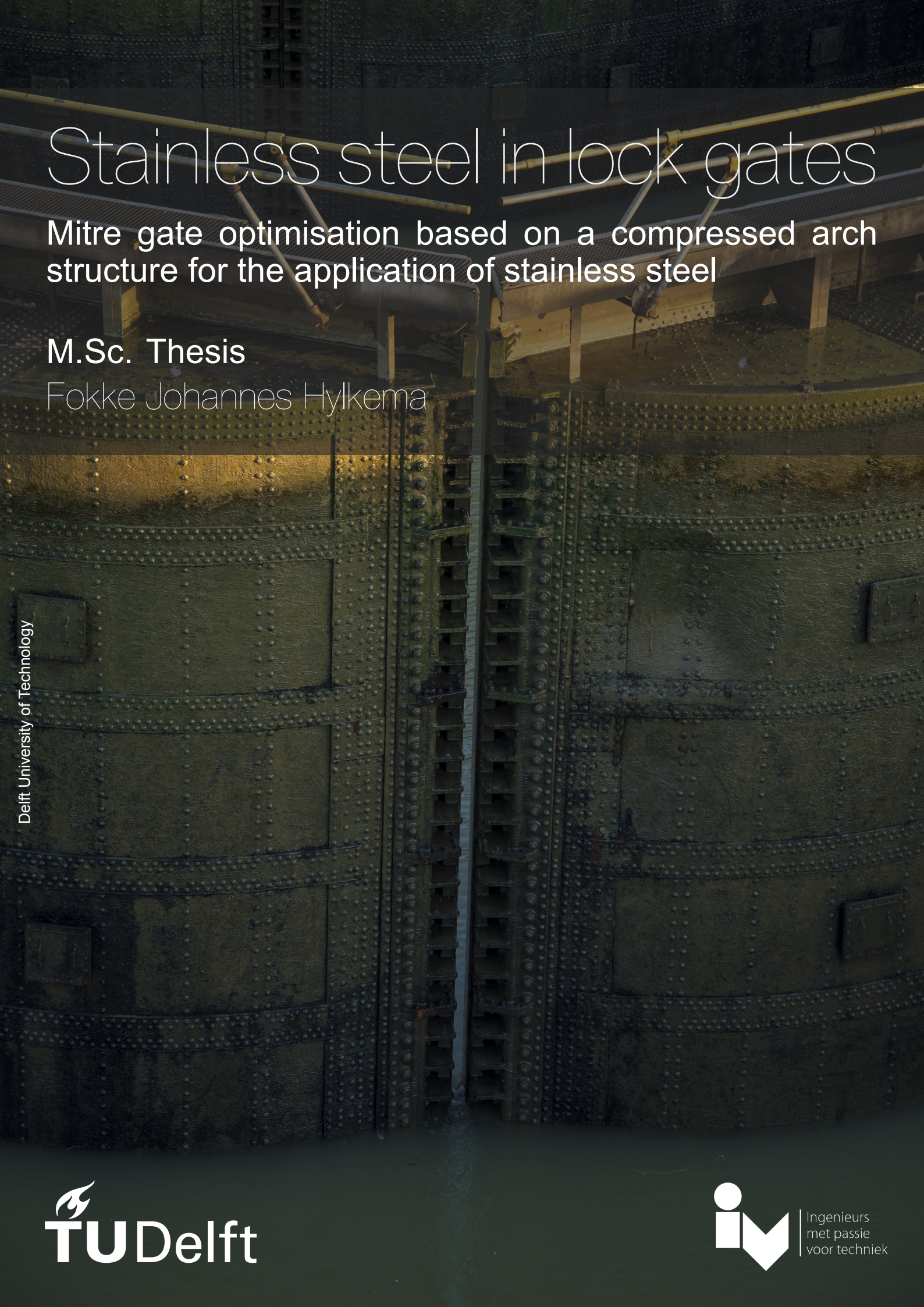

Stainless steel in lock gates

Mitre gate optimisation based on a compressed arch structure for the application of stainless steel

M.Sc. Thesis

Fokke Johannes Hylkema

Delft University of Technology

TU Delft

Ingenieurs
met passie
voor techniek

Cover: by SL Photography, Stockfoto ID:1145264754
Date: 29/4/2019
Title: Panama Canal Miraflores Lock, Panama

Stainless steel in lock gates

Mitre gate optimisation based on a compressed arch structure for the application of stainless steel

by

Fokke Johannes Hylkema

to obtain the degree of Master of Science
at the Delft University of Technology,
to be defended publicly on Tuesday May 16, 2023 at 15:00.

Faculty:	Civil engineering and Geosciences	
Study programme:	Civil engineering; Master's track Structural Engineering; Specialisation Steel, timber and composite structures	
Student number:	4369319	
Project duration:	April 25, 2022 – May 16, 2023	
Thesis committee:	Prof. dr. M. Veljkovic,	TU Delft, Chairperson
	Dr. A. I. Mohabeddine,	TU Delft, Supervisor
	Dr. ir. D. Wüthrich,	TU Delft, Hydraulic structures
	Ing. D. Alsemgeest PMSE,	IV-Infra, Supervisor

Iv-Infra

TU Delft

Preface

When I began my thesis process, I started with the ambition to see if it was possible to reevaluate a common civil structure built with an uncommon material and find advantages to this contrast. After some interviews with various people, I landed at IV-infra where they were eager to set up this research collaboration. The subject of stainless steel in lock gates was one of their aspirations to be investigated. My interest was awakened since I had little knowledge of the matter while the potential seemed to exist. Now, twelve months later, I have finished my thesis and hopefully inspired the use of stainless steel in combination with the gate design resulting from my thesis.

The expertise from my committee that I had at my availability was very valuable to me. First, I would like to express my gratitude to the supervisors from the Delft University of Technology, Milan Veljkovic, Anis Mohabedinne and Davide Wüthrich. Milan Veljkovic, chair of the committee, provided me with the necessary critical insights into my research but also proved very approachable and helpful when I was in the dumps. Anis Mohabedinne gave me the motivation to continue and made sure that I kept on track to reach a point of graduation. Davide Wüthrich gave me the insights to create structure in my project. His enthusiasm for the subject contributed to the feeling of relevance for my project outside the steel constructors' perspective.

The colleagues and supervision from IV-infra, specifically Dennis Alsemgeest, have given me great experience and insight into the world of an engineering firm. Dennis's guidance has been highly insightful in the process of structural engineering from a practical perspective. The passion with which he performs his work and the (brief) moments he used me as a sparring partner for his projects have taught me essential lessons in the world of infrastructure. The other colleagues at IV have welcomed me into their department and helped me in the process of my thesis where possible. In particular, the possibility to ask FEM questions (of which there were many) to Dirk van der Tol and Garry Vandeberg. I am very grateful for everyone their help, support and the chance to be a part of their team.

Lastly, I wanted to thank several people for the support they have given me during this period. My parents made it possible for me to come so far in my education and supported me all these years during the more challenging times. Secondly, my girlfriend was mainly there for me during the process of this thesis. Next to them were my friends and study mates with whom I could always take a break to escape from the project briefly. Thank you all very much for the support when I required it.

Fokke Johannes Hylkema
Delft, May 2023

Abstract

Gates are an essential part of navigational locks, as they are responsible for creating a water barrier and can be repositioned to allow passage for maritime transit. Most lock gates in the Netherlands are based on the mitre gate principle and made of steel. A recent project in Sweden challenged the status quo by constructing the first stainless steel lock gate. The main question of this thesis aims to investigate the possibilities for the application of stainless steel in Dutch mitre gates and how optimisation through implementing a global arch shape can contribute to the material and weld reduction required to do this.

To quantitatively assess the hypothesis of this thesis, Lock Veere was chosen as a case study. The finite element method was selected to simulate the operational conditions of a lock gate. Using the software application 'Ansys', different elastic analyses were performed to find an answer to the effectivity of design. This method was validated by analytical engineering methods based on basic cases.

The first part of this thesis aims to define what needs to be taken into account when designing arch-shaped stainless steel mitre gates. The operational conditions are a combination of boundary conditions and loading conditions. The gate can be positioned in three different setups, which each provide different boundary conditions. Eight different load combinations that could possibly be critical for the gate design of this thesis were defined. These are based on size, asymmetrical positioning or repetitive loading. In addition to the operational conditions, the requirements and limits of stainless steel in lock gates were considered.

The second part of this thesis investigates the feasibility and optimisation of the global shape. The effectiveness of shape is based on the loading system of a structure. For a lock, this is the water level difference that results in a uniform load over the width of the construction. Arches are relatively more resistant to this load, which allows for material reduction. In order to investigate the effect on reaction forces, stresses and buckling shapes, different boundary conditions were simulated to predict the effectivity of the arch shape in mitre gates. Mitre gates have another dominant load situation; a point load with asymmetric support during an obstacle situation. Plates alone are not resistant to this load, so a frame around the plate is introduced. This frame was designed based on low member forces and reduced member use. The feasibility of the components is based on an approximately equal amount of material used compared to the traditional design of lock Veere. Based on the results found in this thesis, both components seem feasible and allow for further material reduction.

The third part of this thesis aims to prove the effectiveness of the gate design by simulating the construction with the operational conditions selected in the first part. The results from part two were used to design a complete gate. The aim of the design was to be as simple as possible in order to meet the demands imposed by stainless steel. This design included lock components and adjustments in the frame such as triangular reinforcements which add structural stiffness and reduce the chance of corrosion. Multiple elastic analysis types simulated the operational conditions on the gate in order to predict behaviour as accurately as possible. Based on the established critical conditions, further optimisation for material reduction was investigated using horizontal stiffeners in the arched plate. The final design allowed for 20% weight reduction and 30% weld length reduction compared to the traditional design. Based on an approximation, the weld thickness was expected to increase and lead to a larger weld volume due to thicker plates being needed at the weld locations.

Based on the results that were found, an answer to the main question posed by this thesis can be formulated. For the operational conditions found in Dutch mitre gates, an arch shape can be applied in combination with a surrounding frame. This reduces the weight, number of welds and weld length. For these reasons, manufacturing is expected to be less intensive and maintenance is more accessible due to component reduction. Global shape was thus able to contribute to the optimisation of Dutch mitre gate design. This optimisation through global shape adheres to the requirements for stainless steel. However, this result opens up interesting possibilities for further research on using global shape in combination with other materials as well.

Contents

Nomenclature

Abbreviations

Abbreviation	Definition
SS	Stainless steel
DSS	Duplex stainless steel
LCA	Life Cycle Analysis
LCC	Life Cycle Costing
LA	Linear elastic analysis
LBA	Linear elastic Bifurcation analysis
GNA	Geometrical nonlinear elastic analysis
GNIA	Geometrical nonlinear elastic analysis with imperfections
EV	Eigenvalue

Symbols

Symbol	Definition	Unit
A	Area	$[mm^2]$
b	Width of the plate	$[mm]$
E	Elasticity modulus	$[GPa]$
F	Force	$[kN]$
g	gravitational constant	$[m/s^2]$
h	Water height	$[mm]$
I	Moment of inertia	$[m^4]$
k_σ	Coefficient for plate vs column buckling	$[-]$
L	Length of the beam	$[mm]$
M	Bending moment	$[kNm]$
N	Normal force	$[kN]$
P	Pressure	$[MPa]$
q	Load over length	$[N/mm]$
R	Reaction force	$[kN]$
t	Thickness of the plate	$[mm]$
u	Normal deformation	$[mm]$
w	Deformation	$[mm]$
ρ	Density	$[kg/m^3]$
ν	Poisson ratio	$[-]$
ϵ	Strain	$[-]$
σ	Stress	$[MPa]$

Denomination

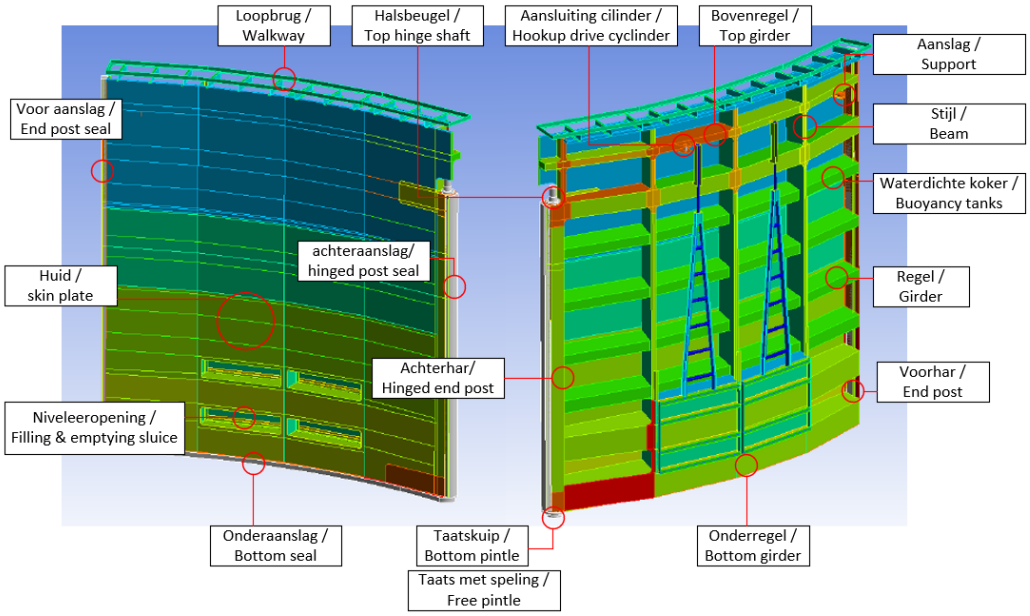

Figure 1: Denomination of Gate members in Dutch and English, labeled.

1 Introduction

The importance of navigational locks in the Netherlands is undeniable. For centuries, the Dutch inland waters have been stocked with the functionality that the construction provides [43]. A navigational lock is part of Dutch flood defences as a water barrier while also providing the service of passage for maritime transit. Aside from safety, one of their main functions can also be to provide a way to regulate the water levels in the surrounding water bodies.

Nearly 20% of freight transport in the Netherlands is done by waterway [7], meaning navigational locks play an essential role. In addition to freight transport, the government also actively works on getting more of the inland transport done by waterways [21]. This means there is a continuous demand for locks and the availability of gate constructions while maintaining water safety.

Navigation locks are a big part of Dutch infrastructure, and at this moment, at least 52 lock gates must be renewed before the year 2040 [29]. Most of these locks were built in the 1950s and the 1960s and have reached their end-of-life phase [27], which means that they have to be replaced to maintain a safe and manageable environment. The design of lock gates is usually contracted to secondary parties which have more knowledge of construction design. IV-infra is an engineering firm that is actively looking for new ways to design these constructions and therefore works with, among others, students from the Delft University of Technology to innovate in the sector.

The design of navigational locks has changed significantly since the production of most of the gate constructions from the previous century [27]. The calculation methods used before the widespread availability of computer-assisted methods led to the over-dimensioning of components and an inability to predict the complex behaviour of constructions fully. New methods of predicting design effectiveness, like Finite Element Analysis for example, were never used on these constructions.

The main building material used for lock gates has over the years evolved from timber [5] to predominantly steel [7]. Steel remains to be a popular construction material, and based on studied literature for certain dimensions, it even seems to be the only viable option [6]. However, the availability of new materials in the civil engineering industry opens up possibilities for the renewal of these kinds of structures and an improved way to design them.

1.1. Motivation

Since a lot of the Dutch gate constructions need to be renewed in the near future, now is a good opportunity to innovate. There is existing literature available on lock gates and the material applications that seem to be evident, but there are currently some options left unexplored. In cooperation with IV-infra, this thesis aims to innovate lock gates by investigating new ways to design these structures.

When compared to carbon steel, there is relatively little research available on the structural application of stainless steel. Structural stainless steel is an upcoming market in the civil industry which has always been held back by the material's relatively lower strength and lack of design codes [2]. There seems to be only one source in literature from Delft University of Technology which studied the implementation of stainless steel in lock gates, published over 20 years ago [16]. This research provides insight into the considerations of the application of the material and gives a preliminary design possibility for mitre gates in the Netherlands. Kruse's study presents an alternative mitre gate design based on

the membrane effect, in which it would be possible to implement stainless steel in a project based on life cycle costing. Yet this study never led to the execution of a gate construction in the Netherlands.

However, twenty years later, Sweden plans to construct the first lock gate completely made from duplex stainless steel [18]. The new project in Sweden is executed in a sector gate, which is different from the design presented in Kruse's study, and is a type of gate which is scarcely found in the Netherlands. Since most locks in the Netherlands are constructed with mitre gates [47], it might be beneficial to focus innovation in the industry on the same type of gate found in the surplus of the structures in the Netherlands.

There are still design options for lock gates that remain to be studied, which can innovate the lock gate industry. This thesis wants to investigate one of these undiscovered possibilities within the lock gate industry; arched global shape optimisation of mitre gates for the application of stainless steel. This design is inspired by the shape effectivity of an arch, as it offers great resistance to the uniform pressure created by water level differences (see figure 1.1). A change in material availability and advances in the calculation methods of complex structural behaviour make it possible to revisit the subject and investigate whether it has potential for innovation in the lock gate industry.

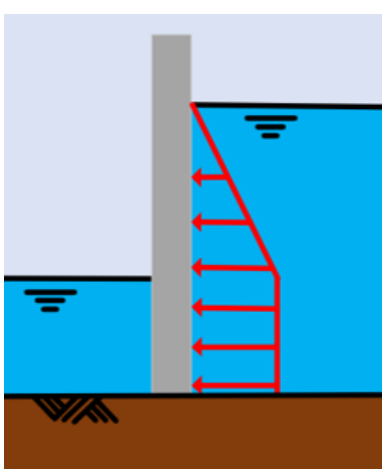

(a) Resultant pressure over the height profile of the gate.

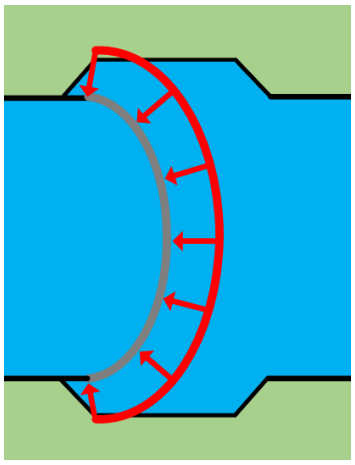

(b) Top view of uniform water load, perpendicular to the local surface due to water pressure.

Figure 1.1: Uniform water load resultant force.

1.2. Research questions

This thesis aims to investigate a main question which was formulated based on studied literature. In order to find the answer to the main question, three sub-questions have been formulated.

Research question:
How can arch shapes be effectively optimised for stainless steel Dutch mitre gates?

The sub-questions are listed below:

- **Sub question 1:** What are the design considerations and requirements for a compressed arch gate construction of stainless steel?
- **Sub question 2:** To what extent can an arched plate be considered feasible for optimising mitre gate constructions and what is minimally required in case it is not?
- **Sub question 3:** To what extent is it possible to optimise the arched gate based on critical operational conditions?

1.3. Objective

The main objective of this thesis is to optimise mitre gates in order to implement stainless steel based on the following aspects: material reduction, minimal welding and a single-skin gate. What is needed in order to achieve this main objective are listed below.

- Get an understanding of the role of global shape in lock gates and how this can be used to advance innovation.
- Define the in- and output required for working with stainless steel in general and specifically hydraulic structures.
- FEM can be used for a complex assembly of components to help predict real-world cases. The behaviour in the model should always be in line with expectations based on simpler cases but can be extrapolated in more complex models. The step by step procedure of model building will aid in this. A systematic approach will help in continuously having a grip on the behaviour of the model and make it possible to understand where the results come from.
- Design a gate construction based on global shape optimisation which can withstand critical load combinations. This design can be further optimised in order to find the best option for global shape application.

1.4. Methodology

The research done in this thesis has been carefully developed, with each step clearly outlined in figure 1.2.

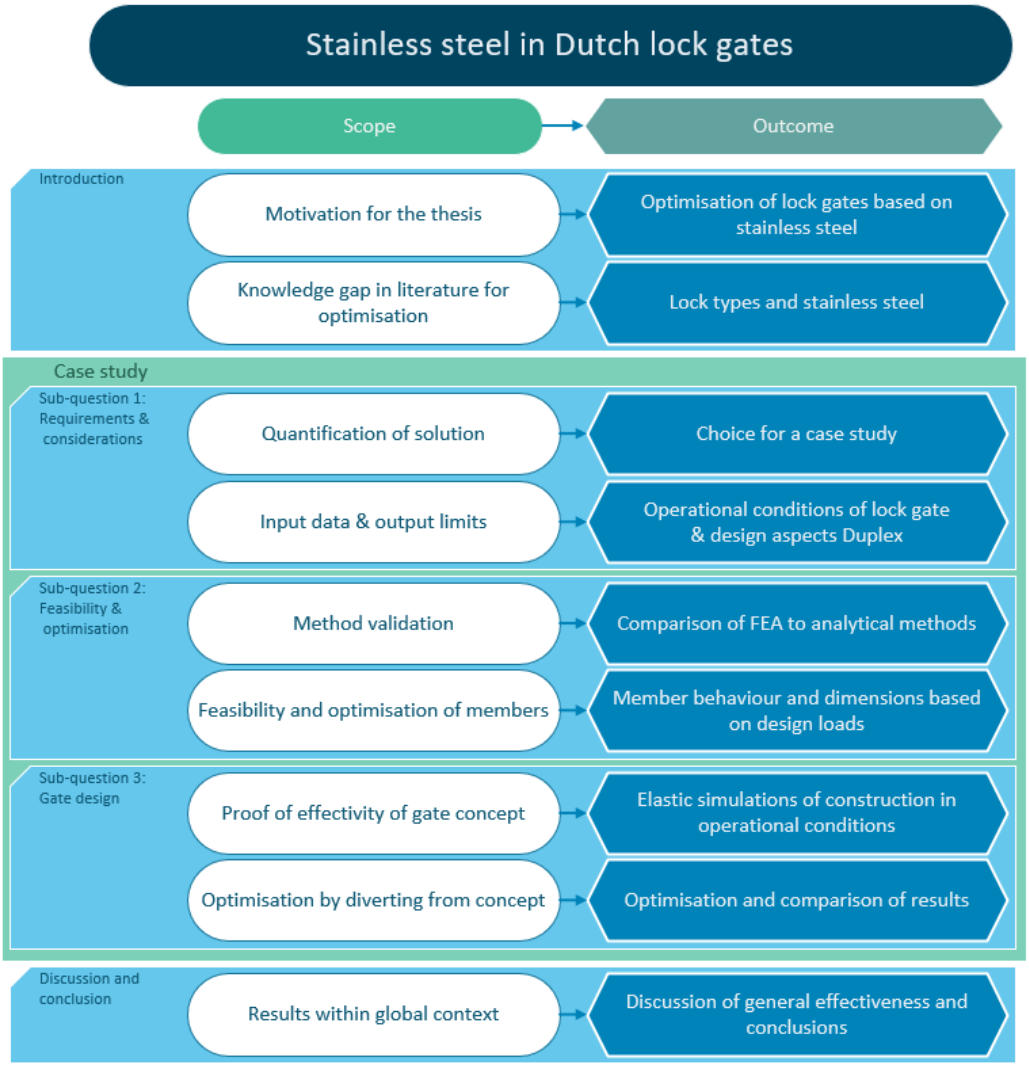

Figure 1.2: Scope and outcome for the steps in this thesis

Figure 1.3 shows the steps that will be taken within the case study presented in this thesis, in order to arrive at the gate design as it is. First of all, there will be an exploration of the components which

will be used in the case study to construct a framework of the available resources and the limits which the model has to adhere to. It shows the process of solid model building and explores the primary feasibility of the main components of the concept. Using the results of this step, a simulation for the circumstances in which the actual lock will be placed needs to be rendered. With the help of FEA a model will be constructed in order to imitate these circumstances, based on which the software will predict the effectivity of the design concept. The design concept is also taken one iteration further in order to see if it can be further exploited than the bare minimum. These designs will be compared with one another.

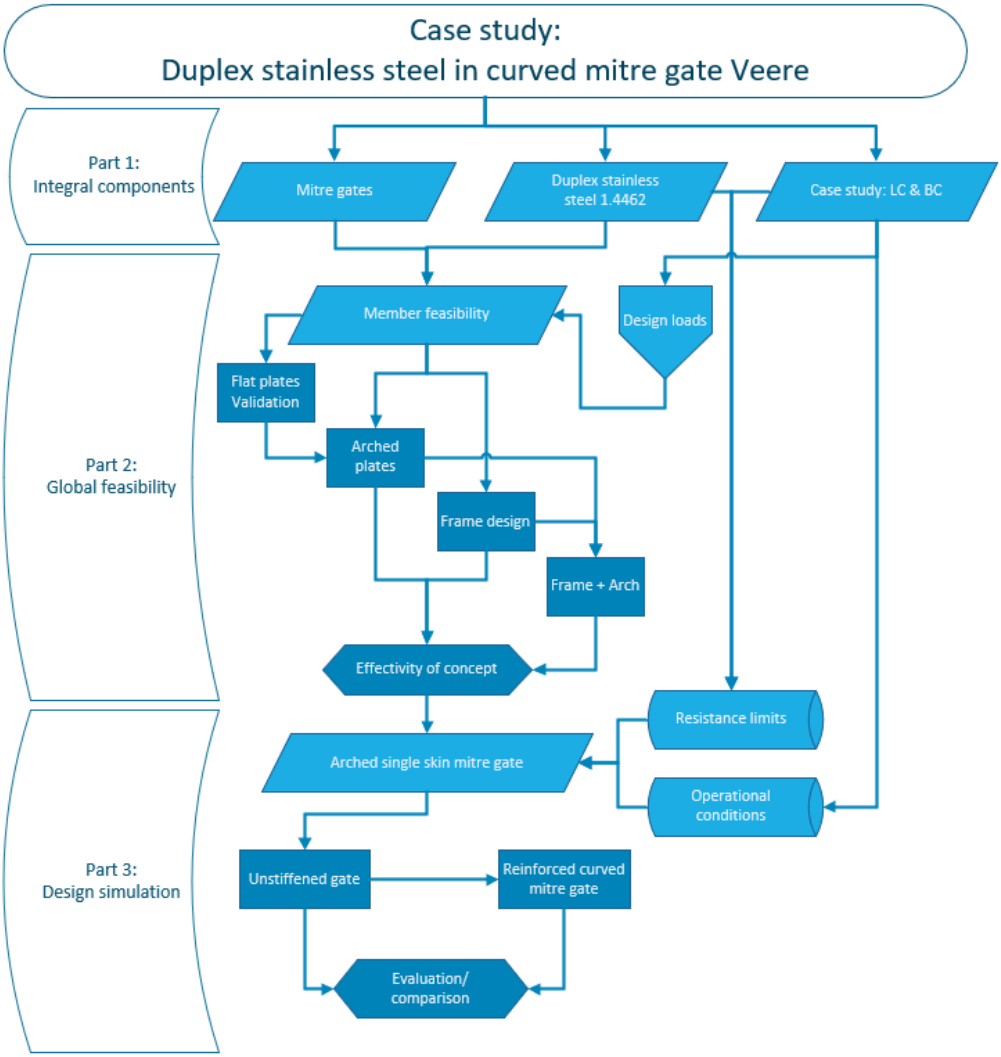

Figure 1.3: The steps taken within the case study of the thesis

1.5. Scope

The scope of this project includes the following components:

- Only Dutch gates will be considered, which implies that only loads which are present in the Netherlands are evaluated.
- The optimisation in this thesis will be focussed on mitre gates. Other lock types in the Netherlands will however be evaluated to see the difference in design and structural mechanisms of the construction types.
- This thesis will only provide the design of a single gate. Modelling one gate will provide a realistic model of the situation of a gate and reduce computation time. The substructure will also not be

part of the structural analysis.

Certain subjects will be left out of the scope of this thesis. These subjects were factors that would not be of relevance to the project or of realistic size for the extent of the thesis. These items will be listed below:

- Plastic analysis was not included in this thesis. The limit for the construction is set at the elastic limit; more complex material behaviour will not be included in this research.
- Extreme incidents like collisions and explosions will be excluded as these are events which use calculation methods that are too extensive for the thesis size next to the work performed. In addition, it is focused on the destructive capacity of the construction, which is not part of the goal of this thesis.
- Proof of the effectiveness of stainless steel against corrosion will not be considered in the case study, as it is considered to be nearly maintenance-free.
- The levelling method applied in the case study is through the use of sluices. One of the main aims of this thesis is optimising an empty plate field. Adding the sluices will cloud this aim. Since there are other levelling methods possible, sluices are not included in the design of this thesis.
- A life cycle costing of the construction will not be included in the thesis.

2

Background

In order to answer the questions posed in this thesis, an investigation on the currently available literature was done. The results of this literature study will now be presented and used to create an understanding of stainless steel and lock gates. In addition, the relevance of the material in civil engineering and for the thesis will be presented. Since this thesis aims to optimise Dutch lock gates, the current state of the art of lock gates needs to be presented, including any knowledge gaps which might be exploited for optimisation. Next, the background of the material will be investigated in order to explore its potential and its characteristics.

To quantitatively assess the questions, a case study was chosen. The lock chosen as a case study is lock Veere, which is a mitre gate with an unoptimised arch shape. The design for lock Veere has to consider design considerations and requirements imposed by the environment, the material and lock gate conditions. These will all be presented and analysed in this section in order to use them for further research.

2.1. Lock gates in general

Lock gates are constructions which are designed with an efficiency-based design method. To know how a structure can be designed efficiently based solely on the operational conditions, it is important to evaluate what conditions are applied to that specific type of structure. The loads which are presented here are relevant for general lock types. Next, the materials which are used will be evaluated in order to see what is commonly used. When the norm with regard to materials has been defined, the lock mechanisms which are used in the Netherlands will be considered and the differences between them will be highlighted. Of these different mechanisms the mitre gate was chosen based on its potential to be optimised for stainless steel application. The mite gate optimisation study starts with the evaluation of global shape use; what use of global shape can already be found in lock gates but is scarcely found in mitre gate design, and thus has the potential to be exploited. This forms the basis for the investigation which will be performed in this thesis.

2.1.1. Lock gates loading conditions

There are general loads which are valid for nearly all lock gates that should be considered for the design of a gate. Since not all locks are similar, and the environment in which they stand can differ significantly, different loads can be chosen to evaluate. The loads which can be considered according to literature [6] are listed below, more information on these can be found in appendix A.

- **Hydraulic loads**, the main load on gates come from all water-related pressures by static or dynamic loads. Movement of the gate can lead to water-induced forces as well, depending on how the gate is moved through the water.
- **Selfweight loads**, as with all other constructions, the material affects loading as well.
- **Loads from gate drive systems**, the moving mechanism exerts a force on the gate.
- **Variable walk, vehicle and service loads**, some locks allow passage of other traffic across the water by means of a passable segment.

- **Sediment, ice and vertical loads**, these loads can increase the weight of the construction and, therefore, the wear in components.
- **Loads from ships and floating objects**, this can be, for instance, the water being moved due to ships or debris floating against the construction.
- **Loads from system malfunctioning**, The system behind the driving mechanism has the possibility of failure and this could lead to forces on the construction.
- **Transport and installation loads**, for transport, there are certain points which have to be able to connect to a crane, for instance.

There are also other conditions under which calamities to which a gate can be subjected and these are briefly described below:

- **Contact behaviour**: since the gate is in the passage of marine traffic, the construction can have a collision with one of the passing vessels.
- **Fatigue**: due to repetitive loading of a gate. Gates are moving structures so depending on the interval of movement gates can be prone to fatigue. The tide may also play a role depending on the size of the load difference.
- **Seismic loads**: when the lock is located in an area where this is relevant it is important to check if it is able to withstand the loads that come with such a situation. Since the
- **Vibrations** in some cases it is possible that due to flow the structure will start to vibrate. This is in combination with water flow in and around the construction.
- **Exceptional calamities** i.e. explosions are possible for construction but are not very common in environments like the Netherlands.
- **Corrosion** that takes away functional, structural material.

When considering the guidelines for working with lock gates, the general guideline for working with constructions is given by the Eurocode. This, however, does not cover the design and loading of lock gates specifically. Therefore the ”Richtlijnen Ontwerp Kunstwerken” (ROK) as an additional guideline has to be used. The ROK forms an additional rule for (hydraulic) structures in the Netherlands which are not covered in the Eurocode. This additional set of rules forms the base for lock gate design. What is noticeable is that unlike other structures, such as buildings, the loads in hydraulic structures like locks are dependent on environmental factors. There is no Eurocode for lock gates at the moment of this thesis. Figure B.1 and B.2 give the load combinations from the ROK.

2.1.2. Lock gate construction materials

Locks can be made from different materials. A comparison by Rijkswaterstaat has been made to compare four different materials for a mitre gate case study. This is part of the ”Multi Water Werk” report [30]. Some conclusions which can be retrieved from this research are presented to gain insight into the application of the material and the consequences.

Steel is the most common material used when constructing lock gates [6]. It is a favourable material based on its relatively high strength and stiffness capacity. It also allows for the largest span possibilities compared to other materials in combination with relatively slender construction possibilities. In comparison to other materials, it has the second-highest life cycle costing (LCC) price and the second-best cost for the life cycle assessment (LCA, environmental impact) analysis [30]. There is a downside to steel that the conservation in relation to corrosion has to be done every 12-17 years [43].

Timber is historically the oldest material used for lock gates. It is relatively low in strength but has a similar density to water, which makes it light in its work and thus accessible for gate removal [6]. As it is a natural material, quality control is harder to uphold. Methods to account for these characteristics have long been developed, allowing this material to be still competitive for smaller and medium-sized gates. This is because there is a limit to the size of available members and the practical dimensions that the gate has. In comparison to the other materials, it has the worst LCC price and the best cost for the LCA analysis [30]. Regarding environmental impact, timber can make a relevant difference in the future. A major downside is that timber gates sometimes do not have a larger life span than 30 years [6], this is a problem when comparing it to the expected 100-year life span of modern gate projects.

Fibre-reinforced polymers are not commonly used in lock gates [6]. The material is relatively new and therefore not often seen in structural engineering. The material is lightweight compared to the

other materials and has relatively high strength. It has average span possibilities compared to the other material options. Compared to the other materials, it has the best LCC price and the highest cost for the LCA analysis due to the environmentally impactful polymer [30].

Stainless steel is not part of the MWW study, but there is a separate analysis for the LCC found in other literature, this source says that the costs of stainless steel can be competitive to carbon steel under the right circumstances [16]. For an LCA there is a conceptual comparison study found in literature [6]. This did not however take stainless steel further into account based on the energy consumption of the material. This is not an incorrect assumption as the material has a high demand for energy during production [8]. In the study, the product used was AISI 316L which is not the strongest type of stainless steel available. This choice of steel led to a design which is heavier than the carbon steel variant he compares it to. Options in stainless steel with better mechanical properties can however lead to a lighter construction, making Daniel's conclusion not definitive.

The study on the implementation of stainless steel in lock gates [16] has some important conclusions which can be used to continue work from. The study concluded with an option for a membrane global gate design and an LCC of the construction. The barrier plate of the final design used as the membrane, has a thickness of 8 mm; see appendix figure C.4. In the study, valuable insights are presented in line with the modern standards of working with stainless steel. There are, however also results of her work which can be improved upon using the knowledge we have acquired on stainless steel since. This thesis will take the following notions into account:

- A membrane design based on the tensile capacities of the material was made. Figure 2.1 presents the concept of the final design. The global shape of the construction provides an option for material reduction and the risk of corrosion is said to be mitigated.
- The membrane gate has a convex side that will point inwards to the canal when the gate is in an open position, it is a hazard for the passing marine traffic to collide with gate components that are in the middle of the canal. When an arch concept is used the gate will be removed from the canal passage and stored away into to post of the substructure.
- The structure proposed in literature [16] does not seem to take into account all loading conditions common in a mitre gate. It is expected that the membrane structure will not be able to offer resistance to asymmetric loads which can be present in a lock. More on these loads can be found later in this chapter. The gate concept is however not found in modern-day locks and is assumed not to be effective enough. New simulation tools could help in a more accurate prediction of the different load types.
- In the report there is no assessment of fatigue. Looking at the edges where the plate is connected to the frame, there is a detail which might prove to be critical as continuous stress is put on one part of the gate as it opens and closes and the water head is created and removed. This can result in fatigue of the detail and is expected to be critical based on the results found in the report. Fatigue must be taken into account in this thesis to define a more realistic structure.
- For stainless steel gates to be competitive, they need to have a predicted life span of at least 90 years. Current life spans for lock gates are set at 100 years which should allow for the approximation of the break-even point.
- A compression-based structure can be less susceptible to stress corrosion than a tensile-based structure [42].

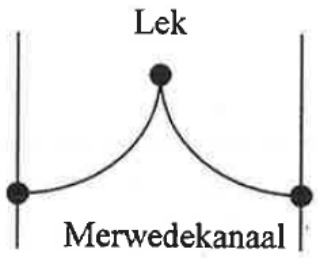

(a) a top view of the gate in which the high water comes from the "Lek" direction.

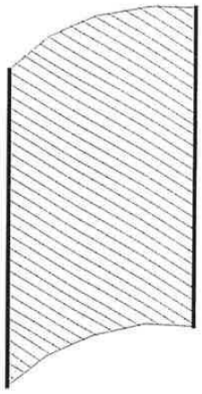

(b) A 3D image to present how the tension plate is thought of.

Figure 2.1: The Kruse design of a solution for a stainless steel mitre gate.

Since the use of stainless steel has become more widespread over the years [2] and the first stainless steel lock gate is being built in Sweden [18], this offers a possibility to investigate what can be done to implement the material in Dutch lock gates. Taking into account the characteristics of the material, which will be explained later in this chapter, and the guidelines by which a gate can become competitive against the traditional gate types. This mainly includes a way to optimise material use and corrosion reduction.

2.1.3. Dutch gate operating mechanisms

The most popular lock gates in the Netherlands are divided into three main types [6]. These types are the mitre gate, the vertical lift gate and the rolling gate. The advantages, disadvantages and mechanisms of all three gate types will be elaborated on as they influence the types of vessels coming through, the manufacturing possibilities and the effect the gate has on the environment. The relation to this thesis is presented in the form to which extent the gates are feasible to be used for the optimisation.

Certain functionalities have to be present in most if not all gate types. Firstly, the gates have to be able to provide passage for inland ships of an according class, meaning the gate must be able to move in and out of the way. Secondly, the gates have to be able to withstand the forces applied to them when the barrier is either in a closed or open position. Third, all locks need to have the capacity to level the water inside the lock. This is often done by means of sluices in the gate or water culverts around the gates. These sluices will have to be of sufficient size in order to provide the lock with enough water levelling speed to support the lock operations.

2.1.3.1. Mitre gates

The most common type of gate in the Netherlands is the mitre gate. A visual representation is given in figures 2.2, the general supports and loads can be seen in this image. The positive aspects of a mitre gate design, otherwise known as a double gate system, for this thesis, are listed below:

- It is a sustainable principle of operation as the three-point truss is self-sealing. The arch principle will benefit from this.
- The forces in the connection of the gate to the substructure can be in the perpendicular and longitudinal direction of the lock. This matches with the arch principle.
- The forces of the water head are divided evenly over the seals of the gate.
- The construction is not overly complex to design and maintenance costs are relatively low. The optimisation investigation is adequate for this project size and provides a decent level of detail.
- The depth of the gate cabin is small, which means the sub-structure itself doesn't need to be deep either.
- The movement for opening and closing is simple and quick.
- Multiple filling and emptying possibilities in addition to some extra mechanisms, can be fit into the gate.

- It is relatively easy to transport.
- This lock is the most applied type, which means that information on the structure is readily and extensively available.

Some negative aspects of arched stainless steel mitre gates are listed below:

- If a vessel collides with this type of gate, the system will open. The arch shape is slender which offers low resistance to these impacts.
- An extra gate set is needed in the structure, as the system can only form a water barrier in one direction. This means that extra gates and therefore material is needed to achieve the same barrier options.
- Larger lock spans have to deal with more motion resistance from the water which leads to a lot of energy being needed by the mechanism. The slender arch design hs to be investigated for this.
- Floating debris can form a problem for opening and closing mitre gates, as it can get stuck between the gate and the substructure, which is located in a nook of the downstream direction. Stainless steel has to be combined with low sediment storage to reduce corrosion chance.
- The inspection possibility underwater is limited and would require some form to be performed.

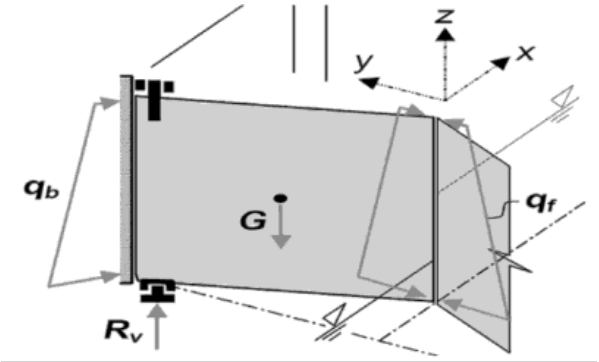

Figure 2.2: Mitre gate system presented systematically, images from literature [6].

2.1.3.2. Vertical lift gate

A vertical lift gate is opened by raising the construction out of the water by means of towers. The towers can either have contra weights to facilitate this lifting motion, or there needs to be another type of mechanism in the tower that is able to lift the weight of the gate. An image has been added to get an idea of the gate in figure 2.3. Some positive aspects of lift gates are listed below:

- It has water barriers on two sides for which the arch is likely to be resistant.
- The design allows for easy inspection, as the gate can be lifted out of the water completely. This is favourable for stainless steel and inspection possibilities.
- The gate is not very vulnerable to sediment or debris in the opening of the gate. This reduces the chance of corossion.

Some negative aspects of lift gates are listed below:

- Forces can only be transferred in the substructure in the longitudinal direction of the lock. The perpendicular force produced by the arch shape has to be evaluated.
- The gate requires complicated guidance systems for vertical movement. This is not fit for all support types.
- The structure is exposed to high wind loads when lifted. This should not be a direct issue for the shape efficiency but the load type can become complex.

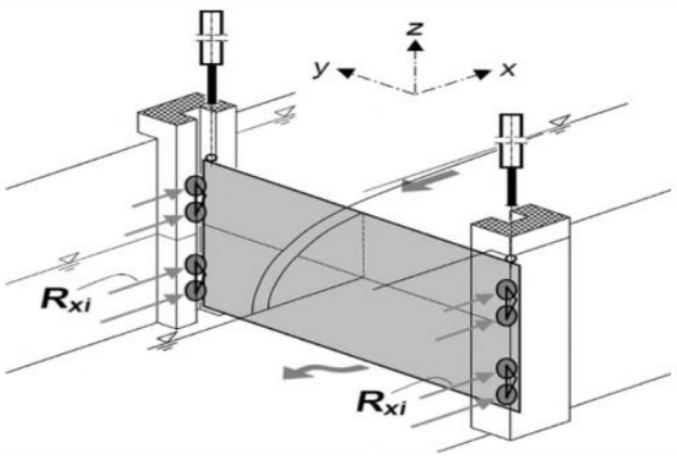

Figure 2.3: The vertical lift gate type, image from book locks and other closures [6].

2.1.3.3. Rolling gate

A rolling gate is a structure where the gate is put on wheels, which ride over a rail system that horizontally allows movement (see figure 2.4. The weight of the gate is carried by the rail system, which can be placed at the top or at the bottom of the structure. Positive aspects of the rolling gate:

- The gate can facilitate a driveway on top, which allows for the combination of functionalities and getting the most out of used material.

Negative aspects of the rolling gate are:

- It is an extremely detailed gate with a complex structural system. It does not really fit the size of this thesis and the detail level it is striving for.
- Forces can only be transferred in the longitudinal direction of the substructure. Not in line with arch shapes.
- It requires an expensive and deep gate cabin, which is combined with a large concrete structure around it. The material is expensive too so the expectation is that this will be difficult to improve on.
- Inspection of the gate is difficult because the most critical component, the rail, is located underwater. Most of the structure is and removing it from the water is not an accessible task. Poor fit for stainless steel.

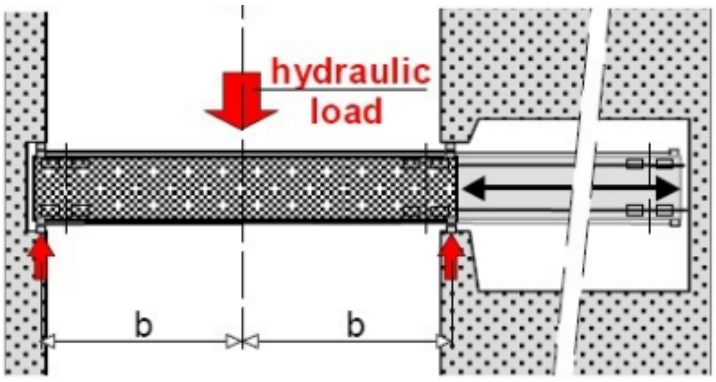

Figure 2.4: The rolling gate type, image from book locks and other closures [6].

The mitre gate in the Netherlands offers an opportunity for research due to its support aspects that line up with the force transfer found in this gate type. Secondly, research on this type can impact most due to its abundance in the Netherlands.

2.1.4. Lock gate global shape

Different lock gates make use of different movement mechanisms, as was seen in the previous section. Gates can also come in different global shapes to transfer loads. These global shapes are mainly used to transfer the water head in the closed set-up of the gate. These different movement mechanisms and global shapes will now be discussed below.

2.1.4.1. Curved gates

Curved gates are not new in the lock industry. They have been used in different lock types and in different end mechanical systems. They can be compression or tension-based constructions.

Several sector gates that have been constructed, have a curved shape in their water barrier. The global shape of sector gates when the gate is closed is not a circular shape but rather an intersection of two semi-circles. Force transfer occurs through the long arms which are attached to the rotation point of the gate. These gates usually have many stiffeners on the skin as reinforcement to make sure the construction stays intact.

The Hartel storm surge is an example of a curved gate which can work in two directions, giving it two functions. First, it can function as a storm surge, preventing water from coming in. In this situation it functions as a compression-based gate. It can also prevent water from streaming into the sea. Here it functions as a tension-based gate. The system is visible in figure 2.5.

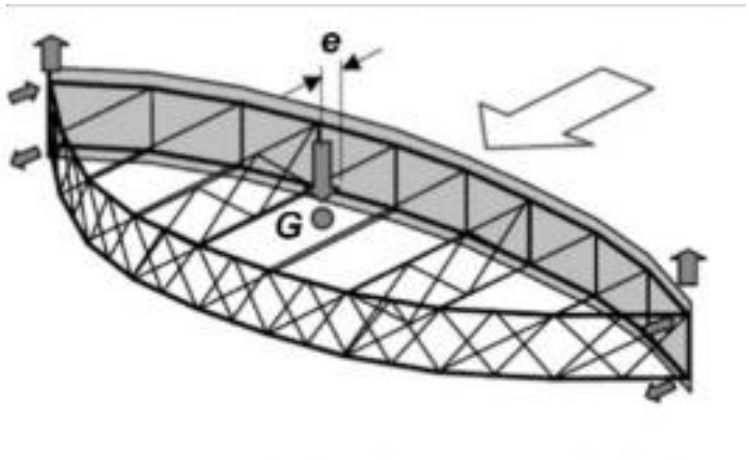

Figure 2.5: Hartel barrier system [6].

Other examples of curved gates are found in radial gates or rotary gates. These structures are designed with a rotational axis in the horizontal axis and the plate is also curved around the rotational axis. The downside of this design is that the water can create omniscient pressure. When there is a water head on two sides the construction has to be able to withstand a force which can be vertical on the plate while also presenting a horizontal force on the plate.

2.1.4.2. Single or double skinplate

Most gates are constructed with some form of double skin, constructed similarly to a sandwich panel. Double skins allow for buoyancy tanks locked within the gate but can also be filled with water in order to prevent the construction from floating. A downside of these tanks is that when water is repetitively put in and taken out, regular inspection and maintenance is needed, which makes an entrance to these tanks essential. Another downside of a buoyancy tank is that when it is filled with air it initiates local bending of the skin plate due to the absence of water on the other side. In the case of repetitive loads, this can lead to fatigue.

Although less common, single-skin constructions are not an uncommon way of executing a lock gate. The single skin is often combined with a network of stiffeners. The downside of a single-skin gate is that there is an asymmetrical centre of gravity, which leads to an eccentric load mechanism. There are some cases in which a plate field is made using a fold plate structure, through which strength is created by the moment of inertia of the plate shape. As all these options require many welds and corners, debris or sediment can become an issue.

The literature presents an optimal shape for curved double-skinned gates which should contribute to material optimisation [23]. Two curved gate designs are the most instinctive and are seen in figure 2.6a, these were assigned a base value of 1 for material use. The optimal value for material use in curved gates lies between 33 and 39 degrees at the base angle of the lock triangle [23]. Figure 2.6b shows this layout and which corner is meant, the right bottom angle. The material value for this gate was found to be 0.88 compared to the base cases. This is a significant improvement. This concept will have to be further evaluated in this thesis if this can be exploited.

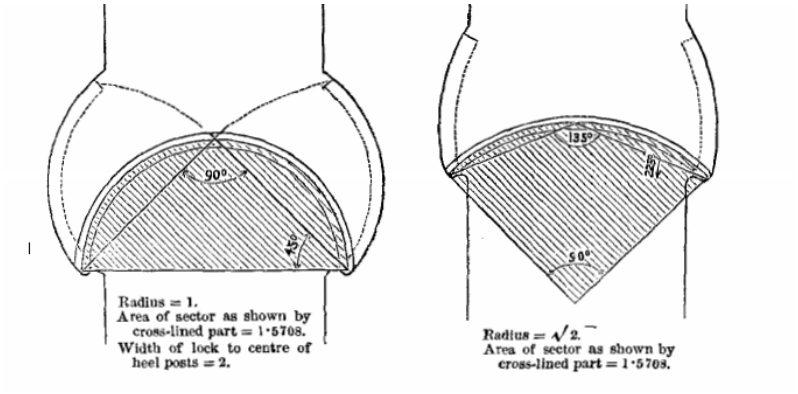

(a) The basic curved gates with material base value 1.

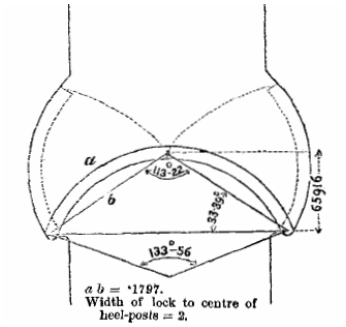

(b) The optimal curved gate shape with material base value 0.88.

Figure 2.6: Phipps curved gate design [23].

2.1.4.3. Curved unstiffened, single-skin mitre gates

When studying literature on lock gates, it quickly became noticeable that there seems to be an absence of arch gate types that are designed to work based on the global shape of a single skin plate. Some gates make use of the arch principle but have reinforced the skin with many stiffeners so reduced member use is not achieved, which in turn requires much manufacturing effort. These constructions also have asymmetric build-up that can lead to problems in mitre gates. A curved single skin can overcome the problem of stiffeners and asymmetry. This could allow weight reduction, manufacturing steps and a better loading scheme of the construction. To see if the global arch shape, which can be very resistant to a uniform water load, can be applied in mitre gates, an investigation has to be done on the effectivity in the circumstances of this construction.

2.2. Stainless steel

The current section will be devoted to an investigation of stainless steel as a material, including what capacities the material has and how that should be accounted for in a lock gate design. Based on these results, the choice this thesis made to use duplex 1.4462 stainless steel as a material will be substantiated. This elaboration includes what the material has to offer and what its limits are.

2.2.1. Introduction

The definition of stainless steel is such: ”In metallurgy, stainless steel is a steel alloy with at least 10.5% chromium with or without other alloying elements and a maximum of 1.2% carbon by mass.” [39]. There are over 200 types of stainless steel available today. Stainless steel is dividable into three main types [42]. Ferritic, Austenitic and Ferritic/austenitic.

Ferritic consists of Fe + 11-18% Cr. In structural application, it is excellent for cold forming and has a relatively high yield strength which makes it attractive for structural application. This type is relatively poor for welding and is often used indoors due to the lower corrosion resistance.

Austenitic consists of Fe + 18% Cr + 8% of Ni. Corrosion resistance is generally high. Welding is not as great as other types but possible if alloyed correctly. The yield strength is generally low which makes it less attractive to structural application.

Ferritic/Austenitic is often called duplex stainless steel (DSS) and it consists of Fe + 21-27% Chromium and 3-5% of Nickel. Welding is well possible for this material but it has its complications [22]. Duplex has a relatively high yield strength and is often used when high corrosion resistance or high strength is

needed. The range of stainless steel types is a characteristic difference in local structure due to the alloy type. This structure is called the phase of the material. Duplex has the characteristic of possessing both phases which are part of the reason for the material properties. The range of phases is based on the assembly of the alloy which is presented in figure 2.7. This is where the implication with welding is presented. Welding changes the local structure with heat input and forming of the phases is only adequate under the right circumstances. This will be elaborated on later.

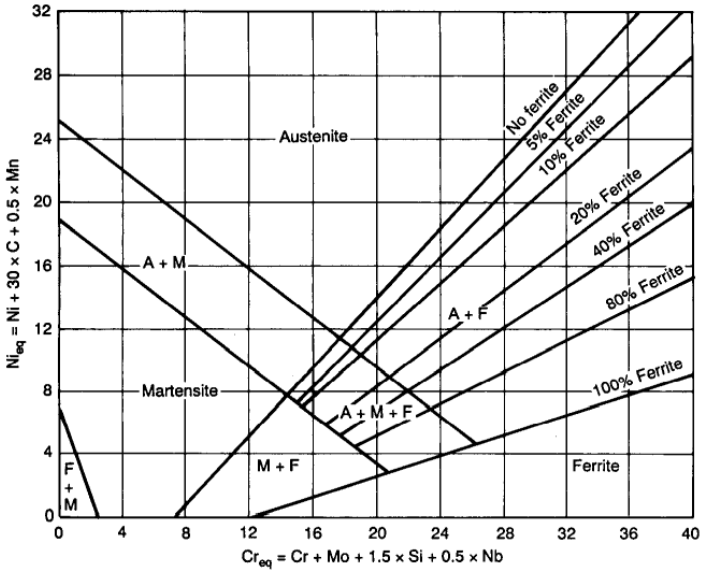

Figure 2.7: Phase diagram of stainless steel [20]

Stainless steel has found its place in projects and constructions, such as bridges.. ”Grade 1.4462 was used for the Millennium bridge footbridge (York, UK), the Cala Galdana highway bridge on the island of Menorca and the Stonecutters bridge towers in Hong Kong. The Cala Galdana bridge contained two types of SS, of which the lesser was used for railing, resulting in a worse deterioration of the weaker grade (1.4401) in the high-level chloride environment. Grade 1.4362 was used for the Padre Arrupe Bridge linking the Guggenheim Museum to the University of Deusto in Bilbao and for the Celtic Gateway footbridge in Holyhead, UK (...). Grade 1.4162 was used for the Siena bridge in Ruffolo.” [2].

2.2.2. Design codes for stainless steel

Eurocode 1993-1-4 prescribes the treatment of stainless steel for structural application. Some critical differences compared to structural steel design code 1993-1-1 are highlighted here to show the difference between the material types.

One impactful difference in the design of stainless steel compared to carbon steel is the applied safety factors. The factors are given down below. The values for the first two factors used for general stresses and stability are 10% higher than the ones used in carbon steel. This most likely results from a lack of research on stainless steel compared to carbon steel. This lack of research might be improved upon in the future. The current values for the safety factors are given here:

$\gamma_{M0} = 1.1$, Resistance to yielding and for local buckling

$\gamma_{M1} = 1.1$, Resistance to instability for elements which are prone to buckling

$\gamma_{M2} = 1.25$, Resistance to tension by cracking and resistance of bolts, rivets and welds.

The design codes do not describe any additional rules for the stability of stainless steel. The factors used to describe the imperfections in pre-fabricated beams deviate conservatively, but there is no difference prescribed in the codes. In contrast to the code, some sources aim to define a calculation method for the nonlinear plastic behaviour of the material concerning stability [45]. This will not be included in the thesis as its limits will be set around elastic behaviour.

Fatigue has to be treated the same way as carbon steel, according to the code. This is supported by other research [9]. The fatigue will be followed according to the fatigue standards used for carbon steel.

2.2.3. Corrosion in stainless steel

”Corrosion is the degradation of materials’ properties due to interactions with their environments, and corrosion of most metals (and many materials for that matter) is inevitable.” [34]. This indicates that materials like steel are prone to corrosion. The ultimate goal of stainless steel is to prevent corrosion from happening. This is achieved by a chromium-rich oxide film on the outside of a component created on exposure to oxygen [9]. To ensure a stable film, the material can be treated by pacifying. This Layer should stay intact for the material to stay corrosion free. It does, unfortunately, not completely out rule the material from forming corrosion spots. The types which can form in stainless steel will be briefly elaborated on here:

- Regular corrosion in aerated environments can be neglected for most stainless steel types due to its ability to maintain an oxide layer. This is supported by the Eurocode.
- Pitting corrosion and splitting corrosion: In case of damage to the chromium-oxide layer, this can self-heal. If, due to circumstances, there is no possibility to oxidise the damaged spot, the corrosion could continue. This could even evolve into an extremely corrosive environment. This can be prevented by careful material selection and decent construction and maintenance [42].
- Galvanic corrosion: when multiple metal types are in contact with each other and an electrolyte is present, this type of corrosion can form. Speed depends on multiple aspects and is unpredictable [42].
- Stress corrosion (SCC): presents itself in Chloride environments in combination with tension stresses. This is not likely in environments under 60 degrees Celsius. As a lock gate is generally situated in cool and stable temperatures, this will not be relevant.
- Intergranular corrosion: can present itself around welds, mainly the temperature-affected zone. There is an interaction between the carbon and the Chrome which depletes the local area of the chrome in the metal. Mainly present in austenitic Stainless steels. Can be prevented by choosing stainless steel with a low carbon volume of less than 0.02 wt %.
- Biological corrosion: Bio growth can occur on the homogeneous oxide layer of SS. Within a week, there is inhomogeneous bio growth on the material. The random spread creates anode and cathode spots of which the clean spots form the cathode. The process of biocorrosion is not corrosion in itself but it is a stimulant for other mechanisms. It stimulates pitting by differences in the oxidation of spots, the speed in which oxide is reduced at the cathode and the new cathodic reactions. Stainless steels alloyed with Molybdeen are relatively well equipped against biological corrosion [16].

To prevent corrosion, the Eurocode has several guidelines. The prevention of dirt accumulation on the structure can be achieved by avoiding horizontal surfaces and inclinations where possible. Use of hollow sections to reduce exposed surfaces. Crevices should be avoided to prevent splitting corrosion. Smooth surface treatment reduces the chance of bio growth on the construction. Welds should be post-treated by removing contaminants on the material and pacifying the material to reduce the presence of unwanted welding products. Treatment of the welds includes mechanical or chemical methods, as brushing is not enough to allow the chromium layer to perform its corrosive resistant effect [22]. The oxide contamination of the weld includes oxidation, tarnish, heat tint and other contaminants. Mechanical treatment includes polishing, grinding or abrasive blasting. Chemical treatment can be a more aggressive form of passivation than that is used in other stainless steel processes.

To indicate how resistant a stainless steel type is, the pitting resistance equivalent number PRE-N value is used to describe resistance to pitting corrosion. The value is determined by this formula: $PREN = wt.\%Cr + 3.3 * wt.\%Mo + 16 * wt.\%N$. The resistance to corrosion in chloride environments is due to the presence of chromium, molybdenum and nitrogen [15]. A higher number indicates more resistance to this corrosion type.

2.2.4. Duplex 1.4462 stainless steel

The choice of the type of stainless steel is based on several aspects. The mechanical properties of the material, the costs and the resistance to corrosion have to be taken into account. This section will touch on these subjects and will start with the application in reference projects.

An example of a lock that was constructed using duplex 1.4462 is the Swedish lock in Sodertalje. The lock is situated between an inland lake and the Baltic sea, forming a connection between the sea

and the lake. In addition to the project in Sweden, another study advised to use the same material type for an inland lock which is connected to freshwater rivers [17]. These projects were the starting point of the decision to use duplex stainless steel 1.4462 in the current study. The study by Arup presents the results of bridge construction in a marine environment, concluding that duplex 1.4462 has an advantage over carbon steel in terms of LCC over a sixty-year span [32].

Duplex 1.4462 is, according to the Eurocode, suitable for high-intensity sea environments and is even considered overqualified for medium situations this is also confirmed by other sources [24]. Lock Veere lies close to the sea and directly interacts with brackish water. This is not a temporary situation so it can be assumed that lock Veere is a high-intensity environment. For reference, the table with the environment classifications has been added in the appendix figure C.2. Regarding the lifespan of the material, the assumption is made that it will be able to withstand the use phase of a hundred-year service life of the construction with adequate inspection and maintenance.

Duplex 1.4462 stainless steel is made up of the following elements presented in the mass percentage of the material 2.1: C (Carbon): 0,02 wt.%, Cr (Chromium): 22.4 wt.%, Mo(Molybdenum): 3.1 wt.%, Ni(Nickel): 5.7 wt.% and N(Nitrogen): 0.17 wt.%. The remainder of the material is made up of iron (Fe). Due to the high chromium content of duplex 1.4462, it offers excellent resistance against uniform corrosion [22]. Molybdenum and nickel are valuable to aid in resistance to pitting and splitting, contributing to the PRE-N value which is 35 for this material [22]. Stainless steels that are alloyed with Molybdeen are relatively well equipped against biological corrosion [16]. Duplex 1.4462 has a high relative weight percentage which makes it resistant to biological corrosion [16]. Nitrogen assists in the self-healing ability of the film [46]. There is a low carbon content, as this would otherwise form high ferrite levels in the heat-affected zone of a weld [12]. Carbon presence is desired for carbon steel as it creates hardness in the arrangement of atoms of the material. The presence of carbon in stainless steel is however less desirable as it forms an impurity [35].

As mentioned before, duplex contains a balance of iron phases in the material. This can consist of ferrite or austenite which represents the structure of a specific spot in the material. When adjusting the material through heat this can change into various compound or intermetallic phases [15]. When this change occurs, the local microstructure differs from the rest of the material. The balance it has is the aspect which gives it resistance to corrosion.

The challenge of welding duplex stainless steel is to maintain excellent corrosion resistance [37]. Welding inserts a temporary change in the temperature of the material. Heat changes the chemical composition which, together with a two-phase microstructure of ferrite and austenite, is responsible for the resistance against pitting corrosion. Manufacturers often provide a guide to welding their material [37]. Some points of attention for welding are:

- It is important to create a weld that is just as resistant to corrosion as the base material is [37]
- 1.4462 can be welded using the following methods: TIG, MIG, stick electrode, SAW, FCW and PAW [22].
- Near the fusion temperature, the structure is completely ferrite. The desired ferrite content is 30-55% which can only be achieved by proper cooling. Too fast cooling can lead to the austenite not reforming and too slow cooling can lead to embrittlement.
- Weld splatter on the surface of base material needs to be removed, as there is no further conservation added in the process.

The ratios in the alloy give duplex its mechanical properties. The Eurocode presents the values that have to be worked with for structural application, they are presented in table 2.1. According to Outokumpu, a stainless steel manufacturer, duplex stainless steel 1.4462 has excellent mechanical properties that even exceed these values [22] which might lead to better results in the future.

Table 2.1: mechanical values for duplex 1.4462 stainless steel according to the eurocode

	<6mm	<75 mm	<250 mm
$f_{0,2\%}[MPa]$	480	460	450
$f_u[MPa]$	660	640	650
$\nu[-]$	0.3	0.3	0.3
$E[GPa]$	200	200	200

Duplex 2205 (1.4462) stainless steel is the most widely available type of duplex, reducing production costs compared to other types [33]. The duplex cost will be compared to S355, which was used for the design by IV-infra. For carbon steel S355 the cost per kg for plate material is found to be 0,8-1,22 dollars per kg [40]. Duplex stainless steel 1.4462 is found to be 4-5 dollars per kg [38]. This means that the costs for the duplex variant would be four to five times higher. Reducing the total amount of materials used is important to keep the total cost of the construction realistic. Certain costs are no longer present when using stainless steel in construction, like conservation and the costs of the process that comes with it. These factors allow the material to be more optimal in the life cycle costing of a lock gate [16].

2.2.5. Stainless steel in lock gates

The aim is to design a mitre gate structure with considerations for the design based on stainless steel. The construction must adhere to a set of rules or guidelines by which it has the highest chance of succeeding as stainless steel structure. The design criteria for lock gates used in this thesis are:

- Design for material reduction. Due to the expensive nature of the material, saving on the total amount of material is essential. Higher material strength and global shape allow for this optimisation.
- Both bolts and rivets will not be used in the design for this thesis, as the chance for pitting or splitting corrosion is higher in an underwater environment due to the crevices which come with the connection type. Welds will be used as the connection method, as this fits the corrosion resistance of stainless steel better as advised by the Eurocode. Welds should be minimised as welds are relatively expensive due to labour costs [31]. This can be achieved by reducing the number of members in the construction. Generally, stainless steel requires higher qualifications for welds but due to the classes of the lock this is not an issue as the execution class demands an equal level of welds for carbon steel.
- Sharp inclinations and horizontal surfaces will be avoided as much as possible to prevent the growth of bio-organisms and sediment storage. The addition of members should be considered to reduce these surfaces, while at the same time preventing an increase of welds. Duplex has relatively good resistance to bio-induced corrosion but is hard to predict the effects [16] and should therefore be avoided. Welds have to be smoothed out to prevent inclinations.
- Maintainability and accessible inspection possibility of the construction should be striven after. This can be achieved by keeping the surface of the construction simple or empty when possible. In order to prevent large maintenance, there should be a method to execute inspection in an accessible manner, meaning the surface of the structure should be accessible.
- A single type of material will be used which comes from the galvanic corrosion possibility. Galvanic corrosion will be minimal in duplex steel when pacified, it is usually the noblest material [22]. Combined types of steel in structures have the issue that the less noble steel parts will deteriorate faster than the more noble components [13]. The exact outcome is unpredictable and such a situation should therefore be avoided.
- The assumption is that 1.4462 duplex will not corrode significantly when under the standard circumstances presented by the case study. Opinions in the Eurocode and literature support this [44]. There will not be a loss of material thickness taken into account in the construction.

2.3. Case study: Lock gate at Veere

As mentioned before, a case study was chosen to be investigated in this study. This section will start with a motivation on why this specific case study was chosen. An investigation of the current situation of lock gate Veere will follow this. There is currently a gate in place which provides a solution for the lock barrier which is presented. In addition, there is also a new design for this gate by IV-infra which could provide useful insights. After the description of the current state, the results gathered from studying these structures will be presented. In addition, the local environment and the layout of the lock will be described in order to get an idea of the function of the structure within its position.

In addition, this section aims to define the operational conditions of this gate construction. The simulations executed in this study are based on input from real-life situations and have to be tested by the limits of the material and other boundary conditions of the circumstances. This chapter will present these limits, followed by the boundary conditions for the moveable structure in different setups. Finally,

it will examine which combinations of the loads are present for these different layouts. The mitre gate in Veere will be used in order to simulate all of the above-described situations. As explained earlier in this chapter the ROK gives the general load cases which have been prescribed. These can in turn be evaluated by an engineer in order to assess which of the loads are considered to be relevant. In the case of lock gate Veere an assessment had already been performed, which was used to decide which loads will be used for the project by IV-infra. Next to these loads other loads that might prove critical will be presented as well.

2.3.1. Choice for this case study project

The reasoning behind choosing this project is based on multiple aspects, which are listed below:

- Mitre gate in the Netherlands of which only the gate has to be replaced.
- The curved gate shape presents an opportunity for a global design. The current design is two skins which might be inoptimal.
- Recently the gate was redesigned, which means that there is an up-to-date design which has been designed with equal simulation possibilities. A comparison could be made with this design or it can be used for reference.
- In terms of lock width this construction is above average, at a width of 20 meters while the average lock width (which are maintained by Rijkswaterstaat) lies at 15 meters [28].
- The maximum water head that occurs at this site is below average as it maxes out at 1.65 meters while the average lies at 3.98 meters [28], this needs to be evaluated at the end of the thesis.

2.3.2. Situation lock Veere

The navigation lock that will be studied is located at Veere in the province of Zeeland, NL. The lock was constructed in a time prior to the Dutch waterworks, meaning that in the earlier use phase of the lock, it was a barrier directly connected to the North Sea [49]. This previous function as a barrier to the sea is still visible, as the head on the north side is installed with two sets of gates to manage the water level in the canal during the high tide from the sea. The nature of this type of gate is to only be able to handle a water head from one side of the lock as seen before. Since the addition of the ”Veersegatdam” and the ”Zandkreekdam”, the ”Veerse meer” was created, a lake located on the north side of the lock. The Veerse lake is completely dammed in, the water is kept at an artificial height by a set of locks in the area. Located all around the lake are dykes, which currently have the fucntion to maintain the lake Due to the completely diked nature of the lake, there is no influence of the tide anymore. The water level is kept at 0.0m +NAP in the summer and at 0.3 m -NAP in the winter.

On the South side of the lock the ”canal through Walcheren” is situated, which is a canal that starts in Vlissingen and is connected to the Western Scheldt. the water level in Vlissingen is influenced by the tide of the sea which tends to be higher than in the canal. The water levels in the canal itself vary very little, as it has been locked in on either side through a navigation lock. The water level is kept stable to allow for inland travel of vessels of an industrial or recreational nature. On the canal side of the lock, there is a water level which is maintained at 0.9 m +NAP, valid all throughout the year.

Both bodies of water are brackish this is a constant situation. As brackish water contains salt, this poses a problem with regard to steel construction [10]. The chloride ions tend to be of great influence on the material and its deterioration. In addition, the salts in the water also allow for different kinds of bio-life on and around the construction than freshwater does. Compared to many other locks in the Netherlands with different surroundings, this is an aspect that has to be taken into account. Another deviant aspect of brackish water compared to other types of water is its density: it has a weight of $1015kg/m^3$, which in turn influences the buoyancy forces that are exerted on the structure.

In order to get an overview of how the doors are put into the chamber of lock gate Veere there is an image added from google maps, 2.8b. The arched shape of the gates is clearly visible in the image. The high water level is located on the lower side of the image, which causes the convex shape to be in the direction of the higher water.

(a) "Veerse meer" in Zeeland, the whole lake is surrounded by dykes. **(b)** Lock Veere top view

Figure 2.8: Location and top view of lock, Source: Google maps, [2023-223] [11].

The class of ships that has to be able to pass this lock is CEMT Va. While this is the maximum class of ships passing through, there are also smaller vessels coming through the lock. Next to the lock, there is a second smaller lock. The purpose of this lock is aimed to provide passage for smaller ships, which are often privately owned for recreational purposes. According to the operator who was stationed at the lock, the canal is now almost exclusively used by industrial vessels that are unable to cross the Western Scheldt due to bad weather. The standard routes used by these ships do not pass through the canal, which means the lock is not as frequently used as other locks in the Netherlands.

The span of the lock that has to be barred is 20 meters. The height that has to be covered is mainly dependent on the water level and the waves that can occur at the lock. There is also a walkway which is at the same height as the concrete to let pedestrians and cyclists pass by. The walkway is at a height of 11.5 meters from the bottom of the lock. An image of this will be given in chapter 4. The mitre gates at Veere are set up in an arched shape as was presented before in chapter 1.

2.3.2.1. Classification of lock Veere

The gate falls in certain categories which demand a certain level of manufacturing or robustness to the design. These are listed down below:

- Consequence class 2 (CC2) is reflected in the safety factors.
- Execution class 3 (EXC3), this has an impact on the level of execution performance and inspection done during construction.
- A 100-year lifetime demand.

2.3.3. Traditional mitre gate design

Since this design of lock gate Veere has recently been renewed by IV-infra there is a fairly new design. Every time a new gate is designed, the then state of the art can be used or defined for a new design. The reevaluation of the design does not necessarily mean it will be state-of-the-art. Practicalities, manufacturing possibilities and extra safety margins tend to steer a design away from its most optimal solution. Examining this new gate design (see figure 2.9) results in usable knowledge and a series of opportunities which can be exploited and are mentioned below:

- The water barrier is based on three straight segments along the curve of the bottom seal. There is no curvature in the plate. which increases the bending moments in the plate and the stiffeners. This means that the shape of the plate currently is not used in a global way to reduce thickness, whereas implementing a curved shape will mean optimal use of the shape. In this design, the manufacturing possibility was valued over the efficiency of material used. This design is a relatively well-executable construction.
- The structure is reinforced in the form of stiffeners in the vertical and horizontal directions. There are 8 horizontal stiffeners and 5 vertical stiffeners. Since the vertical stiffeners are continuous the horizontal stiffeners have to be connected to both sides of the vertical ones.

- This design is not based on rivet connections but on a welded construction. Due to the large number of components, there are many welds to be implemented by the manufacturer of the construction. This will end up in high construction costs compared to the material costs [31].
- The structure is designed with steel type S355. This means that the strength is lower than in the duplex variant chosen.
- There is a sluice for water levelling. On the South side, the lock has been equipped with culverts to perform the levelling of the lock. On the North side, this has not been installed. The client has requested for that to be implemented in the new design, meaning there would need to be a sluice on both sides of the lock. As this can be done by other methods and there is an example of such a method present in this lock the thesis will not take into account that the sluices are present in the gate.
- There is no stiff frame around the complete gate, as is often seen in mitre gates. This frame is usually in place to create initial stiffness [6]. The network of stiffeners instead creates the stiffness.
- The location of the hookup to the cylinder is not at the same height as the top hinge. This creates an additional bending moment to the gate. This is unfavourable when compared to gates which have the hook-up at the same height as the hinge, as that means one less bending moment. Since the concrete structure is not to be changed according to the client of the project, this cannot be adjusted for the redesign of this gate. However, when making a completely new lock this should be carefully considered.
- Two loads specifically, were not taken into account during the design of this gate. Ice loads and a ship collision have been left out of the scope during the design process.

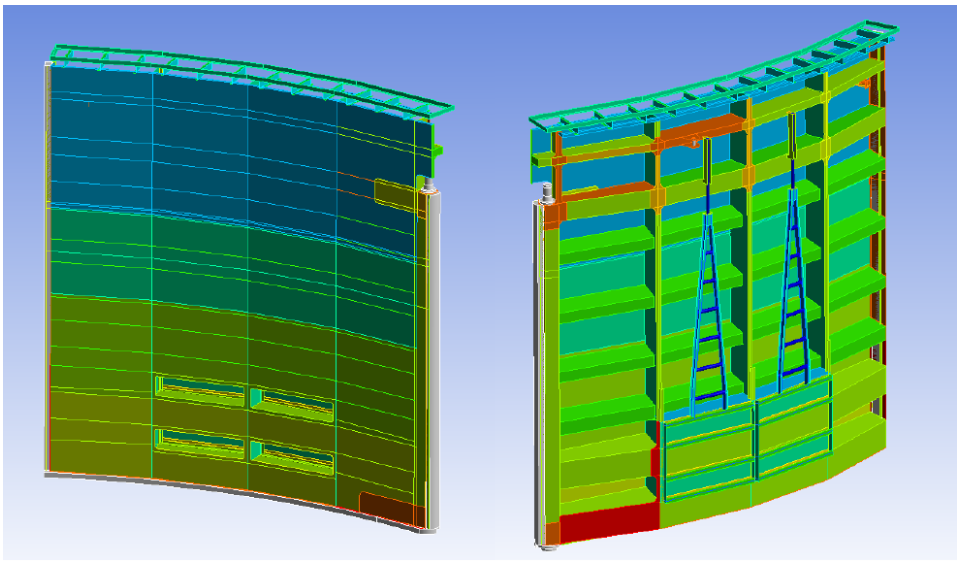

Figure 2.9: Design of lock gate Veere by IV-infra

2.3.3.1. Weight of the construction and buoyancy

The results from the design of IV-infra have been quantified. These results are based on an estimation of the final design from IV. Some of these characteristics have not been quantified by the company and were specifically calculated for this thesis. These characteristics are listed below

- The total weight of the construction is calculated to be 490kN. This does include the system of sluice gates and the required infrastructure for it. The weight for the sluices is found at a total weight of 3.43 kN, excluding the required members to keep the sluices in place and transfer the force adequately. The walkway will weigh 9.6 kN in total.
- By approximation, the buoyancy force is 190kN for the lowest water level present in the lock on both sides.
- To get an idea of the material used in the construction the steel in the construction is theoretically transformed to a single plate which is used to form the water barrier. Based on the weight of the

construction which is divided by the area an equivalent thickness of 40 mm is determined. This thickness will be referred to as the equivalent thickness of the traditional design.

2.3.3.2. Welding in the design

The total length of the welds is estimated as a reference for the needed weld length in a design for this case study. The total length was estimated to be 623.98 meters. Then the volume of the weld is determined to estimate the total volume of welds for the design. This is based on an estimation of a weld that is 0.55 times the width of the plate and is located on two sides of the plate. This assumption is done because the weld is stronger than the base material. The average plate thickness has been estimated and the results was of significant impact since the of 15.6 mm for the design this sums up to a total weld volume of $0.0469m^3$ of which the calculation can be found in the appendix figure D.1.

What is important to notice, is that the weld length of the design is divided over many separate weld segments. All separate components have to be welded to one another while the components are relatively small compared to the main construction. The vertical stiffeners subdivide the welds of the horizontal stiffeners and consist of four separate weld segments in the horizontal span. The segmented troughs have to be welded to the vertical stiffeners as well. The accessibility of the weld locations and the continuity of the welds is very limited. It can be considered when using this design how the construction assembly is possible.

2.3.4. Limit states of the construction

As for all constructions, there are limits up to which the structure has to be resistant. These limits consist of a set of rules made based on previous experiences and testing. These are the limits that have to be met are listed down below:

2.3.4.1. Ultimate limit state

The following limits govern the ultimate limits of the material and the lock gate:

- The Eurocode prescribes the strength for duplex 1.4462 stainless steel and sets it at 480 MPa for thicknesses lower than 6 mm, including safety factor for material properties: $\sigma_{0.2}/\gamma_{M0} = 480/1.1 = 436MPa$. For plates between 6 and 75 mm 460 MPa this is: $\sigma_{0.2}/\gamma_{M0} = 460/1.1 = 418MPa$.
- The value for the plastic strength limit is $\sigma_u/\gamma_{M0} = 640/1.1 = 581MPa$.
- The value for the shear strength limit is $\sigma_V/(\sqrt{(3)} * \gamma_{M0}) = 460/(\sqrt{(3)} * 1.1) = 241MPa$.
- The value for the ultimate strength limit for welds is $\sigma_{u,w}/\gamma_{M2} = 640/1.25 = 512MPa$.
- Stability has to be checked for the plates in the construction. Elastic limit of the material is $\sigma_{0.2}/\gamma_{M1} = 460/1.1 = 418MPa$
- In case of incidental loads the contractor has made an exemption on the elastic limit and allowed for plastic deformations. According to Eurocode 1993-1-4 there are no additional rules for plastic deformation in stainless steel, which should be proven by using experiments.
- If the construction appears to be sensitive to stability issues, the second-order deformations will be of relevance. An imperfect structure has to be modelled to predict behaviour in post-buckling circumstances.

2.3.4.2. Serviceability limit state

The serviceability limits of the material and the lock gate are governed by the following limits:

- For general deformations the limit is 1/250th of the span. This deformation limit is not based on practical limitations and will not be upheld as a limit for the deformation of the plate.
- When the water barrier is created, there has to be a deformation limit at the seals of the lock to prevent any leaks. The deformation that needs to be met is based on the direction of deformation to allow for a correct seal and should be no larger than 1/250th of the span.
- The maximum force that can be transferred to the sub-substructure should not exceed 720 kN on the top hinge. The bottom pintle can take a maximum force of 200 kN in the horizontal and 300 kN in the vertical direction. The limits presented in this section were not kept in the design for the obstacle load in the IV design. The incidental load allows for the exceeding of these values.
- When the gate is in its position its buoyant capacity should not allow it to start floating.

- When the gate is in its post, it should not deform so much in order for the gate to hit the concrete from the post.
- Another practical consideration for lock gates is that they must be able to move the gate in and out of the way to allow ships to pass through.

2.3.4.3. Fatigue limit state

As a lock gate has to deal with repetitive loads, the fatigue limit state needs to be taken into account. The cyclic loading for this gate consists of the opening and closing of the lock.

The minimal requirements for certain points can be determined using reversed calculations of the fatigue damage assessment. As the total cycles are known, the allowable stress for detail categories can also be determined. The construction will not be prone to fatigue if the minimum stress of the lowest category is not exceeded. Based on this minimum stress level per detail category, decisions can be made concerning the execution of details in the construction.

Based on a detail category 36, which is the lowest possible category, the damage of 1 has been checked for 470.000 cycles. According to the calculation method used, the required minimum stress to achieve this damage is a stress of 99.7MPa. This will be used in the fatigue approximation which is done later on in the structure. In every situation and location, the stress and the type of detail governing for the prediction of fatigue has to be assessed. The values can be used to predict if fatigue will be of relevance at all.

2.3.4.4. Design limits imposed by the case study

The aim of the project executed by IV was not to completely renew the lock but only the gates; this presents a set of boundary conditions to which the lock had to comply. The design in this thesis will also adhere to these conditions for a fair comparison later in the thesis:

- The bottom seal, it must be the same shape as the original gate. It is not capable of transferring loads.
- The bottom pintle location and dimensions
- Top hinge shaft location and dimensions
- Front post seal, timber connection between the gate and the opposite gate.
- End post seal, timber connection between gate and sub structure.
- Location height of the cylinder, the driving mechanism used for moving the gate.

2.3.5. Operational conditions mitre gate

A lock can be positioned in different ways to fulfil its function. This is based on different operational conditions. It can be closed, moved or opened. This is presented schematised in figure 2.10 in respective order.

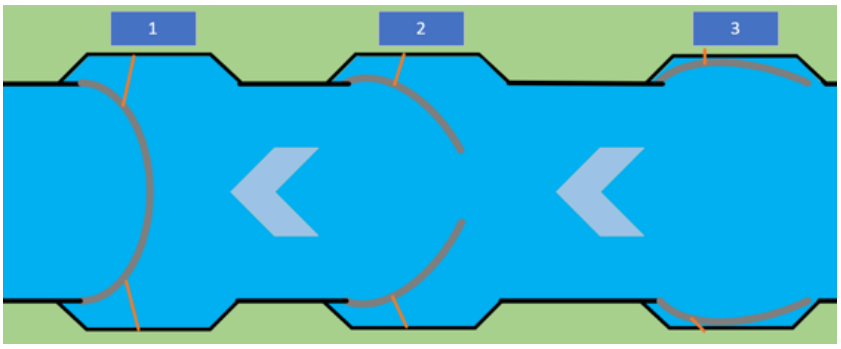

Figure 2.10: The gate in its closed position

For each operational set up there is a series of load combinations possible for the lock. Not all possible load combinations presented in the ROK are present in lock Veere. The combinations are considered per position in which the gate can be positioned. Some load combinations were not considered for lock Veere as these are not applied on the lock in the real-world situation. These load cases will be briefly elaborated on later in this chapter.

2.3.5.1. Closed gate conditions

When the gate is closed, a barrier is formed, which prevents water displacement through the lock. The ends of the two gates stand against each other, touching again at the middle post seal. Figure 2.11 shows a top-down view of this situation. Also visible in this figure is the driving mechanism is completely in an open position. In this layout, there are three main boundary conditions:

1. The bottom pintle functions as a vertical support point; see figure 2.11a.
2. The middle seal functions as a horizontal boundary and blocks movement, as can be seen in figures 2.11
3. The rear seal functions as a horizontal boundary which due to friction can transfer vertical force towards the concrete substructure. The created friction is based on the material interaction between the gate and the seal on the concrete structure. This frictional coefficient is 0.2 for the timber-on-timber interaction.

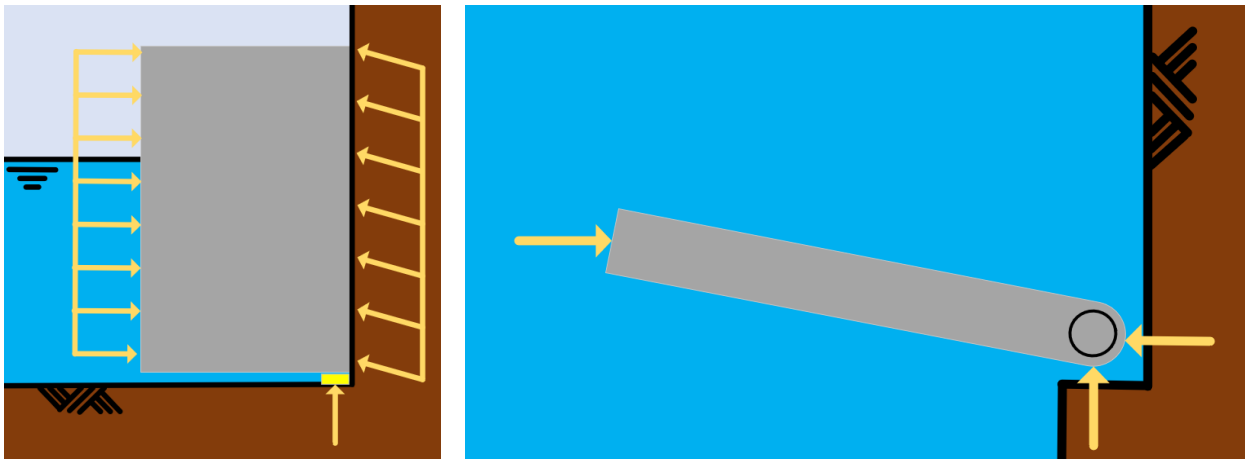

(a) Side view **(b)** Top view

Figure 2.11: Closed gate position and boundary conditions.

The following list are the load combinations which can be present in the closed-gate situation for this case study.

- LC A: Extreme water head in combination with the most extreme wave possible.
- LC C: Differential water head, the regular operational conditions by which the gate will be most often loaded.
- LC D: Loading of the walkway.
- LC E: The propeller load of ships of the maximum class allowed through the lock.
- LC G: Force buildup along the rotation axis
- LC I: Buoyancy tank malfunction

2.3.5.2. Moving gate conditions

The moving condition is not simulated in motion but as a static model. This still represents the situation appropriately but removes unnecessary complexity. Modelled as a static model which represents the situation appropriately. During the movement of the gate, the following conditions apply:

1. The bottom pintle functions as a support in the horizontal direction and as a vertical support
2. The top pintle functions as a horizontal support, see figures 2.12
3. The hookup to the cylinder mechanism functions as a horizontal support

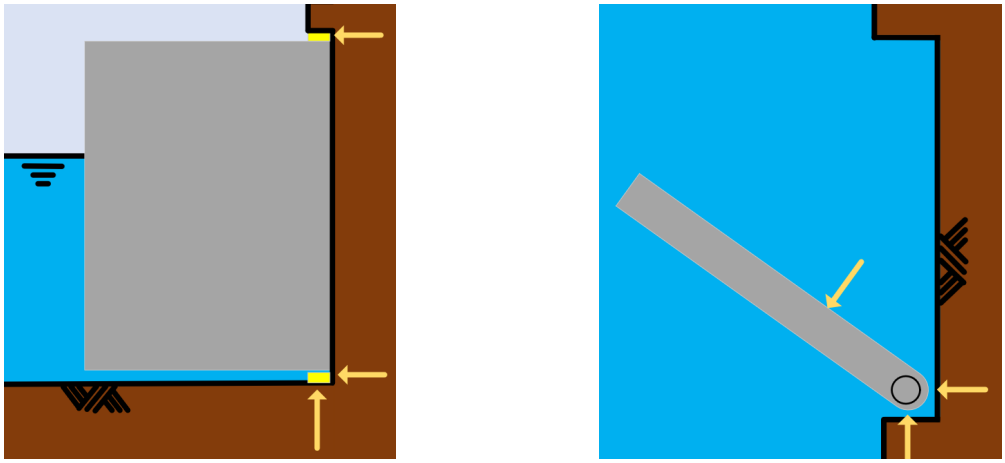

(a) Side view **(b)** Top view

Figure 2.12: Moving gate position and boundary conditions.

The following loads are possible when the gate moves towards its opened or closed position. These loads are considered incident loads, a type of load that usually presents itself in the moving of the gate.

- LC J: Hydraulic loads during movement of the gate
- LC L: Obstacle load
- LC M: Failure of the control system
- LC N: Force buildup along the rotation axis

2.3.5.3. Opened gate conditions

When completely open, the gate is located in its post. The main boundary conditions are:

1. The bottom pintle functions as a support in the horizontal direction and as a vertical support; see figure 2.13a.
2. The top hinge shaft functions as a horizontal support, seen in figures 2.13.
3. The post support in the corner of the frame has an immovability in its normal direction in the horizontal direction, seen in figures 2.13.

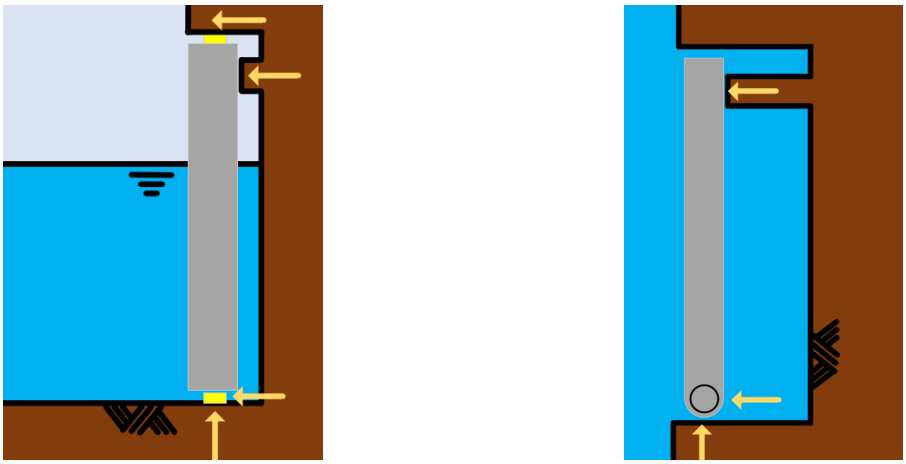

(a) Side view **(b)** Top view

Figure 2.13: Opened gate position and boundary conditions.

When the gate is opened ships are allowed to pass through the lock, it is in its post where the set of loads listed below can be encountered.

- LC A: wind on the gate
- LC B: water level of F17 (this is most likely the force that will not allow the design of M. Kruse to be successful)
- LC G: Force buildup along the rotation axis
- LC I: leak in buoyancy tank

2.3.5.4. Force size on gate

As neither the Eurocode nor the ROK gives instructions on which exact values to use, there is no standard set of load values that can be applied to a mitre gate. This means that these values need to be calculated per case. The loads are calculated for the case study of lock Veere and the results are presented in appendix E. The calculations are presented in the appendix as well. The names of the forces are based on the name that they have been assigned from the ROK.

In order to simulate the model within a realistic computation time and simplify the modelling process, the hydrodynamic loads are all expressed in static loads. This is an accepted method for the simulation of dynamic loads on structures.

2.3.6. Load combinations for arched mitre gates

The aim of this thesis is not to make a definitive design, the aim is to design a structure based on the critical conditions of a mitre gate but also the critical conditions for the construction type. This means that not all possible operational conditions have been simulated on the model. This section is focused on the definition of these critical operational conditions and what needs to be included to make an approximation of real-world situations. The conditions consist of boundary conditions and load conditions. The aim was to include a set of load combinations which resemble others and can thus be covered by them. The conditions which were excluded from the research will be briefly commented on.

When simulating the load combinations, they will not be constructed with all loads, but only with the main loads that take effect. This will generally be based on the relative size of a load. When a load is lower than 10% of the main load it will not be covered in this study.

2.3.6.1. Extreme water head (EWH)

In the lock location there is an extreme water level recorded which is combined with a wind wave. Since the water level difference is the greatest in this case the resultant force will be very large too. This load is therefore included in this thesis as is is expected to be the largest force.

The extreme water head is found in the closed position of the gate. This load case consists of the following loads: self-weight (F0 and F1), water level (F10EWH), wind load (F14), traffic load (F16) and cylinder load (F33). The wind load F14 is less than 10% of the active water load. The walkway load F16, put on top of the gate, is out of scope. Optimising the top of the gate is not in line with the goal of this thesis. The cylinder load F33 is less than 10% of the reaction force found in the seals. An example of the visualisation in Ansys has been added in appendix figure L.12.

This situation is schematised in figure 2.16. The load is uniform over the width of the construction and works in a perpendicular direction to the surface, as seen in figure 2.14b.

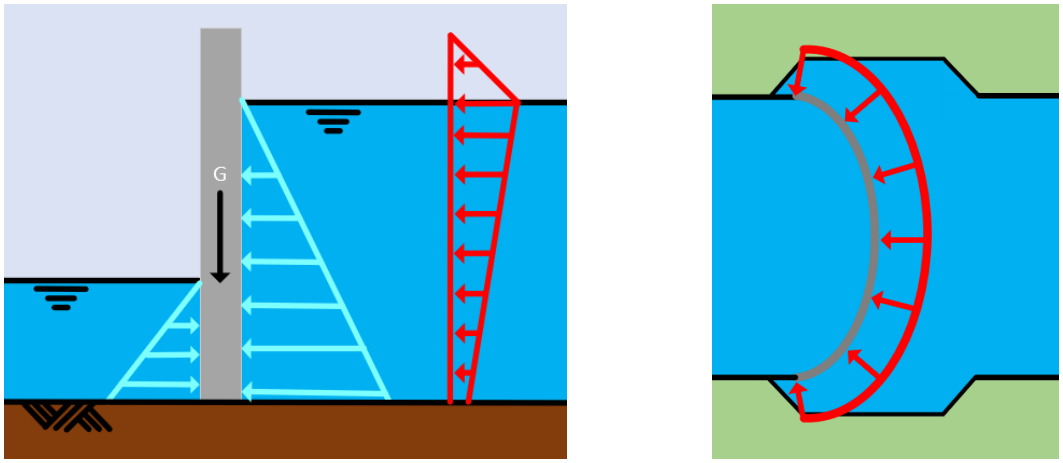

(a) Extreme water level and wind wave load case force schematisation

(b) Top view of the uniform load

Figure 2.14: Load case and uniform load schematisation

2.3.6.2. Propeller load (PL)

When a vessel is in the lock, its propellor produces a propulsion beam when it moves out of the lock. This has a maximum size to which is can be applied to the structure so it is not a uniform load over the construction. It is important to consider that the propeller load can be applied asymmetrically to the surface of the gate. Since the arch is sensitive to asymmetric loading, multiple locations of the propeller will need to be investigated.

The propeller load combination is found in the closed position of the gate. It consists of the following loads: self-weight (F0 and F1), differential water level (F12), wind load (F14), traffic load (F16), cylinder load (F33) and propeller load (F99). Loads F14, F16 and F33 were also exempt from the first load case and are explained there. This situation is schematised from the side in figure 2.15a and from the top in figure 2.15b. Both figures have a generic location for the propellor load which can be moved in a horizontal direction and for the vertical direction the location is linked to the water level. The vertical position is assumed to be most critical when the water level is the highest.

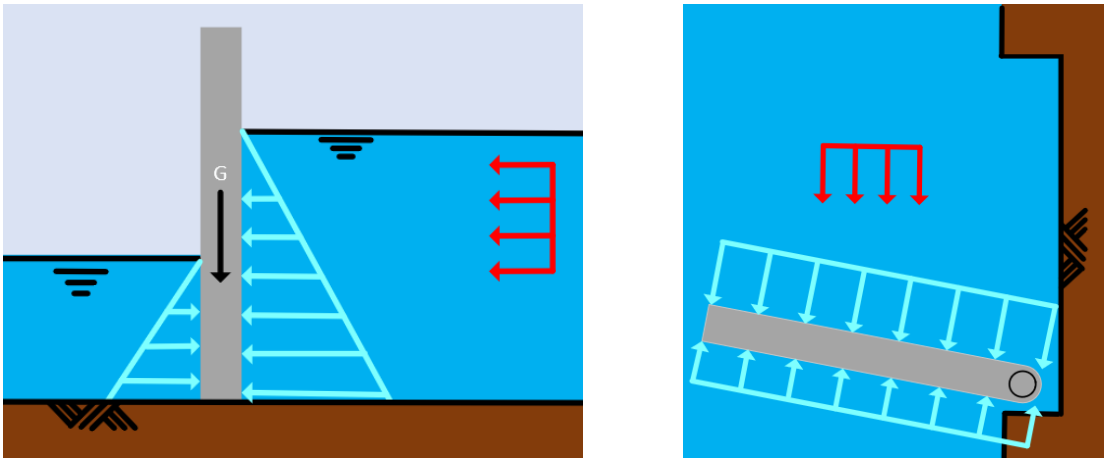

(a) Side view

(b) Top view

Figure 2.15: Propeller load case force schematisation

2.3.6.3. Ice load (IL)

Ice can form at the surface of the water and can float against the gate. The ice load combination is out of scope for the case study, but due to its common presence in the Netherlands and the possible critical local load type to the arch shape due to its asymmetry, it will be considered in this thesis.

The gate position is a closed gate. It consists of the following loads: self-weight (F0 and F1), the water load in operation conditions (F12), wind load (F14), traffic load (F16), cylinder load (F33) and

ice load (F53). Loads F14 and F16 were also exempt from the first load case and are explained there. This situation is schematised in figure 2.16; these are applied uniformly over the width of the gate in the same way as in figure 2.14b.

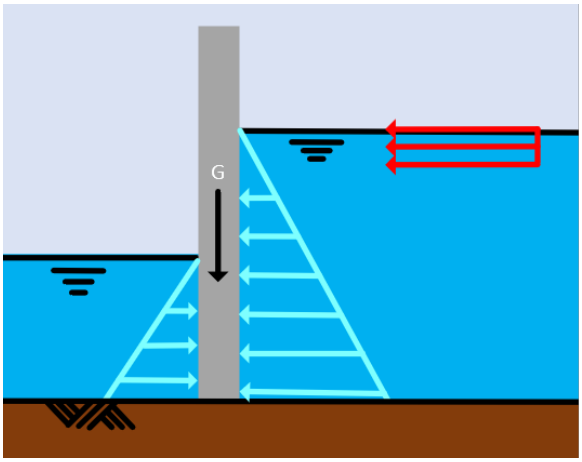

Figure 2.16: Ice load case force schematisation

2.3.6.4. Obstacle load (OBL)

A possible situation in lock gates is an object getting stuck between the gate and one of its seals. Such an object getting stuck is prescribed in the ROK for three locations: between the gate and the post, between the gate and the bottom seal and between the gates themselves. This thesis will evaluate how an object gets stuck in the seal position. This is similarly critical as an object in the post and more critical than an object between the two gates.

The obstacle load boundary conditions are slightly different than those described earlier, and have the following boundary conditions:

1. The bottom pintle functions as a support in the horizontal direction and as a vertical support
2. The top pintle functions as a horizontal support
3. There is a small area located 1.5m from the bottom pintle, immovable in its normal direction.

In this load combination, the main force (F40) is the point loads at the hook-up point. This will be the only force included next to the self-weight. This is because the mass inertia of the water forces is relatively small that it can be neglected, and the water level is equal on both sides and thus will not impose large loads on the construction. The obstacle can be located along the whole length of the gate but the most critical location will be closest to the rotation axis. The ROK prescribes a distance of 1.5 metres from the rotation axis. This situation is schematised from the side in figure 2.17a and from the top in figure 2.17b.

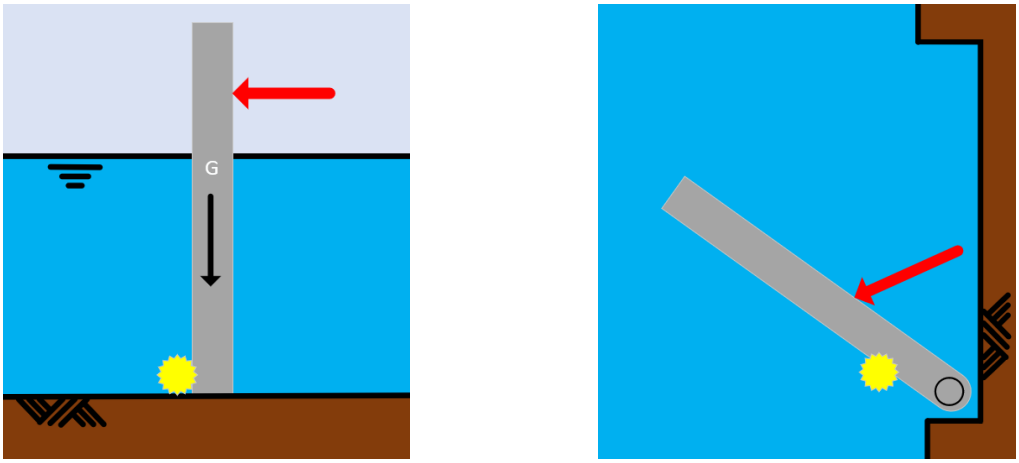

(a) Side view **(b)** Top view

Figure 2.17: Obstacle load case force schematisation.

2.3.6.5. Weight and buoyancy (BU)

The total weight of the construction and how much force that weight transfers to its substructure are important limits for a lock gate. The gate will be considered in its open position for this but there is no effect from the extra corner support in this situation. The loads present are the self-weight (F0) and the water load at the lowest possible level on both sides of the gate. The buoyancy is described by a load that is implied on the gate by the water on horizontal surfaces, it has a separate name to show it is included (F1). When the water is at its lowest level, the load on the sub-structure is most critical. The water level in this situation is F39.

In addition to the lowest water load possible, the highest water level is also relevant to discuss. In case of extremely high water levels, the gate mustn't start to float. F38 water level will allow for the inspection of this situation. These situations are schematised similarly and can be seen in figure 2.18.

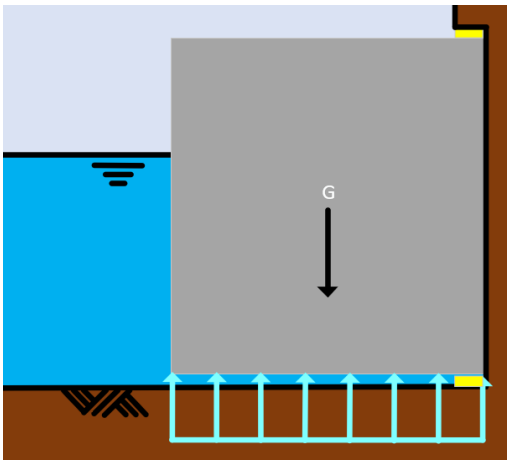

Figure 2.18: Bouyancy load case force schematisation

2.3.6.6. Deformation at closing point (DefCl)

The gate has a serviceability limit state which requires the gate to be closed close to perfectly. Mitre gates which are not symmetrical have been found to generate a torisonal effect in the structure (chapter 2), this negative aspect of the design type has to be checked to assess if the lock will be able to close properly. The boundary conditions are that of the gate in motion. The forces on the gate in this load combination are its self-weight and the buoyant effect of the water. The water head located at the point of the gate closing is approximately equal to the operational lowest water level of the lock. This is levelled at 6100 mm from the bottom of the gate (F39). This situation is schematised similarly to the buoyancy situation in figure 2.18.

2.3.6.7. Gate opened in gate post (GIP)

To assess the forces which can present themself when the gate is opened the following load combination is chosen. This is the most extreme load combination as it has to account for several factors. First, the force (F41) needed to keep the gate open and prevent it from moving out of its post. Second, a water difference ($F17_{in}$)adds to the force which is already directed into the post. Third, the self-weight of the gate. Fourth, the stress is transferred by the frame to a boundary in its corner which is not further loaded. The significance of this force on the frame is a possible point of interest for this study. Finally, the pulling load is used in combination with a water level which can be created by passing ships. This adds to this support by having to take up force. This situation is schematised from the side in figure 2.19a and from the top in figure 2.19b.

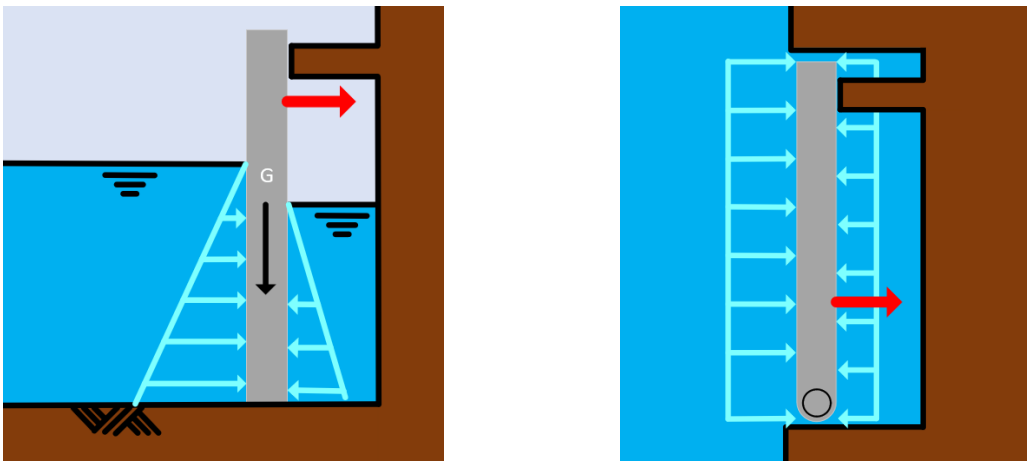

(a) Side view **(b)** Top view

Figure 2.19: Gate in its post load case force schematisation

2.3.6.8. Fatigue load (FAT)

The fatigue assessment for the gate has been assigned to the opening and closing of the gate. Since the gate is not a tidal gate, and the environment of the gate does not produce big waves, these factors do not lead to significant stresses in the material. Therefore, this loading is not further assessed in this section. The opening and closing movement of the gate has been divided into seven steps. These steps are listed below:

1. Gate is in the gatepost and the cylinder load gets applied (F41).
2. Gate is pushed out of the gate post, water load F24 acts on the concave side.
3. Gates are nearly closed and not yet settled into the seals of the end post but remain hanging on the pintle and the hinge shaft. F23 is on the concave side of the gate.
4. The lock is closed and the gates are positioned against each other, the gates are supported by one another and the differential water head is created ($F10_{FAT}$).
5. The gate is pulled back towards the gatepost and the high water wave is created on the convex side of the gate. Load F23 is used for these levels on the convex side (opposite to step 3), and the hookup is used as a boundary condition for horizontal movement.
6. Gates pulled in gate post, F24 water is on the convex side.
7. This step is the same as step 1.

For the benefit of the research, a critical look was taken at the results concerning fatigue load found by IV-infra. The fatigue analysis that was performed presented a constant result in terms of which steps of the cycle led to the highest stresses. These steps are step 3 and step 5 of the fatigue cycle of the gate. As the large plate has the possibility to form large deformations when the water head is active, it might be part of the larger stress situations for the plate. Step 4 of the fatigue cycle was also taken into consideration for the analysis of this thesis due to its possibility to prove to be critical in the fatigue cycle.

The water levels are visualised in figure 2.20 and are numbered per step. The water level differences can be seen in every next figure.

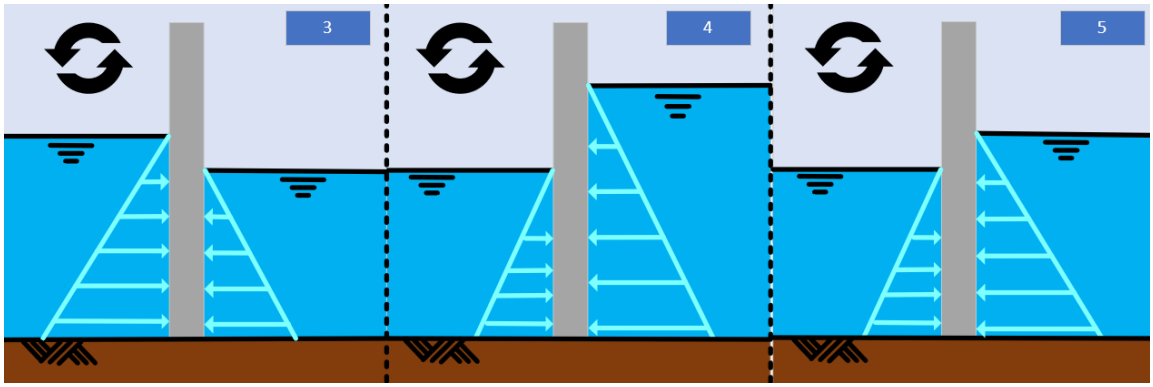

Figure 2.20: Fatigue cycle water levels for step 3, 4 and 5.

2.3.6.9. Load combinations excluded

In this subsection, the load combinations that were excluded from this thesis will be discussed. These were excluded because these loads will either be covered by other bigger load combinations or because the load is not relevant to the research purpose of the thesis.

Closed load combinations

- **Load combination C** is lower than the extreme water head and therefore excluded based on the expectation that it is less critical.
- **Load combination D** is a variation on c and is not covered either.
- **Load combination G** shows that the effect on the vertical beam at the rotation axis is higher in the obstacle load.
- **Load combination I** is dependent on the extreme forces which may be on the sub-structure since the construction is assessed on buoyancy separately. This will be taken into account but not as a load case.

Moving load combinations and incidental loads

- **Load combination J** has hydraulic loads that are smaller than the fatigue loads which can arise, which are covered.
- **Load combination M** is the failure of the control system, which presents a lower force than which the obstacle force would put on the frame, but with better supports and boundary conditions
- **Load combination N** is lower than the obstacle load applies on the rotation axis beam.

Open load combinations

- **Load combination A** is of lower impact than the fatigue loading.
- **Load combination G** is covered by obstacle load.

2.3.6.10. Safety factors for operational conditions

When the load combinations are applied on the model they have to be included with safety factors. The safety factors that are used are presented in table 2.2. Each load case is seen in the table on the horizontal axis with the loads on the vertical axis and the safety factor used for this load. The load cases applied are listed once more:

- Extreme water head (EWH)
- Propeller load (PL)
- Ice load (IL)

- Obstacle load (OBL)
- Weight and buoyancy (BU)
- Deformation at closing point (DefCl)
- Gate opened in gate post (GIP)
- Fatigue load (FAT)

The loads included are also listed once more:

- $F0$&$F1$: self weight and buoyancy
- $F10_{EWH}$: extreem water level
- $F12$: differential water level /head
- $F13$: Windwave at extreme water level
- $F17_{In}$: Schip wave from passing by
- $F23$: Water level difference due to gate moving
- $F38$: High water level equal
- $F39$: Low water level equal
- $F40$: Obstacel cylinder load
- $F41$: Cylinder load opened gate
- $F53$: Ice load
- $F99$: Propeller load

Table 2.2: Safety factors for applied load cases

	EWH	PL	IL	OBL	GIP	FAT3	FAT4	FAT5	DefCl	BU_{cw}	BU_{fl}
$F0$ & F1	1.2	1.2	1.2	1.2	1.2				1	1	1
$F10_{EWH}$	1.5										
$F12$		1.2	1.2				1				
$F13$	1.5										
$F17_{In}$					1.2						
$F23$						1		-1			
$F38$											1
$F39$									1	1	
$F40$				1.5							
$F41$					1.5						
$F53$			1.5								
$F99$		1.5									

3

Method

For this thesis, FEM is used to predict the complex behaviour of the construction design. The different types of analysis will be explained along with their application to this thesis. Ansys Workbench is used as software for finite element analysis. This software uses certain elements which will be introduced and to why they are appropriate for this thesis.

3.1. Finite element method

The finite element method can simulate real-world problems built up of multi-physics, complicated geometry and boundary conditions [26]. This method has three advantages compared to others [26]. The geometry can be defined in a domain and is discretised to make a finite domain of a collection of points. Each element is bound to other elements based on equations which are based on physical relationships that the user can assign. The equations from the elements are combined to form a continuity of the primary and secondary variables, often used to represent the boundaries and loads on an item.

The geometry domain mentioned before is defined based on a mesh with nodes at the intersection of the mesh lines. The mesh must be of an appropriate size to represent the real-world item during the simulation. In chapter 4 the size of the mesh is determined based on the quality of the result and the speed of the simulation.

For this thesis, there will be several FEA types used which are also available in Ansys. Each one will be briefly elaborated on to indicate how it will be used and to what extent it is useful.

Linear elastic shell analysis (LA) is based on small deflection theory and linear elastic material law. It implies that the construction geometry remains that of the undeformed structure. LA is used for constructions which will be subjected to small deformations only. Material behaviour is linear and stresses should not exceed elastic limits to remain accurate. If a construction meets these qualities it can be analysed by this method.

Linear elastic bifurcation analysis (LBA) is used to find the eigenvalues and corresponding shapes in which the construction can buckle. The result provides the shape of the buckled construction and it critical buckling resistance. The analysis can indicate how close the construction is to its buckling point and based on this if it should be included in further analysis or not.

Geometrically nonlinear elastic analysis (GNA) takes into account how deformation in the geometry of a construction can lead to secondary effects. The load will be applied on the initial geometry by a portion of the load and is increased step by step while the geometry is updated under the load. Ansys checks if the system moves toward a stable or unstable system.

Geometrically nonlinear elastic analysis with imperfections included (GNIA) is used to simulate a construction that is not perfect as suggested by the name. It is used for constructions that are dominated by compression or shear. These imperfections are based on deviations which are present due to the manufacturing of a construction. The most critical shape of the construction is often the shape given by its first buckling mode, this shape is used as input for the analysis. The deformations from the buckling mode are subsequently multiplied by a factor relative to the size of the buckle. With this adjusted geometry the analysis has to be performed like the GNA to further inspect the stability of the model.

In the Ansys model that was used for this thesis the elements that were used are ”SHELL181”

elements. These elements are appropriate to use for analysing thin shell structures. The design that was simulated is built up of plates, which have a small thickness compared to its width and length (<1/20). The shell 181 element is a 4-node element with six degrees of freedom at each node and is presented in figure 3.1. This element can be adequately used for linear, large rotation, and/or large strain nonlinear applications [1].

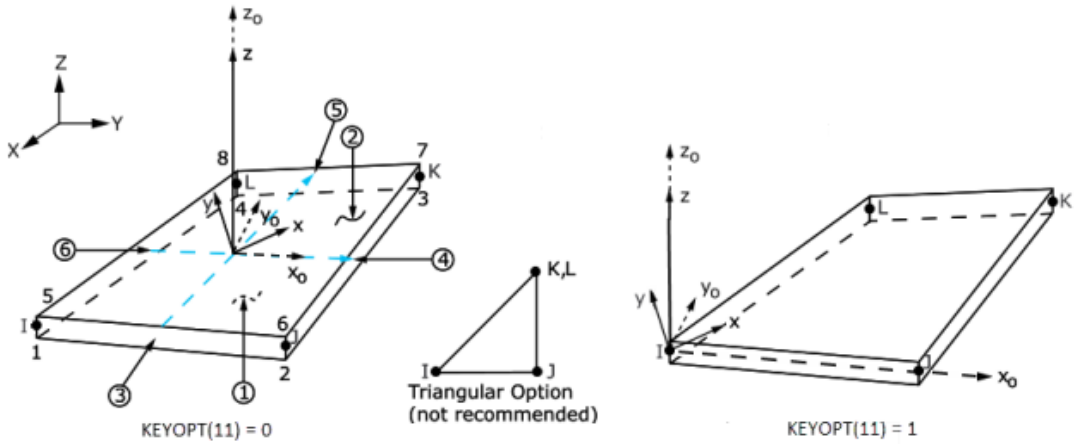

Figure 3.1: SHELL181 element representation.

3.2. Validation with calculation methods from literature

Results of the LA and LBA calculations are compared to results from already established and validated calculations found in the literature. ROARK [48] and mechanics part 2 [14] are examples of these literature parts. These simplified analytical methods, in general, use the concepts of structural relations. Compared to the software which is used in this thesis the methods are expected to be representative but also present minor differences due to the difference in complexity of the methods.

4

Validation of modelling and design assumptions

This chapter will be investigating the feasibility and optimisation possibility of the arch concept for a lock gate construction. In order to achieve this two loads were defined which dominate the design of a lock gate, through which the shape concept will be investigated. These are the uniform water load and a point load from the obstacle situation. The case study is used in order to define general dimensions which the models must fit into, which will be presented in this section as well. The feasibility of the components is then defined by the stresses in the material, based on the equivalent material used in the traditional design.

In order to gain confidence in the modelling with FEM, it will be compared to engineering methods. The results of this comparison will be presented for two load types: plates under bending and plates subjected to axial loading. These represent the resultant force of the uniform load created by the water. Then a plate will be modelled under different boundary conditions in order to check the difference in results from the simulations. The results include reaction forces, deformations, stresses and buckling shapes and plate buckling. Within these simulations, a mesh study is also included.

After the first modelling steps, the feasibility and optimisation of the arch concept will be investigated. In addition, the reaction forces, deformations, stresses and buckling shapes will be determined. Different arch shapes are then modelled to see which shape is the most effective for the uniform load which is investigated in this thesis.

Since plates are ineffective against the point load presented in the obstacle situation, a frame is introduced to add to the structural stiffness. The frame dimensions are presented and a method to determine the layout of the frame was added. Since this frame adds boundary conditions to the plate, the effect of these boundary conditions is investigated for the effectivity of the arched plate.

4.1. Design loads

The main forces which drive the design, which will be referred to as ”design loads”, is the load or loads with the greatest impact on how a structure needs to be designed. In this chapter, the opportunity of the arch concept will be investigated for lock gates and their design loads. The main load mechanism was determined to be the water load as seen in chapter 1. The second load is chosen based on its mechanical difference compared to the water load. Based on the information found in chapter 2 the obstacle situation is chosen. The reason for this choice will be elaborated on this the next section. These are the two most extreme loads of their kind and will represent the dominant loading mechanisms of a lock during this feasibility phase.

4.1.1. Uniform water load on the plate

The design load is based on the water head which creates a resultant pressure of $P = 0.016MPa$. The force is based on the extreme water head as seen in figure 4.1a. This will be applied on the plate as a uniform pressure over the whole surface. When the buckling is validated for simple plates a unity load

will be used that is $F = 1000kN$. This is in line with the size of the reaction force which will be present in the final design.

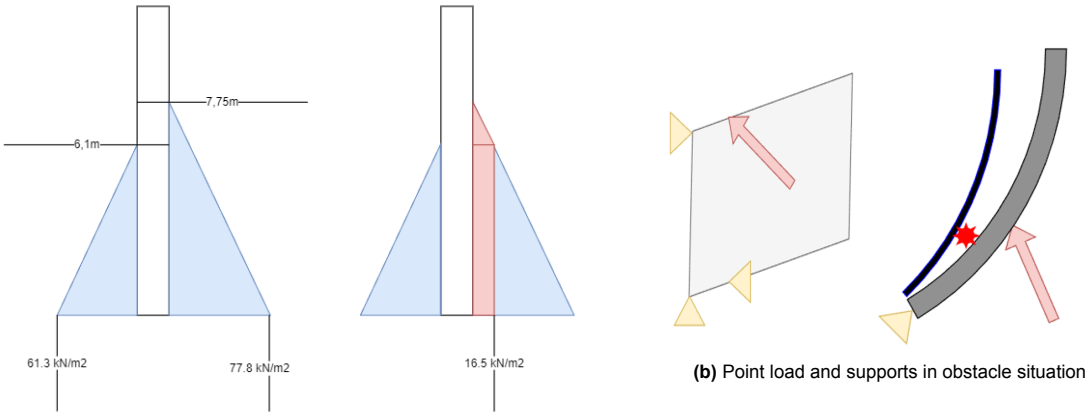

(a) Resultant uniform water load

(b) Point load and supports in obstacle situation

Figure 4.1: Sketches of design loads

4.1.2. Design load on the frame

The obstacle point load has a completely different mechanical effect than a uniform water load. The loads and supports are all at the edge of the body as can be seen in figure 4.1b. The load has to be transferred from the entry point towards the supports while the body is able to rotate around the axis of the two hinge supports. It is an incident situation and therefore not a regular load type but has a similar support-load layout as the moving conditions of the gate. It is the largest load of its kind and, therefore the extreme case that also represents other load cases in terms of a mechanical system.

The horizontal distance from the top hinge to the hook-up is 4000mm. The location of the pintle to the obstacle is 1500mm. The force has a size of load F44 with a safety factor of 1.2 this ends up at $F = 1575kN$. The direction of the load is under an angle of 56 degrees to the local surface of the gate and is presented in the appendix in figure H.1.

4.2. Model dimensions

In order to investigate the validity of the method presented in this thesis and the feasibility of the arch concept, a basic dimension is chosen. As seen in the elaboration on the case study, the width of the lock is 20 metres. Due to the mitre positioning of the gates, the length of one gate is more than half of this span. The length of the model is set at 11400mm. When the arch is added to the plate it will have a circular shape with a radius of 18200 mm. These dimensions are presented in figure 4.2a.

The height of the model is divided into two important heights. For the investigation on the plate, this is set at the height of the top hinge at a height of 9800 mm. The maximum water level never exceeds this, and therefore including more height will not contribute value to the investigation. The height of the frame is based on the hook-up to the opening mechanism. The height of the hookup is 10800 mm from the bottom. This can be seen in figure 4.2b.

The equivalent plate thickness of the traditional design is used to investigate what can be achieved with that amount of material. This thickness is equal to 40 mm. When stiffeners are added to the construction the main plate thickness will be reduced in order to remain at the same equivalent thickness.

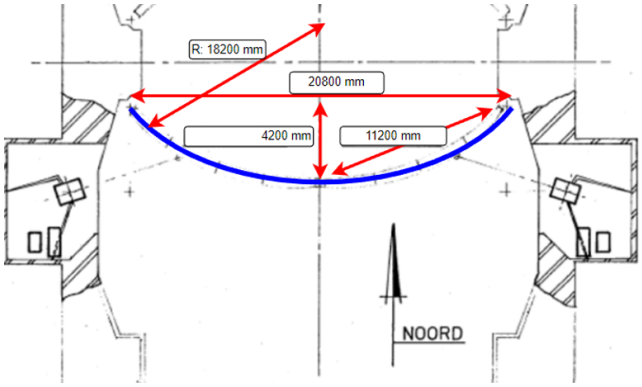

(a) Top view of the lock and the spans of the gate.

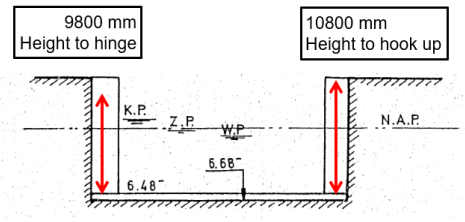

(b) Height levels of the lock from side view.

Figure 4.2: Layout of the basic models based on the gate dimensions.

4.3. Validation of modelling

To gain confidence in the modelling in this thesis, general engineering methods were compared to FEM. The results of this comparison will be presented in this section and also present the order of magnitude in which the members are loaded. The first analysis is based on a plate which is subjected to out-of-plane loading. The results from this analysis include reaction forces at boundary conditions, deformations and stresses of flat plates in bending. Next, the results of a plate subjected to axial loading will be presented, which include a comparison of stresses and buckling behaviour.

4.3.1. Plate loaded out of plane

The set-up of the first two models can be seen in figure 4.3a and 4.3b. The boundary conditions for the left situation are at the edges and are simply supported; in this case, the Y and Z directions have a displacement of 0 mm. The simply supported edge has been indicated by the dotted line. The right model has constrained supported edges, indicated by a continuous line. In this model, the rotation around the X-axis has been locked. The pressure force is applied on top of the surface and is distributed uniformly and is directed in the normal direction of the face.

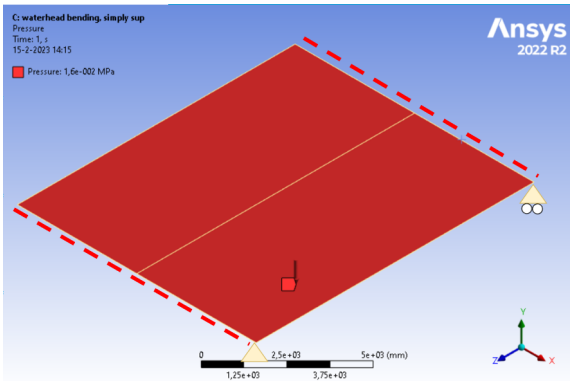

(a) The model of the plate when for out-of-plane loading for simply supported situation.

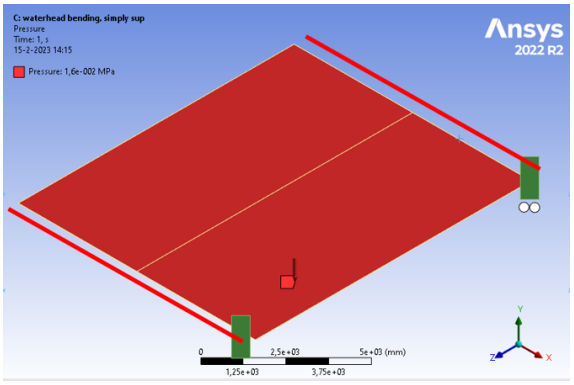

(b) The model of the plate when for out-of-plane loading for a constrained support situation.

Figure 4.3: Model set up of basic plates

4.3.1.1. Results out of plane loading

The results which were investigated are presented in table 4.1. The calculations can be found in appendix F. The results of both methods have been compared to one other and the results are all nearly the same, all values with a difference of 0% are below a level of significant difference. The only difference is found in the bending moment in the middle which is possible as not the exact middle node might have been used to determine a result.

Table 4.1: Results from plate loaded out of plane

Result	Analytical	Ansys	Difference
Vertical Reaction force at support [kN]	893	893	0%
Bending moment at the support [kNm]	1698	1698	0%
Deformations simply supported [mm]	3298	3298	0%
Deformations fixed support [mm]	659	659	0%
Bending moment in the middle of the plate [kNm]	849	846	0.3%

4.3.2. Plate subjected to axial loading

Next, the plate will be investigated under axial loading. This will give the results of the stresses in the plate, the deformations due to compression and the Poisson effect and lastly the effect of column and plate buckling. The methods to determine these values analytically will be presented and the results of both methods will be presented at the end. To ensure that the result from FEM are of quality a mesh sensitivity study has been performed too.

The model set-up is a simply supported plate, it is presented in figure 4.4. The boundary conditions are presented in the figure. The load has a value of 1000 kN.

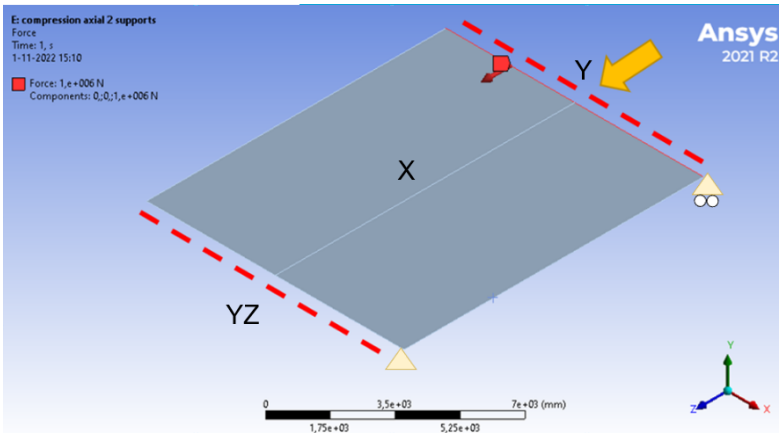

Figure 4.4: Axial loading scheme of the flat plate

4.3.2.1. Results of axially loaded plate

The results of the mesh sensitivity study are based on the eigenvalues that result from the model simulations and are presented in table 4.2. The 50 mm mesh gives a fast result of computation time and the accuracy does not change the result presented by Ansys. The other options led to an eigenvalue difference or longer computation time. The results from Ansys are presented in the appendix section F.2.3.

Table 4.2: Mesh study Eigenvalues

Result	500 mm	50mm	25mm
Eigenvalue	0.7963	0.7939	0.7939

The results of FEM and analytical methods have been compared to one other and the results are all nearly the same. All results are presented in table 4.3. The difference found in plate buckling can be due to an inaccuracy from the ratio between the width and length (a/b) of the plate and the value chosen from the graph of appendix figure F.11b. This graph can be used for an approximate value that needs to be used in the analytical method and cannot be made more precise in some ratios.

Table 4.3: Results from plate loaded axially

Result	Analytical	Ansys	Difference
Normal stress: σ [MPa]	-2,551	-2,551	0%
Strain: ϵ [-]	$-1,275 * 10^{-}5$	$-1,275 * 10^{-}5$	0%
Deformations: u_z [mm]	0,145	0,145	0%
Deformations: u_x [mm]	0,0375	0,0375	0%
Column buckling simply supported: EV [-]	0.793	0.793	0%
Column buckling fixed edges: EV [-]	3.18	3.18	0%
Critical buckling stress simply supported: σ_{cr} [MPa]	12,34	12.29	0.4%
Critical buckling stress fixed edges: σ_{cr} [MPa]	21,79	21.42	2%

4.4. Arched plate optimisation and feasibility

The effectivity of the arch shape is investigated in three ways. First, the basic effect of the arch shape which is found in the case study is investigated. Next, the adjustment of the curvature is inspected, and the implications this has for the lock gate. Lastly, the possibility of a double arch, or shell structure, is explored. The effectiveness of these concepts and their adjustments will be discussed in this section.

4.4.1. Basic arch plates

The first simulation was executed using the basic variant of an arched plate. This includes simply supported boundary conditions and displacements at the edges set to zero. This setup can be seen in appendix figure 4.5. Dimensions are as mentioned earlier in the chapter.

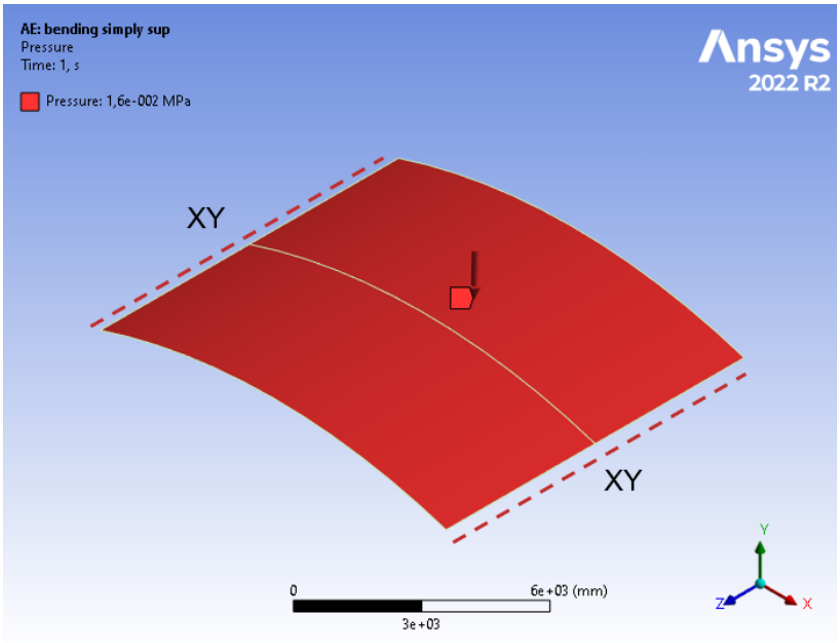

Figure 4.5: Model of the curved plate

4.4.1.1. Reaction Forces

The force reaction at the edge of the plate was expected to be compressed into a vertical and horizontal component. This is confirmed when looking at the result of the simulation. There is a vertical force component of 896 kN and a horizontal force of 2718 kN. The vertical component lines up with the size of the load when approximated with the total vertical force of the flat plate: $R_v = p * A = (0.016 * 9800 * 11400)/2 = 893kN$. The small difference lies in the fact that an arched plate with a perpendicular load on it has more surface area but less vertical force on it at the edges.

This shows that the horizontal component is of significant impact on the reaction force into the sub-structure. The result of this simulation is added in appendix figure G.1. Important to notice is the direction of the reaction force: when inspected from the side the force seems to be in line with the direction of the plate. The direction of the force can be seen in appendix figure G.2.

4.4.1.2. Stresses along the curve

The advantage of an arched structure should be seen in forces in the construction that can be transferred by normal forces instead of by bending moments in the plate. This effect can be seen in the stress contour of the plate when loaded. When the stress is consistent throughout the plate and there is no difference between the top and bottom of the plate, an ideal arch effect is achieved.

The following results on normal stresses along the curve were collected from Ansys and are presented in figure 4.6. The figure shows that the stresses in the plate are not consistent. The right side of the figure represents the bottom of the plate, on which the stresses are of a significantly different size than on the top of the plate. This indicates that bending stresses are still present in the plate. The stresses are however of lower value compared to the yield stress that was defined for the material ($7.6MPa/418MPa = 0.02$).

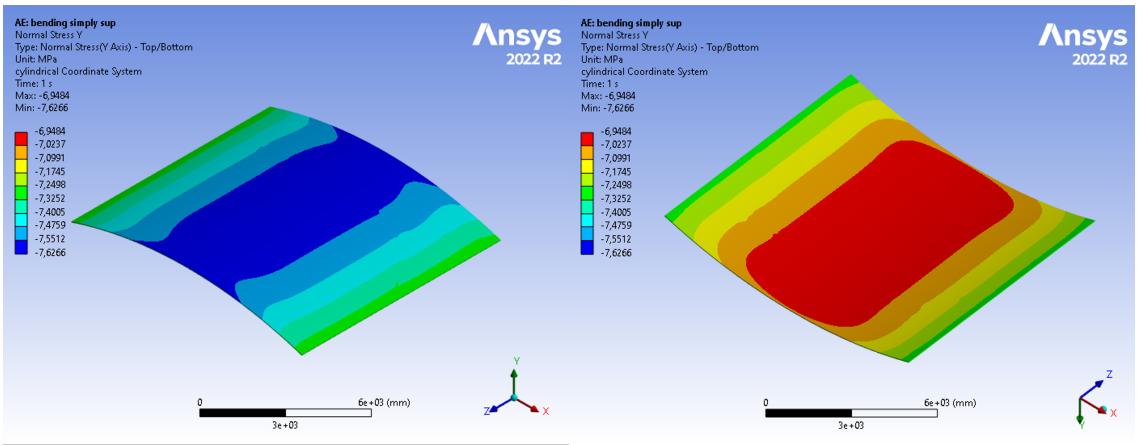

Figure 4.6: Normal stresses along the curve of the plate due to pressure load.

The curve that is used results in an arch that is still in bending. This means that the plate is somewhere in between an arched and a flat plate component. Since the stresses are significantly reduced when compared to the flat plate earlier in this chapter. The stress on top of the plate was 947 MPa (reference in appendix G.3) as compared to 7.6 MPa in the arched plate, it can be concluded that the arch effect is a great addition. The bending stress in the plate is expected to disappear if the curve of the plate is adjusted with a smaller radius, only compression stress will remain. This hypothesis will be studied later in the chapter.

4.4.1.3. Deformation in the plate

The deformation have been checked for the plate as well in LA. The simulation presented that there was only a very small maximum deformation of 1 mm, over a plate of 11 meters; this is very minor. When executed with a geometrically nonlinear elastic analysis (GNA) the result was the same for the deformation. This indicates that there is no possibility for the arch structure to deform more when the arch is compressed into its stiffened shape. Both results were added to the appendix in figure G.4.

4.4.1.4. Buckling of arched plates

Since the plate is a compression-based component it has to be checked for buckling using an LBA. As the buckling in a curved plate is different from uncurved plates, it has to be validated by engineering methods. The formula 4.1 gives the analytical formula to determine the buckling load for a curved plate [48]. The result is a load of $q' = 0,0187MPa$.

$q' =$, Load over the curve
$E = 200GPa$, Modulus of elasticity
$t = 40mm$ Thickness of the plate

$arcAB = 11596mm$, Length of the curve over the plate
$\alpha = 0.5 * arcAB/r = 0.32$, Central angle of the plate
$r = 18200mm$, Radius of the plate
$\nu = 0.3$, Poisson ratio

$$q' = \frac{Et^3(\pi^2/\alpha^2 - 1)}{12r^3(1-\nu^2)} \tag{4.1}$$

When checking the result of the buckling simulation in Ansys, the eigenvalue corresponds to the analytical calculation, as the eigenvalue was 1.15 with a load of 0.016 MPa. This is multiplied to a value of $q = 0,0184MPa$. It is important to note that in the result of the buckling simulation, the plate always has two or more buckles in it. This continuity has been checked for the first ten buckling modes. Figure 4.7 shows the first buckling mode, which has two maximum deflections and an axis of zero deformation in between them. The curve of the plate seems to steer away from a global buckling shape with one buckle in the plate, induced by the resistant shape of the curve.

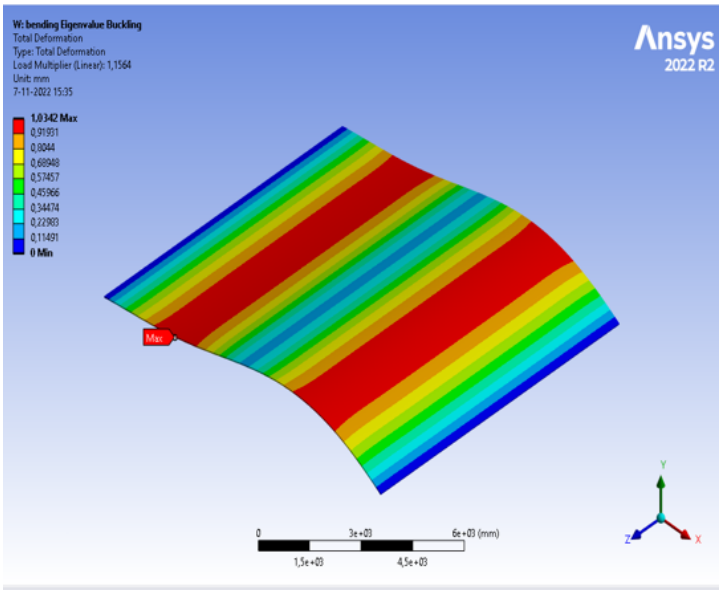

Figure 4.7: First buckling mode of the arched plate under uniform loading.

4.4.1.5. Constrained rotations

The plate will be connected to the construction, preventing the edges from rotating freely as was simulated in the models above. The effects were small but the main difference was the deformation shape found, which presented a double buckle form and a smaller deformation in the middle of the plate, the arch is no longer able to deform into its ideal shape. Next to that, higher eigenvalues and slightly reduced arch effect visible by the larger stress range and larger deflections. All results are in the appendix G.

4.4.2. Alternative curvature possibilities

Among all options available for arches, two important adjustments have to be considered. This concerns a different radius of the plate and the curvature in a second direction of the plate. They are important to explore to assess the effectiveness limits of the shape. Both were evaluated based on the simulations which were done and on what their effect was when used in construction.

The smaller radius did not lead to an optimisation of the gate due to the fact that more material is needed to be used which led to a lower eigenvalue in the buckling mode. It was chosen that the current radius of the gate was more promising. The results of the analysis can be found in appendix G

To conclude on the use of a double curve for lock gates is that it is a global shape which should work very effectively if only under a completely uniform load. Since there are several asymmetrical loads, including the true hydrostatic load, the shell proved to be less effective and is not evaluated any further. The study is included to present that there is no opportunity expected for the lock gate industry which

is a sector driven by effectivity and not aesthetics as in other constructions. This conclusion was based on the input used in this thesis. The results of this analysis can be found in appendix G too.

4.5. Frame optimisation and feasibility

The arched plate investigated so far has some deficits which have yet to be solved. Two main issues present themselves. Firstly, it is not resistant to the second design load, which was determined to be the point load from the obstacle situation in combination with the accompanied asymmetric support system. A sketch is presented in figure 4.1b. A slender plate alone is not very resistant to this operational condition.

Secondly, the plate edge seen in regular locks is often a softer and replaceable part [6]. The thin edge will not be able to transfer loads to the sub-structure adequately as the local stresses will be relatively high. And since this is a component that is constantly moved in and out of its position and thus sensitive to wear, it is not wise to use the main construction as the seal. Also, the two gates have to be able to form a seal against each other in the middle of the lock, but if the plates are thin the chance they close properly reduces drastically.

A possible solution to these two issues would be to introduce a frame to the concept. A frame will add stiffness to the plate for the second design load, and at the same time function as a way to properly transfer the load to the substructure. It will also be able to include a seal that can be replaced separately from the main construction. To see if this frame is a possibility a frame design was made to investigate the feasibility within reasonable limits.

4.5.1. Dimensions of the frame stiffeners

Stiffeners are a standard solution to the reinforcement of plates. To investigate the feasibility of the frame, dimensions are chosen which are in line with regular dimensions for plate stiffeners. The height of stiffeners are based on the rule of thumb for stiffener height: $h = 1/20 * L$. This results in a height of 570 mm and is applied for both the height and width of the rectangular hollow stiffener. The thickness of the plates is chosen based on the values found for boxed beams in NEN-EN1993-1-4 which are valid for at least class 3. This ensures that the beams do not buckle before the plate. The result is 26 mm thick plates for the box girders.

4.5.2. Frame design layout

To determine if the stiffeners chosen are feasible the loading is investigated is done on different options. The frame can be designed in different ways, but there are six conditions to which the frame must comply:

1. The seals of the gate have to be formed by continuous vertical members.
2. A continuous bottom seal that can seal the bottom of the gate but cannot transfer further loads.
3. The hook-up point where the force is introduced at 10400 mm height and at
4. The bottom of the frame where the obstacle is simulated.
5. The bottom corner of the pintle needs to be included.
6. The top hinge shaft has to be included at 9800 mm.

A situation sketch of these conditions is present in figure 4.1b in the appendix. The options for the frame include horizontal and vertical stiffeners; the main goal is to reduce the number of stiffeners used under the water to reduce corrosion chances. The top hinge shaft is above the water line so there is the goal to reduce members of less importance. A second important aspect is the limit of the material, so the member forces must be reduced as well. This is achieved by opting for the lowest bending moments, normal forces, torsional forces and shear forces in the frame. Deformations of the frame are not relevant as this concerns an incident situation. The options considered for this feasibility study are presented in figure H.2 in the appendix.

In order to speed up the frame design process, the choice was made to work with beam models in Ansys Mechanical. This is a method in Ansys which works with beam segments instead of shells or solids. This increases design speed and decreases computation time significantly. The downside of this analysis type is a lack of detail, since it concerns a feasibility study this is acceptable. To perform the beam analysis the interaction of the plate on the frame has to be inspected to see if the results are not biased.

4.5.2.1. Frame plate interaction

To see if there is significant interaction between the components during the obstacle situation a model has been made that has both. The frame has been modelled around the plate made in the previous section. Due to the aim of the feasibility study being to stay in line with material use, the plate has been reduced to a thickness of 34 mm with the added frame. To adequately introduce the load into the frame, an addition of a hook-up point was made. This addition consists of an assembly of two simple plates which are connected by a small cylindrical beam. The horizontal components of the hook-up are directly connected to the top and bottom flange of the boxed girder. The hinges are simulated by two nodes at the top and bottom at one of the vertical members.

Interaction of the frame will be indicated by the stresses in the plate relative to the stresses in the frame. If the stresses in the plate are significantly lower it can be assumed that there is no significant effect of the plate on the frame behaviour.

The results of the analysis show that the stresses in the main plate were less than 10% of the stresses in the frame. This is the situation for a plate which is 34 mm thick. If the plate is thinner than in this model the interaction of the plate and the frame would reduce even further. It can be concluded that if the stresses are as found in this simulation, the interaction is insignificant and a beam analysis can be done without the added plate in the simulation. There always is the interaction between the two components but this will present itself in complex future models. This will also be the case if the arched plate presents to be less slender than expected.

In the result, the frame presents peak stresses but this was not analysed any further as the frame has not been optimised and the focus of this analysis was on the interaction between the main plate and the frame. The result of the analysis can be found in figure H.3.

4.5.2.2. Beam model of frame

The beam models are based on similar dimensions as presented before. Since this is an approximation of the forces present in the frame, there is a basic detail level in the analysis.

The simulation results showed how the beam forces will be present in the frame. One model was chosen to be the most promising, this design can be seen in figure 4.8. It was the option that includes horizontal stiffeners in the top two levels and one small vertical stiffener between them. The benefit of this frame layout is that the two top beams allow for a reduced maximum bending moment at the vertical member as it is divided over two connection points. Resulting in a reduction of $856kNm : 1830kNm = -54\%$. Since the detail around the hinge might become complex this is a possible advantage. Further conclusions for the frame design are given in the appendix H.3.

The frame experiences just over the allowed maximum stress when considering the equivalent Von Mises stress, it has to be designed in further detail in order to conclude if the frame is strong enough. The result does show that the frame is within the same magnitude as the limits of the material, which is the criteria for this analysis.

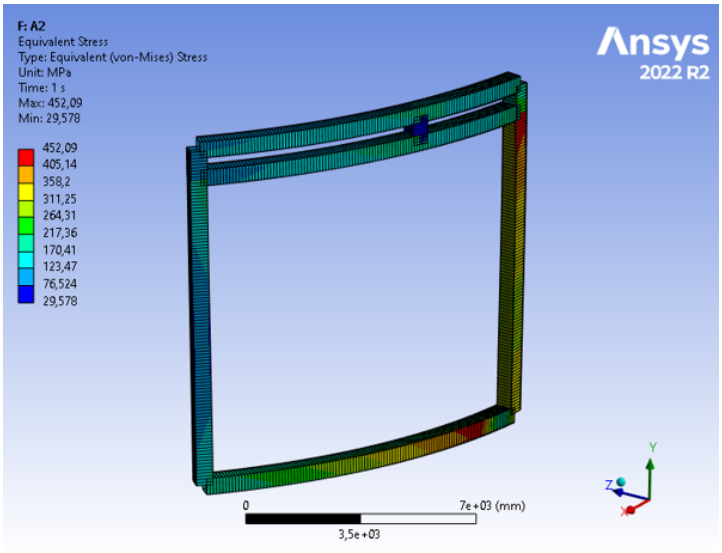

Figure 4.8: Equivalent stress in frame

The chosen frame design has no vertical members in the main plate field. Designs with a vertical member in the main plate have been included in the process, these showed that the extra stiffener adds to the maximum member forces in the frame and reduces deformations. In combination with the main plate field being disrupted and adding extra weight and welds, this option is not preferred as the aim is lower forces and deformations are not relevant. For comparison, the results have been added in figure H.5.

The member forces for the final design can be found in figure H.4 in the appendix. The limit of the rectangular hollow sections will be provided by using methods from Eurocode 1&4 in appendix H.4.

Based on the approximation done for this thesis the frame seems to be a possibility for the obstacle load situation. The material use is in line with the traditional design and the stresses are within the range of the material limit. This indicates that it is on the limit of its possibility to be optimised but a more detailed design will be needed to draw further conclusions.

4.6. Stiffeners and plate interaction

It has been proven in the previous section that the plate does not affect the frame. However, this has to be valid the other way around as well. Several aspects need to be investigated in order to see if the plate remains to be effective and therefore, feasible for optimisation.

The effect of stiffeners on a plate in compression will now be evaluated. Then, the deformation capacity of a beam relative to the stiffeners will also be evaluated. Next, the effect of stiffeners on buckling shapes is inspected as to what their impact can be when added or left out. Once the effect of stiffeners on flat plates is studied, the effect of stiffeners on arched plates is then also investigated. The principle of arch behaviour is based on the shape of the arch being able to deflect as a whole and it supporting itself in its deformed shape. So when the boundary conditions at the free edges change due to the implementation of a frame, the arch still has to be effective.

4.6.1. Plate behaviour with stiffeners

The plate behaviour of a flat plate with stiffeners has been investigated. The effect of the stiffeners lead to an inability of the plate to deform which led to stresses around the edge of the stiffener to the plate. Next to that, the buckling shape of the plate has changed due to a change in boundary conditions, this has a positive effect on the eigenvalue of the buckling modes as the multiplication factor increases. Further findings can be found in appendix F.

4.6.2. Arch effect with frame

To see if the arch effect last with the addition of stiffeners to the plate the model has been built step by step to see where certain effects come from. The first model only has stiffeners at the free edges.

The next model will include stiffeners on the edge that was simulated as a boundary condition before. An addition was made to this section to see if further optimisation would be possible for the plate with more stiffeners in the plate field. This analysis is in line with the first analysis of this section.

4.6.3. Stiffeners along the curve of the arch

The model of the simulation is given in figure I.7. The uniform water load is applied on the surface of the plate and not to the stiffeners. Similar behaviour as in the flat model is expected which includes increased stresses at the plate to stiffener connection. The buckles will be smaller and a clamped effect will be at the edge.

The effectivity of the arch should become evident based on the direction of normal forces in the plate. When they are directed at the stiffeners, the arch effect will not be present while if the stresses are along the curve of the plate to the model boundaries the arch will be effective. The deformation of the plate is also evaluated as part of the arch effectivity lies in the plate being able to deform into its stiffened position. The relative stiffness of the boxed stiffeners to the plate might interfere with the edges of the plate that are not able to deform while the slender plate will likely deform more.

The results of the simulations show that the stresses in the plate are in accordance with the expectations. The arch effect is still evident in the plate field. The normal stresses in the direction of the curve are larger than the stresses directed at the stiffeners: $\sigma_{curve} = -8.3MPa : \sigma_{stiff} = -8.4e^{-}2MPa$ for in the plate field and near the edges the stresses towards the stiffeners increase: $\sigma_{stiff} = -3.2MPa$ (see figure I.8 and I.9 in the appendix as reference). The deformation in the plate is also larger than at the stiffeners which allow the plate to settle into its compressed arch position. The deformation is approximately 20% ($u_{stiff} = 0.2mm : u_{plate} = 0.9mm$) of the deformation that presents itself in the plate field (see figure I.10 in the appendix as reference).

The effect of the stiffeners has been seen to increase the number of buckles in the plate. There are now 4 buckles in the first mode compared to the two in the free edge situation (appendix figure I.11). The buckles are located within the plate instead of continuing to the edges. Since the free edges are now being supported by the boxed stiffeners, both in displacement and in rotation the buckles are confined to the plate alone. The eigenvalue also increased with the addition of the stiffeners.

4.6.3.1. Stiffeners in the curved plate field

To inspect if there are possibilities to optimise further the concept one side study is done, steering away from the base concept a model is made with stiffeners in the arched plate field. If there are stiffeners in the curved plate field it needs to be inspected if the effect of the arch will remain active. The plate will be simulated to check if stiffeners that are closer to each other will result in the plate transferring load to the nearest support, or if the curved plates remain to transfer loads in a horizontal way. The model used is presented in appendix figure I.12.

The added plate stiffeners are of similar size as was used for the box girders. The total height is 500 mm but since it is on two sides the effective height on either side is 250 mm. The thickness is 13 mm as this is the required thickness for class 3 in combination with the transverse height.

The normal stresses along the plate curve continue to be formed in the stiffened model. The stresses along the curve are around the same size as seen in earlier models. The normal stress is nearly constant along the middle of the open plates. The forces around the stiffeners seem to increase as seen in the boxed stiffeners on the edges. The stresses in the perpendicular direction are significantly smaller than the stresses along the curve which indicates that the curved plate still performs in the desired way: $\sigma_{curve} = -11MPa : \sigma_{stiff} = -1MPa$. The results of the simulations are in appendix figures I.13 and I.14.

4.6.3.2. Arched plate with all-round frame

In the last step of the curved plate towards the assembled model, there are vertical stiffeners added at the end free edges of the plate where the supports were modelled before. These boxed stiffeners will have to transfer the force to the substructure. The boundary condition for these stiffeners is a zero displacement of the rear plates of the box. The vertical frame stiffeners are the same dimensions as the horizontal boxed stiffeners.

The deformation of the plate is different from earlier models. There are two large deflection bulges on the left and right sides from the middle. Behaviour is similar to the deformation given in the free-edged situation with constrained rotation at the supports seen before. Deformations are also larger

than before, this is not strange as there is a larger effect of the deformation of the vertical stiffeners. The deformation in the vertical stiffeners is very small. Figure I.15 is added in the appendix to show the result of the deformation.

The normal stresses along the curve of the plate seem to change with the deformation of the plate as there can be higher stresses seen in the locations of the top of the bulges. This means that there are larger bending moments in the plate than before. This resembles the effect of the constrained edges at the basic curved plate simulation and is therefore logical. The result is visible in appendix figure I.16.

The equivalent stresses have been checked to find if there is any change to the extreme stresses of the construction so far. There was relatively high stress found in the model since the start of the design sequence, the stress was located at the plate in the boxed stiffener that holds the plate. On further inspection, it is found that the plate is in bending and the normal stress in the width of the plate is high in the middle. This stress is still well below the yield limit (117 MPa /418 MPa=0.27).

The buckling shape found in the plate due to the pressure on the plate is in line with all previous results from the thesis. There are multiple buckles which are formed within the plate and do not transfer in the frame. Their buckles are of larger size in the height of the plate than along the curve. Higher buckling modes have similar shapes but the location of the buckles can vary. The shape of the first two modes is seen in figure 4.9a and 4.9b. The buckles seem to be shaped as if there are vertical stiffeners without there actually being placed stiffeners. The eigenvalue for these buckling modes is higher than for the unstiffened plate which was started with.

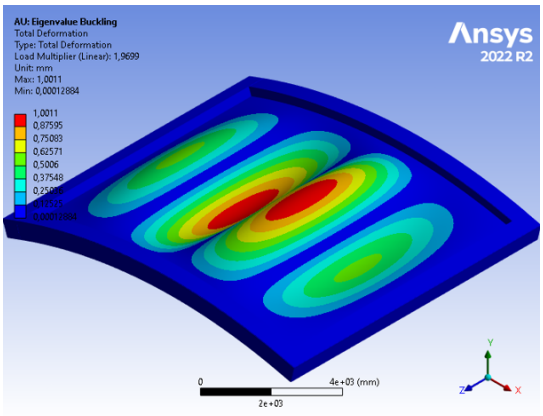

(a) Buckling mode 1 of plate with frame

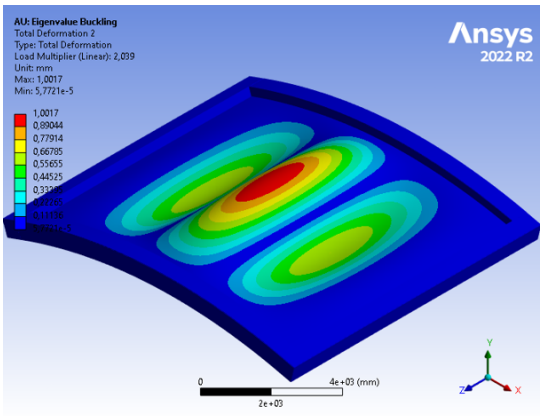

(b) Buckling mode 2 of plate with frame

5

Finite element modelling of arched mitre gate

This chapter aims to provide insight into the proposed design of the gate and how it is modelled with FEM. First, the design will be presented; this includes the dimensions used and the additional members added to the framed arch shape resulting from chapter 4. Then the final gate is presented which is part of an optimisation including stiffeners in the plate field to further reduce weight without compromising the concept too much. Lastly, the modelling options which are used to simulate the construction as realistically as possible will be presented.

5.1. The design

A complete model of the mitre gate has been generated using SpaceClaim, the design software package that can be used for Ansys Workbench. To clarify the model used to run the simulations, the design dimensions will be presented in this section. This model has been used in all the separate simulations. However, some simulations have been conducted in a sub-model of this general model to speed up the calculation process.

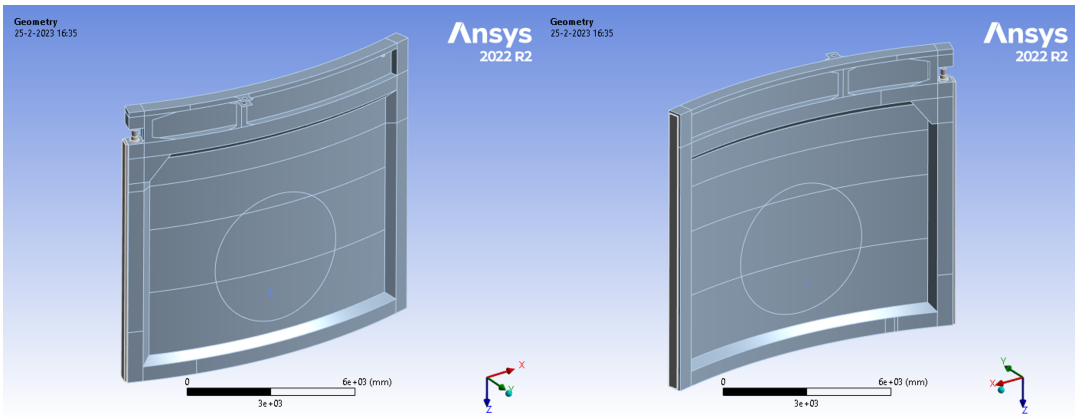

Figure 5.1: Design of mitre gate with arched unstiffened main plate and frame

The design presented in this study results from the iterative model building starting in chapter 4, which was refined through the steps taken in that chapter. The result of the design includes the top segment of the gate with hookup point and support, the front and rear seal, diagonally placed stiffener additions and solid members for rotational hinges. The front and the rear are presented in figure 5.1.

The span of the gate and the radius that describes the curvature of the main plate, which are two of the main components of the design, are presented in figure 5.2. This curvature is aligned with the bottom seal of the concrete substructure present in Veere. In order to meet the requirements needed

for a gate replacement for the project in Zeeland, there is no adjustment of the curvature. Previous results found in this thesis (chapter 4) did not require redimensioning of the radius.

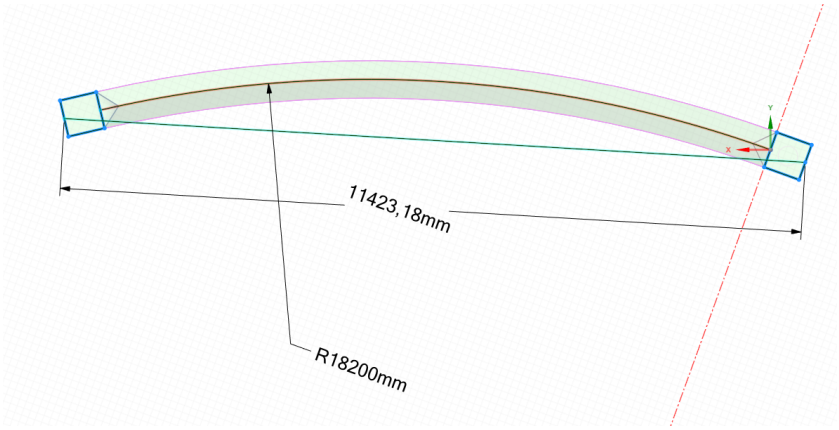

Figure 5.2: Span of the gate and the radius that describes the curvature of the main plate.

Figure 5.3 shows the dimensions of the boxed stiffeners that form the gate frame. These dimensions are valid for the frame in both vertical and horizontal directions. The stiffener dimensions are based on rules of thumb for stiffener design which is a height of 570 mm. The stiffeners have a thickness that ensures a class 3 member, which means a thickness of 26 mm for the 570 mm plates. The plates that holds the main plate have span of 285 mm which means the thickness can be reduced to 13 mm. The diagonal members have a span of 400 mm and a thickness of 20 mm.

The panels at the rotational axis have a thickness of 30 mm to reinforce the cantilever that is created due to the hookup location. These dimensions are chosen to prevent stability issues with the frame members of the construction. The remaining dimensions of the design, such as heights, the location of the hookup and the extra support, have been presented in appendix J.1 and J.2. Further plate thicknesses in the design are given in appendix figure J.3.

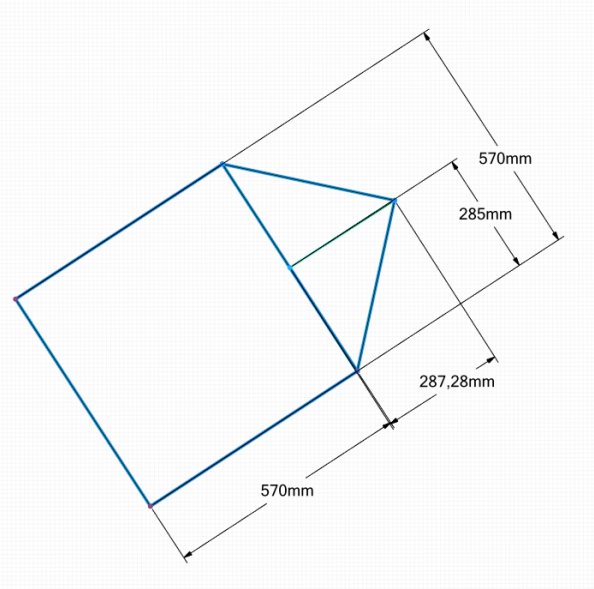

Figure 5.3: The dimensions applied in the boxed stiffeners that form the frame of the gate

5.2. Ansys Model

The modelling has been split up in boundary conditions, loads individually in Ansys and the load combinations which were made as a combination. Each will be briefly commented on what is the reason for this modelling and how it works in the basis.

The mesh of the model is set at 50mm per element, which is the same as the mesh determined in chapter 4. The number of elements in the smaller components has been taken into account and was refined to a smaller mesh. The solid elements have been given a separate mesh of 25 mm in order to accurately predict the results.

Welds are not simulated in the model. Rigid connections are made which connect components to one another. This is not an accurate representation of reality, but it is however still an appropriate way to run a simulation, as welds can be assumed to be of equal or higher strength than the base material. Checking the stresses at the connections is part of the interpretation of the results.

5.2.1. Boundary conditions

In the closed set-up of a lock gate, force is transferred from the plate through the frame into the seals and away into the substructure (appendix figure K.3). This is primarily a horizontal load, but due to friction, there is a vertical force transfer as well. This vertical force is only present at the end of the lock system where the gate is in contact with the substructure. In the middle of the lock, there is no vertical support for the gate which makes it impossible for the gates to transfer vertical loads to one another. Since the vertical support is only on the rear side of the gate, it creates an asymmetric boundary condition. This feature can be modelled in Ansys Mechanical under the ”connections” and ”contact” tabs. Specifying a ”frictional” contact between two members allows for a frictional coefficient. It determines how high the force transfer will be, based on the normal stress that builds up between two members. In the appendix, a figure K.1 is given to present this in Ansys.

To adequately model the rotation of the gate around the rotation axis when it is not in either the closed or opened position there, has to be rotational freedom for the hinge face. The hinge will not be able to rotate when the nodes are locked in the horizontal direction by a “deformation” boundary. Instead, a joint can be simulated by the joint-type connection of ”body-ground”. This feature allows a surface (or body) to be unlocked of displacement and or rotation by the shape of the selected surface. The modelling of this situation can be seen in K.2.

Next to the plate members, there are also solid members in the lock gate, plate elements will not simulate those members correctly. This can be accounted for in Ansys by using a solid element instead of a shell element. This method is used for the bottom pintle and the top hinge, as the shell elements are inappropriate for modelling a solid component. Using this method will produce more accurate results for the two components than using shell elements.

Any additional boundary conditions and the way they are modelled for the closed, open and moving conditions can be found in appendix K.

5.2.2. Loads in Ansys

To run the simulations of the different load combinations, Ansys Mechanical software was used. In part 2 of this thesis, several modelling options for these simulations were presented. In this section, the options which were not used in part 2 will be elaborated on.

The self-weight of the model is a standard option in Ansys and is automatically applied to all members. In the simulations for this thesis, the self-weight has been modelled as an acceleration; this is done to implement the safety factor adequately. Figure L.1 shows how the self-weight of a member is presented in Ansys.

In order to simulate the water on either side of the gate there is a load option in Ansys that allows modelling hydrostatic loads. These loads can be applied to a number of faces and act on a reference height from which it will simulate a linear static load which increases over its depth. By using two different loads on the model the water head is created (see figure L.2). All hydrostatic loads can be seen in appendix L

5.2.3. Load combinations in Ansys

The operational conditions have been combined in the different simulation setups. The setups for these individual situations are presented in appendix L. The figures show the combination of applied loads and the boundary conditions implied on the model.

5.3. Design of stiffened gate

A second design is presented for a final optimisation which has been performed at the end of the thesis. The main plate of the design will be constructed using multiple plates. As the arch is easier to apply over the longest edge of a plate, the individual plates will be placed above each other to form the main plate. The stiffeners are placed in between two panels that are spaced 2500 mm from each other. This is a common size for plates produced by steel manufacturers (for instance found at Salomon's metalen bv), which is why this study will use these dimensions. Other dimensions of plates can also be used, but these will be left out of consideration for the purpose of this thesis.

Using the available plate width from manufacturers provides a practical solution for an optimisation of the plate thickness and more weight reduction. The edges that are used to connect different plates to one another in the unstiffened design are welded. This weld is inevitable and must be present to connect two plates. Since this weld is inevitable, there can also be a stiffener put in between two plates. This adds one more weld but also the possible advantage of a weight reduction. An iteration of the plate resulted in a 14 mm main plate. The plate stiffeners have been designed with similar dimensions as the frame stiffeners. The total height of the stiffeners is 500 mm. This means that the height of the stiffener that protrudes out of the plate is 243 mm. The stiffener is a class 3 profile and is hence 13 mm thick. How the stiffeners are located in the plate can be seen in figure 5.4

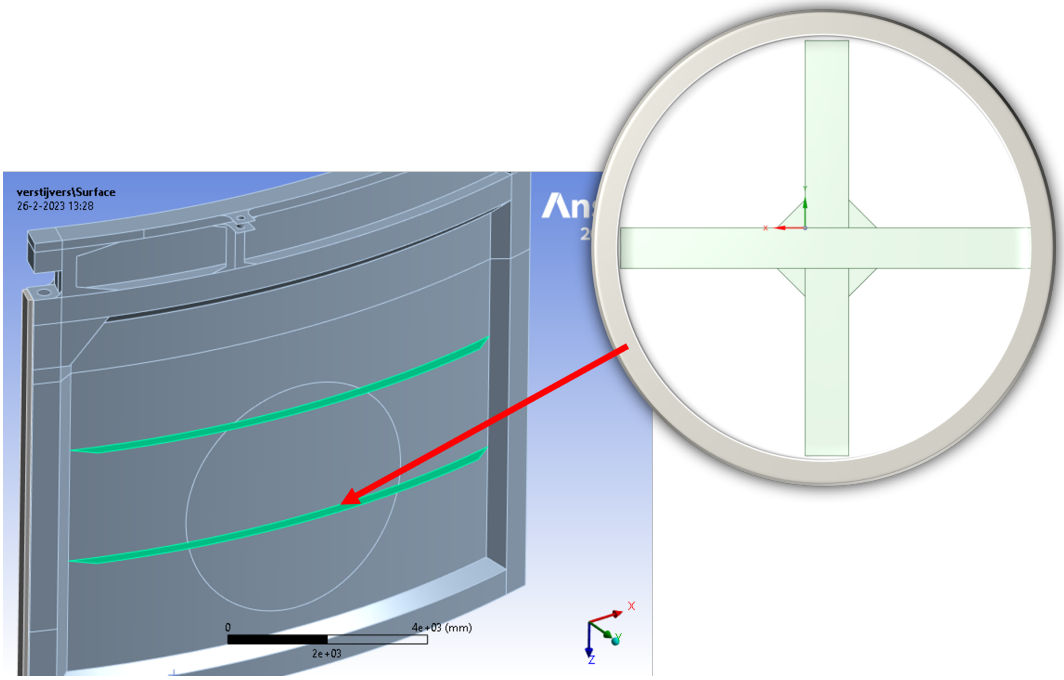

Figure 5.4: Design of mitre gate with arched stiffened plate and frame

Complications can occur at the vertical edge of the plate where the plate stiffener ends and the frame begins. To prevent these details from forming, the stiffener is not continued into the frame and not through the diagonal members. This allows for the stresses to remain outside of the boxed frame and be dissipated in the same way as the plate does. To prevent the stiffener from having sharp inclinations that tend to create stress concentrations, a slanted end has been added to the stiffener ends. The stiffener mainly functions to create stiffness against buckling and to prevent forces from transferring to the frame. This design of the stiffener is seen in figure 5.5.

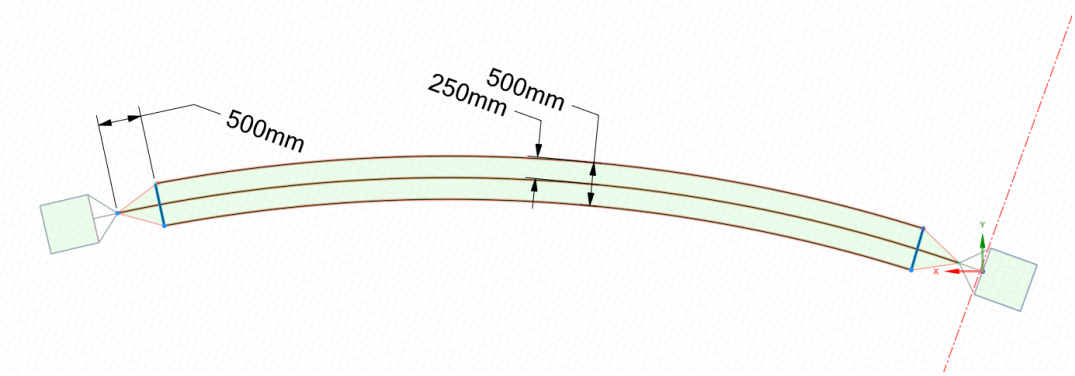

Figure 5.5: Design the stiffeners placed in the main plate.

6

Results and final gate design

This section will present the results from the simulations of the model as seen in chapter K, for the load combinations as presented in chapter 2. These results support the effectiveness of the design against the imposed loads. The main results are from the simulations of the initial design, which is unstiffened in the main plate field and is locked in by a frame on the outside. Additionally, a final design optimisation was implemented and checked for its validity based on the extreme results found for the initial model. The final design will be elaborated on in this chapter, substantiating any design choices that were made. Concluding remarks on the findings provided at the end of the chapter will include a comparison of the results from the traditional design and the thesis design.

6.1. Results of simulation of load combinations

In this section, the results of the simulations of the design will be presented, along with the corresponding boundary conditions and load combinations. The results are an approximation of how the construction would behave in reality. These results are based on the gate model as seen in the previous chapter. Each operational condition will be presented separately to clarify the steps which were taken to come to the presented conclusion. The initial design is being considered for this section of the thesis which means there are no extra stiffeners in the plate field.

6.1.1. Extreme water head and windwave

The simulation of the first load combination includes the extreme water head and the wind wave that can be present at the same time. First, the reaction forces on the boundary conditions will be checked to see if they comply with the expected reactions. Then the deformation of the construction will be considered to investigate whether the stresses match the deformations found. The model will be checked for buckling based on the loads which are applied. The LBA predicts its critical shape under the applied loading conditions.

This buckling shape will be used to simulate a GNIA. The start of this analysis is the buckling shape with a predetermined imperfection. This simulation is closer to the real-life loading of the construction in case of buckling.

6.1.1.1. Reaction forces

The reaction forces on the boundary conditions were checked first. The reaction forces in the horizontal direction are in balance with the load that is put on the model. The vertical reaction of the pintle is relatively small compared to the vertical force that is created by the rear seal of the gate. This is expected based on the principle of a mitre gate; it transfers the loads from the gate to the substructure through a horizontal force, due to friction there is a vertical force transfer which is a component relative to the size of the force perpendicular to the surface. The size of the load depends on the size of the gate and the water head which is created. Arched gates work similarly to general mitre gates; the main difference between arched gates and straight gates is the force transfer in the gate itself. This effect is presented in figure 6.1. The other results are given in figures M.1, M.2 and M.3.

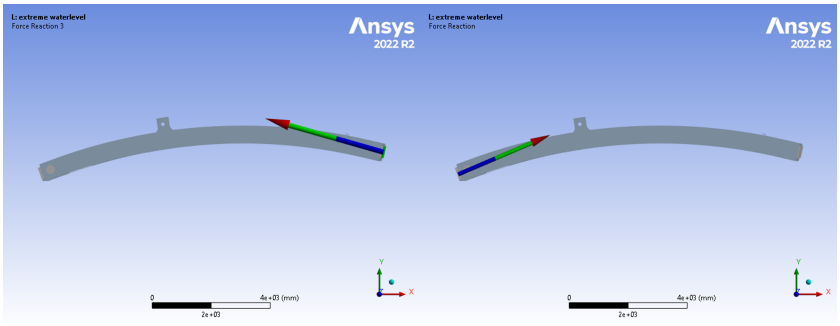

Figure 6.1: The first order deformations of the construction with the extreme water head and wind wave

Seal force distribution The force transfer in the seals must be inspected to see if the concept does not distort force transfer to the sub-structure. When evaluating the result from the seal in the normal direction of the plate it is visible that the stresses are almost constant over the height of the structure. There is an increase in stress around the height of the horizontal frame members. There is an absence of stresses at the top segment of the seal which can be explained by the main force on the model being located on the bottom of the structure. The consistency of the stress over the height proves that there is no direct problem presented in the force transfer to the structure due to the design concept. The results of this can be found in appendix figure M.4.

6.1.1.2. Deformations

Figure 6.2 presents the result of the total deformation, which is induced by the loads. These deformations are in line with the expectations of the model. The largest deformations can be found in the plate field, which is the least stiff component of the design. These deformations match with the deformations found for the fixed edges in chapter 4. An asymmetric deformation can be seen in the left side of the plate field, which conforms to expectation as the boundary conditions are also asymmetric (vertical support on the left side). The frame itself is barely deformed, except for the middle, where the span is the largest compared to the supports. The observed deformations are within the limits of tolerable deformation, yet these are deformation created by ULS loading and do not have to be tested on the limits from SLS.

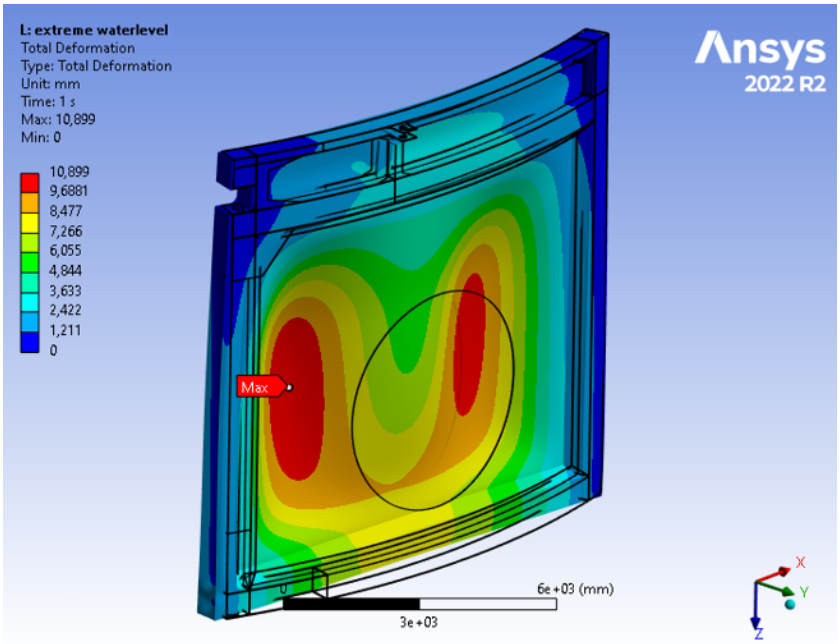

Figure 6.2: The first order deformations of the construction with the extreme water head and wind wave

6.1.1.3. Elastic stress limit

Figure 6.3a presents the equivalent von Mises stresses. The Von Mises stress shows whether any nodes in the model would approach a point where the material would start to yield. The maximum stress found is 280 MPa in the frame at the location of the seal, which is not close to the limit of yielding at 418 MPa. The maximum stress can be found on the connection point between the gate and the rear seal post. This complies with expectations as the forces that are transferred to the boundaries at the rear and middle seal have to be carried by the frame.

Figure 6.3b presents the normal stresses in the plate in the middle of the nodes. The large blue field visible in the middle of the plate represents the compression-based arch working in the plate. At the edges of the plate there is more disturbance from the rest of the construction, resulting in the normal stress being less consistent. The top of the plate has no loading and is partly activated in bending as the lower part is deformed and bending is created on the location where the load stops.

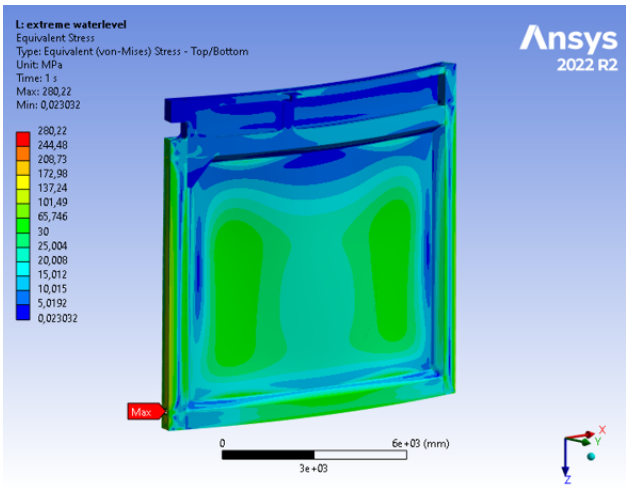

(a) Von Mises stress due to EWH.

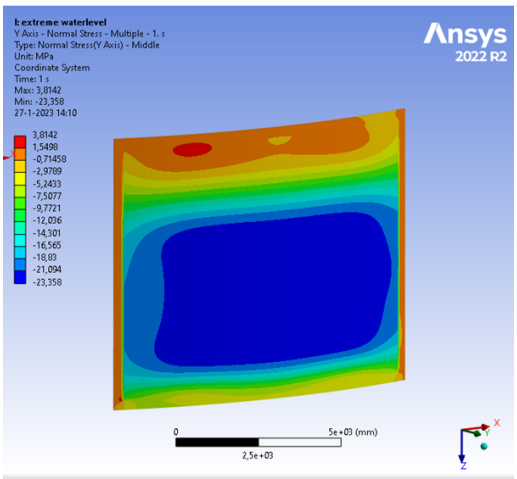

(b) Normal stresses along the horizontal curve of the plate.

Figure 6.3: Results of LA for the EWH load case.

6.1.1.4. Eigenvalue buckling analysis

The plate of the concept researched in this thesis is prone to stability issues. As presented in chapter 4, plate buckling is likely to happen for the slender type of plate used as the critical force is approached or exceeded. A buckling analysis can also be performed for more complex models and multiple loads. The result from the eigenvalue buckling analysis of the EWH load combination on the final design will be presented here.

Figure 6.4a gives the results from the first buckling mode and figure 6.4b from the second mode. The shapes are similar to the shapes found at the framed arched plate in 4 when the stiffeners were attached to the plate. The second buckling mode has an eigenvalue which lies close to the first mode and therefore has a likelihood of presenting itself. Both will need further investigation to assess which leads to a more critical situation.

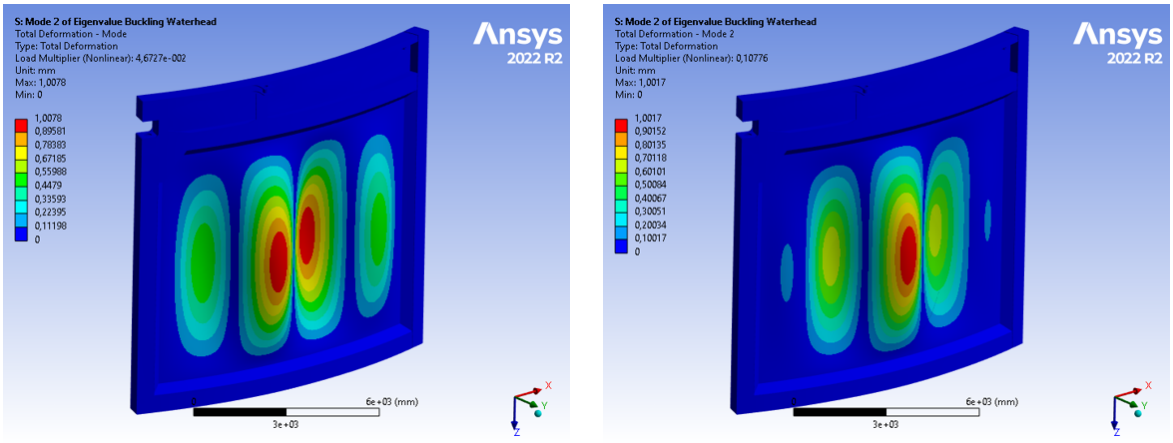

(a) First buckling mode. **(b)** Second buckling mode.

Figure 6.4: Buckling shapes of the first two buckling modes for the extreme water head load combination.

6.1.1.5. Buckling behaviour of the gate

The Eurocode standards from 1993-1-5 dictate that the total imperfection must be the minimal value of b/200 or h/200. The buckles have been conservatively estimated in size; the height is equal to the total plate height, which is 8460 mm. All horizontal buckles are of similar width but the largest buckle span in the plate is in the middle. To employ a conservative approach, a quarter of the total plate width is used which is a span of 2460mm for the largest buckle. This calculation can be seen as conservative as the buckles seem to be slightly smaller than that. The imperfection must be 12 mm, with a multiplication factor of 12 as the deformations in figure 6.4a are based on 1 mm deformations or slightly higher.

This imperfect shape is used to simulate the shape of the model and the same loads were applied to it. This simulation is done with GNA. Since it concerns a stability calculation, the geometry of the construction has to move towards a stable situation. This can be seen by the results from Ansys for the GNIA analysis. The result of the simulation done for this load combination is added in the appendix in figure M.5. It proves that the construction is stable as the simulation does not fail to find a stable point at the end of the simulation.

Figure 6.5a shows the results from the directional deformation of the second-order calculation of the first buckling mode. The largest deformation is found on the right side of the middle; this is the location of the largest deformity given by the buckling shape. It is expected that this part will deform even further as the resultant load is in the same direction. The opposing buckle on the left side of the middle is bent slightly out of the undeformed plane by the moment which is created on the right side of it. The deformations are relatively large compared to the LA results, This is due to the second-order effects. Deformations of this magnitude are no longer in line with the preferred deformation limit set before. However, to optimise the construction the deformations were assumed to be acceptable as the stresses of the construction remain within the elastic region of the material.

The equivalent Von Mises stress result is presented in figure 6.5b. The stresses do not exceed the limits of the material and no yielding would be present. The highest peaks of the stress are found at both the bottom and the top of the largest deformation buckle. To determine whether the stress peaks at these locations are within limits, they will now be inspected further.

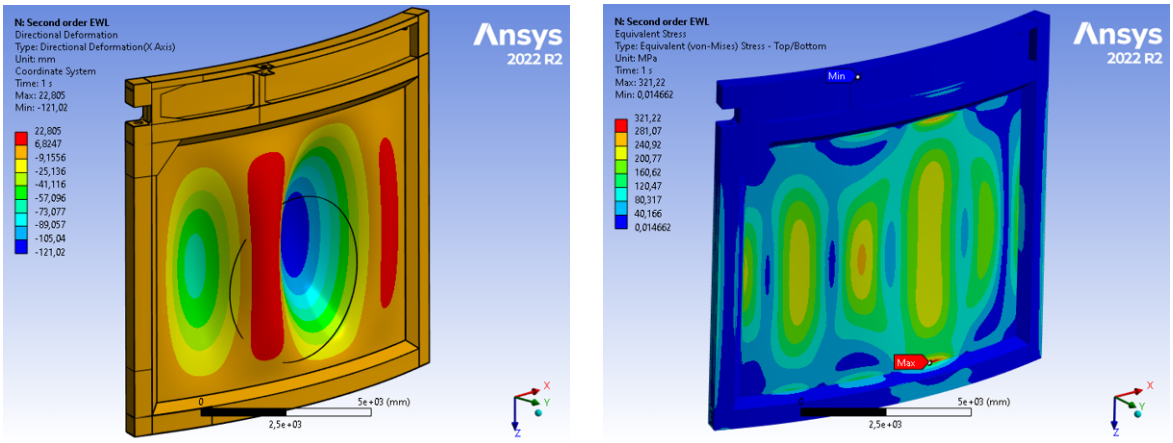

(a) Deformation of the construction

(b) Equivalent von Mises stress.

Figure 6.5: Results of second order simulation of the first buckling mode.

The results of the stress maximum in the equivalent stress is found in the normal stresses of the plate, both in the horizontal (figure 6.6a) and vertical (figure 6.6b) direction there is a stress concentration in the same location. The vertical stress is the largest of the two stresses, and it occurs at a logical location: the deforming of the plate in the direction of the force creates a bending moment at the point where the plate is held in place and prevented from rotating. The peaks of the normal stresses end up at the top and bottom of the plate. This load combination is not a cyclic presence in this project, which excludes it from fatigue risk. It is however important to be aware of this effect for this design type, the differential head (which is cyclic) cannot be of this size due to the result found in the GNIA simulation.

The arched behaviour of the plate is reflected by the results from the horizontal normal stresses in the plate (Figure 6.6a). When comparing this figure to figure 6.3b it can be concluded that the consistent normal stress that was found in the initial simulation would no longer be present. Due to the deformations that were implemented in the model, there is no longer a continuous arch present. A curved arch is ideal for the transfer of loads in the direction of the curve, but this effect is no longer dominant when the arch shape is disrupted. Since the limits of strength are not exceeded, and the analysis did not become unstable it can be concluded that the remainder of the construction in its imperfect shape can withstand the load.

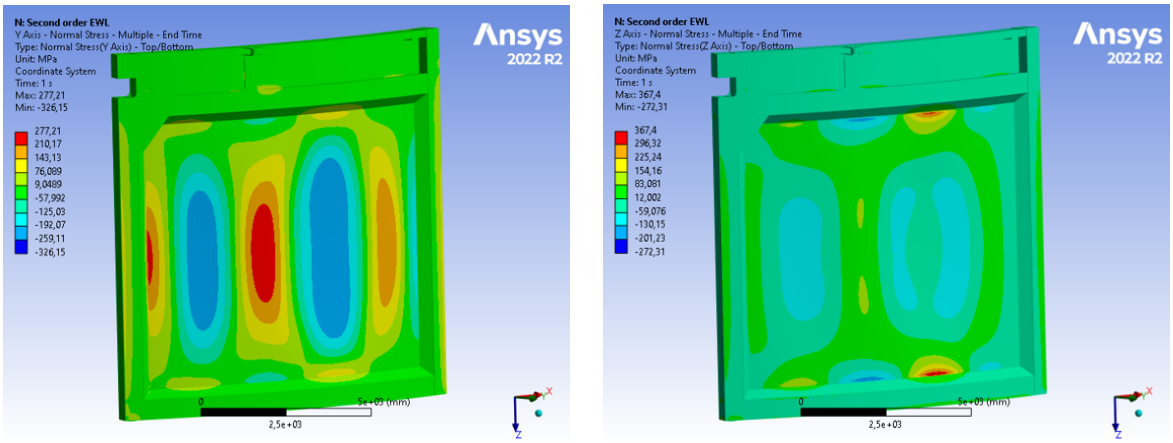

(a) Stresses along the curve of the plate.

(b) Vertical stresses in general Z direction.

Figure 6.6: Normal stresses in the plate for second order simulation.

Second buckling mode as imperfection Because the second eigenvalue of buckling lies close to the first, it is checked if this is not more critical than the first. The second buckling mode is similar to the first mode in the vertical sense. The GNIA analysis was performed and the results have been added to appendix M.1.

For this study the first mode is assumed to be critical, this is based on the results found in the EWH load combination. Higher buckling modes have been found to present more buckles on the plate which lead to smaller imperfections. Smaller imperfections in the plate lie closer to the perfect design in which the arch working of the plate is dominant, meaning that forces can be transferred more efficiently due to the global arch effect.

6.1.1.6. Deformation with imperfections

The total deformation of the plate with imperfections under SLS loading of the EWH loads is equal to 94 mm. This is found in the location of the largest buckle in the direction of the load. This exceeds the initial limit but it presents no practical problems in the lock as the deformation does not even bend out of the perimeter of the frame. The Ansys result of the plate deformation in GNIA is presented in appendix figure M.8.

6.1.2. Propeller load

A propeller load has the potential to be a critical load case for this design. As opposed to the hydrostatic loads it resembles a point load, which is unideal for arched plates. Point loads can be applied in different locations. To assess whether propeller loads form a problem for the design, simulations have been run with the load on multiple locations. The most obvious location for the load to be critical is the middle of the plate, which creates bending moments in the plate. The second most critical location would be if the load is present at the location of the largest imperfection deformation of for instance the imperfection shape of the EWH buckling shape. The location of the largest deformation is usually surrounded with the largest stresses, meaning an increase by a local load might result in a critical stress. This situation where the propeller load is on a pre-buckled location has been simulated in order to check if this will not have a larger impact than is expected in the basic propeller load case.

6.1.2.1. Propeller load first order analysis

The largest deformation can be seen in the middle of the plate, which is where the load is located. This location is in accordance with a beam which has a point load in the middle; the largest deformation will present itself in the middle. The maximum deformation is in the middle of the plate, while the force is applied on the lower segment of the gate just beneath the water line. This situation causes a deformation to be superimposed on the less supported part of the plate. This deformation is larger than in the first-order analysis of the EWH load case. There are no extreme stresses in the equivalent Von Mises stress. The stress image for the frame is similar to the results found for the EWH load simulation. Further reference is given in figure M.9 and M.10, found in the appendix.

The previously mentioned arch effect is present but in a less consistent fashion, see figure 6.7. The normal stresses are not consistent over the plate. The top/bottom stresses show this effect more than the middle stresses in the node. Normal stresses can be found around the location of the propeller load, as this is a bending point of the plate. Around the buckles on the left and right side of the main deformation the stresses also increase. The stress pattern is similar to the situation in the GNIA of the EWH. The Stresses in the middle of the nodes give a much more consistent image as can be seen in figure 6.7b. The lower value of the loads in the middle of the plate indicates bending stresses in the plate, proving the arch effect is not absent in this load simulation.

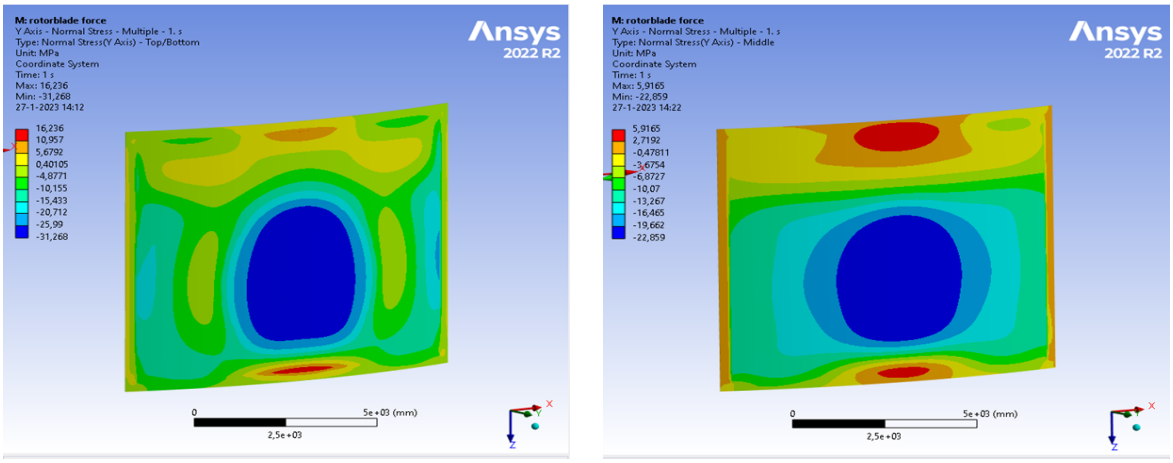

(a) Normal stresses at the top and bottom of the plate.

(b) Normal stresses at the middle of nodes.

Figure 6.7: Normal stresses for the first order analysis of the propeller load.

6.1.2.2. Propeller buckling and imperfection analysis

Similar to the EWH load combination, the propeller load is also checked for behaviour in GNIA. The results are similar to the results found in the first buckling mode of EWH. The results can be found in figure M.11 in the appendix. Since the result of the buckling shape is similar to the previous result, it can be assumed to be dominated by the hydrostatic load instead of the propeller load. We can thus conclude that the propeller load is not a leading cause for the buckling shape, as a buckle would have appeared in the middle in the first mode would have shown a buckle in the middle if this were the case.

When considering the deformation of the propeller load this is different from previous results. Figure 6.8 shows the deformation result from the imperfection analysis. The deformations observed in this simulation do exceed the 45mm limit, which is acceptable since this limit was discarded based on stresses not surpassing the elastic limit and the loads are for ULS. When the equivalent stresses from the same simulation are evaluated, there are no peaks over the limit and is valid for this load case too. All stresses are lower than in the EWH load case. This result can be found in figure M.12 in the appendix.

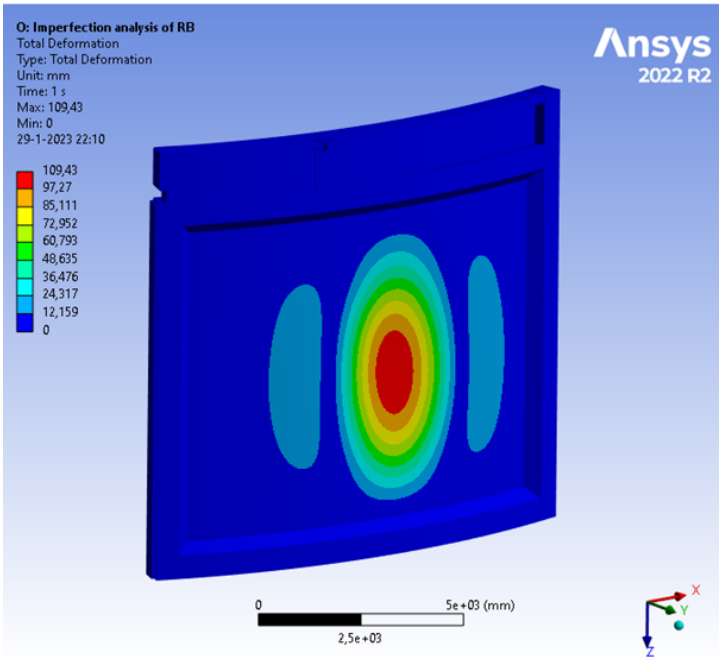

Figure 6.8: Deformation of the model due to the propeller load in the GNIA.

The normal forces in the vertical z-direction are similar to the results seen in the EWH load situation. The stresses remain below the yield stress and are less critical than the EWH load presents. For reference, the result is visible in the appendix in figure M.13. The normal forces in the horizontal direction do not give any significant results, as seen in appendix figure M.14.

This load combination less extreme then the EWH load but is applied more often. It does however not present itself in this exact configuration every cycle. The assessed situation is only valid when a ship passes through the lock in one specific direction, not if the ship travels in the opposite direction. In addition, it is only the heaviest vessel class which can produce this load, meaning not every ship passing through the lock will create this situation. The location of the load can also vary, which will be assessed later. If the stresses are at the same spot as this analysis a fatigue check has to be performed.

6.1.2.3. Propeller load GNA analysis

As in the GNIA, the option to make a multi-step can also be activated in the first-order analysis. Making use of this option will always result in a better approximation of reality than a first-order analysis, as the loads are applied gradually and simulation allows the structure to redistribute stresses. To compare the results of this multi-step option with the buckling behaviour, a simulation was run. These results are not more critical than the GNIA and these can be used to more accurately determine the most critical situation of the model. The results of the comparison between these simulations are given in figures M.15, M.16a and M.16b.

6.1.2.4. Propeller load on unideal location

While not critical in the already simulated situation, the propellor load has the possibility to be critical if placed in a different location on the gate. As the buckling shape of the first mode of the EWH presented the largest issue thus far, it was used to determine the most critical imperfection shape in this situation. The asymmetrical propeller load will not be more critical than in the original location. The location of the stress peak is in a different location than in the load in the middle of the plate model and therefore fatigue can be discarded for this load situation. The results of this analysis can be found in appendix M.2.

6.1.3. Ice load

The ice load presented an asymmetric load to the gate in a vertical sense. The load type resulted in a compression situation for the arched plate. Just like the other loads that had this effect a LA has been performed which led to no extreme results (see results in appendix M.3).

The next step was to investigate the behaviour in case of an imperfect structure. For this, the first buckling mode imperfect shape of the extreme water head has been chosen. The result of the ice load led to similar stresses as found in earlier load cases at the top edges of the arched plate. It did however not surpass the elastic limit of the material. The extreme result can be found in appendix figure M.26, the other results can be found in appendix M.3.

6.1.4. Obstacle load

The obstacle load situation was already studied in chapter 4. The results from the detailed gate are found here and led to some changes in the approximation. When working with the first-order simulation the stresses are well out of bound. This is not considered since the simulation also indicates that there are large deformations. These deformations are in the region of 500 mm which is too extreme to be evaluated solely in the first order.

Therefore the obstacle load is simulated with a Geometrically nonlinear elastic analysis (GNA). The calculation time is reasonable and the deformation of the structure is essential to allow the rotation in the top hinge. Also, stress redistribution is possible for the construction which improves the results since it is closer to true behaviour. In figure 6.9 the equivalent von Mises stress can be seen for this simulation. There seems to be no yielding of the material.

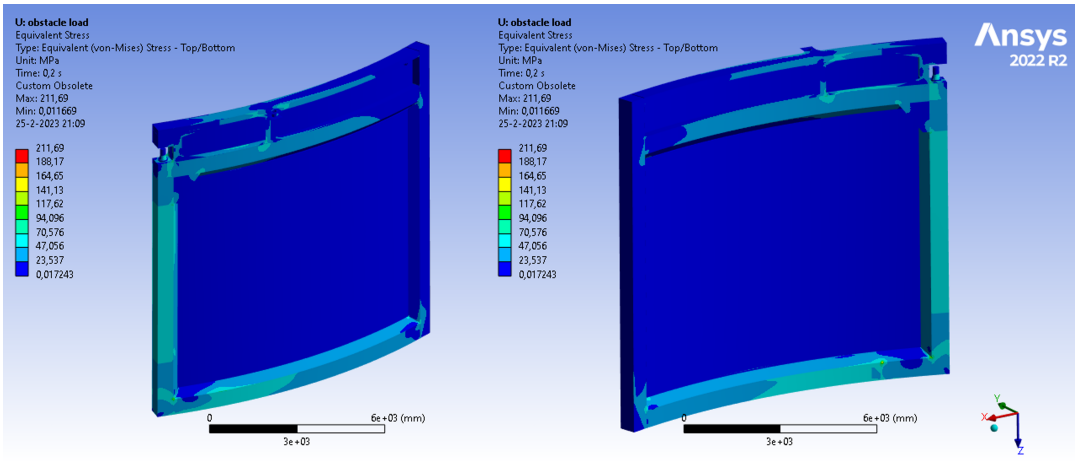

Figure 6.9: Results of the equivalent Von Mises stress for the obstacle load combination in GNA simulation.

It is, however not enough to base the result only on the equivalent Von Mises stress. Local stresses have to be further inspected, and when this was done, several results came back, which are important to consider. Important to note is that the stresses in the corner of the connection from the horizontal to the vertical beam can be easily resolved by adding a corner connection. This was not included in the most recent model but will gradually transfer loads instead of the hard inclination which is currently designed. Future design should include this in the design to mitigate the peak stresses.

The most critical result is found in the normal stresses along the curve (local Y axis), see figure 6.10, and mainly the negative/compressive stresses are found and will present an issue. These are located on the location where the obstacle is put. These stresses will lead to local buckling of the plate, it exceeds elastic limits and creates plastic deformation or even exceed the ultimate strength. This will be further commented on at the end of this section.

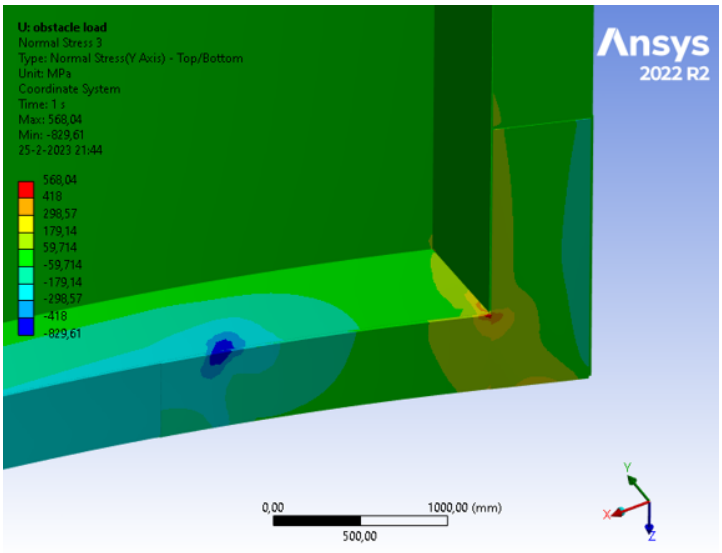

Figure 6.10: Normal stresses along the curve of the plate.

Normal stresses perpendicular to the plate, in the general y direction, present peak stresses, these are singularities as the peaks are in single nodes. This effect will lead to stress redistribution and is negligible for the true structure. The result can be found in the appendix figure M.28.

Normal stresses in the general Z direction are only small peaks which arise due to the limit in the modelled design. There were several detail simplifications implemented which are executed as sharp inclinations which can be executed as curved details in the final design, the stresses in these spots are likely mitigated when executed correctly. In the appendix figure M.27 shows where these low-quality

details are located.

Due to the load at the top which has to be transferred to the boundary at the bottom, a torsion force has to be taken up by mainly the vertical rear frame member. This component will be under shear loading and the shear limit should not be exceeded. When considering the shear resistance of members in the Eurocode the maximum shear can be determined in members. This has a maximum shear load stress of 241 MPa. For the frame, there is no exceeding of the shear limit in the vertical frame member. The shear limit is only exceeded in the location of the obstacle where the normal stresses spiked too. This detail will be commented on separately at the end of this section. The Ansys results of the shear are added in the appendix in figures M.29, M.30 and M.31

The obstacle load has several peak stresses which exceed the prescribed limits and will lead to local deformation. This is inevitable due to the nature of the load case and how it will present itself. The nature of this problem lies in the random location of the boundary due to the obstacle as it can present itself along the whole bottom of the construction. There cannot be designed for all these situations without dimensioning beyond reasonable sizes. When the incident happens, it has to be taken into account how the construction behaves globally and there has to be an inspection done on the impact location. The fact that the stress peaks are presented locally in a GNA indicates that effects remain locally, it is not likely for the whole structure to fail when it happens. Plastic analysis in geometrically and materially nonlinear analysis (GMNA) needs to be performed to adequately assess the effects on the bottom horizontal beam. GMNA is not in the scope of this thesis.

The results do indicate that the frame of the gate is ductile in a way that the rest of the frame will allow for deformations while a fold is created at the obstruction location. The nodes with the peak stresses remain to be in a small group which indicates that it will remain local. Plastic deformation might adjust this but needs to be studied to conclude on.

6.1.5. Fatigue load

Fatigue loading of the structure has been simulated and the results will be given in this section. Fatigue limits were approached in chapter 2 but will be slightly further elaborated upon in this section. There is a difference made between the fatigue stresses in the plate and in the frame. The plate has been simulated in a GNIA to more accurately predict the stresses of the main plate. The frame has been approximated with a first-order analysis.

6.1.5.1. Fatigue damage methods

Based on the reversed engineering of the fatigue damage assessment the minimal requirements for certain points can be determined. As the total cycles are known the allowable stress for detail categories can be determined. The construction will not be prone to fatigue when the minimum stress of the lowest category is not exceeded. Based on this minimum stress level per detail category, choices can be made in the execution of details in the construction. As mentioned in 2 the required minimum stress for fatigue to be relevant is a stress of 99.7 MPa. As a reference to the increment of the detail category on the maximum stress another detail was calculated for the damage method. Based on detail category 71, which is a detail that is a minimum for many details or can be achieved by proper treatment, a damage value of 1 has been calculated for 470.000 cycles. The required minimum stress to achieve this damage is a stress of 197 MPa. If stresses approach this value further study on a higher detail must be done to assess the fatigue stresses.

The detail in the plate where the plate is connected to the stiffener is detail 6, found in table 8.4 of 1993-1-9. Based on a detail category 80, which is the lowest possible category, damage of 1 has been implemented with the number of cycles, 470.000. The calculation method provides the answer to the minimum stress to achieve this damage and that is a stress of 222 MPa.

6.1.5.2. Normal stresses in the plate

The stresses in the plate have been simulated with GNIA. Since stresses were higher in this analysis and it is a step further in the direction of the real-world prediction these results will be used for the fatigue of the main plate. The first buckling mode from the extreme water head load combination was used as the imperfect shape.

The main plate is loaded in two directions due to fatigue which is in steps 3 and 4 of the cycle. The most critical stress proved to be in the vertical direction and is located at the bottom of the plate. Figure 6.11 shows this location in the left image on the bottom and the opposing stress on the right side of the

figure. The total stress difference is approximately 33 MPa in the vertical direction at the weld. This value is well under the limit of the critical fatigue value. Other results of fatigue stresses in the plate can be found in appendix figures M.32, M.33 and M.34.

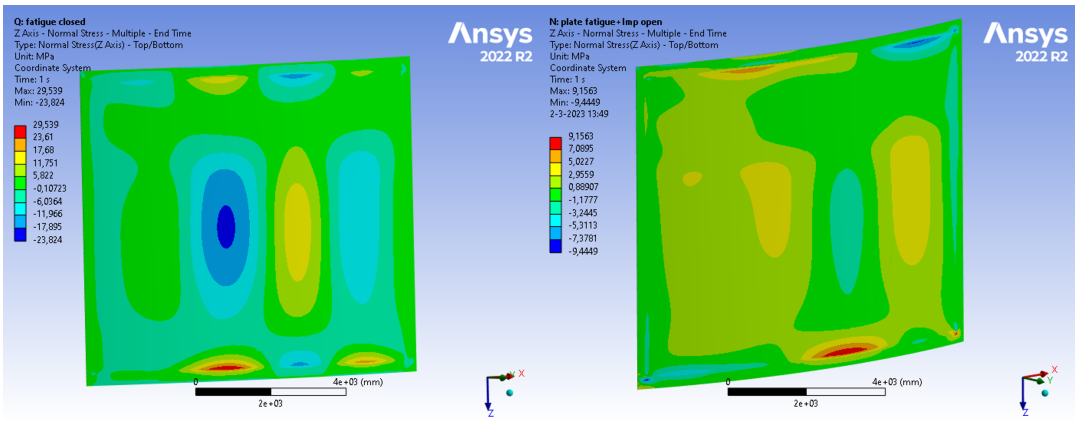

Figure 6.11: Vertical normal stresses in plate due to fatigue loading steps 3 and 4

6.1.5.3. Normal stress in the frame

There are multiple details in the frame which are prone to fatigue damage. These locations have been evaluated based on the results from fatigue load combinations that were simulated

The peak stresses in the vertical z-direction of the gate are found around the stiffener between the top and middle horizontal beam. This is logical as there is a moment transfer to the height of the hinge by the force on the hook-up location. The detail of the connection between this stiffener and the beam is either in the form of detail 6 from table 8.4 or detail 1 from table 8.5 from the Eurocode. For both details the category would be at least 71 since the thickness of the welds and plate is lower than 80 mm. Figure 6.12 shows the stresses at the stiffener and presents the difference is 186 MPa. This is lower than 197 MPa which is set at the limit for these details but the approximation of the simulation has to be further studied in order to adequately assess the fatigue stresses.

There can be something done about the stress of the stiffener and that is adding another stiffener in between the horizontal beams and placing them at an equal distance next to the hook-up point. One can be closer to the rear seal and the other to the middle seal. This will result in a distribution of vertical force in the two stiffeners. and reduce the peak stress at the connection of the stiffener to the frame.

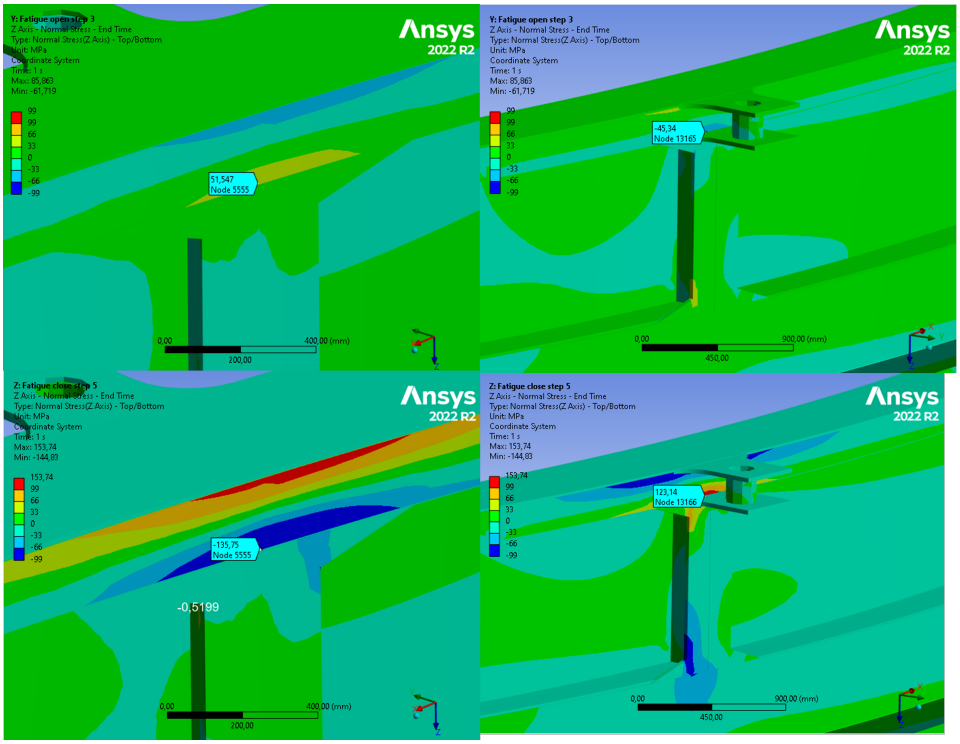

Figure 6.12: Vertical normal stresses in the frame due to fatigue loading.

The stresses in the horizontal Y-direction along the curve of the gate present peaks at which there is now a connection simulated. These stresses add up to 127MPa which exceeds the minimum limit for the det. cat. 36. The plate at the girder is 26mm thick and this will create a weld thickness of approximately 28mm. The total thickness of plates and welds will be just over 50 mm which puts it in construction detail 1 with category 71 of table 8.5 from the EN1993-1-9. If this is used as the reference detail there will not be a problem as the stresses are lower than 197 MPa. Since this is only an approximation further study needs to be done on these details if the construction is unchanged. Appendix figure M.35 presents the results of the normal stresses in these locations.

What is also a possibility is the adjustment of the weld and its location. It is possible to shift the connection out of the critical zone where it is located now. Creating a separate L-shaped plate which is located in the corners of the frame and shifts the weld location further into the beam, where the stresses will be lower. This mitigation can be done in all corners of the frame to prevent these peak stresses from being of importance to fatigue.

The normal stresses in the X-direction, which is perpendicular to the normal of the main plate (cylindrical axis system) present peak stress around the hook-up point of the cylinder mechanism. These stresses are based on hard angles which were not further detailed and create stress concentrations on the connection of the members. This can be dissipated by introducing circular angles instead of triangular members. The hookup presents peak stresses to the girder. The detail class is the same as in the Y direction mentioned above. This detail class has a higher tolerance than the stress found. The connection of the hookup could be fixed by not welding the hookup to the girder but making it out of the same plate. The results from the simulation can be found in figure M.36.

6.1.6. Deformation at closing

The water barrier function of the plate can be assessed by the load combination for the deformation at the closing of the gate. This is the moment right before the gate closes and it has not yet created a water head which pushes the gate into its rigid arch shape. If the sway of the gate is too large the gate will likely not properly close. When the gates do not meet correctly in the middle, water seepage will occur at the seals and the lock does not function properly. If major deformations take place on the scale of the gate this will form an issue. As a limit, the deformation limit of 1/250 is used.

The result of the simulation can be seen in figure 6.13. The maximum deformation of the gate is 15

mm in the bottom corner. This indicates that the chance that the gates will connect adequately remains unaffected. The deformation direction is even in favour of the gate closing properly as the bottom will make contact first and the mechanism at the top can push the top of the gates against one another.

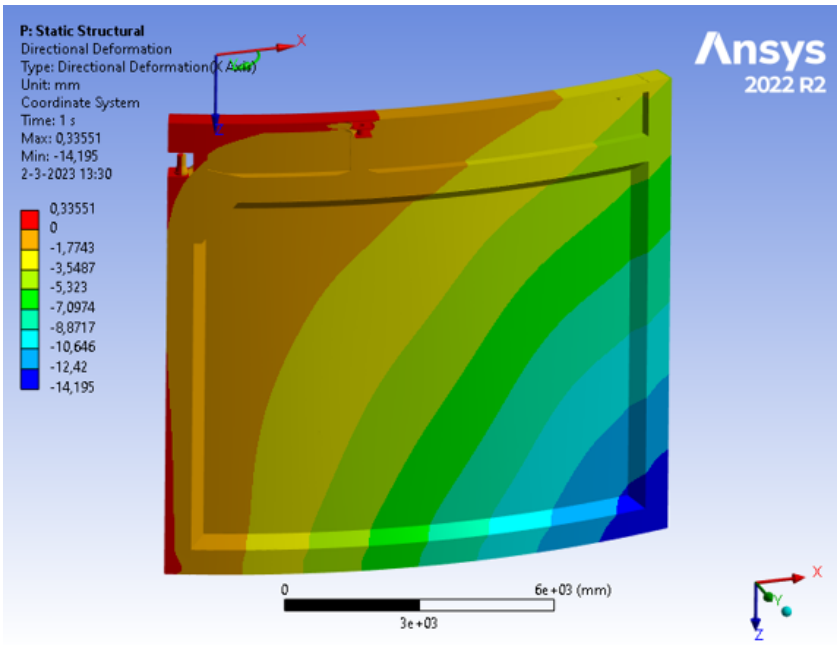

Figure 6.13: Deformation before the closing of the gate.

6.1.7. Gate opened in gate post

The gate has to be checked for the load combination which has a likelihood of being critical in the opened set-up. The load combination of the gate opened in the post while a wave of a passing ship is applied. The modelling of the load and added boundary conditions are presented in the appendix in figure L.11 and K.5.

The result from the simulations shows that there are no significant stresses in the frame outside the support of the gate. Proof of this can be found in figure M.37 in the appendix. The maximum stress in the support is a singularity with an extreme of 403 MPa in the node (figure M.38) which is located at the connection of the support to the horizontal top beam. Other stresses at the top support max out at 313 MPa. Both values lie below the yield limit of the material.

6.1.8. Buoyancy and weight

In this subsection the weight of the structure will be presented, it has been determined in Ansys mechanical. The buoyant force capacity will also be presented. The weight is an indicator of the possible reduction of the material used. The weight that is calculated takes into account the welds and their weight.

The weight of the construction is determined by Ansys and modelling the structure with only one load, which is the self-weight without any safety factors. If in combination with a single load only one boundary condition is applied for the vertical direction, it will calculate the total force reaction which can be interpreted as the weight of the construction. The total weight for the unstiffened construction is 412 kN. This result can be seen in figure M.39.

To calculate the critical buoyancy situation, the water load is put on the model at the lowest level possible on both sides of the gate at 6100 mm, in this set up the minimum amount of lift is created. The water is also not meant to be lower at any given moment when the construction is in the lock. This setup determines the maximum load which can be present at the substructure. The weight of the construction is 322 kN when the buoyancy is put on the construction. This means that the total buoyancy that is created is 90 kN of lift. The maximum load on the bottom pintle would be exceeded in this situation. There is a possibility of one of the compartments leaking and losing its buoyant capacity. Since the

construction is not buoyant enough for the substructure the loss of an air body is not extra critical for this situation as it exceeds the limit. The result is given in the appendix figure M.40.

If the gate were to be in an extreme water level situation, it is important that it will not start floating. This is a risk for the gate which is installed at the moment and needs to be checked. When the water is at the extreme level of 7750mm from the bottom. The result of the calculation is 308 kN for the weight of the construction on the sub-structure and 104 kN of buoyancy. The buoyancy must be 412 kN for the construction to start floating. This upwards force is not critical and will not lead to the gate floating upwards. The result is given in the appendix figure M.41.

6.2. Welding length of arched gate design

The total length of welding for the design was calculated, which resulted in 438.98 meters of welds. With an average plate thickness over this length of 23.4 mm, the total weld volume is approximated. When taking a weld thickness of 0.55 times the thickness of the plate, which is equal to the approximation used in chapter 2, and a weld at two sides of the plate, this is a total of $0.0752m^3$. The corresponding calculation can be found in the appendix in figure M.43.

The weld locations in this design concept have to be considered in terms of the accessibility of the weld locations. Most welds are long segments which run parallel with a component and are uninterrupted. There is only a minor set of welds which are not easily accessible and need more attention.

6.3. Stiffened arch-mitre gate

To further optimise the gate, another design iteration was made as presented in chapter K. This design was then tested for the most extreme load found in the previous section, of which the results will be presented in this section. The effect of stiffeners on the plate has been investigated in chapter 4, and the application of stiffeners in this design will aid in reducing plate thickness. First, the design will be presented and then the results of the simulation will be evaluated. Finally, the conclusions that can be made based on the results from the simulation will be presented.

6.3.1. Results of stiffened design

Not all load combinations have been simulated for the stiffened gate design. To assess what the effect of the plate stiffeners is on the plate, only the most critical load in terms of strength from the clean gate will be simulated: the EWH load and the wind wave, which can form simultaneously. This load combination in the closed layout will be used in the simulation. As was done in the clean gate, a GNIA will be executed to inspect buckling behaviour. Because the EWH load is the most critical load induced by hydrostatic loads, all other water-induced loads are expected to be of lower impact. The frame remains unchanged, so loads mainly affecting the frame will not present different results.

The first-order analysis results present no problems for the design, and the deformations and stresses found are similar to the results from the first-order calculation in the EWH simulation. The most prominent difference between the two is that the stiffeners in the plate give extra reinforcement to the plate, which works as a stiffened plate field under bending as seen in chapter 4. For further reference see figure N.1.

In figure 6.14 the first buckling mode and the equivalent stress are presented respectively. The lowest buckling modes are all of a similar shape, where the buckles are formed in the middle plate of the gate model. The stiffeners prevent the forming of buckles in the vertical direction as was found in the unstiffened model earlier in this chapter. The stresses in the Von Mises stress do not exceed the yield stress limit.

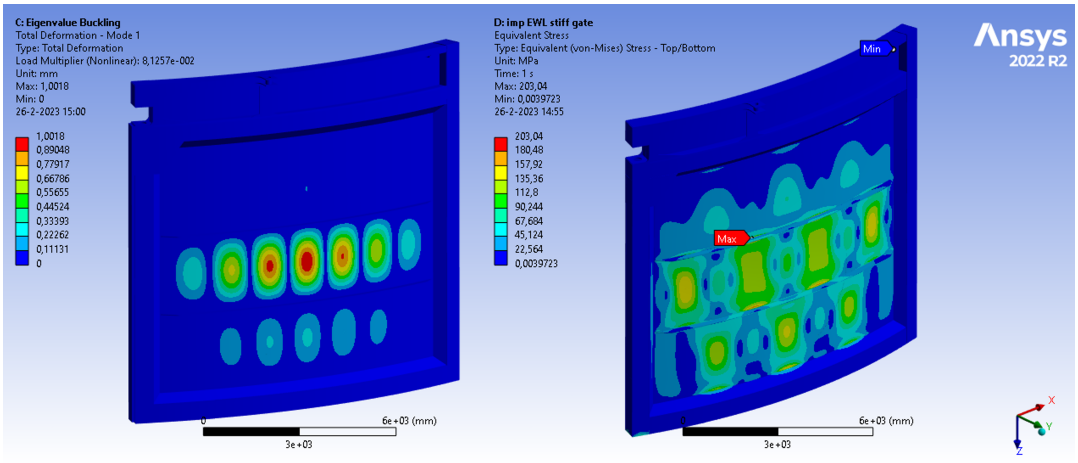

Figure 6.14: Deformations and equivalent stress of mitre gate with 14 mm plate.

The deformations are found mainly on the same spots where the buckling mode presents the buckles. The direction of the deformation is equal to the load and forms small buckles in the counter direction in between the larger deformed buckles (see Figure N.2). To determine whether the stiffeners in the model are simulated correctly, the stresses in the vertical direction of the plate have to be inspected. The vertical stresses are semi-consistent, as presented on the left in figure 6.15. Higher stresses can be found at the edges of the large deformations. This conforms to expectations based on previous load combination results. Stresses form at the point where the plate is prevented from rotating, as the stiffener will take up bending forces which are translated into stresses in the transverse direction of the stiffener. This effect can be seen on the right in figure 6.15. As in the model the stiffener also prevents rotation and takes up bending forces the modelling is correct. On the other side of the stiffener, opposite from the stress peak on the plate, the stress peak will not be present because there is no deformation on the plate at that side (see figure N.2). The vertical stress of the plate is equal to the stress on its opposite side at the areas where no large deformations are found in the plate. In these areas, the stiffener should have equal vertical stress on the top and bottom to be in balance. This process is observed in multiple spots on the plate.

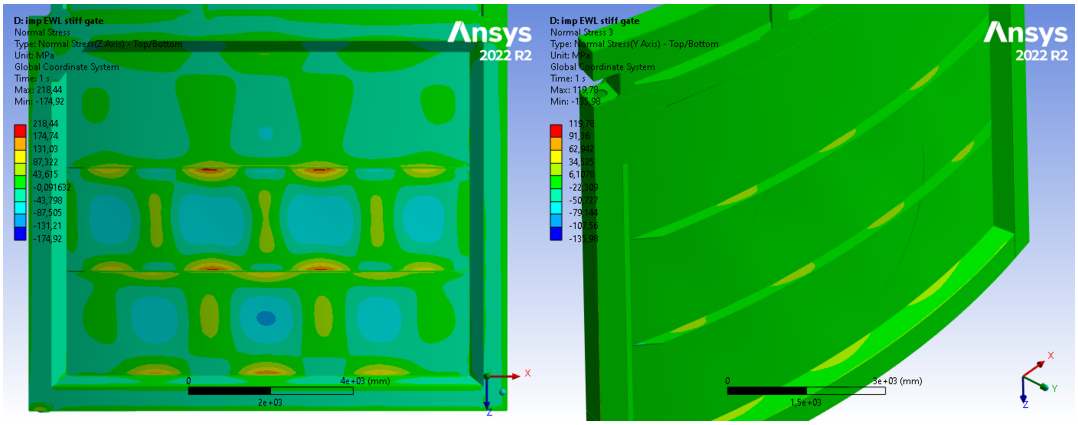

Figure 6.15: Stresses in the plane and vertical stress in the plate for the model with 14 mm plate.

The thinner plate was not tested for fatigue situations, as the stress in the extreme case that was simulated is lower than the stress in the plate that was found in the weld locations from the unstiffened design. It is, however possible that the fatigue stresses are lower for this stiffened design if the effects of the loads are interpolated. A definitive answer to the height of the stresses is possible but will not be further calculated for this thesis.

6.3.1.1. Thinner plates

Since the design is not at the elastic limit of the material a further iteration was alos performed. The results became more complex to work with due to the difference in the buckling shapes of the lower modes. A prestudy was done on this matter to see if the results would lead somewhere, the results are given in the appendix N.

6.3.1.2. Weight of construction

To determine the weight of construction the same method is used before in this chapter. The weight of the construction with stiffeners is 367 kN. The buoyancy is equal to the unstiffened design and will be 90 kN for the lowest and 104 kN for the highest water level. This result is given in figure M.42. The critical weight on the sub-structure is 277 kN, which is below the limit that has been prescribed in chapter 2.

6.3.1.3. Leaking of the buoyancy tanks

There is a possibility that a buoyancy tank will fill itself with water due to an unforeseen construction issue. It is, therefore, essential for this construction that the size of the buoyancy tanks is not larger than 23 kN of buoyancy. This is feasible for the boxed frame stiffeners if the length of a compartment of buoyancy is no longer than 7 meters long. This is more than half of the span of the gate. It is advisable to make these compartments half the frame's length to ensure the impact is low enough when the air tanks start leaking. These added plates in the construction would have to be inspected for fatigue as these welds fall in detail category 71 or 80.

6.3.2. Welding length for the stiffened design

The total welding length has been calculated for this design and resulted in 459.91 meters of welds. The average plate thickness to determine the approximated weld is 21.85 mm, leading to a total weld volume of $0.0664m^3$. The calculation can be found in the appendix in figure N.6. It is lower than the initial design as the plate thickness of the long welds in the main plate are much thinner.

6.4. Summary on gate design

Based on the found results it can be concluded that the unstiffened design is possible with buckling as part of the deformation of the main plate. This is within elastic behaviour so the plate will return to its original form. All other load combinations were concluded to be within safety margins of the limit states.

Fatigue is not calculated using exact methods, but an approximation of the local stresses was performed and the detail types have been discussed. With the assessment performed to this level of detail, it could be concluded that based on the simulated fatigue steps there is no risk of fatigue in the structure.

Table 6.1: Unity check for applied load cases

	EWH	PL	IL	OBL	GIP	FAT	DefCl	BU_{cw}	BU_{fl}
Limit	418 MPa	418 MPa	418 MPa	241 MPa	418 MPa	197 MPa	40 mm	300 kN	412 kN
Result	367 MPa	328 MPa	378 MPa	217 MPa	403 MPa	186 MPa	15 mm	322 kN	104 kN
UC	0.76	0.68	0.90	0.90*	0.96	0.94**	0.34	1.07***	0.25

*Extra explanation is given on this result in the text.

** Fatigue stresses have to be further studied if the design is unchanged; mitigations for change in the design have been discussed in this chapter.

*** The buoyancy is not further designed for as this problem would be resolved by adding stiffeners in the final design.

6.4.1. Stiffened design

The plate thickness is reduced to 14 mm with the addition of two stiffeners. The stiffeners are 500 mm high and 13 mm thick. The unity checks for the simulations of this design can be seen in table 6.2.

Table 6.2: Unity check for applied load cases

	EWH	BU_{cw}	BU_{fl}
UC	0.48	0.92	0.28

6.5. Comparison of results

When comparing the results of the design concept to the traditional design, it is important to keep in mind that some essential differences in design were not taken into account for the thesis. This includes the levelling sluices and the walkway on the construction. The total weight of the IV design without these components was approximated to be 455 kN. The total weld length of the IV design was approximated to be 635.17 metres and had a total weld volume of $0.0469m^3$. The result of the thesis compared to the original design is presented in table 6.3. What is noticeable is that the thesis designs both can reduce the weight.

One aspect that has to be considered for the thesis design and the traditional design is the weld assembly. The original design was made with many components, which led to a larger total weld length. The design proposed in this thesis would result in a lower weld length, as can be seen in table 6.3. The total weld volume however would be bigger for the thesis design. Two aspects relevant to welding are however not reflected in these values: the accessibility of the weld location and whether the welds can be applied in a continuous process. When comparing the weld locations of the IV design to the weld locations in the thesis design, it can be concluded that the locations of the thesis design are more favourable as these segments are interrupted less. However, further research is needed to determine the exact effects of the weld locations.

Table 6.3: Weight and weld comparison for thesis designs and IV-design

	IV-design	Arched plate gate	Diff. to IV	Stiffened gate	Diff. to IV	Diff. to unstiffened
Weight $[kN]$	455	412	-9%	361	-21%	-12%
Weld length $[m]$	635,17	438,98	-31%	459,90	-28%	5%
Weld volume approximation $[m^3]$	0,0469	0,0725	55%	0,0664	42%	-8%

7

Discussion

This chapter aims to define how the results of the thesis can be interpreted and what can be achieved with the gained knowledge. All conclusions ans suggestions made from the results are also based on the knowledge found in the literature study. In order to discuss the results found in this study and enable them to be used more broadly, it is therefore relevant to highlight some of the themes found during the literature study.

7.1. Type of gate

The results found in this thesis have the possibility to be relevant to other structures as well, making them more widely applicable. However, there are also some limits to the model. Both of these will be discussed here.

7.1.1. Mitre gates

The results found in this thesis could benefit the design of other mitre gates as well. Some variations of the mitre gate will be discussed here.

Mitre gates with smaller gate spans could certainly benefit from the design method posed by this thesis. The frame can be of lesser format and will work more effectively over smaller spans. Larger gate spans would have to be further studied in order to find where the limit lies in the concept. It does however seem like some gate spans would be impossible due to the fan-out effect.

Locks which have to be completely renewed, meaning including the concrete structure, can profit from the renewed design. The radius used in the case study was not further optimised, but can be differentiated. The result in chapter 4 provided the insight to not over-dimension the gate to get a smaller radius; there might be a further reduction of buckle size in between the two dimensions tested. A parametric study could assist in investigating this by finding an optimal design based on a simulation of different combinations.

7.1.2. Rolling gate

The rolling gate is relatively difficult to inspect and therefore does not lend itself to stainless steel as a material. The arched shape of the gate can however be considered for the smaller application of rolling gates with spans similar to the one in this thesis. There are other hydrodynamic loads at play in rolling gate locks, such as the asymmetric hydrodynamic load around the gate. The effect of such loads will need to be simulated or calculated in order to predict the behaviour of the gate adequately.

7.1.3. Vertical lift gate

Stainless steel would be an interesting option for vertical lifting gates as they are moved in and out of the water regularly. This presents the possibility for frequent inspection of the gate but also for performing small maintenance in the form of cleaning, making these processes much easier than for the mitre gate type. This lock type is known to be expensive already due to other components than the gate, so it might not be the best option to reduce relative costs. Another issue is that the support system is not adjusted to transfer of loads in the perpendicular direction to the lock. This means the structure

might require a gate that can internally support the loads or extra systems allowing this transfer to the substructure.

7.2. Material applied

Stainless steel has been the driver for this thesis but the design concept it proposes can be of value to other materials as well. This same design concept could be feasible for (high-strength) carbon steel variants too, for example.

The higher modulus of elasticity of carbon steel presents more resistance to buckling, and will prevent buckling under lower loads. Next to the elasticity modulus, the safety factors used for carbon steel up to S460, as seen in NEN-EN1993-1-1, are more favourable than for stainless steel. This offers a direct advantage of the material of 10% in, for instance, the elastic limit of the material.

Lower-strength materials could also be potentially used for the design proposed in this thesis, but it will have to be further investigated whether the weight reduction will be in line with the design. If this is not the case, there might still be an advantage to be had when making use of the simplified construction and weld length reduction.

It needs to be mentioned that other characteristics of the material have not been taken into account in this discussion, as this could possibly affect the outcome of the advantage. This would need to be further investigated.

7.3. Operational conditions outside the case study scope

In this thesis, a series of loads has been chosen to represent the critical loads for the arched gate design. Some other load types will be expanded upon in the next sections.

First of all, it is important to mention that not all forces were taken into account in this thesis. For example, the 10% threshold which was used to exclude smaller forces has to be taken into consideration. Additionally, the elastic limit of the material is not fully reached, meaning that the forces which were left out of the scope would have room to have an effect as well. It can therefore not be guaranteed that the design will be sufficient if these loads would be included. These other loads are however not located at the same place as the loads which were taken into account, which means they will probably result in stresses on other locations than the critical locations found in the thesis. For lock gates, there is always a difference in load size for future gate designs due to environmental factors. The chosen loads represent the loads on mitre gates and the reduction is likely possible for many gates.

7.3.1. The weight of the structure

The weight of the construction without stiffeners is deemed too heavy for the sub-structure. This would only be the case for this case study as the limit of the weight on the substructure can be increased. The set limit is a result of the concrete and pintle which were already present in the project, and the client is not planning to replace them. If a completely new project would be set up, this would create a possibility to increase the weight tolerance on the sub-structure.

If the structure proves too heavy for the substructure, including the buoyancy, there is an option to interchange the mid-plate stiffeners used with hollow stiffeners, which would in turn contribute to buoyancy tanks. Boxed girders can take up the same function as simple stiffeners and be fitted between the arched plates. The stiffeners would add extra height in between the plates, which should not present any problems. The size of the stiffeners can be determined based on the size of the required buoyancy tanks. Additionally, there is also an option to adjust the dimensions of the frame members to add or reduce buoyancy.

7.3.2. Water heads closer to Dutch average

The Dutch average water head was found to be at 3.98 meters, which is relatively large. Hoewever, the design is now tested for a rather small water head. Checking whether the concept would hold for larger heads can be simulated in a quick prediction.

The plate can be made thicker in order to increase the resistance of the plate, with the limit of the increased plate thickness being at the point where plates are no longer able to be formed adequately. When plates reach a thickness of 75 mm a reduction of strength occurs, indicating that the quality of the material is not guaranteed for larger plates.

Also quite relevant is a higher differential water head to the fatigue resistance. This effect is not further simulated but can be interpolated from the found results. The stresses found in the fatigue simulation during the post-buckling behaviour were relatively low in terms of fatigue. However, when the differential water head approaches the levels at the extreme water head, the stresses run up and surpass the level of fatigue. The unstiffened design is not able to withstand the extreme water head with the number of cycles that the gate will make in its lifetime. The stiffened design has lower stresses at the stiffeners than the unstiffened design. The detail category is the same so it can be expected that fatigue will not be more critical for the stiffened design.

7.3.3. Sluices on the gate

Sluices in the gate were left out of the scope of this thesis. However, many locks do use this system as it is relatively cheap. The sluices add a load at the point where they are supported in the form of a line load on the plate. This needs to be transferred to the frame of the structure. In the traditional design, this transfer was done by stiffeners. The thesis design might achieve this in the same way but without the addition of vertical stiffeners. If the horizontal stiffeners can take up the sluice load, it might perform somewhat similarly to the line load from the ice loads. The size of the sluice loads is not studied, meaning it has to be calculated in order to predict the effectivity of this concept accurately.

There are also some possible alternatives to the sluice design. For example, there are options which include smaller sluices which could fit in the bottom frame member. These are small cylindrical valves which make it possible to level the water through the gate. It would have to be investigated whether the additional components do not interfere with the main functionality of the frame. Fatigue might also play a role in this, as there will be extra welds in a beam which was already not stress-free in the fatigue cycle.

Another alternative to the sluice design is a method already used on different sized gates, where the gate is positioned in a slightly opened position, creating a gap through which the water can flow. This does impose a new load type on the gate as there is flow around the ends of an opened mitre gate, which is supported only by the moving boundary conditions. This flow could also produce vibrations against which the arched concept with the frame has not been tested. The relatively flexible frame might not be resistant to this load type.

7.3.4. Incidental loads - ship collisions

The advantage of this arched gate, when compared to the membrane gate found in literature, is the fact that the arched gate's convex side is completely placed in the post, out of harms way. In contrast, the convex side of the membrane gate is positioned towards the middle of the lock, where it is not safely stored away from passing vessels. This already prevents collision in normal opened position situations.

The unstiffened gate is not expected to be very resilient to ship collisions. The incident type was however left out of the project's scope as the client of the case study had not witnessed any incident in their current gate life span. There is an advantage to the mitre gate type due to its shape. Research shows that ships tend to collide on one side of the lock, meaning the mite-shape of the gate allows the gates to open up with relatievly low resistance to the collision. The new, unstiffened design has a similar situation on the concave side of the gate. It has to be checked if the ultimate strain of the material is within limits for it not to break for this type of load. An indication for this would be that duplex is known to have a similar strain capacity as carbon steel [22].

Next to a gate's behaviour during a head-on collision, there are also lower impact gate incidents which are more common. The resilience of the gate in these situations is important as it has to be able to maintain its function for as long as possible. Smaller collisions will take effect like a point load, which is unfavourable for the arched plate. This could be solved by using timber cladding over the surface of the arched plate, but this would then take away the advantage of a clean surface for maintenance. Due to this complication it might be best to find a solution which would prevent the ships from coming close to the gate at all when the gate is in its closed position.

7.4. Manufacturing

Welding calculations of the construction were out of the scope of this thesis, but it was expected to increase due to the thickness of the plates at the welds. The type of weld being used might also have an impact on the complications of the welding process. The thesis design has relatively fewer and

longer weld segments which are, most of the time, in easily accessible positions. The accessibility of the weld positions is relevant as welding in hard positions is more complex during the assembly process, and requires welding to be done by experienced workers. A more easily accessible weld position could allow for a more straightforward/simplified or, for instance, automated welding process. This could benefit the design greatly in terms of manufacturing advantage.

The welding volume presented in this thesis is an approximation. Both for the traditional and the thesis design, this volume was approximated to give and indication for the possible outcome. It is a rough approximation as it is based on a full-strength weld on both sides of a plate, which is completely unoptimised and not based on the stresses found in the simulations. Next, the approximation was based on a double weld on two sides of the plate but due to the inability to reach all weld sides, this might be a double overestimation. This was done for both designs so the comparison would remain fair. Further calculations would need to be done before drawing any definitive conclusions.

In this thesis the assumption was made that the arched plate is not under pre-stress when in its shape. There is a possibility to work with a pre-tensioning of the plate in order to achieve advantageous stresses which might aid in the pre-tensioning of the plate. There might also be a possibility that the plate contains opposing stresses, which means that a negative effect might occur when the plate is not properly formed.

When making a simple approximation using methods found for deformations in beams [14], the plates could easily be bent in shape based on their self-weight. This means that the plate will not have to be formed into its shape, but can be positioned into its arch by simply supporting it in the desired shape and connecting it to the frame. This makes the manufacturing process much easier, and also makes forming the connection between the plates much simpler because there is a lower chance of misalignment.

The tolerances provided by construction manufacturers have to be taken into account as well when manufacturing the gate. Assembly lines have tolerances that allow them to divert from the design as was made in slight ways. The tolerances of the plate provided are based on measurements done for more regular-sized members. The imperfection for larger members, as used for this thesis, might not represent the right tolerances. At the same time the imperfections used for the GNIA have to be considered; these are based on regular structure types, as opposed to the irregular shapes used in this thesis.

7.5. Maintenance

The maintainability of the gate has not been quantified in this thesis, as such an aspect is hard to quantify. The result of the thesis however does present a construction design which is much less complex and exists out of fewer components. Additionally, the total surface of the construction is also likely to be reduced as there are fewer horizontal surfaces from troughs. These factors make the construction easier to inspect and also easier to reach the entire surface area in regular maintenance, which leaves less room for mistakes which could lead to corrosion, among other things.

7.6. Life cycle costing

The life cycle cost of the construction was left out of the scope of this thesis. There is always a driving force from the civil industry to create a cost-optimal solution for civil structures due to its (often purely) functional design. The project in Sweden did not seem to have taken extra measures to create a different construction based on material preferences. In the Netherlands, constructions must be of the most cost-optimal configuration in order to be chosen for execution.

There is a set of costs which has to be defined in order to know that the renewed design will have an advantage over the traditional gate design. Based purely on the material reduction of 20% and the weld length reduction of 30%, the new gate seems to have an advantage. The price of duplex can easily be more than four times that of carbon steel, which is not made up for by the material reduction. Other factors like the costs of welding, accessibility of the construction, absence of conservation and pacifying of stainless steel are not defined and would have to be part of the sum for construction costs. The advantages of the thesis result are evident but not yet quantified enough to uphold a competitive position. The literature does provide some examples of a similar quantification, but these cannot be used to accurately quantify the structure proposed by this thesis.

8

Conclusion

The last chapter of this thesis will be discussing the conclusions regarding the main question and sub-questions. First, the sub-questions will be answered in order of introduction in the thesis. Following these conclusions the main question of this thesis will be answered, followed by an evaluation of the study and recommendations for further research.

8.1. Conclusion

The first sub-question this thesis presented and tried to answer was as follows:

What are the design considerations and requirements for a compressed arch gate construction of stainless steel?

The operational conditions of locks have been evaluated and a set of conditions was defined that have a likeliness of being critical for the arched lock design. How critical they were was defined by size, loading of a specific part of a construction and repetitiveness or opposing effect to the uniform load system of a lock. Lock Veere, chosen as a case study, has a unique set of loading conditions that was determined in order to assess the thesis quantitatively. A more slender construction due to the higher material strength is accompanied with stability issues and higher stresses for fatigue loading, and should both be critically evaluated.

Based on the studied literature, duplex stainless steel type 1.4462 was chosen for this case study because of its corrosive capacity in marine environments and its favourable mechanical properties. Its mechanical limits were defined for the ultimate limit state. The serviceability limit state has been defined based on the allowances set by the practical limits of mitre gates and the environment of the case study. An approximation was made for the fatigue limit state. In addition, stainless steel has several design preferences that must be implemented in order to reduce the chance of corrosion.

To what extent can an arched plate be considered feasible for optimising mitre gate constructions and what is minimally required in case it is not?

Based on the uniform water load which is dominant in lock gates, arched plates can be considered feasible for application in mitre gates. However, as the second dominant load is a point load with asymmetric supports, the plate alone is not enough. A surrounding frame has to be combined with the plate for it to be able to withstand this second load. Both components were optimised with different design possibilities and were considered to be feasible. They were also concluded to be even further optimisable based on the material use and the amount of material used compared to the traditional design.

To what extent is it possible to optimise the arched gate based on critical operational conditions?

A complete gate was designed using the components investigated in part two of this thesis. The gate

design was kept as simple as possible to meet the demands imposed by stainless steel. For example, these demands include a relatively empty surface with few components for assembly and maintainability. Next to that, a reduction of horizontal surfaces was achieved with diagonal members that at the same time add structural stiffness to the connection of the frame and plate. Lock gate components like hinges and seals were included in the design to simulate more realistic conditions.

The complete gate design was based on the critical conditions defined in part one of this thesis, and was then simulated with FEA to check the limit of the construction. The arched plate without any additions was reduced to a thickness of 22 mm based on the loads used in this thesis. When the plate was optimised with stiffeners in between plate components the plate was able to be reduced to a thickness of 14 mm with the addition of 13 mm stiffeners. This result was still conservative as material limits were not approached. The gate can be reduced by 21% of material weight and 28% of weld length with approximately a fifth of the number of weld segments when compared to the traditional design. In an approximation, the total weld volume is however expected to increase due to thicker plates at the weld locations.

These answers to the subquestions presented above support the answer to the main question, which will be presented here.

How can arch shapes be effectively optimised for stainless steel Dutch mitre gates?

Based on the input and results found in this thesis, it can be concluded that global arch shape can be used for the implementation of stainless steel in mitre gates. This is based on material and weld reduction in the construction while still maintaining a simple construction. It is important to consider that while total weld length is reduced, the total weld volume is expected to increase due to plate thickness. In addition to weld length, stainless steel also demands other adjustments to be made to the structure such as a combination of corrosion chance reduction and structural stiffness while also maintaining an accessible surface. The global shape was thus able to contribute to the optimisation of stainless steel in Dutch mitre gates by reducing weight, weld length and component complexity.

The result of this thesis might be of more relevance to the application of steel like S460 in combination with the arch shape. Equal strength properties with better stability resistance, and better safety factors, could for example possibly result in an even more optimised construction. Design rules like the empty construction surface needed for stainless steel could also be beneficial for carbon steel and its maintenance. The arch shape that led to a lighter construction in combination with reduced weld length presents an advantage for mitre gates constructed out of other material types too.

8.2. Evaluation

In the next section several shortcomings of this thesis will be commented on in order to demonstrate what some possibly critical points of this thesis are.

- This thesis does not include levelling sluices or a walkway in its design. If these were to be included they could affected the end result used for the comparison. As the addition of sluices would have interfered with the results of the main plate too much, it was decided to leave them out of the scope of this thesis. Although compensations were made for leaving them out, the exact effect the sluices would have had on the design cannot be qantified. The walkway did not seem to have any substantial influence on the structure and was left out based on the limited time availability.
- The calculation methods presented in the Eurocode were set up with the goal of creating structures that are in line with the ideas worked with in the Eurocode. This thesis had the aim to innovate the structural sector, meaning the design itself is also innovative. It can however be questioned whether the methods provided in the Eurocode are of relevance and accurate proportions for an innovative design.
- GMNA (plastic analysis) for the obstacle load of the structure was not performed. The effect of the stresses was assumed to be low but results from a plastic analysis could possibly have led to further plastic deformation of the frame than was assumed. In the traditional design, the dimensions for the bottom stiffener were of lower thickness as well, but the comparison is not

completely valid due to the rest of the traditional construction being stiffer in general due to the stiffeners around the obstacle location.

- In the fatigue approximation, the fatigue stresses have been approximated based on the local stresses due to a lack of time. These stresses do not represent the exact stresses that could appear on the structure. Other methods can be used to more accurately determine the stresses in the structure like the hot-spot-stress method. These results would be definitive with regards to the true fatigue state of the structure.
- The weld calculation performed was based on an assumption of weld thicknesses and was not further supported by weld calculations due to time limitations. This resulted in an inaccurate and unoptimized result.

8.3. Recommendations

Based on the results found in this thesis there are several more subjects which should be investigated in further future study. Some possibilities for further research will be indicated here:

- In order to know where the limit lies with regards to the spans of the gate in this arch gate concept, further study using larger gate spans is necessary.
- Further study of the difference between stainless steel and carbon steel application can identify if the construction would have better odds of being competitive when making a cost comparison. At this moment there is a difference in the welding method of both constructions, but what the effect would be on manufacturing costs is yet to be determined.
- Further study on the effect of vibrations on this type of construction needs to be conducted. For instance, the addition of sluices might lead to vibrations due to water displacement. The effect of these vibrations on the arched plate needs to be investigated.
- The long-term resilience of stainless steel in harsh environments needs to be established in order to definitively make the material competitive.
- Further research might want to explore the accuracy of the Eurocode for constructions as designed in this thesis, as tolerances of constructions are generally not aimed for application as seen in this thesis.
- Further research should investige whether the frame of the construction can be further reduced, while still taking the local buckling of plates into account.
- The different gate mechanisms that have been considered could benefit from the result found by this thesis, but due to the difference in the support system the exact possibilities are yet to be investigated. The single leaf gate or lift gate that can withstand the horizontal reaction forces internally might be a solution for weight reduction, but this should be investigated by future studies.

Eurocodes & guidelines

Table 8.1: Eurocodes and guidelines

Code reference	
NEN-EN	1090-2
NEN-EN	1990:2021
NEN-EN	1993-1-1
NEN-EN	1993-1-4
NEN-EN	1993-1-5
NEN-EN	1993-1-6
NEN-EN	1993-1-7
NEN-EN	1993-1-9
RTD 1001	ROK

References

[1] Ansys-help. *SHELL181 Element Description*. 2018. URL: https://www.mm.bme.hu/~gyebro/files/ans_help_v182/ans_elem/Hlp_E_SHELL181.html.

[2] N.R. Baddoo. “Stainless steel in construction: A review of research, applications, challenges and opportunities”. In: *Journal of Constructional Steel Research* 64.11 (2008). International Stainless Steel Experts Seminar, pp. 1199–1206. ISSN: 0143-974X. DOI: https://doi.org/10.1016/j.jcsr.2008.07.011. URL: https://www.sciencedirect.com/science/article/pii/S0143974X08001831.

[3] Charles L Bretschneider. *Generation of wind waves over a shallow bottom*. Tech. rep. TEXAS A and M RESEARCH FOUNDATION COLLEGE STATION, 1954.

[4] Chris R Calladine. *Theory of shell structures*. Cambridge university press, 1983.

[5] Mike Clarke. “The history and replacement of lock gates”. In: *Proceedings of the Institution of Civil Engineers-Engineering History and Heritage* 167.1 (2014), pp. 10–21.

[6] Ryszard Daniel and Tim Paulus. *Lock gates and other closures in hydraulic projects*. Butterworth-Heinemann, 2018.

[7] Ryszard A Daniel. “Mitre gates in some recent lock projects in the Netherlands (Stemmtore in einigen neuen Schleusenanlagen in den Niederlanden)”. In: *Stahlbau* 69.12 (2000), pp. 952–964.

[8] H Fujii et al. “How to quantify the environmental profile of stainless steel”. In: *SETAC North America 26th annual meeting*. 2005.

[9] Leroy Gardner. “The use of stainless steel in structures”. In: *Progress in Structural Engineering and Materials* 7.2 (2005), pp. 45–55.

[10] GK Glass and NR Buenfeld. “Chloride-induced corrosion of steel in concrete”. In: *Progress in Structural Engineering and Materials* 2.4 (2000), pp. 448–458.

[11] Google. *Google maps Veerse meer*. 2023. URL: https://www.google.nl/maps/@51.5505069,3.7512668,11122m/data=!3m1!1e3.

[12] Robert Gunn. *Duplex stainless steels: microstructure, properties and applications*. Woodhead publishing, 1997.

[13] Harvey P Hack. “Evaluating galvanic corrosion”. In: *ASM International* 13 (2003), p. 563.

[14] Coenraad Hartsuijker and Johannes Wijnand Welleman. *Engineering Mechanics: Volume 2: Stresses, Strains, Displacements*. Vol. 2. Springer Science & Business Media, 2007.

[15] D.H. Kang and H.W. Lee. “Study of the correlation between pitting corrosion and the component ratio of the dual phase in duplex stainless steel welds”. In: *Corrosion Science* 74 (2013), pp. 396–407. ISSN: 0010-938X. DOI: https://doi.org/10.1016/j.corsci.2013.04.033. URL: https://www.sciencedirect.com/science/article/pii/S0010938X13001686.

[16] Margriet Kruse. “het ontwerpen van een sluisdeur in roestvast staal”. Delft University of Technology, 1998.

[17] Margriet Kruse. “Roestvasstaal voor constructive toepassingen”. Delft University of Technology, 1998.

[18] Walter Langedijk and Jan de Graaf. “Duplex steel segment gate Södertälje (Sweden)”. In: *ce/papers* 3.3-4 (2019), pp. 743–748. DOI: https://doi.org/10.1002/cepa.1129. eprint: https://onlinelibrary.wiley.com/doi/pdf/10.1002/cepa.1129. URL: https://onlinelibrary.wiley.com/doi/abs/10.1002/cepa.1129.

[19] Wei Bing Liu, Mamtimin Gheni, and Lie Yu. “Effect of mesh size of finite element analysis in modal analysis for periodic symmetric struts support”. In: *Key Engineering Materials*. Vol. 462. Trans Tech Publ. 2011, pp. 1008–1012.

[20] Michael F McGuire. *Stainless steels for design engineers*. Asm International, 2008.

[21] Binnenvaartbranchevereniging van Nederland. *Goedkeuring van de EU voor 22,5 miljoen euro steun aan vervoerssector*. 2022. URL: https://www.binnenvaart.nl/nieuws/544-goedkeuring-van-de-eu-voor-22-5-miljoen-euro-steun-aan-vervoerssector.

[22] Outokumpu. *Duplex stainless steels, Outokumpu Forta range datasheet*. 2023. URL: https://www.outokumpu.com/.

[23] GH PHIPPS et al. "DISCUSSION. ON THE STRENGTH OF LOCK GATES." In: *Minutes of the Proceedings of the Institution of Civil Engineers*. Vol. 31. 1871. Thomas Telford-ICE Virtual Library. 1871, pp. 339–357.

[24] Yunan Prawoto, K Ibrahim, and WB Wan Nik. "Effect of pH and chloride concentration on the corrosion of duplex stainless steel". In: *Arabian Journal for Science and Engineering* 34.2 (2009), p. 115.

[25] P. Ray. *Why does buckling occur in columns?* 2018. URL: https://www.quora.com/Why-does-buckling-occur-in-columns.

[26] Junuthula Narasimha Reddy. *Introduction to the finite element method*. McGraw-Hill Education, 2019.

[27] Rijkswaterstaat. *Dammen, sluizen en stuwen*. 2022. URL: https://www.rijkswaterstaat.nl/water/waterbeheer/bescherming-tegen-het-water/waterkeringen/dammen-sluizen-en-stuwen.

[28] Rijkswaterstaat. *Multi Water Werk sluis inventarisatie*. Tech. rep. Rijkswaterstaat, Jan. 2014.

[29] Rijkswaterstaat. *MultiWaterWerk*. 2015. URL: https://www.magazinesrijkswaterstaat.nl/zakelijkeninnovatie/2015/01/mww.

[30] Rijkswaterstaat. *Standaardisatie van sluisdeuren*. Tech. rep. Rijkswaterstaat, Mar. 2021.

[31] A. Romeijn. *Steel bridges Dictaat deel I*. Delft University of technology, 2006.

[32] Erik Schedin and Andy Backhouse. *Stainless steel composite bridge study– A summary of ARUP reports*. Tech. rep. Outokumpu, Feb. 2019.

[33] Zach Schulz, Paul Whitcraft, and Devin Wachowiak. "Availability and economics of using duplex stainless steels". In: *CORROSION 2014* (2014).

[34] Barbara Shaw and Robert Kelly. "What is corrosion?" In: *The Electrochemical Society Interface* 15.1 (2006), p. 24.

[35] Cyril Stanley Smith. "The discovery of carbon in steel". In: *Technology and culture* 5.2 (1964), pp. 149–175.

[36] Hongqing Song. *Engineering fluid mechanics*. Springer, 2018.

[37] Outokumpu Stainless. "How to weld type 2205 Code Plus Two® Duplex Stainless Steel". In: *Outokumpu Stainless, Inc* 425 (), pp. 60173–3218.

[38] Duplex steel and engineering company. *1.4462 Material*. 2023. URL: https://www.duplexplates.com/14462-stainless-steel-material-grade-supplier.html.

[39] PH Stainless Steel. "What is PH Stainless Steel–Definition". In: ().

[40] Tritonalloysinc. *BS EN 10025 S355 Structural Steel Sheet Supplier at reasonable rate, view S355 Steel Standard Plate Thickness*. 2023. URL: https://www.tritonalloysinc.com/s355-steel-plates.html.

[41] M Veendorp and J Niemijer. "Leidraad kunstwerken". In: *L15 DWW2003-059-isbn 9026955440* (2003).

[42] A Vrijburcht. "onderhoud van roestvast staal". In: *ISBN 90-369-3305-6* (2000).

[43] A Vrijburcht. "Ontwerpen van schutsluizen". In: *ISBN 90-369-3305-6* (2000).

[44] Bengt Wallén. "Corrosion of duplex stainless steels in seawater". In: *Avesta Corrosion Management and Application Engineering* (1998).

[45] F Walport, M Kucukler, and L Gardner. “Stability design of stainless steel structures”. In: *Journal of Structural Engineering* 148.1 (2022), p. 04021225.

[46] Qingchuan Wang et al. “A self-healing stainless steel: Role of nitrogen in eliminating detrimental effect of cold working on pitting corrosion resistance”. In: *Corrosion Science* 145 (2018), pp. 55–66.

[47] T Wilschut et al. “Similarity, modularity, and commonality analysis of navigation locks in the Netherlands”. In: *Journal of Infrastructure Systems* 25.1 (2019), p. 04018043.

[48] Warren C Young, Richard G Budynas, and Ali M Sadegh. *Roark’s formulas for stress and strain*. McGraw-Hill Education, 2012.

[49] Zeeuwsarchief. *Kanaal door Walcheren en sluisregisters Veere*. 2013. URL: https://www.zeeuwsarchief.nl/blog/kanaal-door-walcheren-en-sluisregisters-veere/.

A

General loads of locks

Hydraulic loads Figure A.1 presents the main loading types that are present in lock gates. It states that these are the main loads and are part of its main function. Other loads facilitate this function, such as gate drive loads and self-weight is part of its main function.

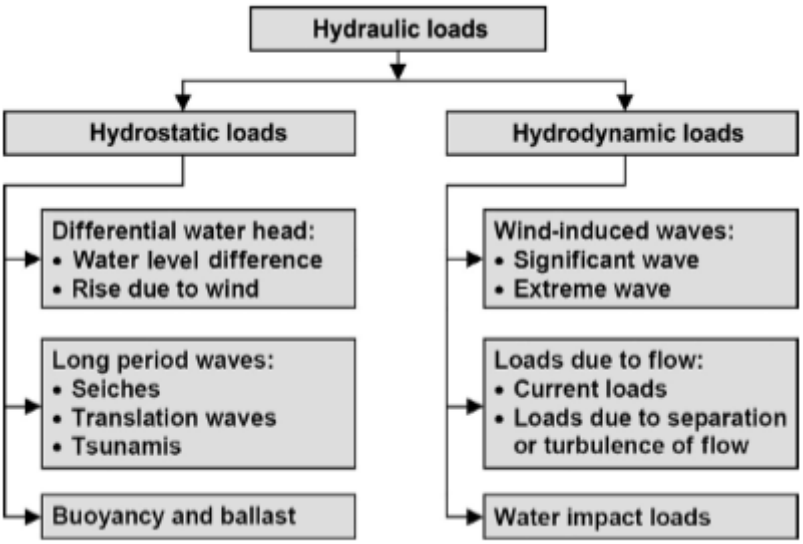

Figure A.1: Hydraulic load types

Based on the register from Rijkswaterstaat [28] the average water head in locations where locks are applied in the Netherlands lies at 3.98 metres. This number is based on data from 127 gates in 54 different locations.

Selfweight loads In all structures the self-weight of the material needs to be taken into account. In locks, this self-weight can increase over time due to the natural growth of marine life. How the self-weight is distributed is important for the way the structure loads the supports. The centre of gravity can determine if a gate wants to deform under minimal loading conditions in the form of sway, this is especially present in mitre gates [6]. In many lock gates there is also space for ballast. In larger structures like ”Zeesluis IJmuiden”, ballast is used to increase the weight of the gate when it is at a standstill and reduced to lower loads when it is on the riding rail [6]. Ballast and buoyancy add forces to the locations where tanks are applied and have to be taken into account when designing the structure.

Loads from gate drive systems There are loads which are imposed on the structure due to the driving mechanism that opens and closes the gate. This force is also present when the lock is in

its unmoving condition to prevent water movement from moving the gate. The mechanism itself can consist of multiple machinery types such as gear + arm (Panama canal linkage or Ohio river linkage), rack + pinion or a hydraulic pump (direct or indirect). It is usually seen as a point load on a gate.

When the gate is being moved, the initial load on the gates should always be as low as possible. Once the gate is in motion the force can be increased. Whether there are any additional forces occurring on the gate due to movement, can be discovered through testing over the years. Some of these conclusions that were drawn through continuous testing are:

- Increased submergence and speed result in increased hydraulic forces.
- Closing forces (going into the static closed system) are bigger than opening forces (going into recess).
- Hydraulic resistance increases as the bottom clearance of the door is decreased (since less water can travel under the door)
- Hydraulic resistance increases when the length of the lock chamber is increased.
- Asynchronous opening of the gates results in lower peak torque.

Variable walk, vehicle and service loads In case there is a need for traffic to cross the lock it can be considered to include a traffic lane on top of the gate, on the condition that the traffic is of a low intensity. ”Zeesluis IJmuiden” is an example of a gate on which traffic is possible. Many other gates only allow for foot traffic, see for example the ”Sluizen van Vlissingen”. The advantage of having a traffic lane on the lock is that there is no need for a bridge like had to be done at the new lock at Terneuzen. When designing, the codes that apply to bridges as this loading occurs need to be kept in mind.

Sediment, ice and vertical loads The most frequently found issues in gate locks due to sediment or marine life is listed below:

- Global increase of gate weight
- Local increase of component mass
- Silting up of water inlets, outlets or clearances for operation
- Increase of wear in details
- Attracting plant growth, mosses, bacteria, vegetation
- Accelerated corrosion

Ice will behave similarly to sediment, but it will not contribute to the self-weight. Instead, the self-weight will slightly decrease as ice is less heavy per volume than water.

If ice forms in the lock there is a possibility that it gets pushed against the gate, which is a force on the construction. There can be glaze ice that is formed by freezing ice that is from splash and leaking fluids. When ice is forming there is a process of expansion which puts pressure in the horizontal direction

Loads from ships and floating objects Vessels that pass the lock bring different types of loading situations with them [43]. For usual loads this includes; loads from propellers, waves from passing ships and loads by floating debris. For unusual loads this includes: ship collisions that cause damage but no operational loss of gate, sunk, or otherwise failed vessels obstructing the gate movement. And for extreme loads this includes: ship collisions that cause damage and operational loss of gate or large uncontrollable floating objects carried by floodwaters.

In the Netherlands, Rijkswaterstaat tries to minimise the risk of collision as proactively as possible, but due to the intensive use of the Dutch waterways, the probability of a collision remains high. Therefore the preferred measures include applying fenders on gates and providing spare gates on location in case of a severe collision. When the gate is opened, it needs to be withheld in its post substantially. A last measure is to minimise the consequences of a collision with a gate. This is for example done by allowing for a gate to be compromised but making sure that if that happens the supports remain intact.

Loads from system malfunctioning The driving mechanism to open and close the gate is operated through a system. This system, like any other system, can malfunction. One of the possible consequences of such a malfunction is the driving force becoming larger than its usual size. This error thus can put loads on the gate when it is in an opened or closed position and is an irregular force on the structure based on format.

It is also possible for an obstacle to get stuck between the gate and its opened or closed position. Since locks are moving structures there are multiple places and setups in which this can happen. During the presence of the obstacle, the driving mechanism will not immediately be alerted of the obstacle and will continue to increase the load until the driver can be stopped.

Transport and installation loads A gate has to be able to be transported and lifted into its position, meaning it has to be able to withstand several different types of forces. Transportation requires the gate to be stiff enough to be lifted by a crane, and that there are hoisting locations that will be loaded in the form of a point load. Lifting also requires the gate to be rotated, which can possibly be done while it is still underwater as well. When the gate is transported it needs to be able to be held up on supports and be able to withstand the impacts that can be present during transportation.

B

ROK load combinations

Figure B.1: ROK Load combinations and safety factors for closed lock layout

Tabel 5-8: Belastingscombinaties Keermiddelen gesloten

belastingcombinatie Belasting	**A**	**B**	**C**	**D**	**E**	**F**	**G**	**H**	**I**
Eigen gewicht (F0,F1,F2)	1,25	1,25	1,25	1,25	1,25	1,25	1,25	1,25	1,25
Max pos vervalbelasting (MHW) (F10) Windgolfbelasting bij MHW (F13)	1,5								
Max neg verval (F11) Windgolfbelasting bij max neg verval (F13)		1,5							
Vervalbelasting bij max schutpeil (F12) Windgolfbelasting bij max schutpeil (F13) translatiegolf bij max schutpeil (F15)			1,5	1,2	1,2	1,2	1,2	1,0	1,0
Verkeersbelasting /bordesbelasting (F16)	1,2	1,2	1,2	1,5	1,2	1,2	1,2	1,0	1,0
Windbelasting	1,65	1,65	0,5	0,5	0,5	0,5	0,5	0,5	0,5
Voorspankracht uit bew. Werk (F33)	1,2	1,2	1,2	1,2	1,2	1,2	1,2	1,0	1,0
Schroefstraal schip					1,5				
IJsdruk (F53)					0,8	1,5			
Krachtsopbouw langs de draaias; zie (1.9)							1,5		
Aanvaren deur (F54)								1,0	
Lekraken drijfkist (F55)									1,0

Figure B.2: ROK Incident loads

Tabel 5-9: Belastingscombinaties openen/sluiten keermiddelen

belastingcombinatie Belasting	**J**	**K**	**L**	**M**	**N**
Eigen gewicht (F0,F1,F2)	1,4	1,25	1,25	1,25	1,25
Belastingen uit het bew.werk	1)	1)	2)	3)	1)
Hydraulische belastingen tijdens bewegen + wind (restverval, windgolven. Translatiegolven, wind, golfweerstand e.d) (F13+F14 +F15+F20+F22+F23+F24)	4)	4)			4)
Massakrachten (keermiddel + water) (F21+F30+F31)	4)	4)	4)	4)	4)
Obstakels (F40)			1,25		
Ijsdruk / ijsgewicht (F53)		1,5			
Falen besturingssysteem				1,25	
Krachtsopbouw langs de draaias; zie (1.9)					1,5

C

Stainless steel

Tabel 14 — Technische kennis van het coördinatiepersoneel — Constructiekoolstofstaal [*]

EXC	Staal (staalgroep)	Referentienormen	Dikte (mm)		
			$t \leq 25$ [a]	$25 < t \leq 50$ [b]	$t > 50$
EXC2	S235 t/m S355 (1.1, 1.2, 1.4)	EN 10025-2, EN 10025-3, EN 10025-4, EN 10025-5, EN 10149-2, EN 10149-3, EN 10210-1, EN 10219-1	B	S	C [c]
	S420 t/m S700 (1.3, 2, 3)	EN 10025-3, EN 10025-4, EN 10025-6, EN 10149-2, EN 10149-3, EN 10210-1, EN 10219-1	S	C [d]	C
EXC3	S235 t/m S355 (1.1, 1.2, 1.4)	EN 10025-2, EN 10025-3, EN 10025-4, EN 10025-5, EN 10149-2, EN 10149-3, EN 10210-1, EN 10219-1	S	C	C
	S420 t/m S700 (1.3, 2, 3)	EN 10025-3, EN 10025-4, EN 10025-6, EN 10149-2, EN 10149-3, EN 10210-1, EN 10219-1	C	C	C
EXC4	Alle	Alle	C	C	C

Tabel 15 — Technische kennis van het coördinatiepersoneel — Roestvast staal

EXC	Staal (staalgroep)	Referentienormen	Dikte (mm)		
			$t \leq 25$	$25 \leq t \leq 50$	$t > 50$
EXC2	Austenitisch (8) Ferritisch (7.1)	EN 10088-4:2009, tabel 3 EN 10088-5:2009, tabel 4 EN 10296-2:2005, tabel 1 EN 10297-2:2005, tabel 2	B	S	C
	Austenitisch-ferritisch (10)	EN 10088-4:2009, tabel 4 EN 10088-5:2009, tabel 5 EN 10296-2:2005, tabel 1 EN 10297-2:2005, tabel 3	S	C	C
EXC3	Austenitisch (8) Ferritisch (7.1)	EN 10088-4:2009, tabel 3 EN 10088-5:2009, tabel 4 EN 10296-2:2005, tabel 1 EN 10297-2:2005, tabel 2	S	C	C
	Austenitisch-ferritisch (10)	EN 10088-4:2009, tabel 4 EN 10088-5:2009, tabel 5 EN 10296-2:2005, tabel 1 EN 10297-2:2005, tabel 3	C	C	C
EXC4	Alle	Alle	C	C	C

Figure C.1: Qualifications for welding of carbon steel and stainless steel.

Tabel A.1 — Voorgestelde roestvaste staalsoorten voor atmosferische toepassingen

Staal-soort volgens EN 10088	Type van omgeving en corrosiecategorie											
	Landelijk			Stedelijk			Industrieel			Zeelucht		
	Laag	Middel-matig	Hoog	Laag	Middel-matig	Hoog	Laag	Middel-matig	Hoog	Laag	Middel-matig	Hoog
1.4003 1.4016	Y[I]	X	X	Y[I]	X	X	X	X	X	X	X	X
1.4301 1.4311 1.4541 1.4318	Y	Y	Y	Y	Y	(Y)	(Y)	(Y)	X	Y	(Y)	X
1.4362 1.4401 1.4404 1.4406 1.4571	O	O	O	O	Y	Y	Y	Y	(Y)	Y	Y	(Y)
1.4439 1.4462 1.4529 1.4539	O	O	O	O	O	O	O	O	Y	O	O	Y

Corrosieomstandigheden:

Laag: Het minst corrosief voor dit type omgeving. Bijvoorbeeld gevallen met lage vochtigheid en lage temperaturen.

Middelmatig: Redelijk typisch voor dit type omgeving.

Hoog: Corrosie is waarschijnlijk hoger dan typisch voor dit type omgeving. Bijvoorbeeld hoger door blijvende hoge vochtigheid, hoge omgevingstemperaturen of bijzonder agressieve luchtverontreiniging.

Verklaring

O	Vanuit het oogpunt van corrosie mogelijk te hoog (overschatting).
Y	Waarschijnlijk de beste keuze met het oog op de corrosieweerstand en de kostprijs.
Y[I]	Uitsluitend voor binnentoepassingen. Het gebruik van ferritisch roestvast staal voor cosmetische toepassingen behoort te zijn vermeden.
X	Waarschijnlijk grote corrosie.
(Y)	Kan in overweging worden genomen op voorwaarde dat er geschikte voorzorgsmaatregelen worden getroffen. Dat wil zeggen er behoort een relatief glad oppervlak en en een regelmatige reiniging te zijn voorgeschreven.

Figure C.2: Type of material which is known to be effective in certain environments.

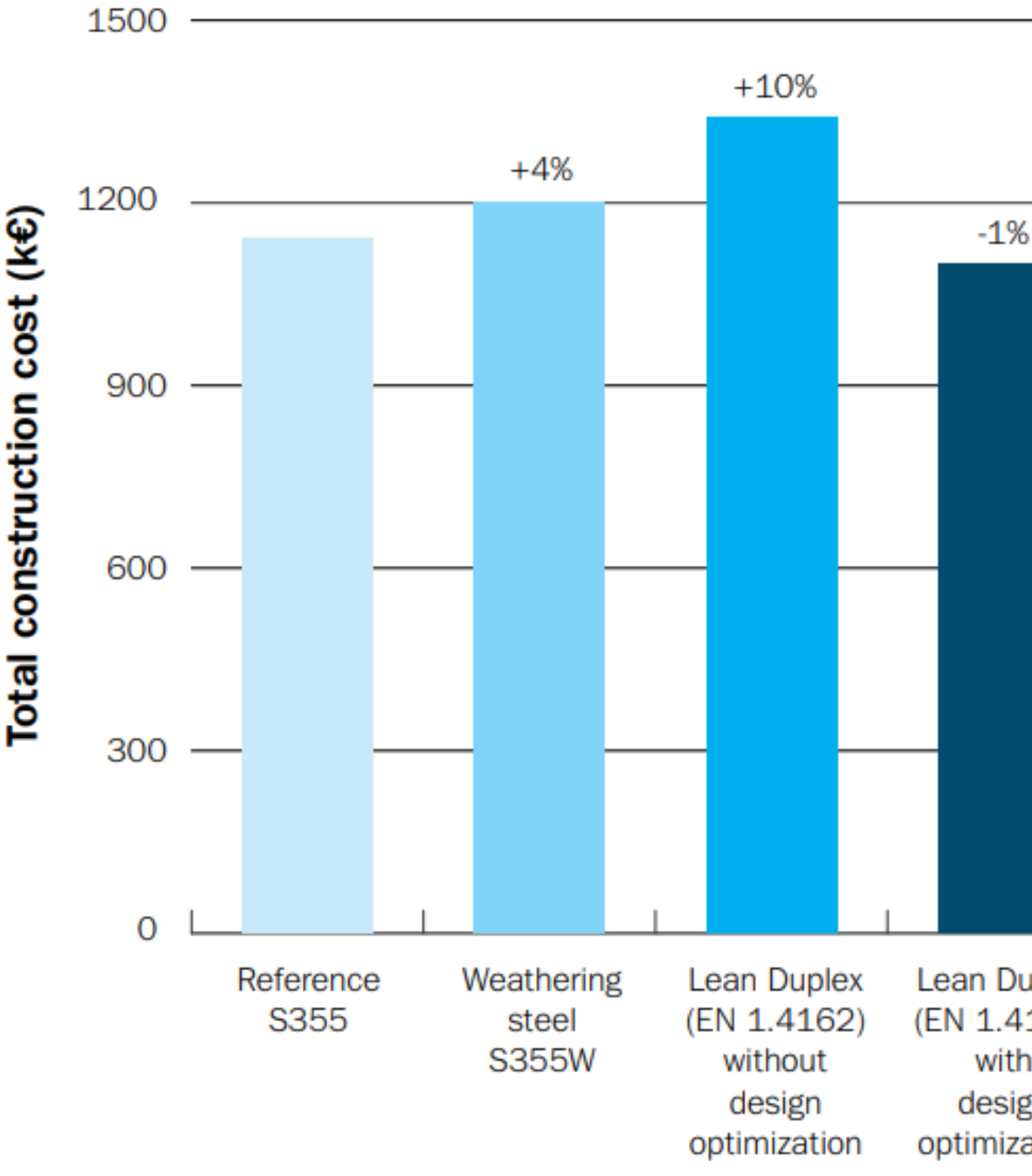

Figure C.3: Construction costs for bridge types [31]

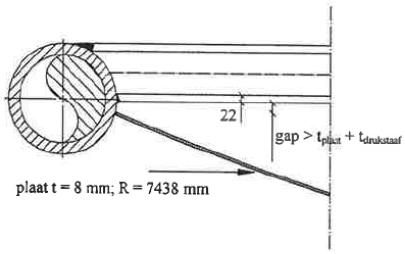

Figuur 8.13: Aansluiting elementen op achterhar.

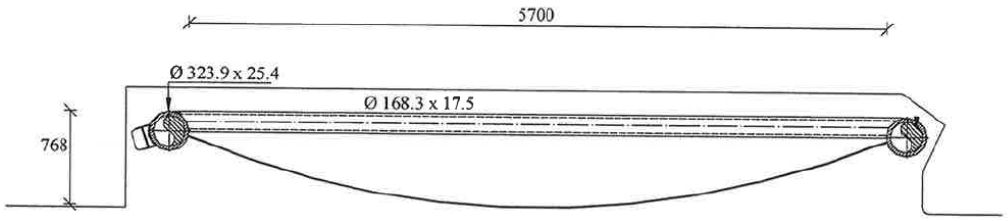

Figuur 8.14: Constructie hoogte.

Figure C.4: The membrane gate top view and detail [16]

D

Weld length of traditional design

welds	veere 2.0						
	height between hinges	10798					
	length along curve	11600					
	hoogte koker achter	400					
	aantal troggen	8					
	aantal lassen per trog	4	32	lengte van lassen		358400	
	aantal verticale verstijvers	6					
	aantal lassen per vert verstijver	2	12	lengte van lassen		129576	
	aantal lassen tussen huidplaten	3		lengte van lassen		33600	
	lassen rondom trog en ver verstijver			102400			
	aantal rondlassen door trog verstijver verbinding			64			
	aantal per trog			4			
	aantal per verstijver			2			
	lengte van een rond las	300	650	1600			
			totale las lengte			623976	mm
						623,976	m
			las volume is			0,55	x plaatdikte
			gemiddelde plaat dikte			15	mm
			lasdikte			8,25	
			weld area			34,03125	
			#welds per side			2	
			las volume			0,042469367	m^3

Figure D.1: Calculation of the weld length approximation of the traditional design by IV-infra

E

Force size

F0 F0 presents the self-weight of the construction, including an additional percentage to model the extra weight of welds and possible conservation material. Self-weight based on material properties and an added weight of 8% for welds bolts and conservation in the project of IV-infra. This estimation is rather conservative when considering [6], which indicates that a 1.5-2% of the total material weight should be added for account for welding weight. To account for the total material weight for welds and coating, another 3-5% can be added. IV based their value on a request of the client to be on the safe side with regard to the estimation. For the design concept, it was assumed that the total added weight for these materials is 2% for two reasons. First, no weight was added in terms of a conservation layer, which is on all top surfaces and is likely to be the largest segment of added weight. Secondly, the goal is to reduce the amount of welds for the design. Based on these factors, the assumed value for the added weight is 2%.

F1 F1 presents the buoyancy force, which depends on the local water level and the airtight compartments. This force will be added to the construction by a water load on the bottom of the structure. If a compartment is fully submerged, the top of the compartment will also be loaded, making it effectively only present on the volume of the compartment.

F2 F2 presents the weight of water and bio growth on the construction. This weight is not further taken into account, as this is comparable to the density of water meaning it does not effectively add any weight to the construction.

F10 $F10_{EWH}$ presents the extreme water heads that have been measured at the lock at Veere 0.4m - NAP and 1.1m + NAP. The ROK prescribes a robustness addition of 0.15m for water levels. The method used for calculating the water pressure on the bottom is presented in equation E.1. This equation was found in [36].

ρ = 1015 kg/m^3, The density of water.
g = 9.81 m/s^2 Gravitational force.
h = [m] The local height of the water level.

$$P = \rho * g * h \tag{E.1}$$

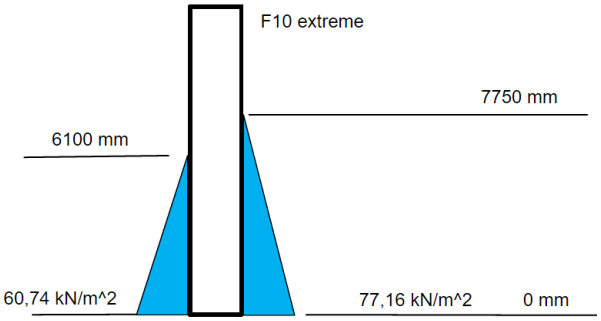

Figure E.1: F10 Extreme water head

F12 F12 there is a different water height for the regular water levels which has heights of NAP -0.3m and 0.9m + NAP. This is the differential water head and this is at a level of 6200 mm and 7400 mm.

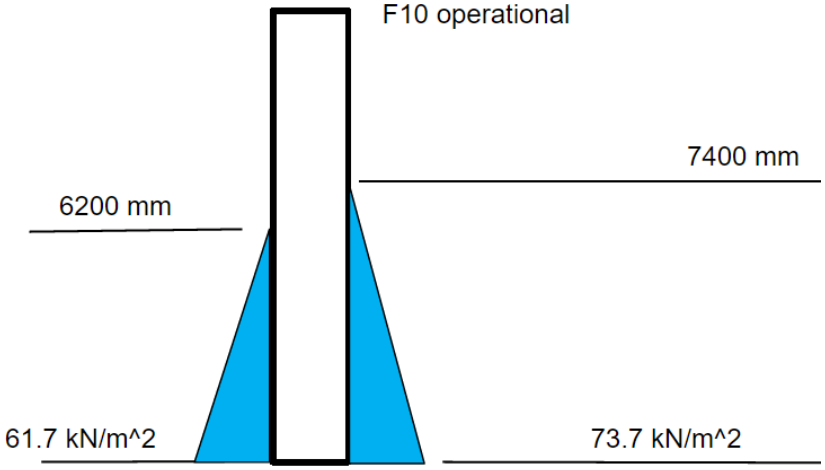

Figure E.2: F12 Differential water heads

F11 F11 represents the negative water level in the lock. This is however not relevant as the water level is always lower on the side of the lake because the lock functions as a one-sided barrier in which the high water is always on the same side. Therefore, negative water levels are not taken into account.

F13 $F13_{50}$ represents wave loading due to wind, to account for the extreme water head. This wave is calculated by IV-infra and has a reference period of 100 years. Max wind loading was calculated with a water level of 1.10m +NAP on the curved side. The wind wave was calculated according to Eurocode 1991-1-4 standards. The calculation for the wind speed can be seen here:

Figure E.5 presents the final result of this calculation. These results will be applied in this thesis.

v_b= basic wind speed, on 10m above land

c_{dir} = 1, wind direction factor

c_{season} = 1, season factor

$v_{b,0}$ = 27 m/s, fundamental value of basis wind speed (= 27 m/s for wind sector II)

$$\nu_b = c_{dir} * c_{season} * v_{b,0} = 27m/s \tag{E.2}$$

To compensate for the probability of the two actions at the same time, a factor for adjusted wind speed was calculated in equation E.3.

c_{prob} = A probability factor

K = 0,234, Shape parameter (= 0,234 for wind sector II)

p =0.01, Annual exceeding probability (= 1/reference period = 1/100 = 0,01)

n = 0.5, Exponent dependent on the wind sector the construction is in. (= 0,5 for wind sector II)

$$c_{prob} = \left(\frac{1 - K * ln(-ln(1-p))}{1 - K * ln(-ln(0.98)} \right)^n \tag{E.3}$$

To adjust the wind speed for the probability factor the equation E.4 is given to take the possibility of this speed actually presenting itself into account. This calculation is based on a height of 10 metres above the ground.

$$v_{b,prob} = c_{prob} * v_b = 28m/s \tag{E.4}$$

By using the Bretschneider formula [3] seen in equation E.5 the wave height can be determined.
h = 7.6 m, Water depth at the lock
f_L = 1.7 km, Length for wind wave creation, see figure E.3.

$$H_s = v_{b,prob}^2 * \frac{\left(0.283 * tanh(0.0125 * \frac{g * f_L}{v_{b,prob}^2}\right)^{0.42}}{g} = 0.94m \tag{E.5}$$

Figure E.3: The distance over which a wave can be built up in the canal [11]

The Goda formula can be used to express the wind wave as a water pressure [41]. The assigned values for the model can be found in figure E.4 and are determined by the formulas in E.11 E.12 E.13.

$\beta = 0°$ Angle of the wave with the normal direction of the gate
$\lambda_1 = 1, \lambda_2 = 1, \lambda_3 = 1$ Modification factors for a vertical plate
$H_d = 0.94m$ Governing wave height
$T_p = 4.26s$ Wave period
$L_d = 26.78m$ Wave length at construction
$L_0p = 28.33m$ Wave depth in free water
$D = 7.6m$ Water depth on top of the threshold
$h' = 7.6m$ Water level on the foundation layer
$h = 7.6m$ Total water depth in the canal
$h_c = 3.87$ Height difference between the waterline and top of the gate

$$\alpha_1 = 0.6 + 0.5 \left(\frac{4\pi h/L_d}{sinh(4\pi h/L_d)} \right)^2 \tag{E.6}$$

$$\alpha^* = \alpha_1 \tag{E.7}$$

$$\alpha_3 = 1 - (\frac{h'}{h}) \left(1 - \frac{1}{cosh(2\pi h/L_d)} \right) \tag{E.8}$$

$$\alpha_4 = 1 - \frac{h_c^*}{\eta^*}, h_c^* = min(\eta^*, h_c) \tag{E.9}$$

$$\eta* = 0.75(1 + cos(\beta))\lambda_1 H_d \tag{E.10}$$

$$p_1 = 0.5(1 + cos(\beta))(\lambda_1\alpha_1 + \lambda_2\alpha^* cos^2(\beta))\rho g H_d = 12.77 kN/m^2 \tag{E.11}$$

$$p_3 = \alpha_3 p_1 = 4.18 kN/m^2 \tag{E.12}$$

$$p_4 = \alpha_4 p_1 = 0 kN/m^2 \tag{E.13}$$

$$p_u = 0.5(1 + cos(\beta))\lambda_1\alpha_1\alpha_3\rho g H_d = 4.18 kN/m^2 \tag{E.14}$$

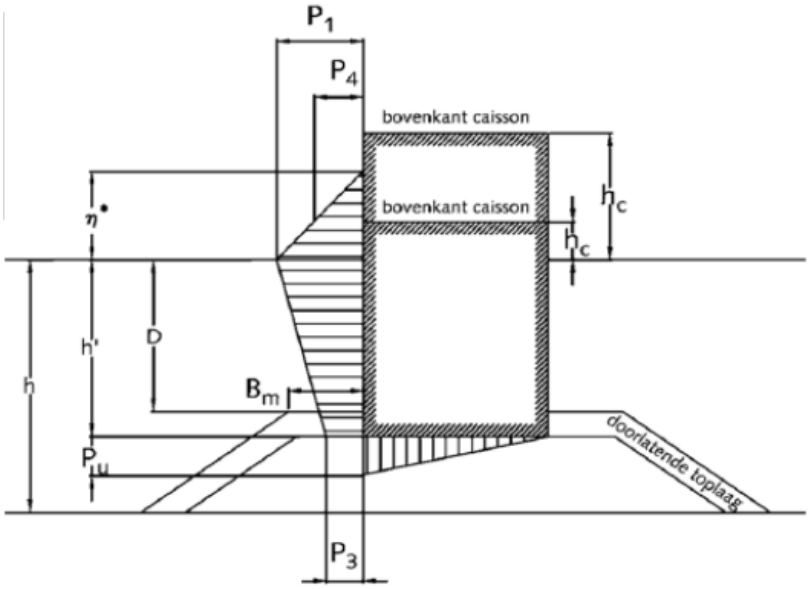

Figure E.4: Goda wave pressure model

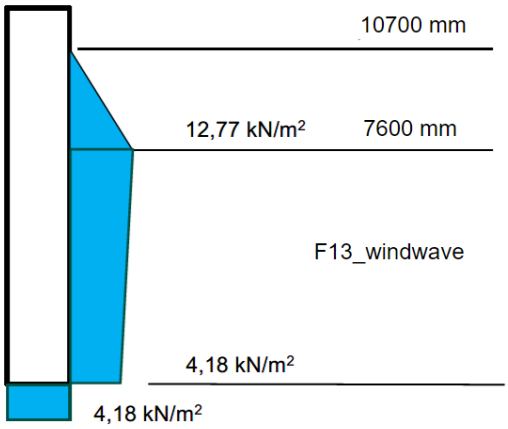

Figure E.5: F13/50 represents the wave load during an extreme water head for the 100-year reference period

F13_VOBB represents wave loading due to the wind, during the opening and closing of the gate. The value was calculated with the same method as $F13_{50}$. The waterlevel of the wave is at 7400 mm and the top of the wave is at 8750 mm. Appendix figure E.6 shows this visual representation.

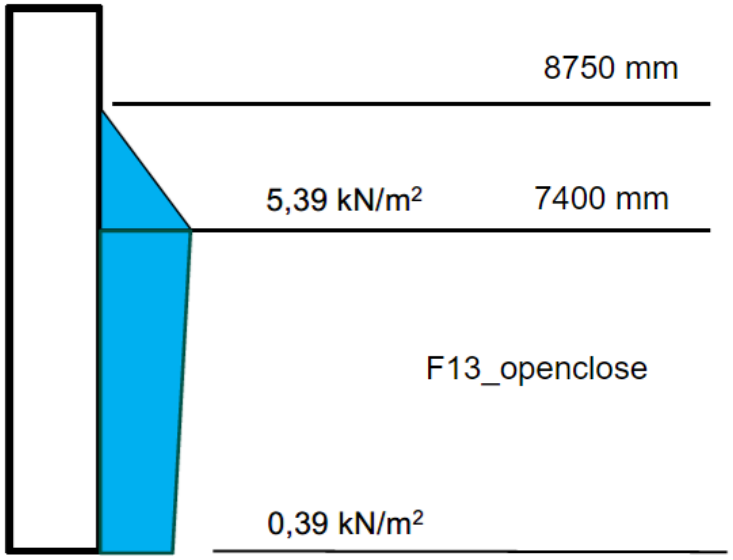

Figure E.6: F13 is the wind load that can act during the opening and closing of the gate

F14 F14 wind loading maximum level of water and during opening and closing.

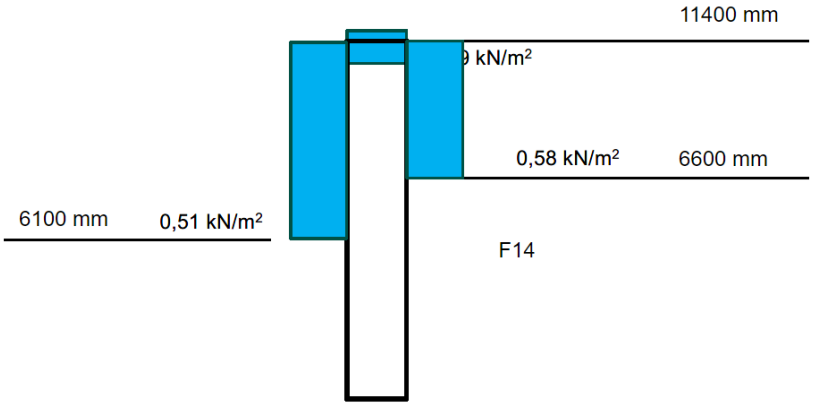

Figure E.7: F14 is the wind loading which can act during extreme water heads

F15 F15 translation wave that can originate from the lakeside of the gate. This is a load that is induced by for instance a passing ship in the lock next to the lock being considered for this thesis. The load is an increase of the water level on the concave side of the gate with a difference maximum 400 mm as prescribed by the ROK. For the case study in Veere the difference was set at a maximum of 150 mm based on measurements. This load has a positive effect in situations when there is a low water level on the concave side so an increase of the water level will only result in a lower resultant force. It will not be further considered.

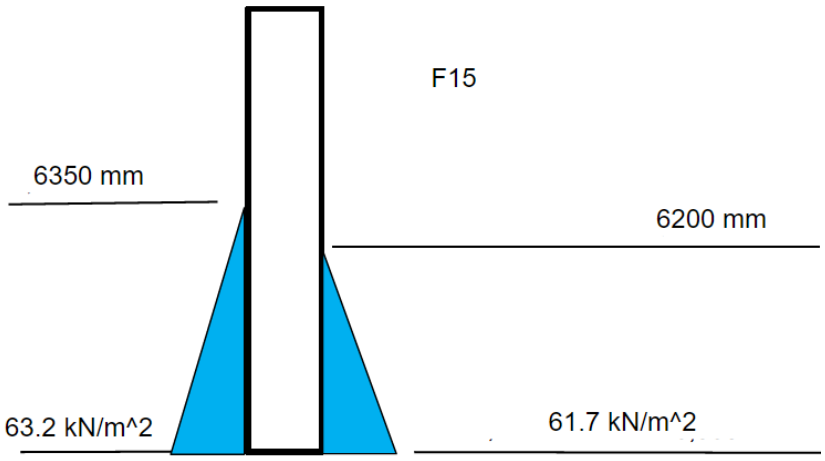

Figure E.8: F15 which can occur due to waves from the lake side

F16 F16 represents the traffic on the lock which can be present when the gate is closed. This traffic has a value of 5kN/m^3 and can be effective on the 1 meter walkway that is on top of the gate.

F17 $F17_{in}$ represents loading due to water traffic entering the lock. This load is a hydrostatic representation of the mass inertia of the water created by a moving vessel. The high water level is at 6670 mm and the low level is at 6200 mm.

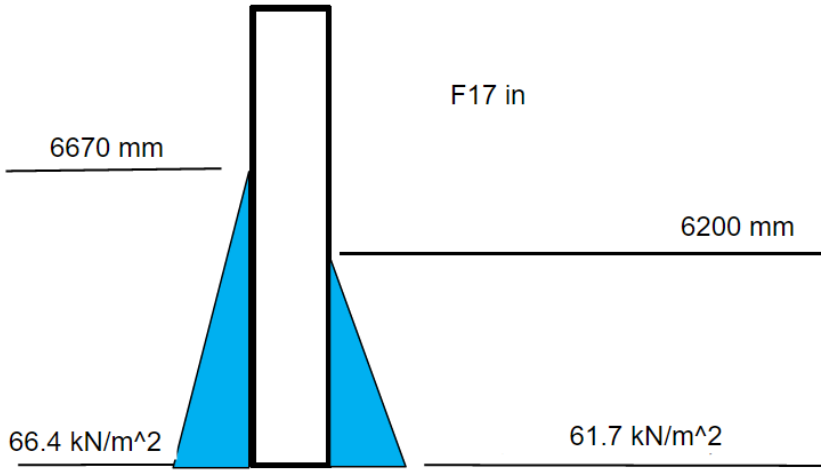

Figure E.9

$F17_{out}$ represents the loading when a vessel leaves the lock. The level is 5520 on the low side and 6200 on the high side.

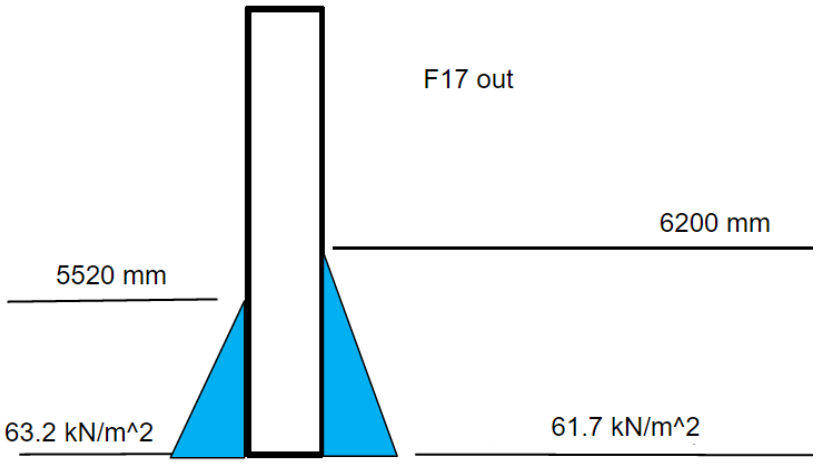

Figure E.10

F20 F20 represents the load which can come into existence due to a small water head when the gate is opened before the water is completely levelled. 6300 mm on the high side and 6200 mm on the low side.

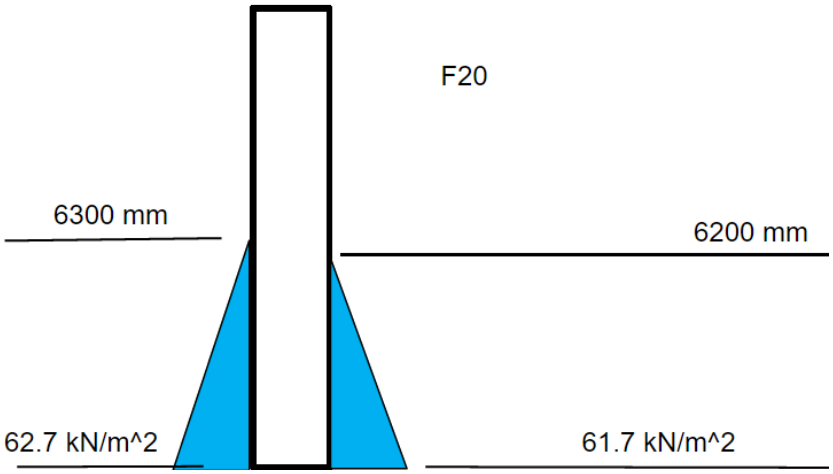

Figure E.11

F21 F21 represents the mass inertia of water while the gate moves. This is calculated using the formula E.15 and E.16. When the gate is moving there is a buildup of inertia that can be considered as a load when simulated as a static situation. This is expressed in terms of a moment around the axis of the lock.

M_a = Moment build-up around the rotation axis
a_a = added mass inertia around the rotation axis
$\frac{d^2\phi}{dt^2} = 0.0007 rad/s^2$ angular acceleration
a_h' = 0.63 Coefficient of added mass inertia in the horizontal area, this value is taken conservatively.
$\rho = 1015 kg/m^3$ Density of water
h_k = 7.7m Water level in the lock
z_d= 0 m Level of the bottom of the gate
l_d = 11.57m Gate length

$$a_a = \rho * a'_h * (h_k - z_d) * l_d^4 = 8.71 * 10^7 \tag{E.15}$$

$$M_a = a_a * \frac{d^2\phi}{dt^2} = 63kNm \tag{E.16}$$

If this moment is transformed to a force on the gate the total force is 11 kN over a depth of 6200 mm, this equals a pressure of approximately 0.00016 MPa.

F23 is the water buildup due to the movement of the gate. The situation can be created on both sides of the gate and the high level is 6400 mm and the low level is 6200 mm.

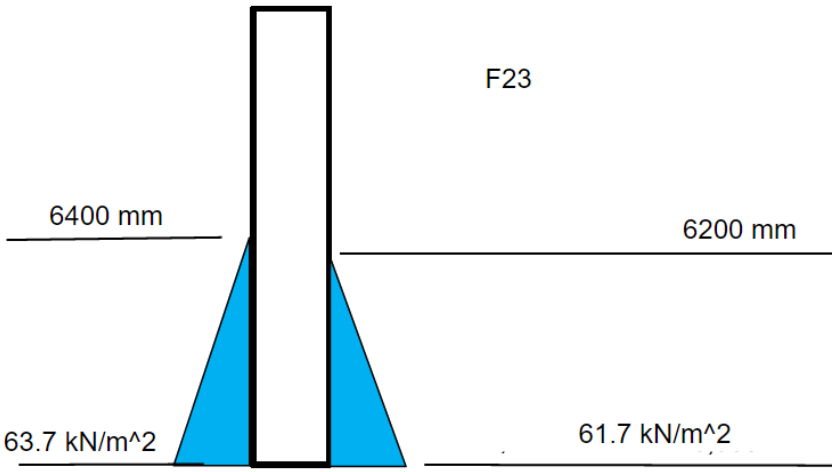

Figure E.12: F23 water buildup due to movement of the gate

F24 F24 water builds up in the gate post due to the movement of the gate when closing. The water level in the post is at 6240 mm while the level in the lock is at 6200 mm.

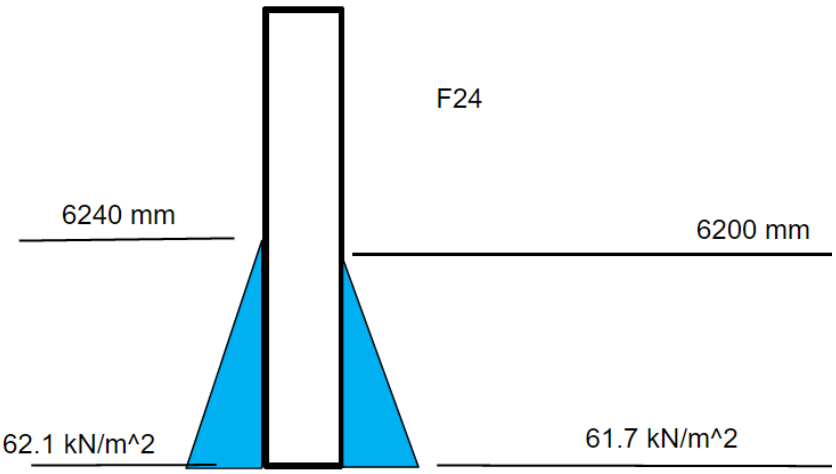

Figure E.13: F24 water resistance in the gatepost

F33 F33 represents loading due to the hydraulic cylinder mechanism. This mechanism creates the force that is put on the gate to open it. This force is located at the hookup point on the top beam of the gate. The force created is 137 kN when the gate is closed and 422 kN when it is in its opened position.

F38 F38 represents an equal high water level in which the water is at the highest possible level. When the water is at its highest level it sits at 7750 mm from the bottom of the gate. This water level is used to assess the flotation of the gate.

F39 F39 represents an equal low water level in which the water is at the lowest possible level. When the water is at its lowest level it sits at 6100 mm from the bottom of the gate. This water level is used to assess the deformation of the construction when closing the lock and the critical weight on the substructure.

F40 F40 represents the obstacle loading - incidental load that occurs due to the force build-up of the movement mechanism. The mechanism is not able to measure that there is an error in the system quickly enough. This causes a peak load in the hook-up point.

The maximum size of the force delivered by the driving system is 1641 kN. According to the ROK this force can be at a maximum of 80% during an incident situation. This 1312 kN is located on the hookup point. This force is set at an angle as the gate is in a position between being fully opened or closed. This direction can be seen in figure E.14

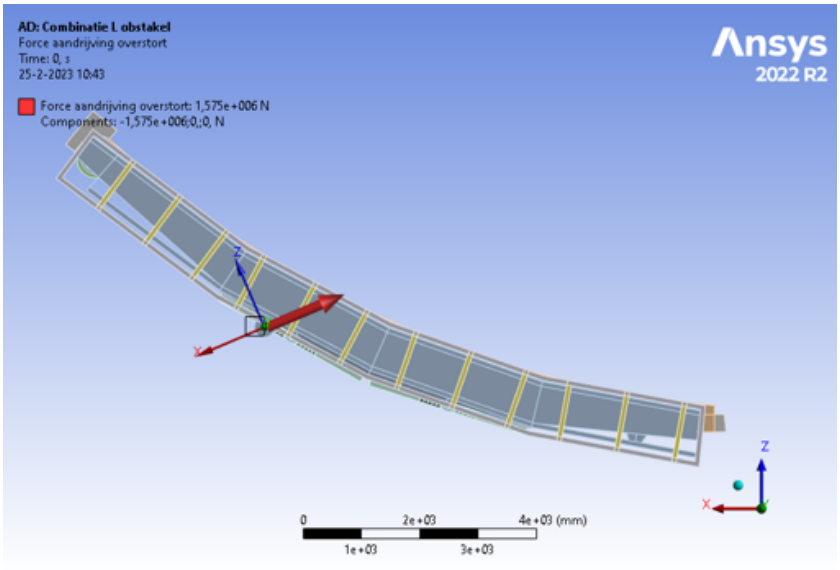

Figure E.14: F44 Obstacle load exerted by the driving mechanism.

F41 F41 represents the driving mechanism force that occurs during the opened position of the gate. The gate is pulled into its post, and the force is applied to ensure that the gate will not start to move in its post. The size of the force is 422kN.

F53 Iceload. The value of the ice load is prescribed by the ROK as $250kN/m^2$ over a height of 24 cm at the height of the differential water head.

F55 F55 represents a leakage in the buoyancy tanks - incidental load. This is assessed by leaving out the most critical air chamber in the lock. The load translates to an absence of an upward force.

F99 F99 represents loading due to the thrust of a propeller on a ship of the heaviest class that is allowed to pass through the lock. The load is present on a circular area with a diameter of 5m. The pressure that is created on the spot is 6.24 kN/m2

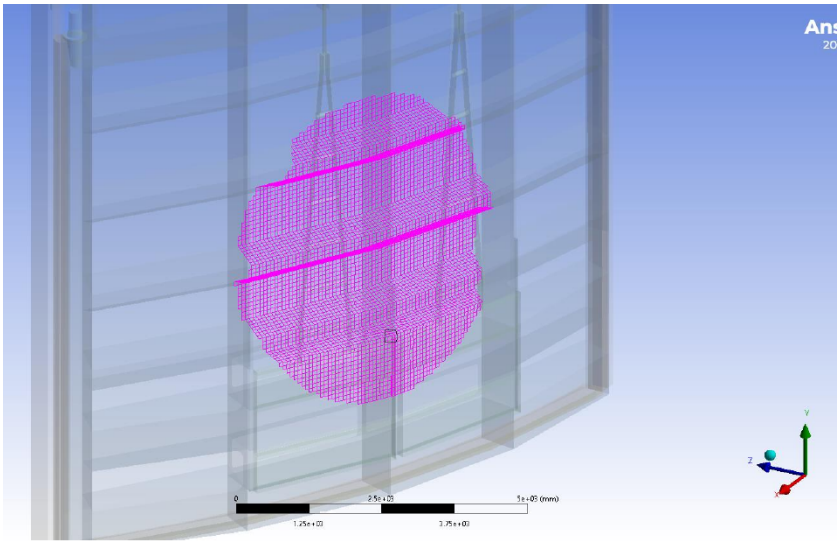

Figure E.15: The pressure load on the gate which will be created due to the propeller of a ship of class

F

Validation

F.1. Out of plane loading

F.1.1. Reaction force

The force reaction at the boundaries has to be equal to the force which is applied to the model. This is calculated by the analytical formula F.1 [14]. The visual results for the FEA are added for reference in appendix figure F.1. For the bending moments of a constrained beam at the support, the value is defined in the formula F.2.

$P = 0,016MPa$, Pressure
$L = 11400mm$, Length of the beam
$b = 9800mm$, Width of the plate

$$F_{vert,support} = P * L * b/2 \tag{F.1}$$

$$M_{support} = 1/12ql^2 \tag{F.2}$$

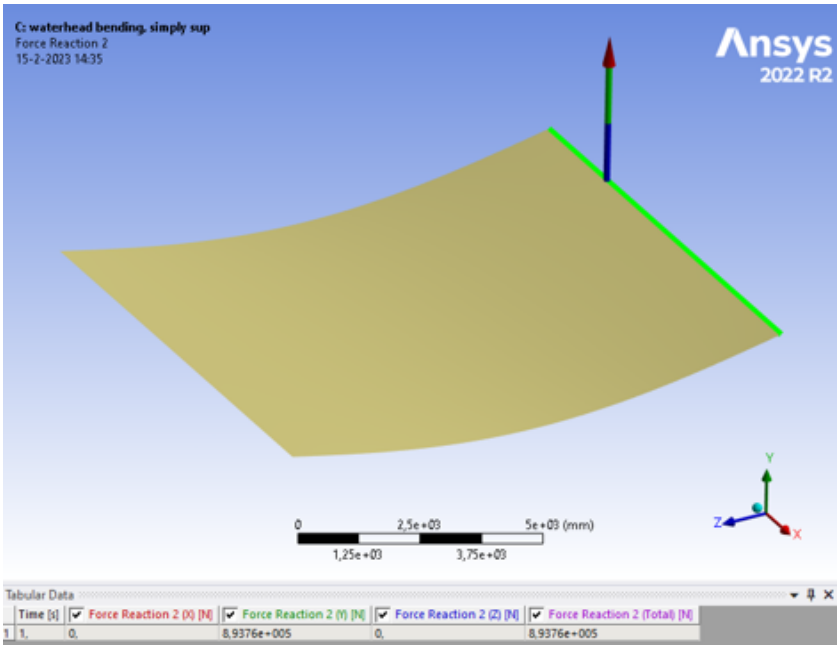

Figure F.1: Vertical support reactions of out of plane loading of plate.

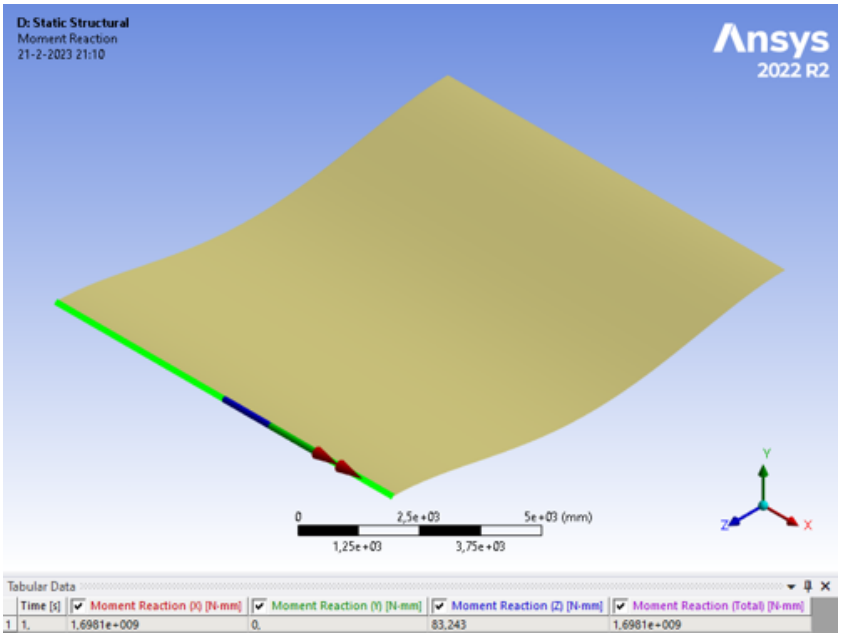

Figure F.2: Moment reaction at the support.

F.1.2. Deformations

The deformations of the plate due to the force are calculated in a linear elastic analysis (LA). The results of the deformations are given in figure F.3a and F.3b. Important is that the results are only comparable when the Poisson ratio is set to a value of 0. When the Poisson ratio is turned on there will be an extra effect on the free edges of the plate which have an added deformation effect due to the longitudinal stresses in the plate. The Poisson ratio will be turned off until this is desired. The effect is however important to take into accoutn later on as this is closer to real world behaviour. Further effects of the Poisson ratio will be discussed later. The appendix figures F.3a and F.3b in the appendix show the deformation of the plate in a visual representation.

The analytical method for the deformation can be found in literature. The formula F.3 gives this for simply supported beam and formula F.4 for the constrained beam [14].

$w =$, Deformation in the middle
$b = 9800mm$, Width of the plate
$q = b * P = 9800mm * 0.016MPa = 156N/mm$, Load over length
$L = 11400mm$, Length of the beam
$E = 200000MPa$, Elasticity modulus
$h = 40mm$, Thickness of the plate
$I = \frac{bh^3}{12}$, Moment of inertia

$$w_{hinged} = \frac{5qL^4}{384EI} \tag{F.3}$$

$$w_{constrained} = \frac{qL^4}{384EI} \tag{F.4}$$

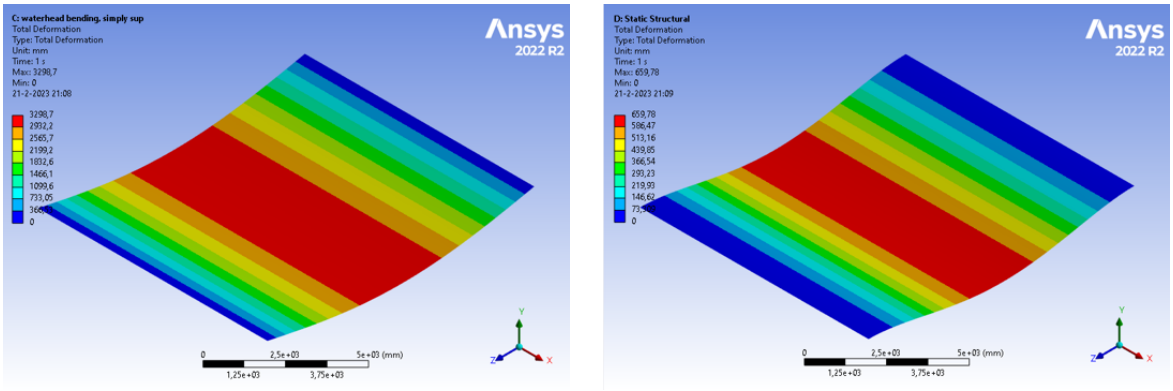

(a) Simply supported bending

(b) Constrained supported bending

Figure F.3: Deformation of plate with different boundary conditions

F.1.3. Stress in the plate

The model with constrained edges is used to inspect the stress in the middle of the plate which will be investigated. The bending moment in the middle of the beam is given by formula F.5.

$q = 156N/mm$, Load over length
$L = 11400mm$, Length of the beam

$$M_{mid} = 1/24q * L^2 \tag{F.5}$$

The result of Ansys will be given in stresses on top of the plate which need to be transformed to a bending moment. This is done with the help of the formula F.2.

$\sigma_{top} = 324MPa$ value from ansys,
$b = 9800mm$, Width of the plate
$h = 40mm$, Thickness of the plate

$$M_{bend} = \sigma_{top} * 0.5h * 2/3 * 0.5h * b \tag{F.6}$$

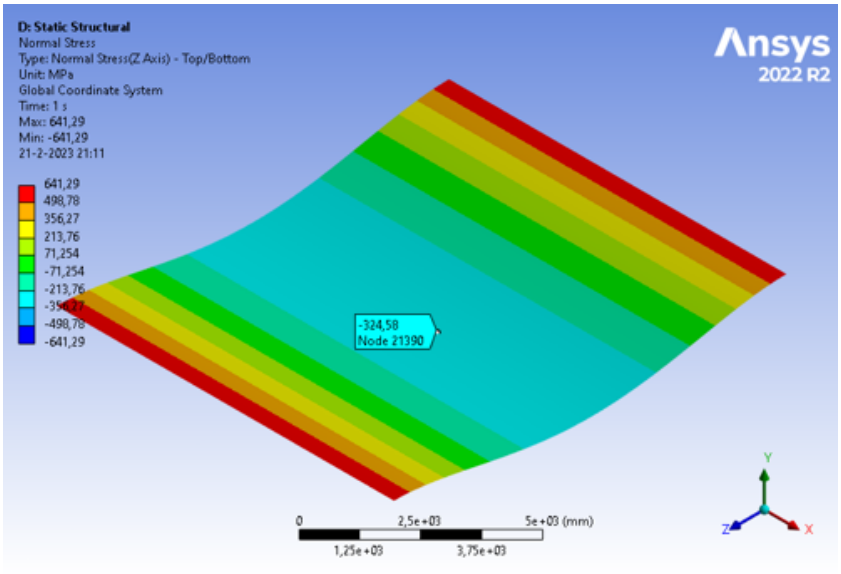

Figure F.4: Normal stress in Z in the middle of the plate.

F.2. Axial loading

F.2.1. Stress and strain in the plate

The stress can be calculated analytically with the formula F.7. The result is positive but this is dependent on the definition of the directions. It is important to check if the directions of reactions match the forces which are applied. In this case, the analytical value should be negative as the system is in a compressive state. The strain is calculated by the formula F.8. The appendix shows the results of the stress and strain in the direction of the force in figure F.5a and F.5b.

σ_{norm}, Normal stress
$F = 1000kN$, Force on the plate.
$A = b * h = 40 * 9800 = 392000mm^2$, Area of the plate.
ϵ, Strain

$$\sigma_{norm} = F/A \tag{F.7}$$

$$\epsilon = \sigma/E \tag{F.8}$$

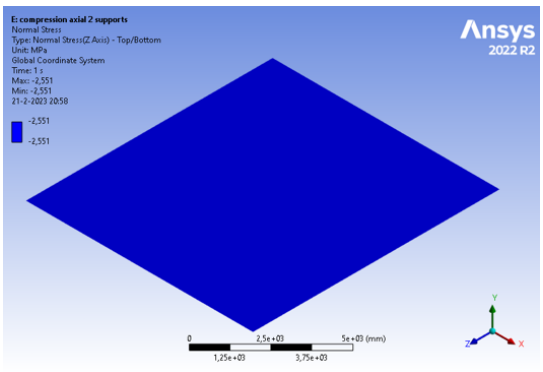

(a) Stress in the direction of the force due to compression.

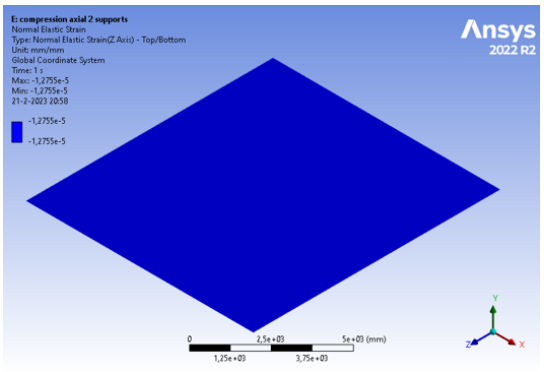

(b) Strain in the direction of the force due to compression

F.2.2. Deformation

Determining the deformation in the force direction is done with formula F.9 [14]. The deformation results in Z and X-direction in Ansys are given in figure F.6a and F.6b.

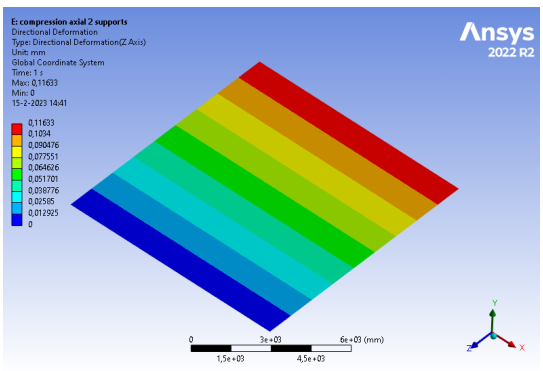

(a) The deformation in Z direction

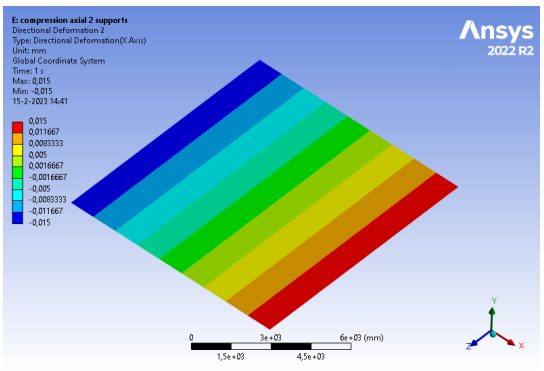

(b) The deformation in X direction due to Poisson effect

Figure F.6: Defroamtions of the compressed plate

u_z, Deformation in Z-direction
$N = 1000kN$, Deformation in Z-direction
$A = 392000mm^2$, Area of the plate.
$L = 11400mm$, length of the plate

$$u_z = \frac{N}{EA} * L \tag{F.9}$$

The Poisson ratio is turned on for this simulation to inspect what the effect is in the model. The deformation in the perpendicular direction of the force depends on the Poisson ratio and has to be determined with the strain of the plate, this is done with the formula F.10 [14]. In appendix figure F.6b the effect of the Poisson ratio can be seen. There is deformation in the perpendicular direction to which there is a force.

$u_x =$, Deformation in X-direction
$\nu = 0.3$, Poisson ratio
$b = 9800mm$, Width of the plate

$$u_x = 0,5 * b * \epsilon * \nu \tag{F.10}$$

The Deformations in Ansys are given relative the original position of the node. In the model the middle of the plate was locked from displacements so the free edges are both displaced in the opposite direction. The total deformations in the horizontal direction have to be added to each other.

F.2.3. Buckling

Since the plate is now being loaded in compression, buckling will also play a role in the analysis of the plate. Buckling is different for plates and columns. The Euler formula F.11 gives the result for the critical buckling load of column buckling. A linear elastic bifurcation analysis (LBA) is done with Ansys. Important is the mesh size that is used, as it has an impact on how the results turn out. A mesh sensitivity study is performed to ensure quality results within a reasonable computation time [19].

The large mesh has an Eigenvalue of 0.7963. The calculation time was very quick for this simulation. The mesh is seen in figure F.7a and the buckling result is found in F.7b. The medium mesh has an Eigenvalue of 0.7939. The calculation time was reasonable for this simulation. The mesh is seen in figure F.7a and the buckling result is found in F.7b. The small mesh has an Eigenvalue of 0.7939. In this simulation the time ran long, meshing was a large part of this which make it too extreme to use. The mesh is seen in figure F.9a and the buckling result is found in F.9b. The medium mesh is of the same size in the first four significant digits which indicates smaller meshing is not adding to relative precision.

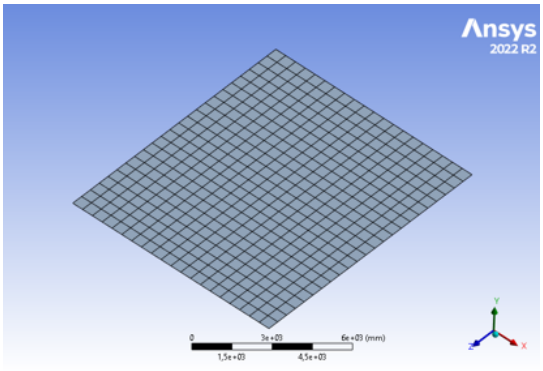

(a) Large mesh of 500 mm

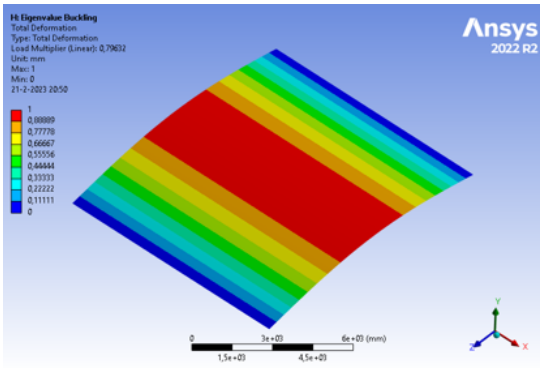

(b) Buckling result large mesh

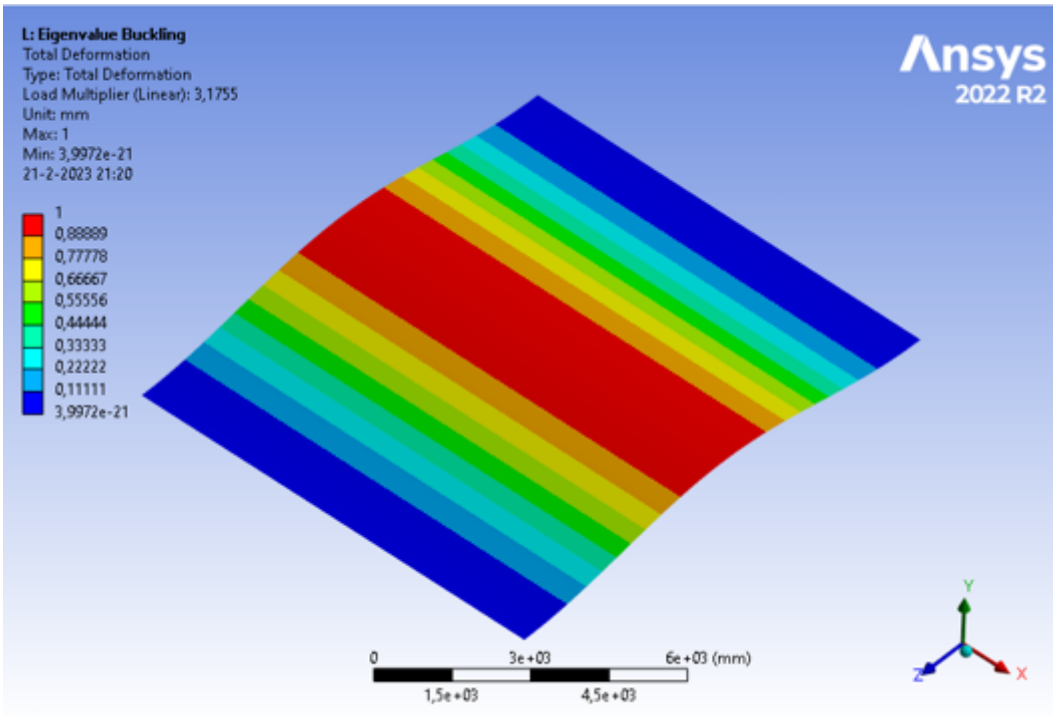

Figure F.10: Result of constrained buckling

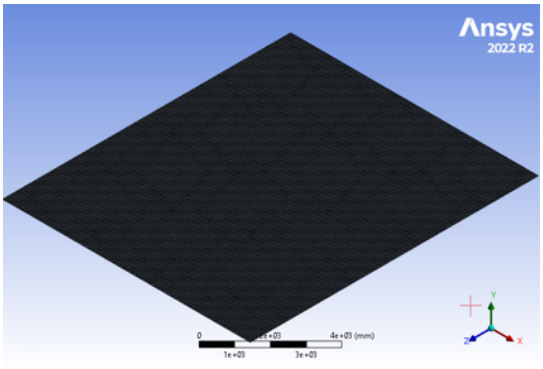

(a) Medium mesh of 50 mm

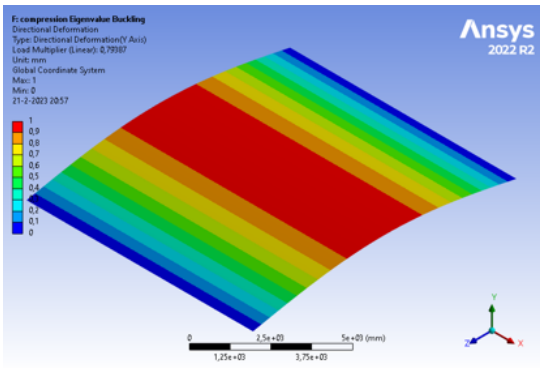

(b) Medium mesh buckling mode 1 result.

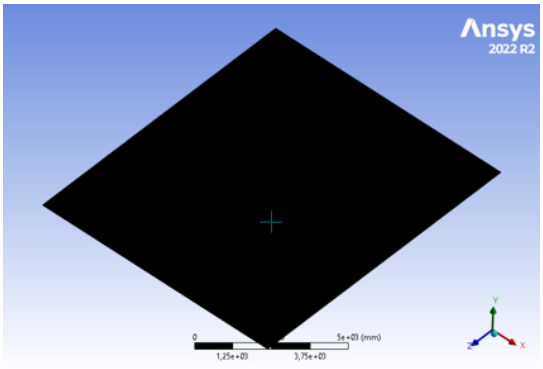

(a) small mesh of 25 mm

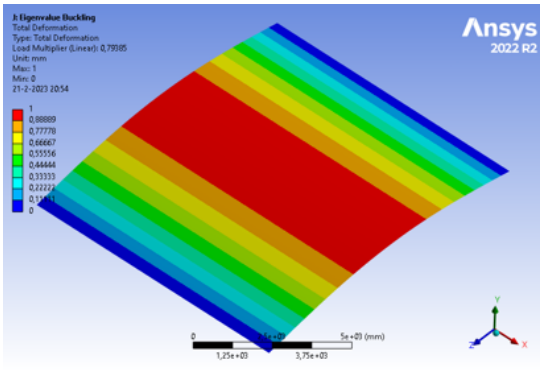

(b) Small mesh buckling mode 1 result.

The Euler formula F.11 is used to find an analytical result. Also for a constrained edge the result is checked to see how boundary conditions affect buckling. Figure F.11a gives the critical lengths for

these support systems.

N_{cr}, Critical buckling load

$L_{cr,simp} = 11400mm$, The critical buckling length for simply supported plate.

$L_{cr,constr} = 11400/2 = 5700mm$, The critical buckling length for constrained supported plate.

$$N_{cr} = \frac{\pi^2 * EI}{L_{cr}^2} \tag{F.11}$$

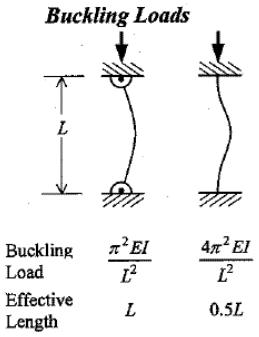

(a) Critical length of different supported beams [25].

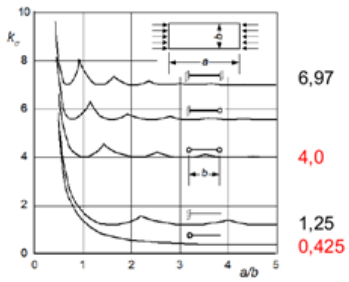

(b) The values for factor k_σ based on the boundary conditions at the plate [48].

Figure F.11: Column buckling and plate buckling

When the Euler formula is used for the different buckling calculations the results are 793 kN and 3175 kN respectively. The critical buckling load can be rewritten to an eigenvalue with formula F.12.

$$EV = \frac{N_{cr}}{F} \tag{F.12}$$

The Ansys result can be seen in the appendix in figure F.8b which gives the result of simply supported and figure F.10 presents the constrained buckling situation. The shape of the buckling modes is evaluated later on for other support systems but it is important to mention that the results in Ansys match the results from figure F.11a.

Plate buckling is different from column buckling. The difference is investigated with different models which have adjusted boundary conditions and a difference in Poisson ratio. The model for the plate is seen in figure F.12. The figure shows the direction of the edge that is locked from displacement. There are no rotational restrictions in this model. Important to state is that the Poisson effect is turned on for this analysis but the edges are free to move in the X direction. This means that there is no restraining effect on the horizontal direction of the plate.

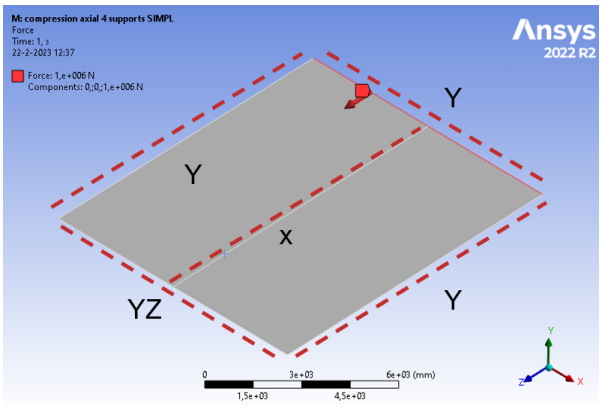

Figure F.12: Model for the simply supported plate buckling simulation.

Analytically, plate buckling can be studied with the formula F.13 [48] which is dependent on factor k_σ. The values for this factor can be found in figure F.11b. The k_σ value is a variable which is based on support conditions of the edge parallel to the force and the ratio between plate and column buckling. Next, the critical stress is calculated analytically with formula F.13, the values used are listed below.

$$\sigma_{cr} = \frac{k_\sigma \pi^2 E}{12(1-\nu^2)}(\frac{t}{b})^2 \tag{F.13}$$

$k_\sigma = 3.37 * 12/\pi^2$, Coefficient for plate vs column buckling.
$N_{cr} = \sigma_{cr} * A = 4836kN$, Ciritical buckling load
$EV = N_{cr}/1000 = 4.83$, Eigenvalue based on ciritcal buckling load.

When the buckling simulation is done with Ansys, the buckling shape result is as seen in figure F.13a. The buckling shape is as can be expected when the edges are all prevented from deforming in the vertical direction.

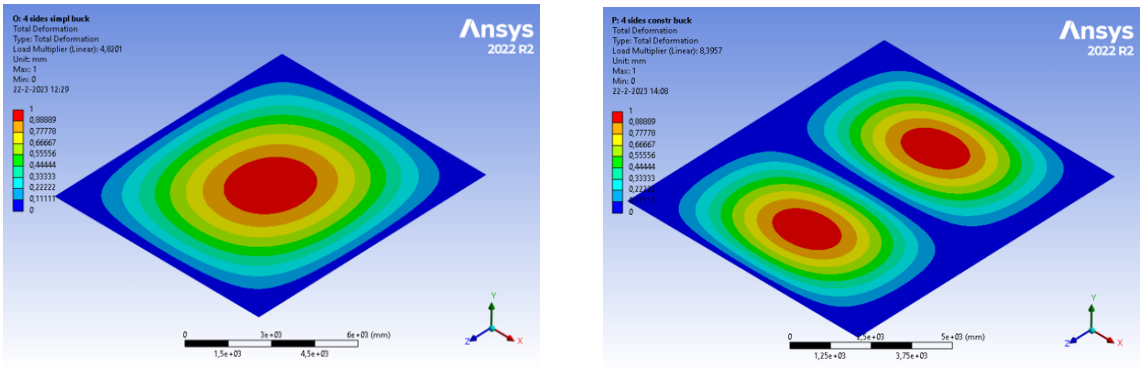

(a) Simply supported edge

(b) Constrained edges

Figure F.13: Buckling mode 1 shape due to compressive force

There is also a model simulated with fixed edges. The value for $k_\sigma = 5.95 * 12/\pi^2$ is used for the fixed sides. The formulas and the figure can be seen in the appendix F.2.4. The shape of the buckling mode is different from the first mode of the simply supported edges. There are two buckles in the plate now which can be seen in figure F.13b. The boundaries can determine how the plate buckling shape will look like. When looking for a higher buckling mode, there is a buckling shape which has only one large buckle. The force needed to allow one large buckle over the width of the plate is higher than the force needed to create the two smaller buckles.

F.2.4. Costrained plate buckling

$k_\sigma = 5.95 * 12/\pi^2$
$\sigma_{cr} = 21,79MPa$
$N_{cr} = 8540kN$
$EV = 8.54$

F.2.5. Plane strain effect

When the edges parallel to the force are fixed in the X-direction, which will be the case when the plate is part of a construction, the result of buckling is different. The edge nodes cannot be displaced in the transverse direction like it was seen in figure F.6b. Stress is presented in the plate in the perpendicular direction to the force due to the Poisson effect and the fixed edge. This stress adds to the load which induces buckling. The eigenvalue is reduced by 30% as it is now 3.43. the reduction of the buckling load is consistent with the size of the Poisson ratio. The Poisson effect transfers 30% in the perpendicular direction which will roughly be added to the compressive stress in the plate. This is called the plane strain effect and will be present when a plate is constructed within a frame. The model's set-up can be seen in the appendix in figure F.14a and the result from the simulation in Ansys can be found in figure F.14b.

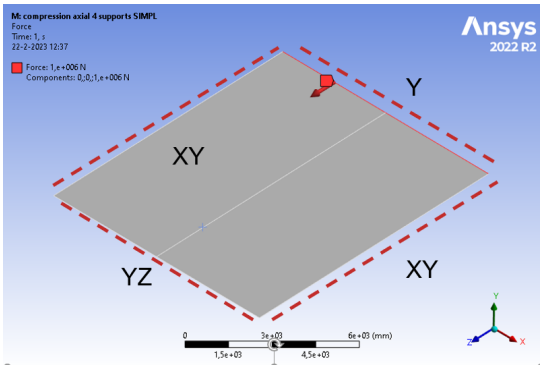

(a) Set-up of the plate for buckling analysis with restricted edges in the perpendicular direction of the force.

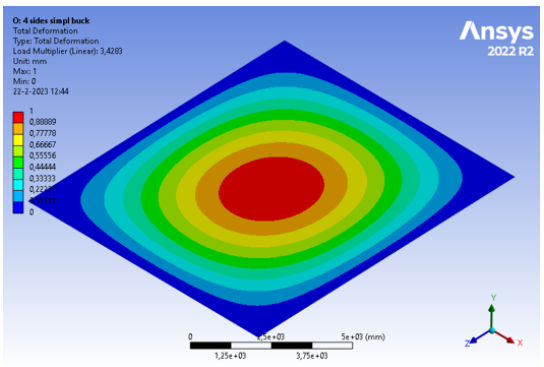

(b) Plane strain effect on plate buckling.

G

Arched plate feasibility

G.1. Simply supported

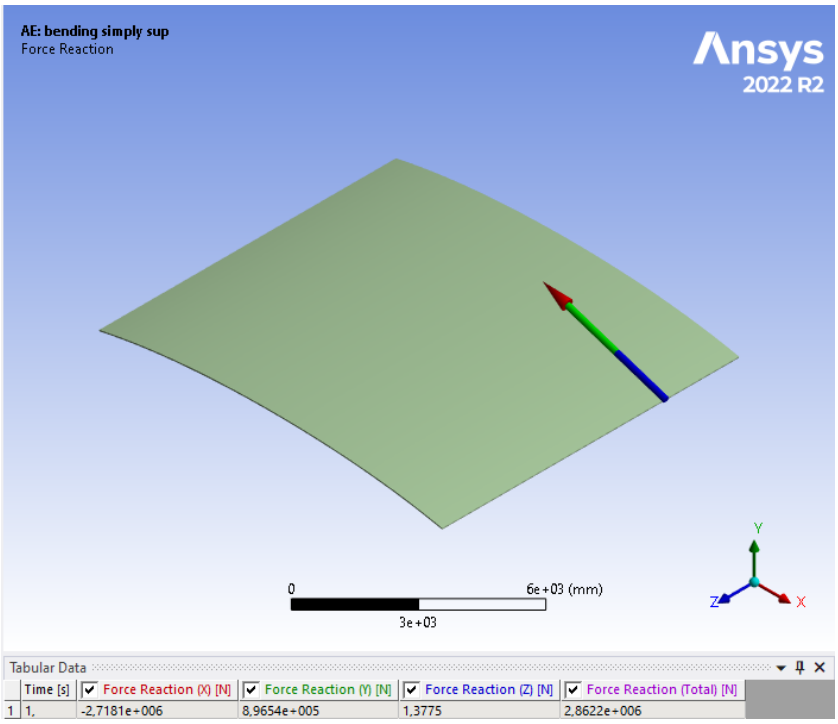

Figure G.1: Reaction force at the boundary of the simply supported edge.

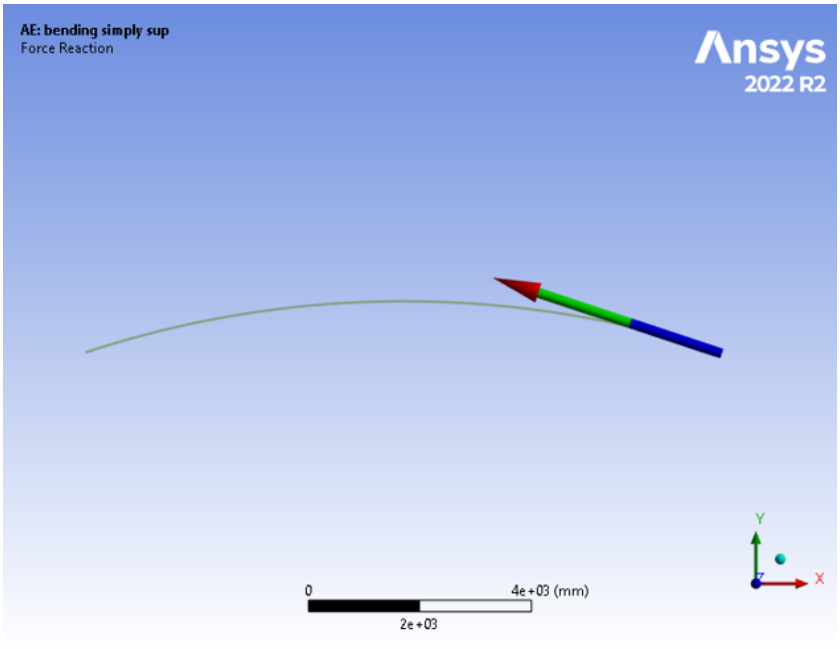

Figure G.2: Reaction force at the boundary of the simply supported edge seen from the side.

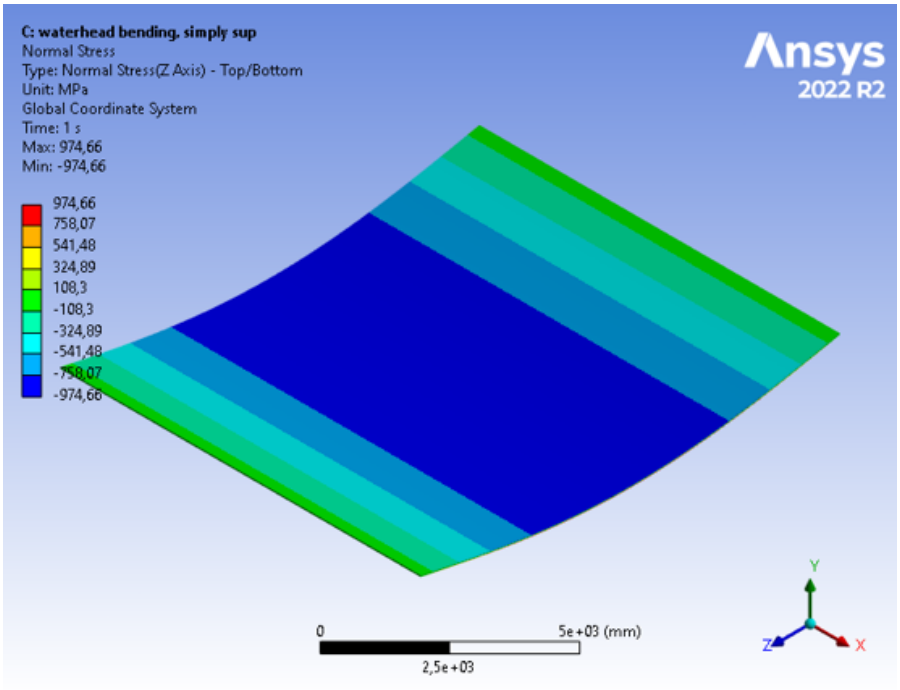

Figure G.3: Normal stresses along in the flat plate due to bending.

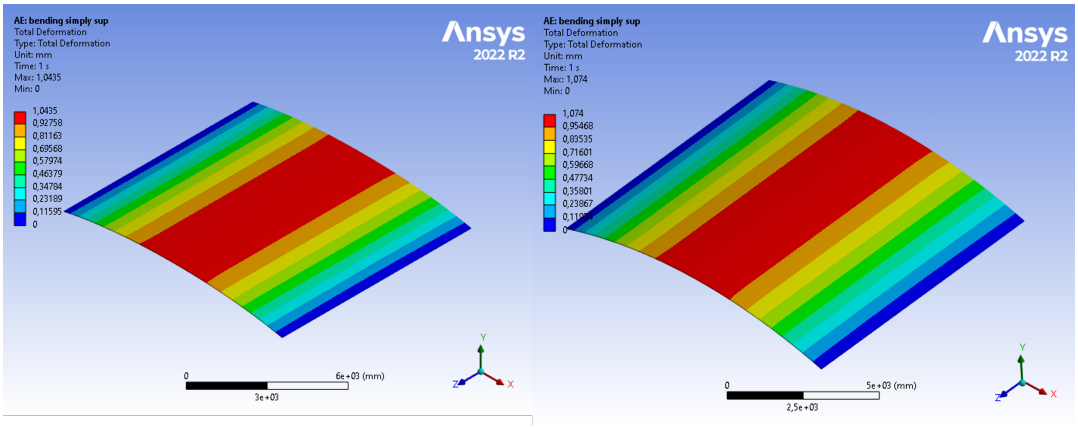

Figure G.4: LA and GNA deformation result of the curved plate.

G.2. Constrained rotation at boundaries

When the supports are constraint, as seen in figure G.5 from rotation there is an effect on the arch working Deflections are bigger 1.25 mm, minimal effect but 25% larger than unconstrained

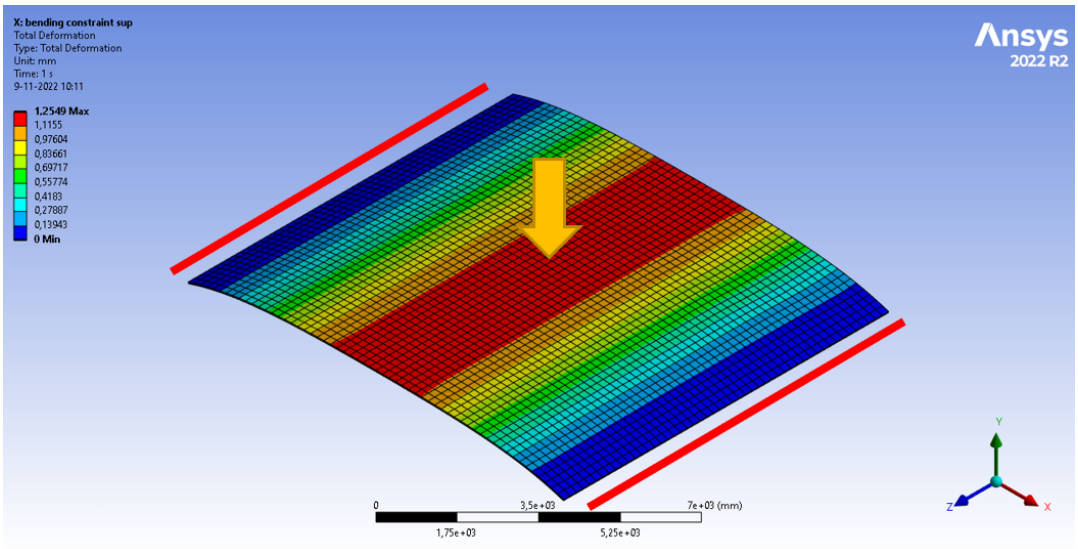

Figure G.5

The normal stresses have a larger range and differ top and bottom which indicates there are moments in the plate but as all stresses are still negative the compression is dominant. G.6

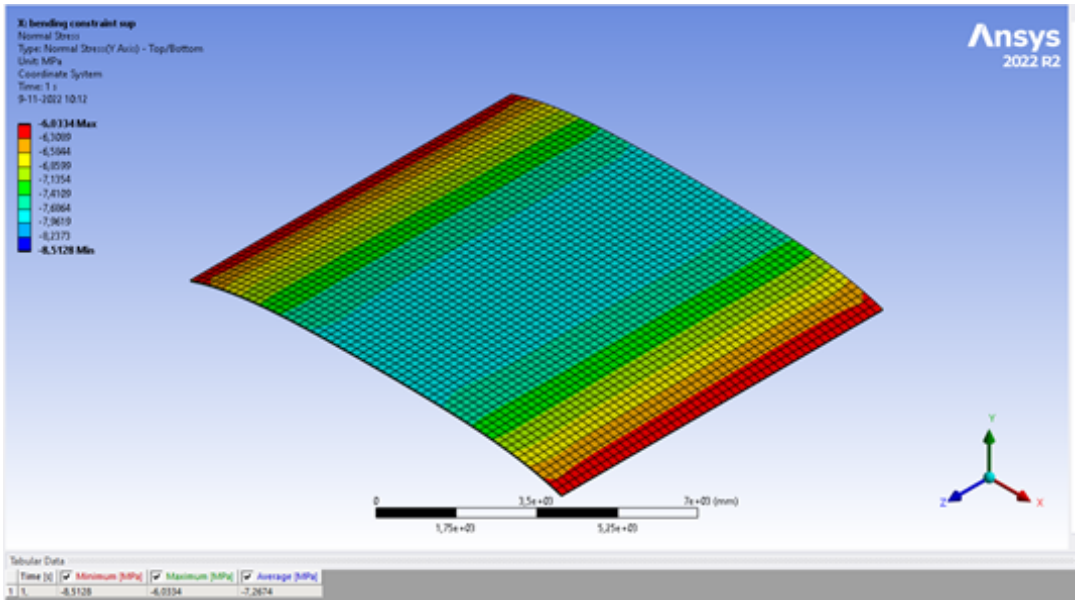

Figure G.6

G.7 EV is larger as it goes to 2.39 so stability increases due to constraints Next EV-modes as visible in the figure

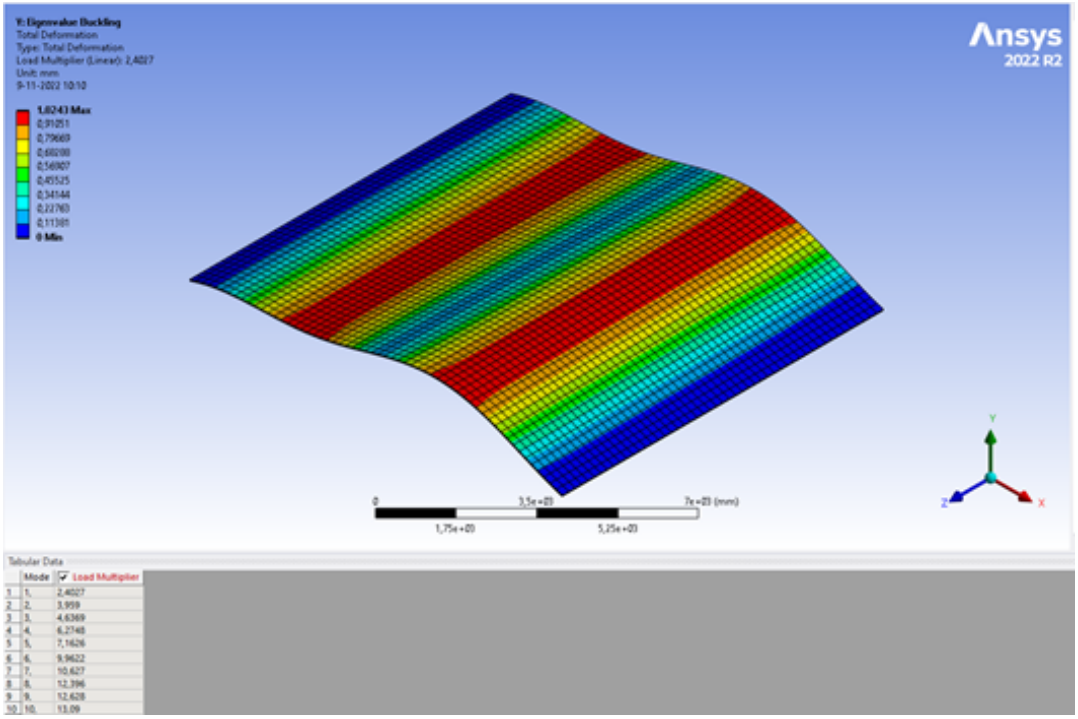

Figure G.7

G.3. Alternative curves

G.3.0.1. Smaller radius for curved plate

As mentioned before, the adjustment of the radius of the curve should remove bending moments in the plate and create the uniform compression arch, which is based on normal stresses only. In chapter 2 a source was presented that claimed to have developed an optimal shape for a curved gate [**Phipps**]. In order to see whether this shape provides the answer to the optimisation possibility in terms of material

used, it will be put to the test.

In order to test the shape, a plate was used with a base angle of 35 degrees. This creates a lock layout in which the span of the lock increases to 12940 mm and the radius of the curve reduces to 11292 mm. The reduced radius leads to an increased arc length of 13770 mm, adding 18% in length to the construction. Figure G.8 shows a top-down view of this situation. An increased span also means increased load on the construction, since the water head is a uniform load. In order to make a fair comparison of the needed material and the resistance of the plate, the same amount of material was used. The plate thickness is reduced to 34 mm, which is equal to the equivalent material of the original curved plate.

The reaction force is redirected into the vertical direction. The total force is lower than the smaller curve and the more vertical direction has to be carried by the substructure (appendix figure G.9). The normal stresses in the plate along the curve are more consistent than in the original curve, but a small bending moment still remains in the plate. The value of the stresses is lower (5.4 MPa) which means that the plate could be constructed thinner than the original curve (figure 4.6).

The buckling of the structure was also simulated. The result of Ansys presented that the eigenvalue of the first buckling mode was 0.79 (appendix figure G.11). This is lower when compared to the eigenvalue of 1.15 of the original plate. A smaller eigenvalue indicates that the load has to increase less to achieve the buckling of a structure. Since buckling is likely to play a dominant role in the arched plate, the decision was made to work with the larger radius in the arch.

In addition to the fact that it seems more prone to buckling, a downside of a lock with a smaller radius is that the total size of the gate is larger, both in length and in the curve. This means an even bigger structure has to be moved into a post in the substructure when the gate is opened. In some cases, this is a limiting environmental boundary condition.

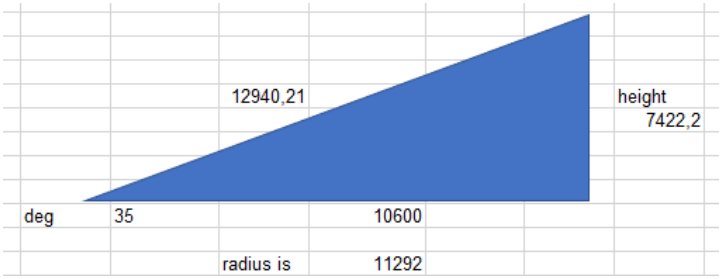

Figure G.8: Lock layout when an adjusted radius has been applied. Top-down view of the construction triangle that is created.

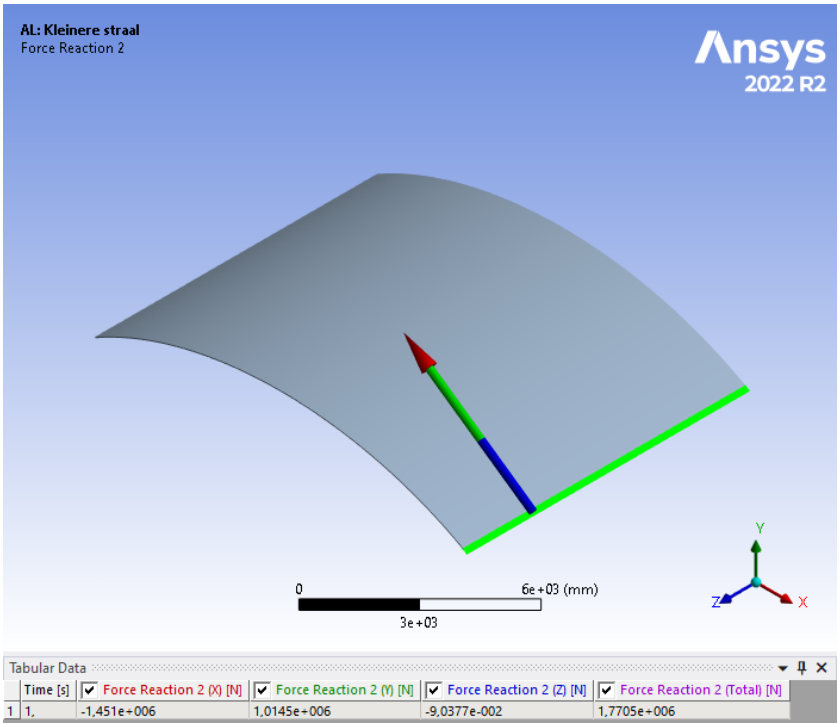

Figure G.9: Reaction force of the smaller radius gate

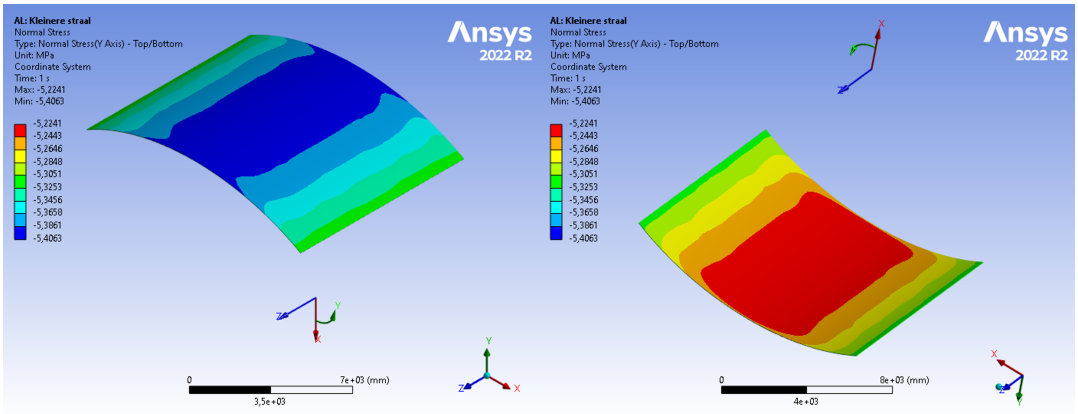

Figure G.10: Normal stresses along the curve of the plate. Plate with a smaller radius.

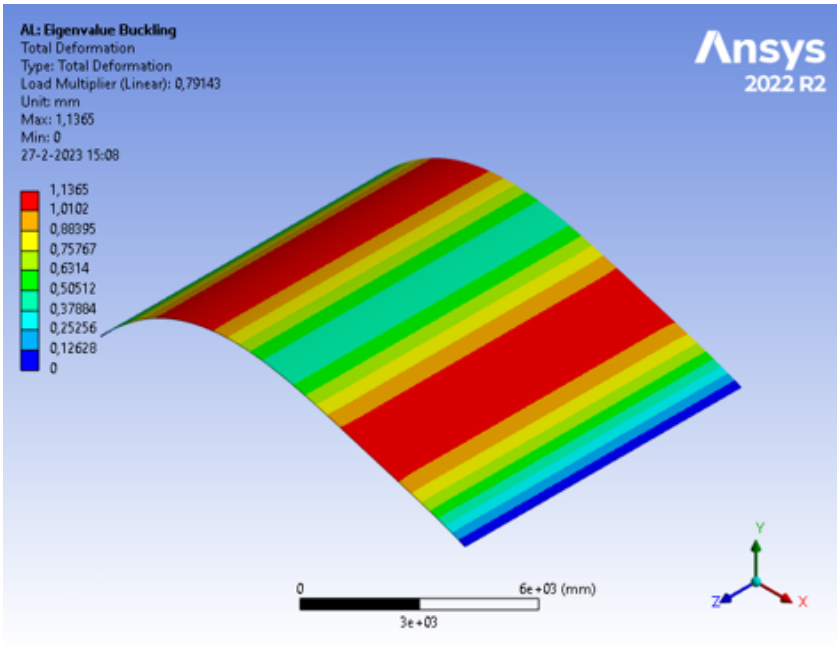

Figure G.11: First buckling mode of the plate with a smaller radius.

G.3.0.2. Shell plate

Shell structures have been used to design members which prevent buckling [4]. This design shape might be beneficial to the optimisation of plates in lock gates. To investiagte if there was any advantage to using a double curve in the plate field, simulations were done to find an answer. In order to study the effect of shell structures in lock gates, simulations were executed for the uniform load situation and with a hydrostatic load on two sides.

The dimensions of the model were based on the frame of the single arched plate, Height: 9800mm, Span: 11400mm. The thickness of this simulation was reduced to 10 mm, based on the fact that stresses so far have not been extremely high. The radius of the shell structure is 18644 mm, which is based on the curve of the bottom of the plate which aligns with the single curve shape. Supports were made all around the frame with simply supported edges in order to simulate the frame (see figure G.12).

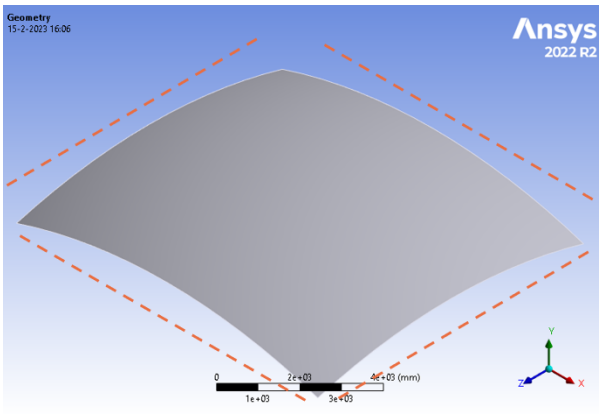

Figure G.12: Support situation of the shell plate based on a sphere shape.

The reference plate was made with a radius of 18200 mm with equal dimensions and was simulated in similar conditions. The result was a larger number of buckles in the plate, which resembles the effect of the flat plate with boxed edge stiffeners. The eigenvalue of the arched gate was 0.25 for the pressure of 0.016 MPa. The result for the shell structure with regard to uniform loading was an eigenvalue of 5.24. This is much higher than that of the arched structure, and the model's shape is also subdivided

into many smaller buckles instead of several larger ones. The effect is bi-directional and somewhat symmetrical. This means that buckling is more difficult in the shell structure. The results of the uniform loading have been added to the appendix in figure G.15a and G.15b.

The normal stresses in the shell resemble the stresses found in the arched plate, but are directed in two directions. This means that the forces are transferred both horizontally and vertically in the plate. This implies that when placed in a lock gate, the load has to be transferred through the top and bottom horizontal beams. The top and bottom beams are not directly connected to the substructure, which means that these members have to transfer the load to the next members which then transfer them to the substructure. This is not a desirable option but might work when further analysed. Appendix figures G.16a and G.16b show these normal stresses.

Hydrostatic load on shell By simulating a hydrostatic load on the shell shape, the effectiveness of the shell plate can be predicted for lock gates. Ansys was used to simulate a hydrostatic load on the arched plate and the shell plate. Since lock gates have water on two sides, this simulation was executed for these plates as well. The water level on one side sat at 6100 mm from the bottom of the gate, the water on the other side at 7750 mm from the bottom of the gate. This is equal to the extreme water head that the pressure load was based on. The visual representation of one of the water loads on the surface of the plate in Ansys has been added to the appendix in figure G.13.

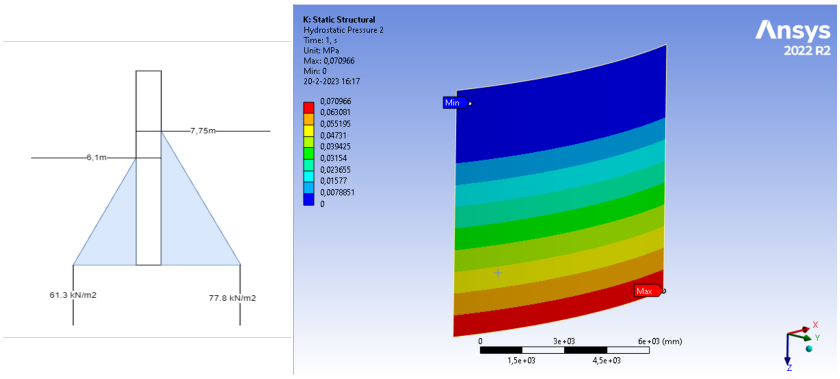

Figure G.13: Support situation of the shell plate based on a sphere shape.

The results of the buckling analysis in Ansys provide the answer to the effectiveness of the shell structure. The eigenvalue for the arch plate is 0.28 which is a slight increase compared to the arched plate, while the shell has an eigenvalue of 3.14 which is a relative decrease. Figure G.14a shows the first buckling mode shape of the arched plate and figure G.14b shows the first buckling mode shape of the shell structure. In uniform loading, the effect on the shell structure has become one-directional instead of a fairly symmetric shape. The effect of the hydrostatic load is completely transferred to the bottom half of the plate. The buckles are smaller than those of the arched plate which still indicates that the effect is better than the single arch.

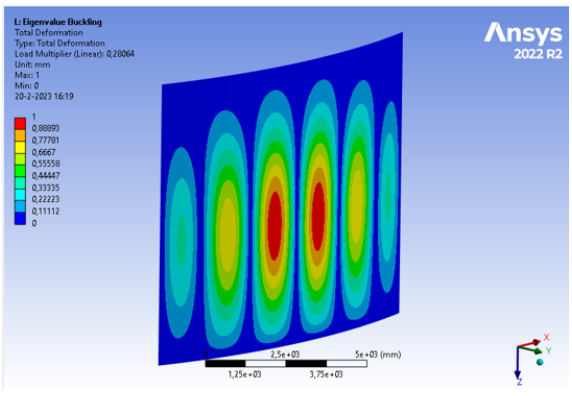

(a) Arch buckling under hydrostatic load.

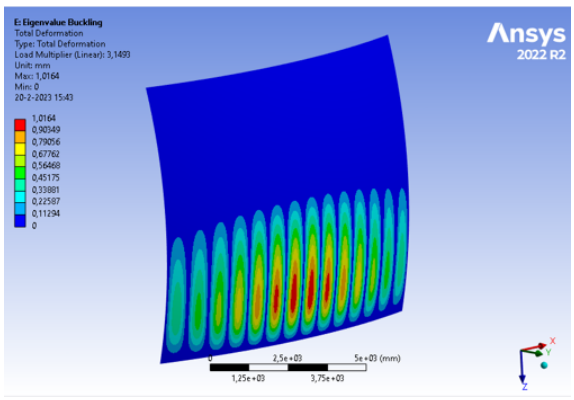

(b) Shell buckling shape under hydrostatic load

Some downsides to the shell structure have not been presented in these results yet. First of all a shell member is very strong against uniform loading. In chapter 2 it was seen that asymmetrical loads are present in a lock. The shell structure would allow for material reduction based on the uniform water load but would later probably require an increased thickness to withstand the propeller load. The optimised thickness for the shell under uniform loads will have little surplus in the component to resist other types of loads.

Secondly, it is not easy to manufacture a double-curved shell structure in the format used in the lock gate. Not only does a double-curve need to be implemented in the structure, but as the component cannot be made out of one plate, different plates need to be connected in a specific way for the shell structure to work efficiently. Shell shapes are not often seen in hydraulic structures, indicating that their cost efficiency might not be optimal. The thickness of the material seems to be able to be reduced, but the effect this will have on fatigue is, although complex to predict, likely not positive.

Lastly, locks have two different water levels, which will create an upwards resultant force on the horizontal segment of the shell due to the lower pressure exerted by the low water level. This upwards force will add to deformations in the shell, which will deviate it from the ideal shell structure. It is, therefore important to maintain the strength of the shape.

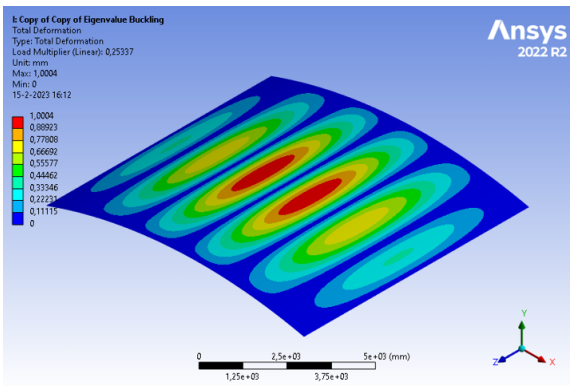

(a) First buckling mode of the single arch plate.

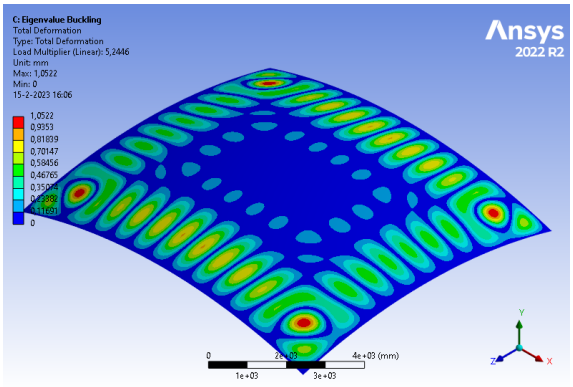

(b) First buckling mode of the shell plate.

When looking at the stresses in the plate this gives a fairly constant normal stress in both directions. G.16a and G.16b present this result. This shape can be very favourable, apparently. the production of such a shape on the scale which is needed for lock gates leaves to question if this will not be extremely expensive. In the infrastructure industry, the costs are often driving.

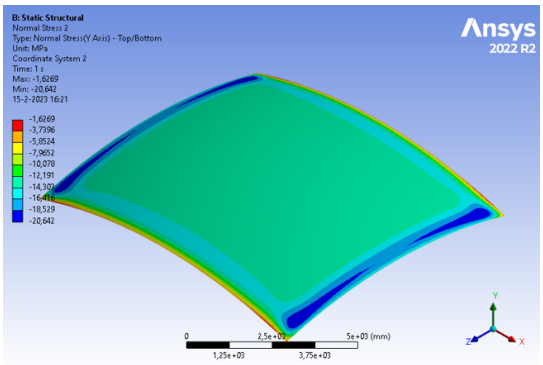

(a) Normal stresses along the curve in the global X direction

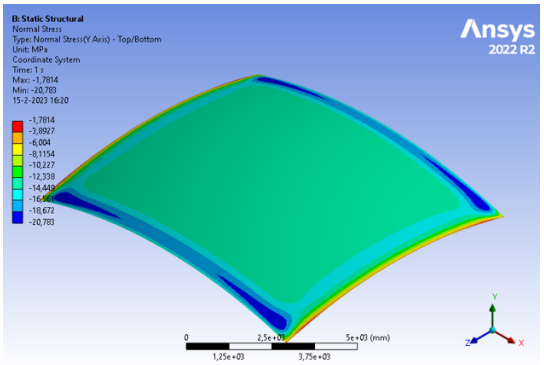

(b) Normal stresses along the curve in the global X direction

H

Frame feasibility

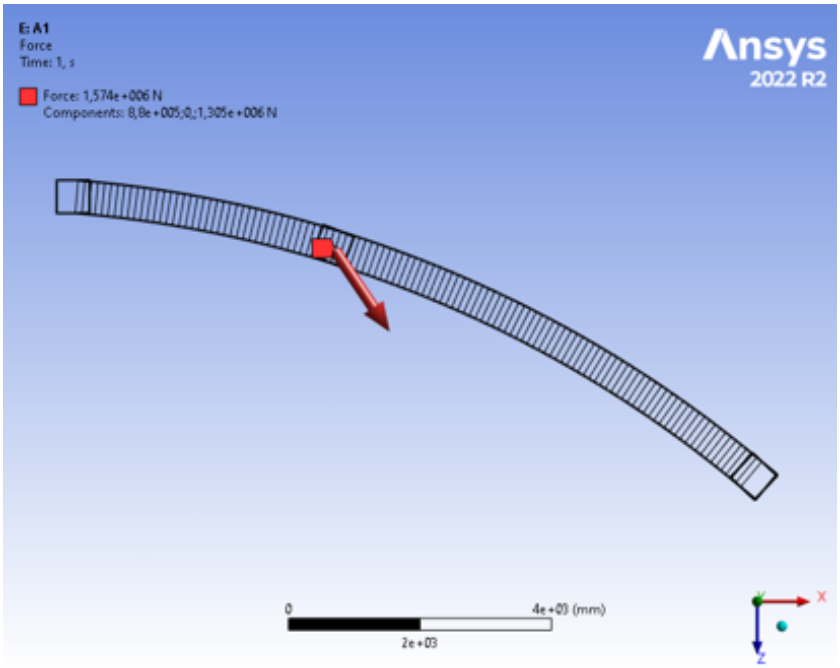

Figure H.1: Direction of the obstacle load in the incident load situation.

H.1. Frame design layout

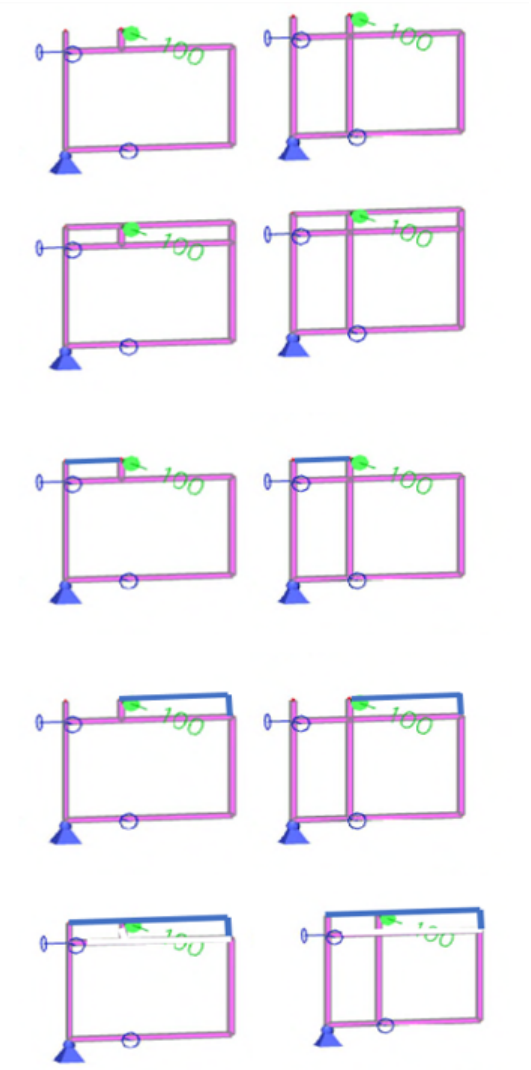

Figure H.2: Options which were considered for the frame of the gate.

H.2. Plate and frame interaction

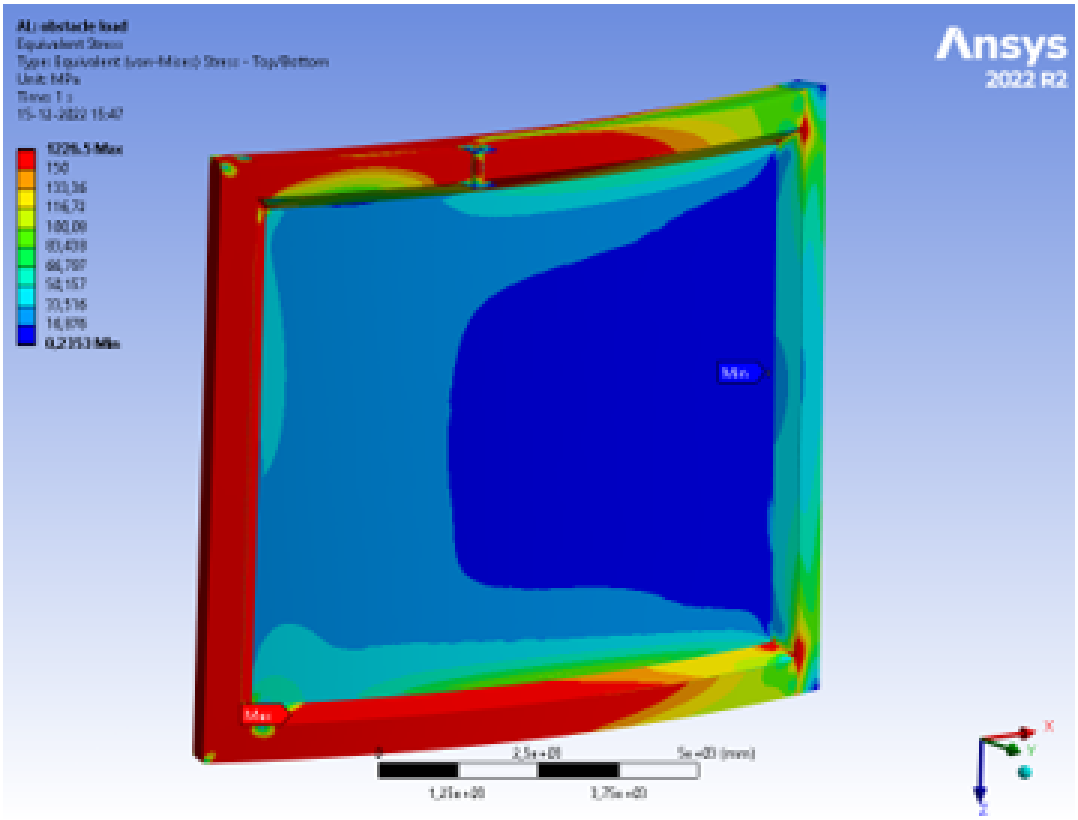

Figure H.3: Interaction between the plate and the frame.

H.3. Conclusions on frame design

Conclusions per adjustment The intermediate conclusion made up on 15-12: the double top frame is best for reducing stresses around the frame. The middle beam is not effective enough.

Vertical beam in the middle This beam gives lower deflections and higher stresses. It also has to go through the field where the arch is which disturbed the empty arch field. This is not desired so the beam is not a good option. Double top Beam

Reduces the moments on the connection to the vertical support with the hinges by half. This option is a realistic one as it does not disturb the part of the arch that has to withstand the extreme water level. It also seems that the moment at the bottom connection is reduced. This indicates that the whole frame is activated rather than just one side. Comparing it to A3 model it is proven that the moments on the left top side are similar but slightly higher for the A3 model and the moment on the bottom side is therefore also larger. Adding the second level is advisable.

Top or middle (top) beam Torsion in the top beam is reduced by 50% for top beam use. The moments are very similar but there is an extra moment in Y direction which also creates the torsion.

Extra beam top left Better than the single beam for moment reduction. Further comments made in double top beam

H.4. member limits

The beam limits for the hollow section are calculated based on the methods found in the Eurocode.

$N_{Rd} = 24213kN$
$M_{pl,Rd} = 6583kNm$
$M_{el,Rd} = 4102kNm$
$V_{pl,Rd} = 6826kN$

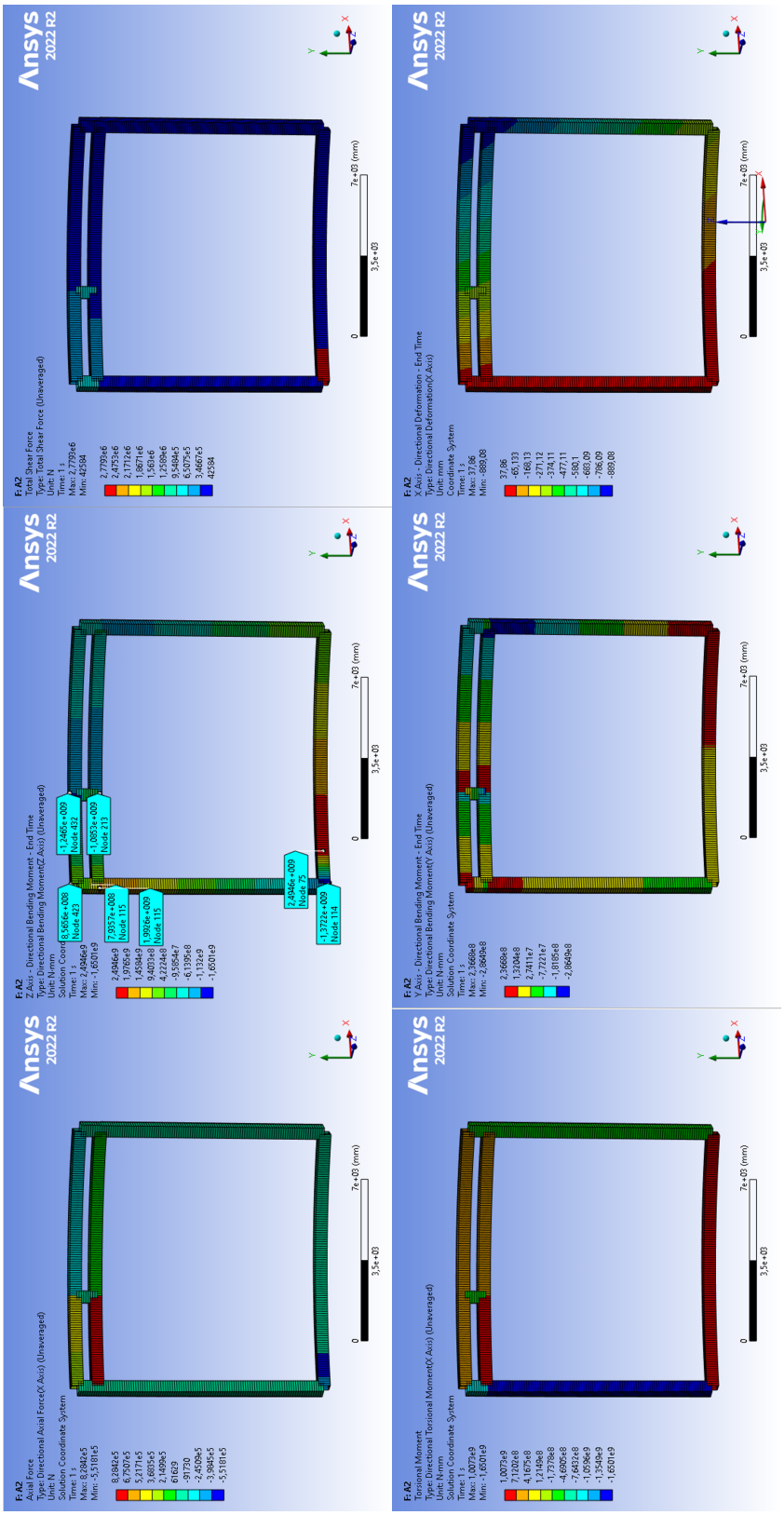

Figure H.4: Member forces present in frame.

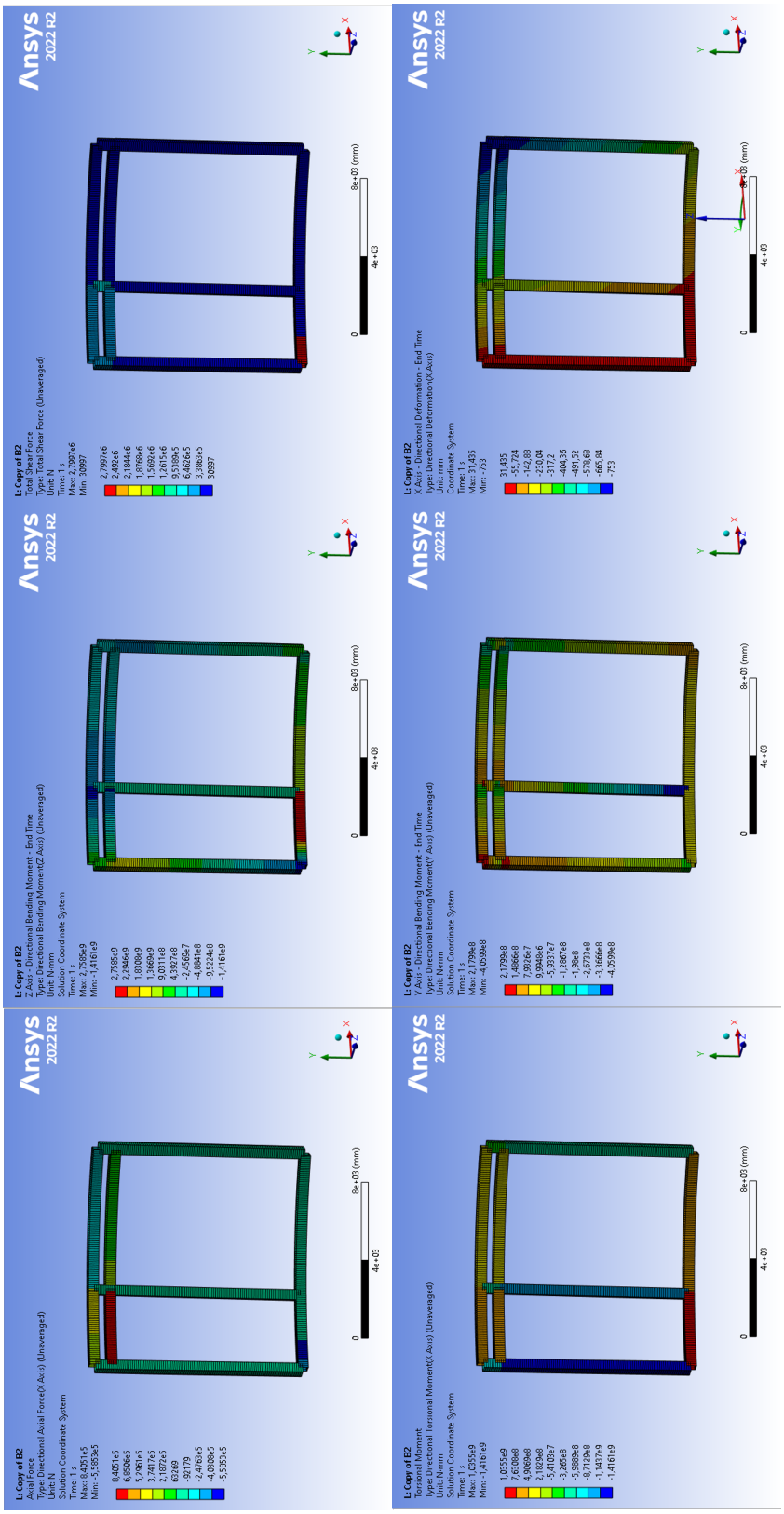

Figure H.5: Member forces in frame with vertical member in main plate field.

Stiffened plate

I.1. Boxed stiffener

To investigate the effect of stiffeners on the plate behaviour, a model has been made that has boxed stiffeners at the edges. The stiffeners should function like vertical support as they increase the local moment of inertia. The same is valid for the horizontal support perpendicular to the force. The plate cannot deform symmetrically like in the unstiffened plate (reference appendix figure F.6b). Next to the vertical and horizontal support, the stiffeners should also limit the rotational freedom of the end of the plate. The plate should behave somewhat similarly to the constrained boundaries seen before. The plate has a reduced thickness of 34 mm to maintain the equivalent thickness of the original design. The setup is seen in figure I.1.

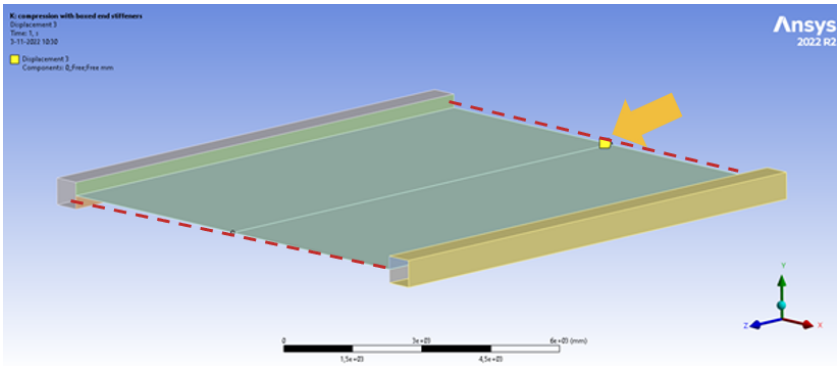

Figure I.1: Plate with boxed stiffeners at the edges.

Since the girders would be attached to a vertical member, the vertical displacement of the stiffeners has been set to zero. This prevents rotations at the end of the stiffeners, bringing them closer to the actual structure. The buckling shape of the structure can be seen in figure I.2 and this shows that there is one larger buckle and one smaller. Three things are noticeable. There is no vertical deformation of the stiffeners. The stiffeners have no horizontal displacement, and the girder is very slightly rotated in the middle of the plate. This means that the effect of the stiffeners is somewhere between the simply supported and constrained edges but is behaving as was expected.

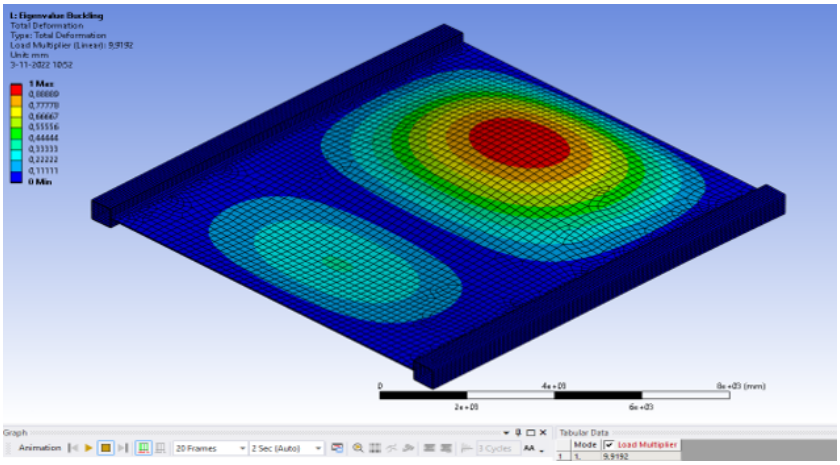

Figure I.2: Buckling mode 1 of the plate with boxed stiffeners.

To investigate how the boxed stiffeners affect plate bending, a simulation has been done in which there is pressure on the face of the plate. The bending effect is minimal on stiffeners, while the plate seems to deform most. There is a small deflection in the girders which proves that they will not function as a complete vertical boundary; the size of the deformation in the stiffeners is small, however, as it is only 10% of the maximum deflection in the plate. This result of an out-of-plane load applied on the stiffened plate can be seen in figure I.3 in the appendix.

The normal stresses in the plate are no longer uniformly distributed. The stiffeners prevent the deformation of the plate along the connected edge to the stiffener. The middle of the plate has a gradient in stresses. Figure I.4 is referenced in the appendix.

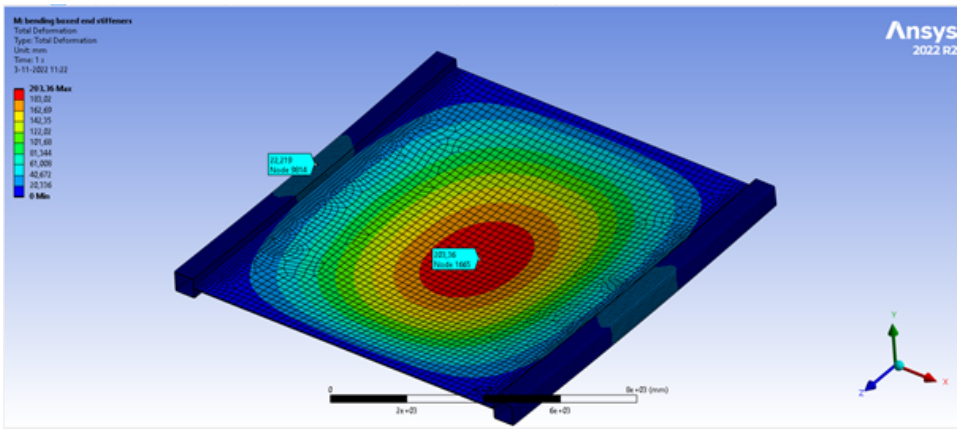

Figure I.3: Plate with boxed stiffeners in bending under plate pressure conditions.

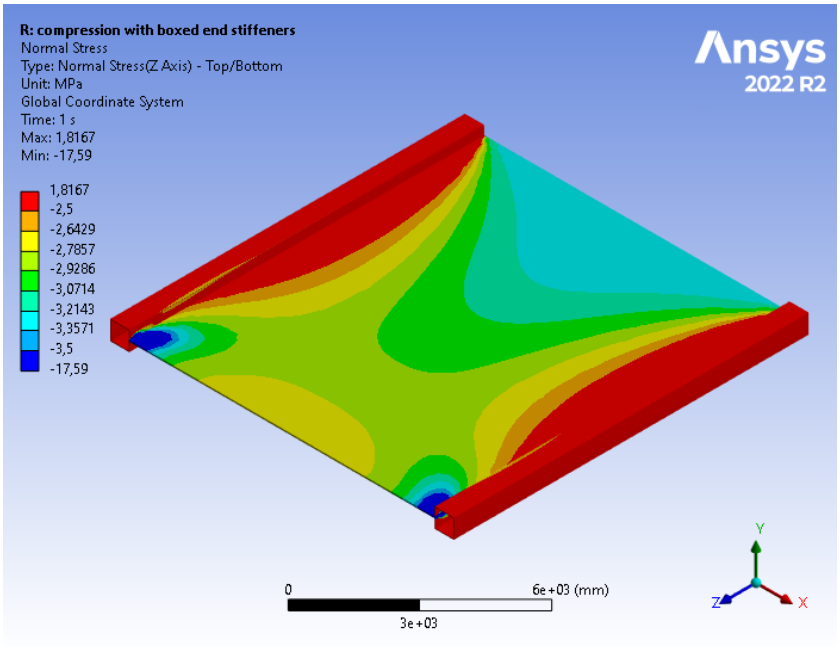

Figure I.4: Normal stresses in the plate with boxed end stiffeners

I.2. Plate with stiffeners in the field

The effect of stiffeners in the plate field has been simulated for this thesis as well. The effect on buckling was for both very obvious as the buckles in the plate started forming around the stiffener. Only in higher buckling modes, there was minor deformation in the stiffeners. The effect of stiffeners could be described as additions to the plate field in order to determine the size and location of buckles.

Effect of field stiffeners on buckling and relevance in bending and buckling. The goal of the new design is not to add these field stiffeners. The effects however are relevant to be studied as it might be unavoidable to add them at one point. The axial forces that lead to buckling modes and bending of the plate can be reduced by adding stiffeners. The first model has been made using one T-stiffener. The aim was to use an equal amount of steel as compared to the original plate. First, the webs and flanges will need to be determined.

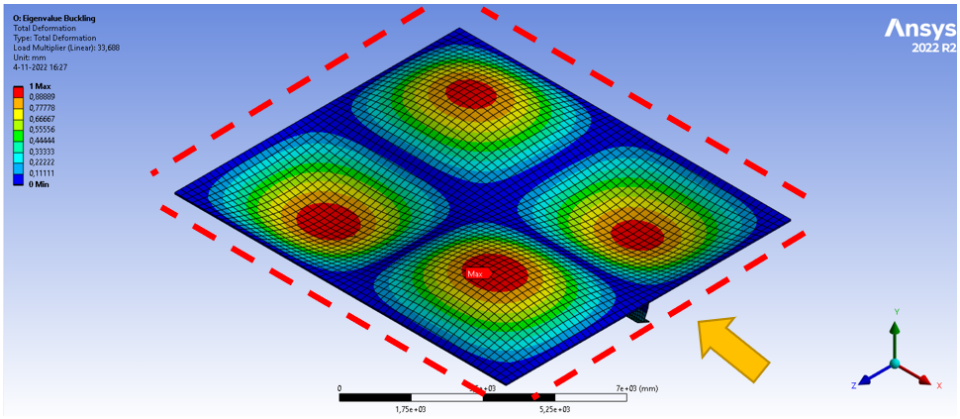

Figure I.5: Middle stiffener in flat plate, buckling mode 1

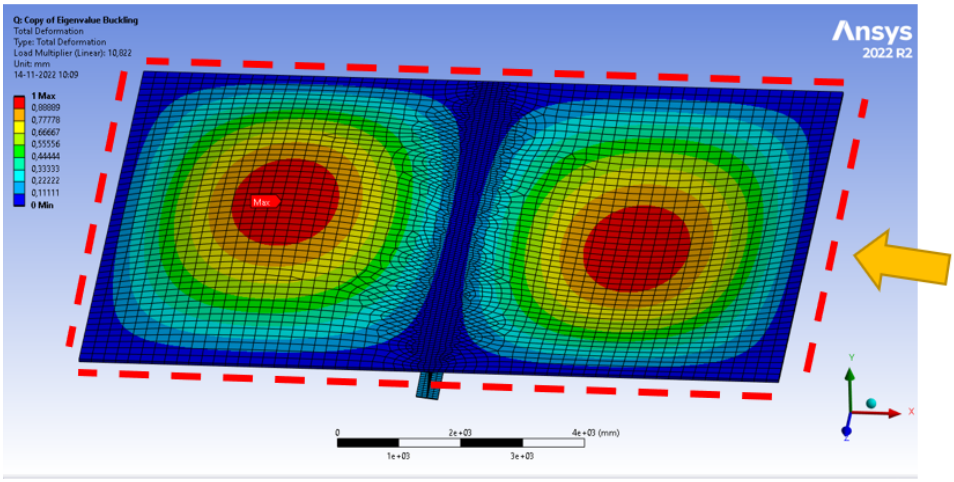

Figure I.6: Middle stiffener perpendicular to the load direction in flat plate, buckling mode 1

I.3. Arched plate box stiffeners

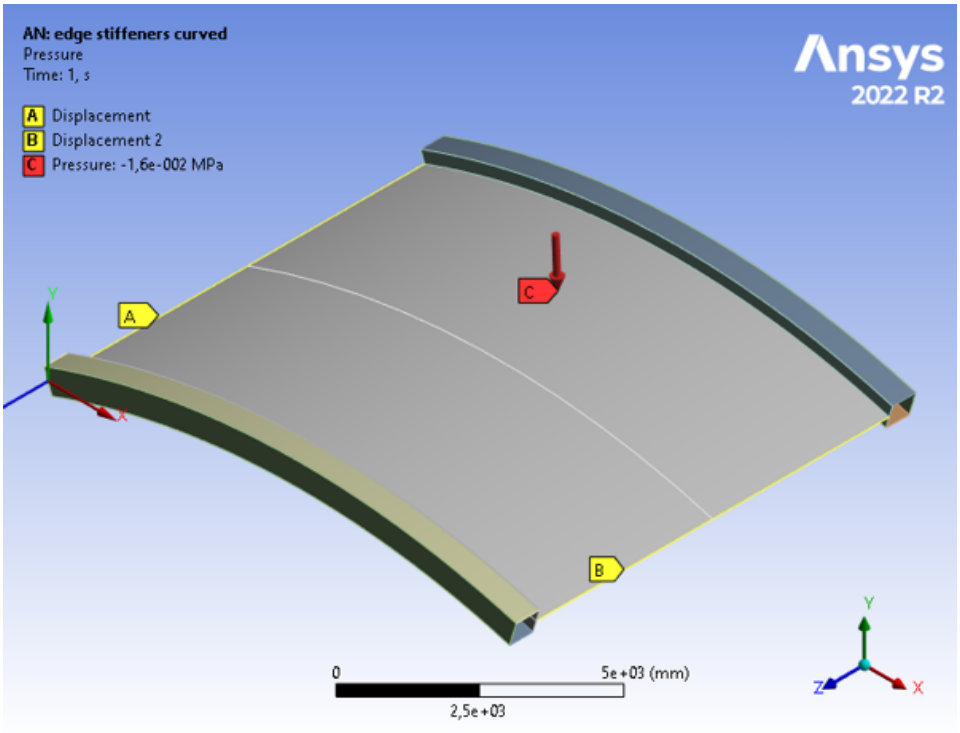

Figure I.7: Set up of the boxed frame

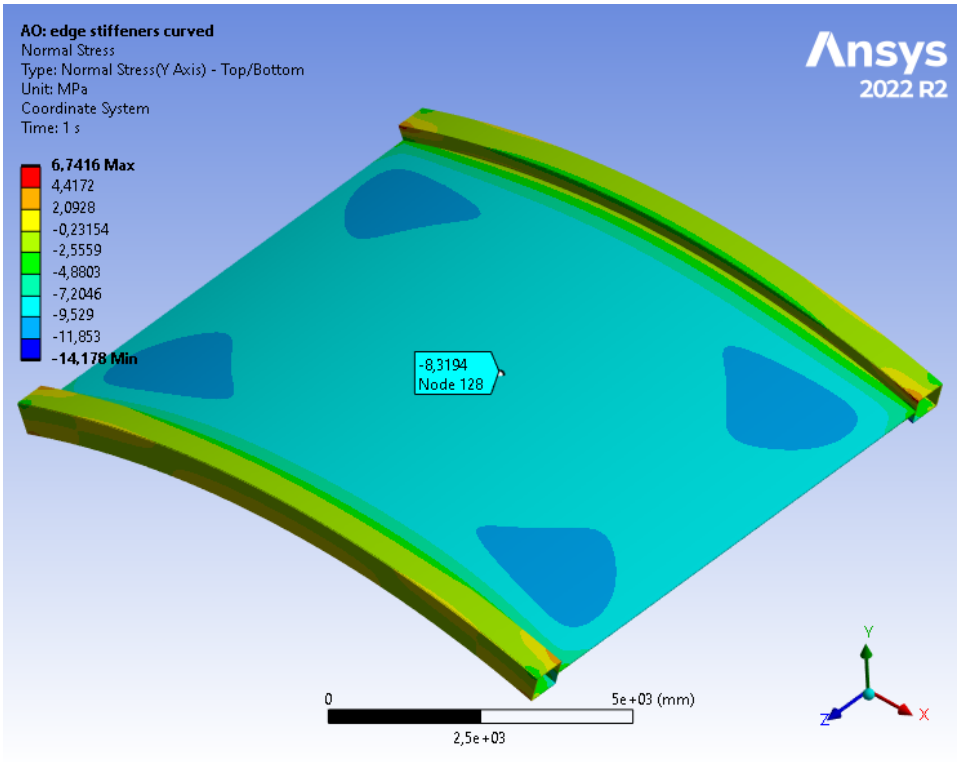

Figure I.8: Normal stresses along the curve of the boxed stiffener plate

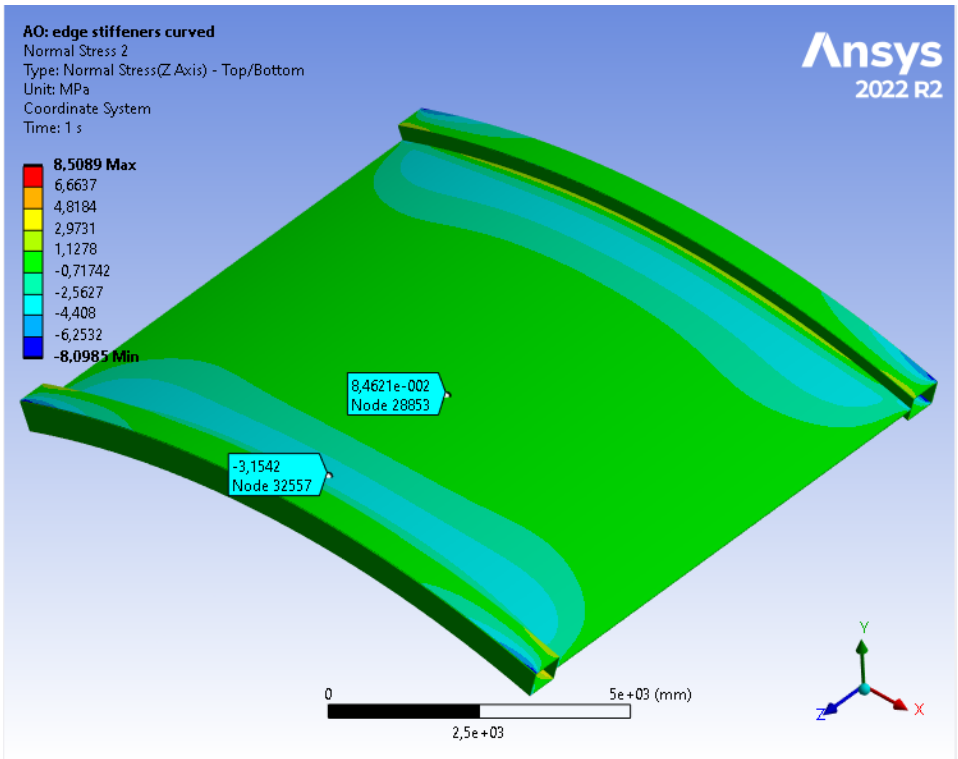

Figure I.9: Normal stresses towards the boxed stiffeners in the plate

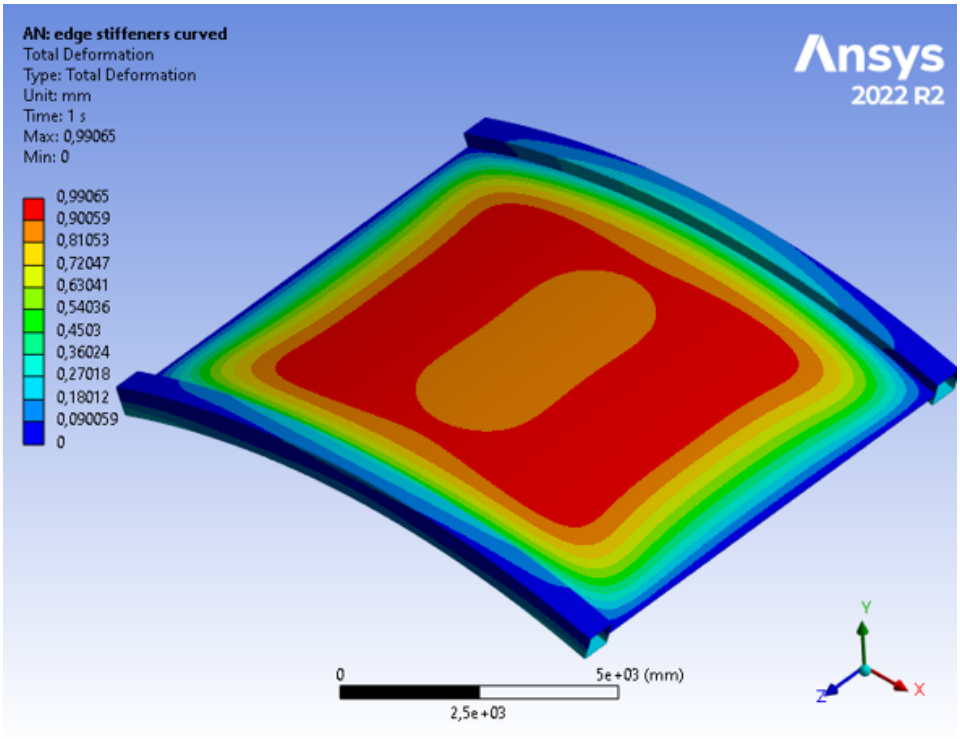

Figure I.10: Deformation of the boxed stiffener plate

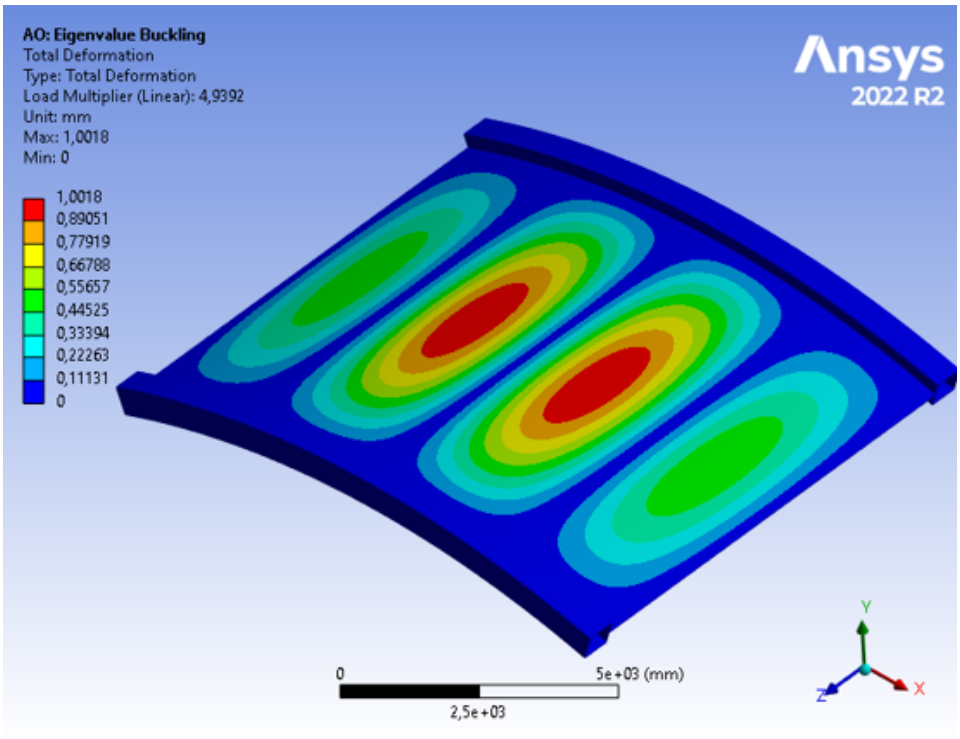

Figure I.11: Buckling mode 2 of the boxed stiffener plate

I.4. Stiffened arched plate field

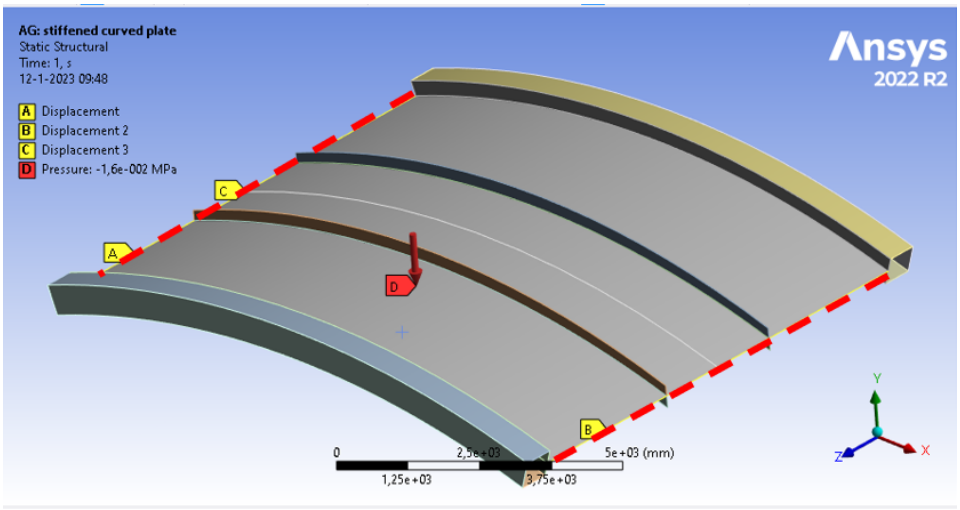

Figure I.12: Model set up for stiffened plate field

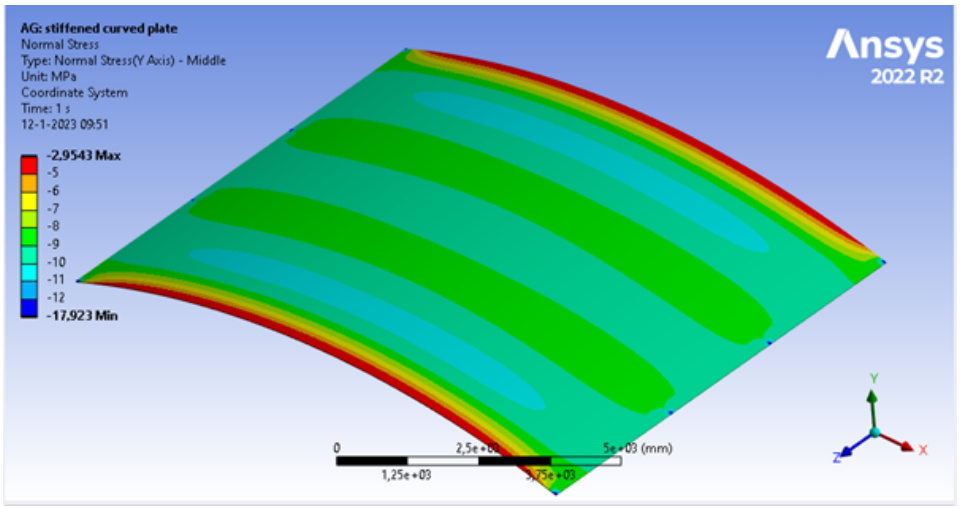

Figure I.13: Normal stresses along the curve of the plate

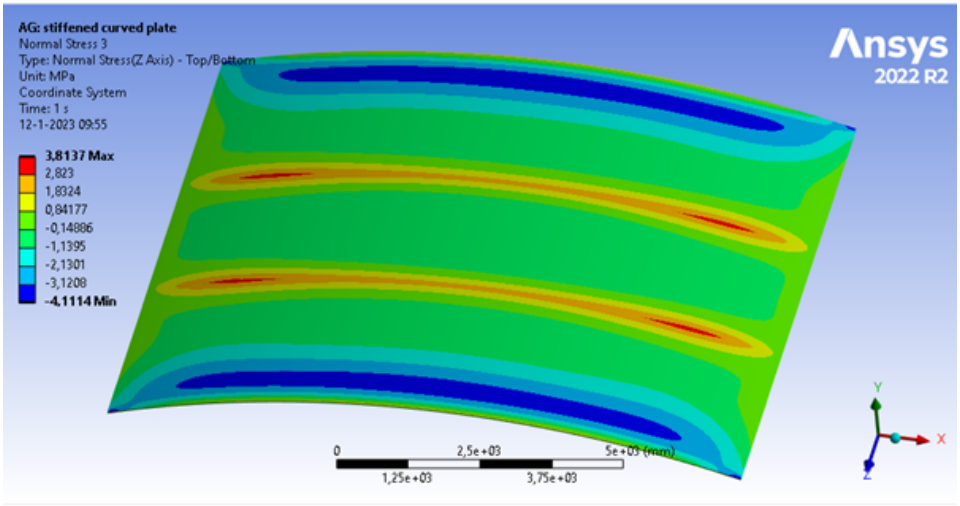

Figure I.14: Z axis stresses in stiffened curved plate

I.5. Frame around the curved plate

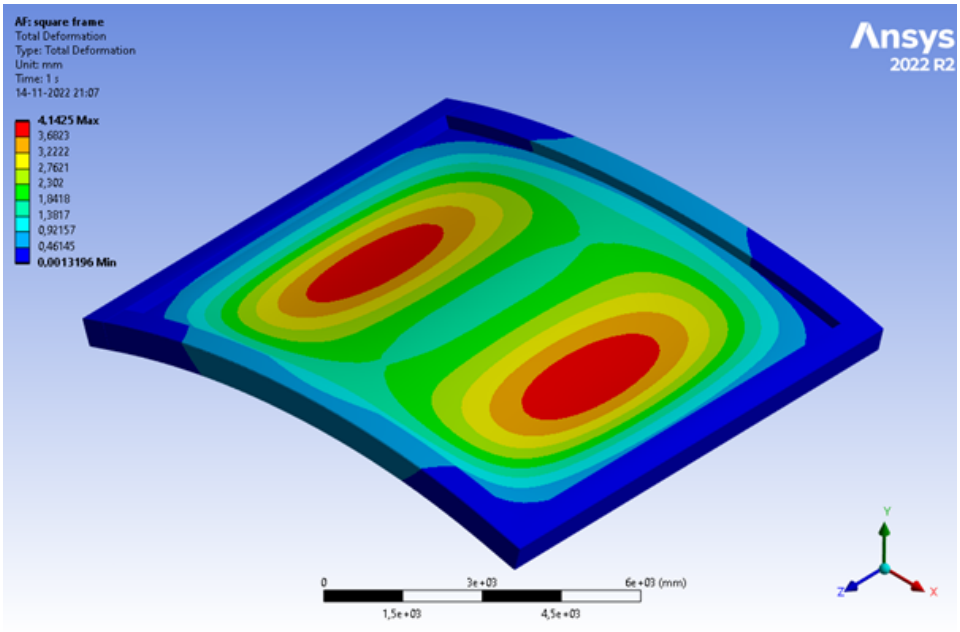

Figure I.15: Deformation in the framed arch plate.

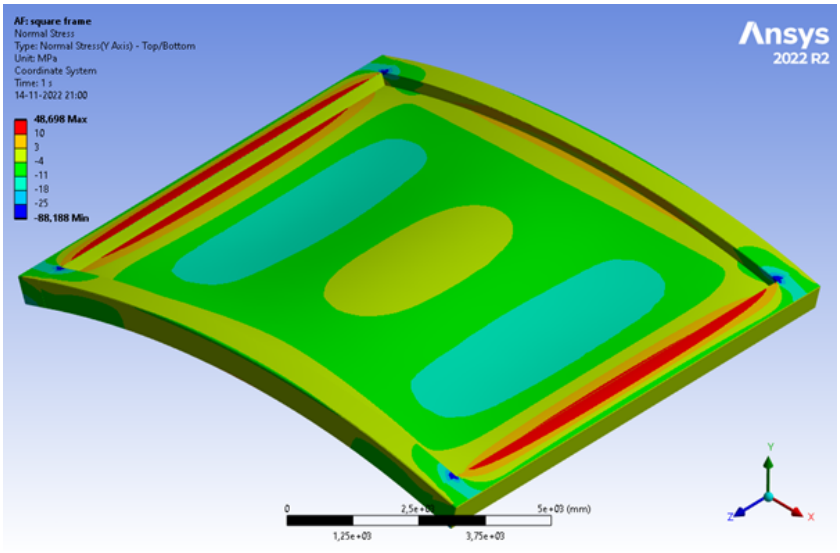

Figure I.16: Normal stress along the curve of the curve for the framed arch plate

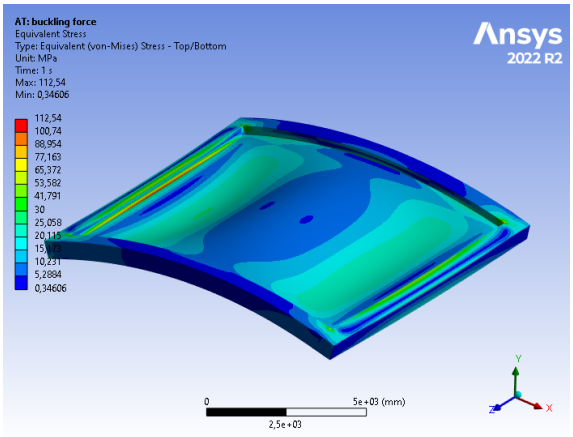

(a) Von Mises equivalent stress for the framed plate.

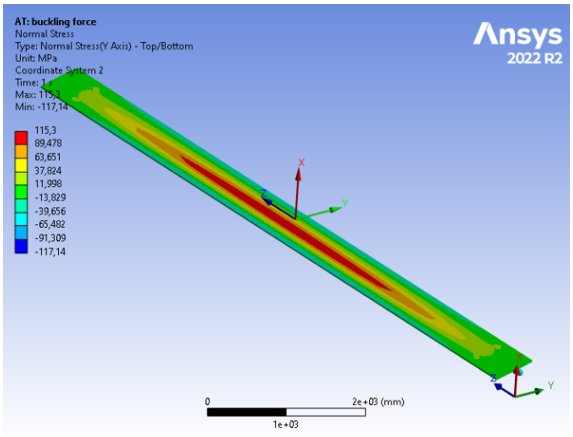

(b) Normal stress in the plate of the boxed stiffener.

J

Gate design

J.1. Design

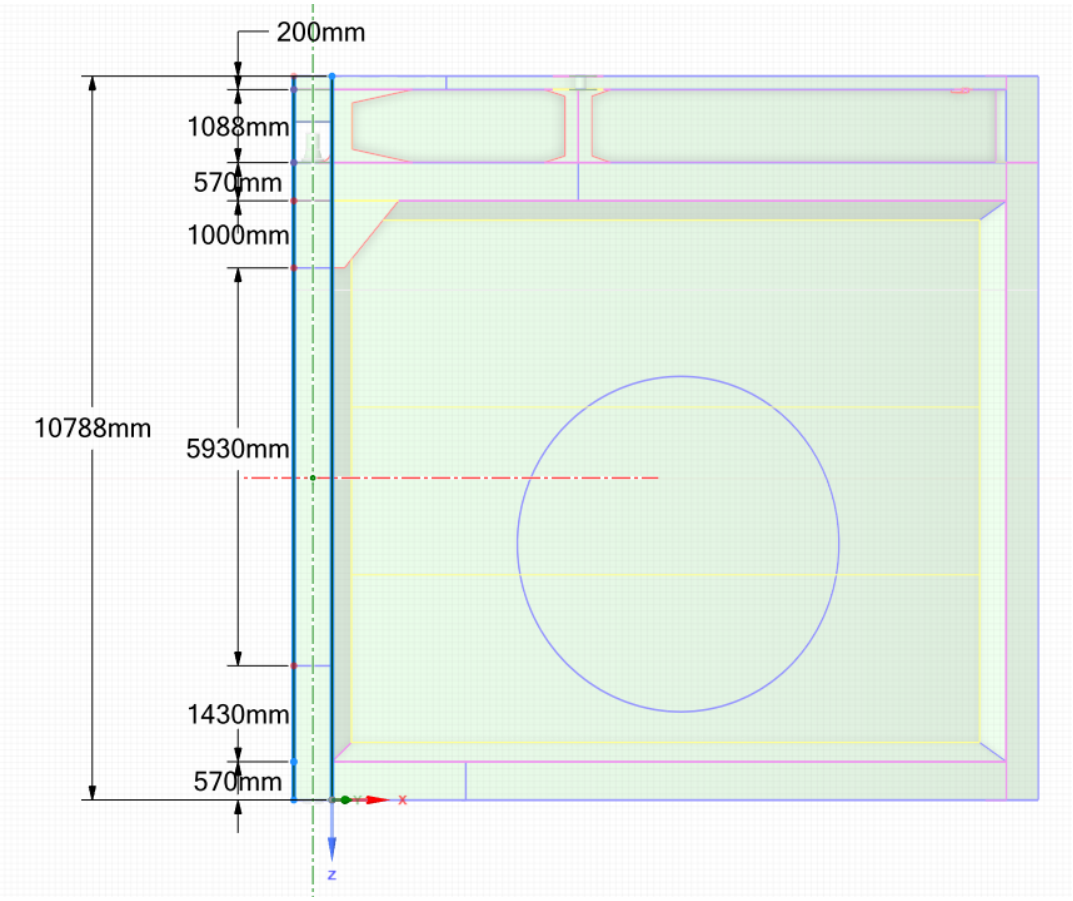

Figure J.1: Design of mitre gate with curved unstiffened plate and frame

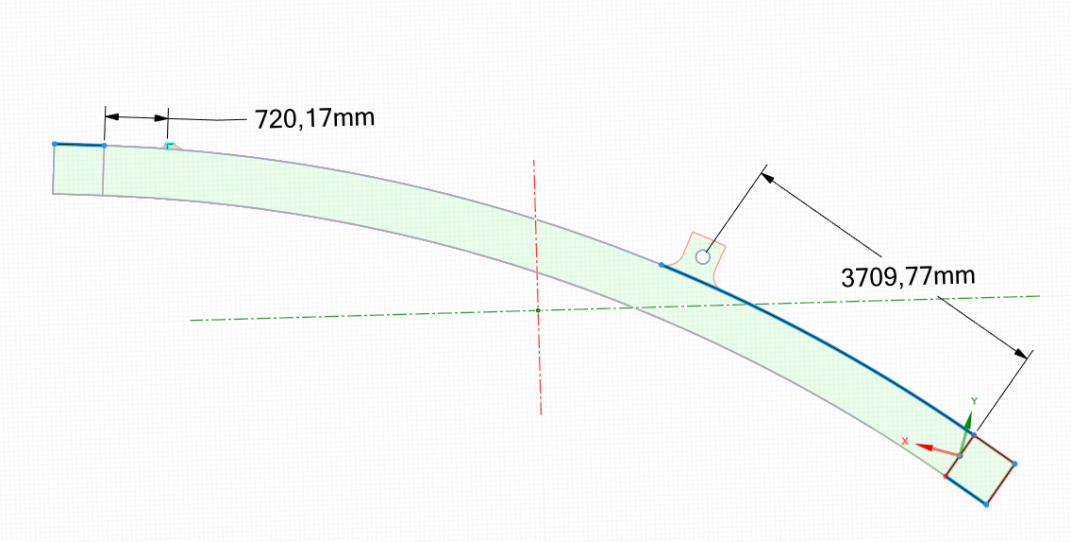

Figure J.2: Hook-up location and support location

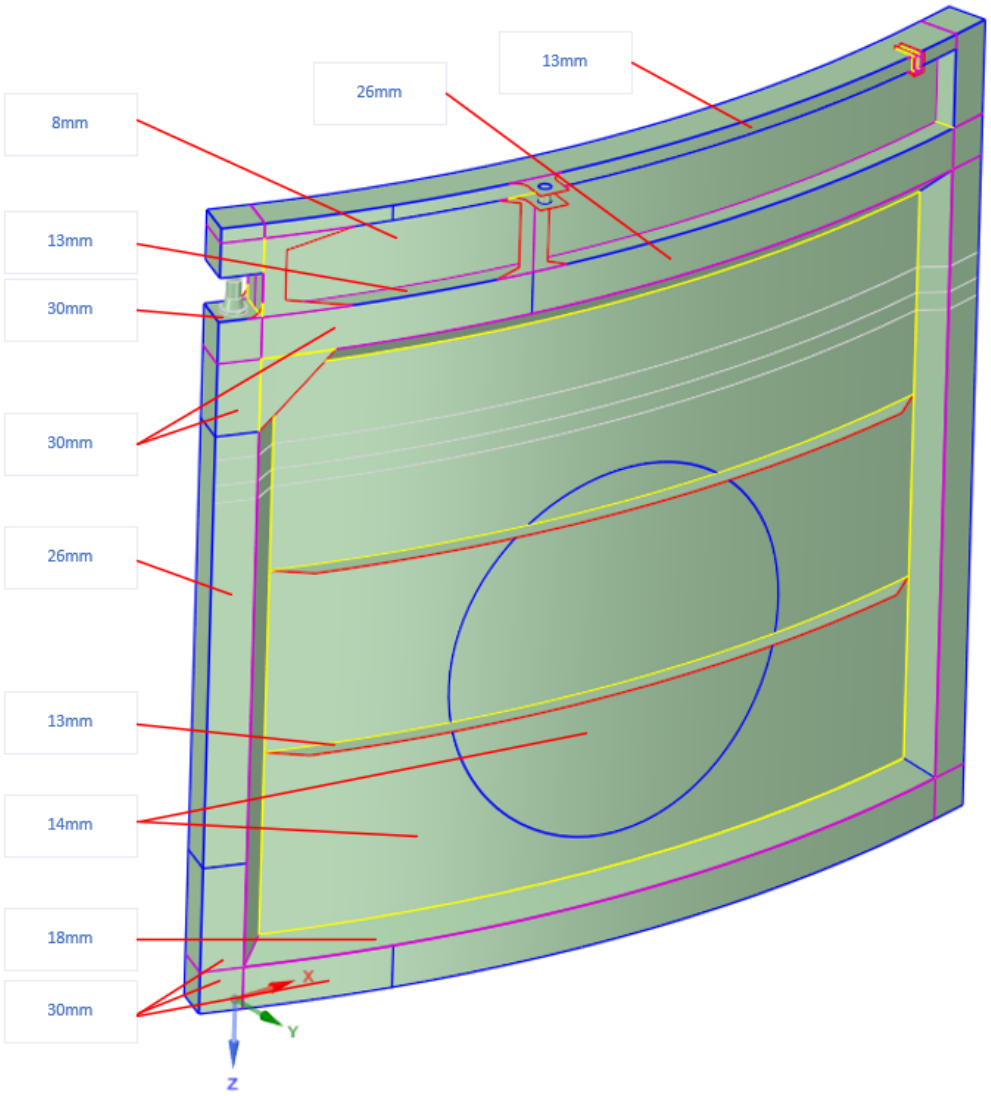

Figure J.3: Thickness of plates in the gate design.

K

Gate moddeling Ansys

K.1. Ansys modelling

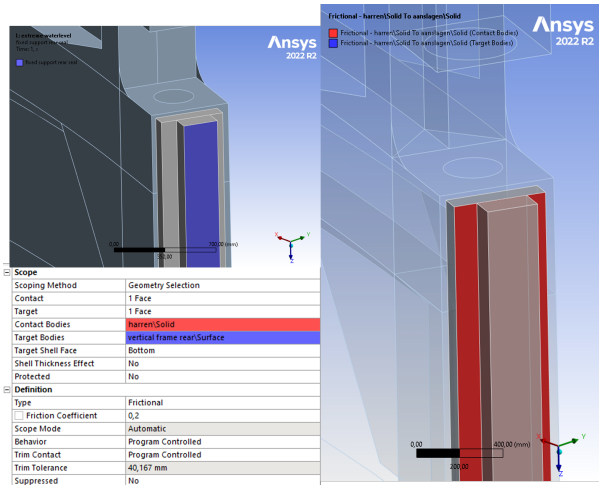

Scope	
Scoping Method	Geometry Selection
Contact	1 Face
Target	1 Face
Contact Bodies	harren\Solid
Target Bodies	vertical frame rear\Surface
Target Shell Face	Bottom
Shell Thickness Effect	No
Protected	No
Definition	
Type	Frictional
Friction Coefficient	0,2
Scope Mode	Automatic
Behavior	Program Controlled
Trim Contact	Program Controlled
Trim Tolerance	40,167 mm
Suppressed	No

Figure K.1: The surface to surface connection of the seals that is based on a frictional relationship.

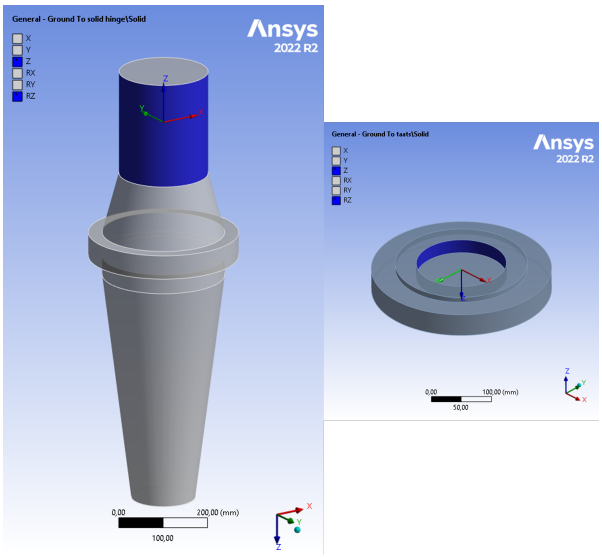

Figure K.2: The faces which are being used for the joint connections in the pintle and the hinge

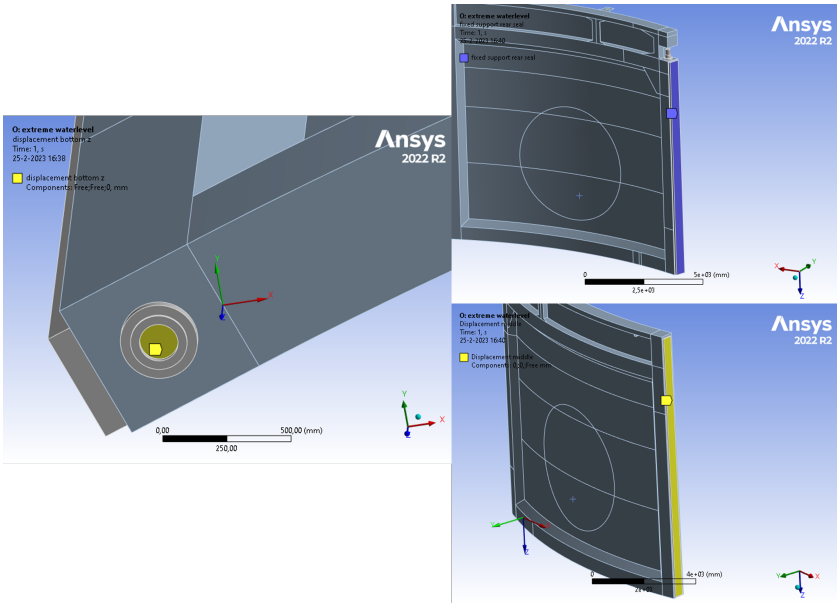

Figure K.3: The boundary conditions for the closed gate

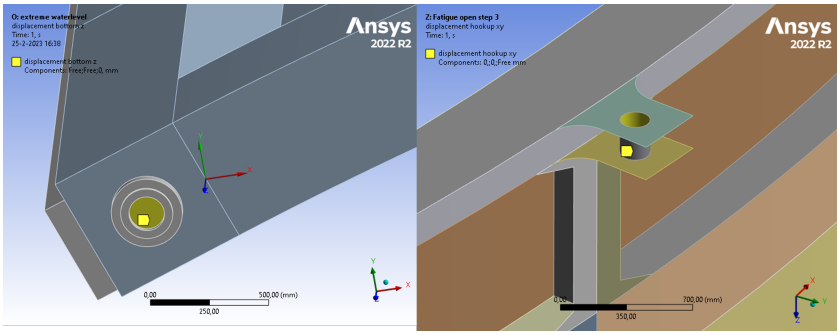

Figure K.4: The boundary conditions for the open gate

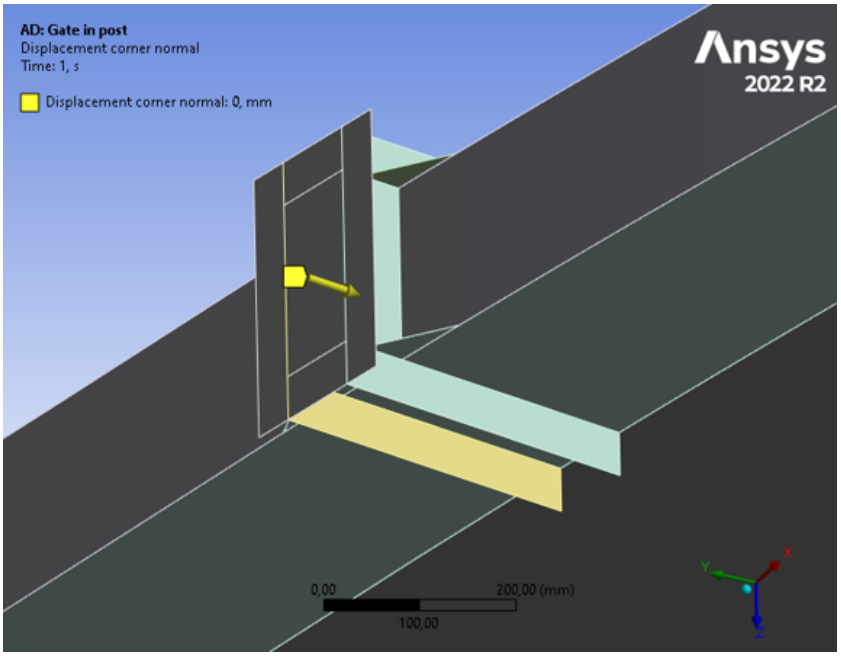

Figure K.5: The post which is used as a support to the gate when in its post.

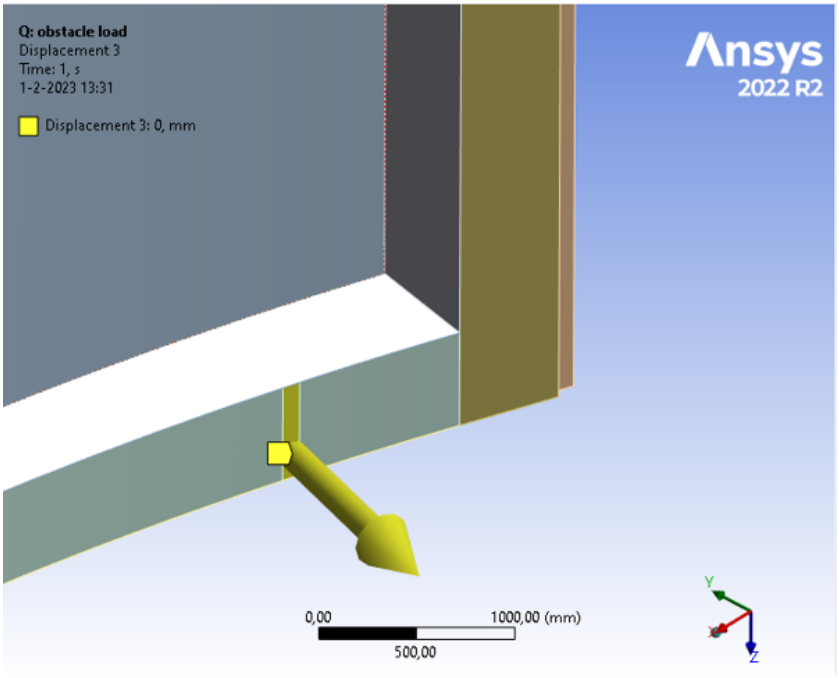

Figure K.6: Obstacle boundary condition on the bottom horizontal frame member.

Loads and combinations in Ansys

L.1. Forces

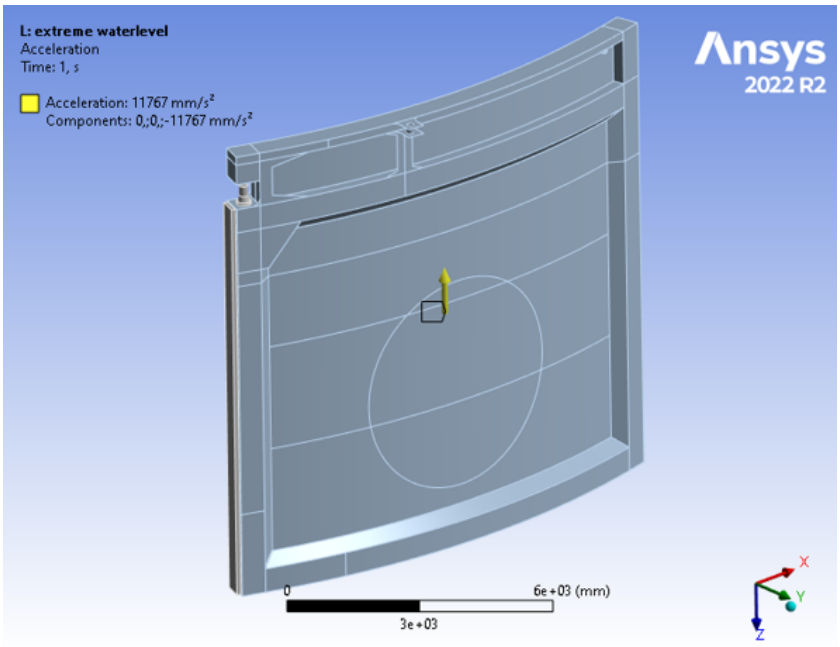

Figure L.1: Acceleration as modelled in Ansys

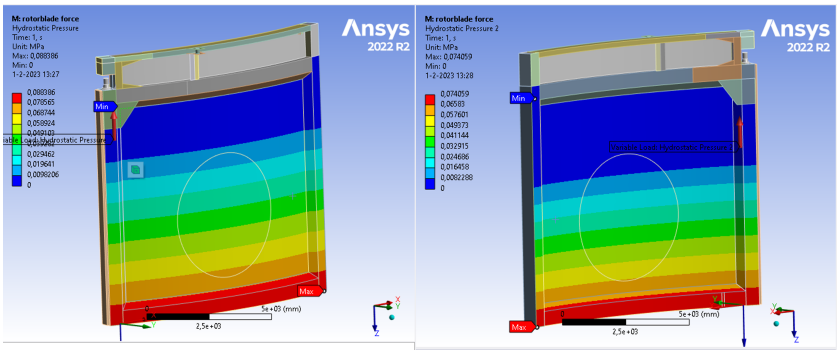

Figure L.2: Hydrostatic loads on both sides of the model.

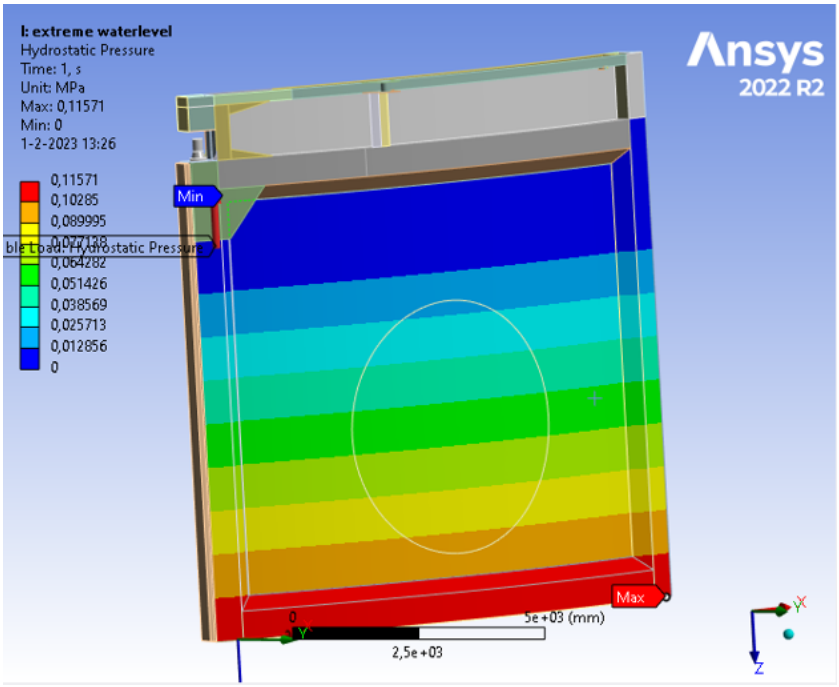

Figure L.3: Extreme water level high pressure as modelled in Ansys

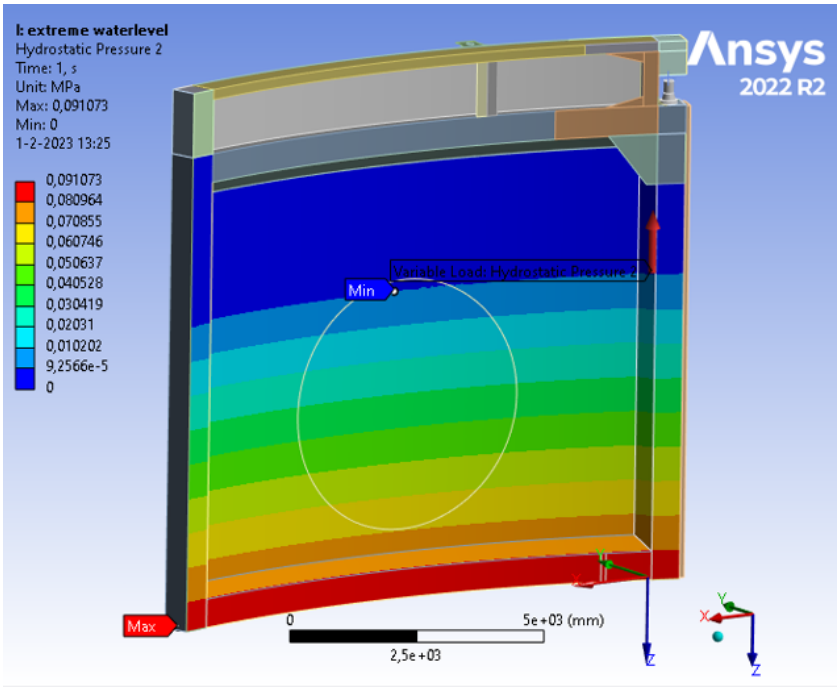

Figure L.4: Extreme water level low pressure as modelled in Ansys

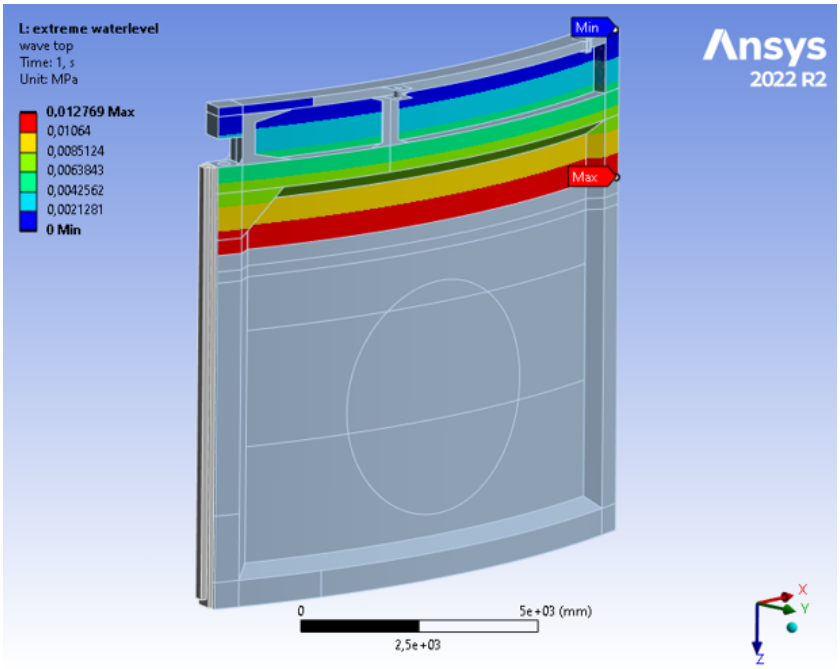

Figure L.5: Windwave top side pressure as modelled in Ansys

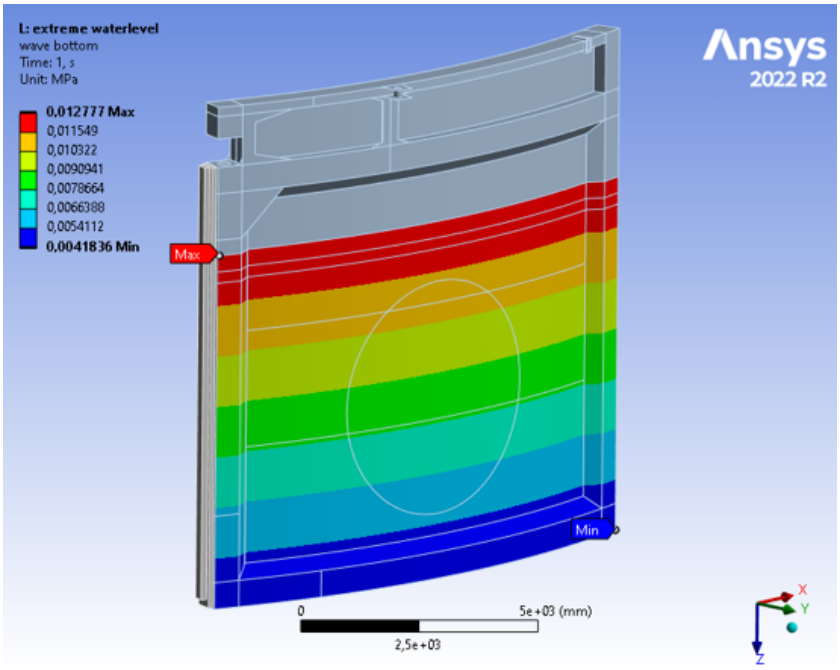

Figure L.6: Wind wave bottom pressure as modelled in Ansys

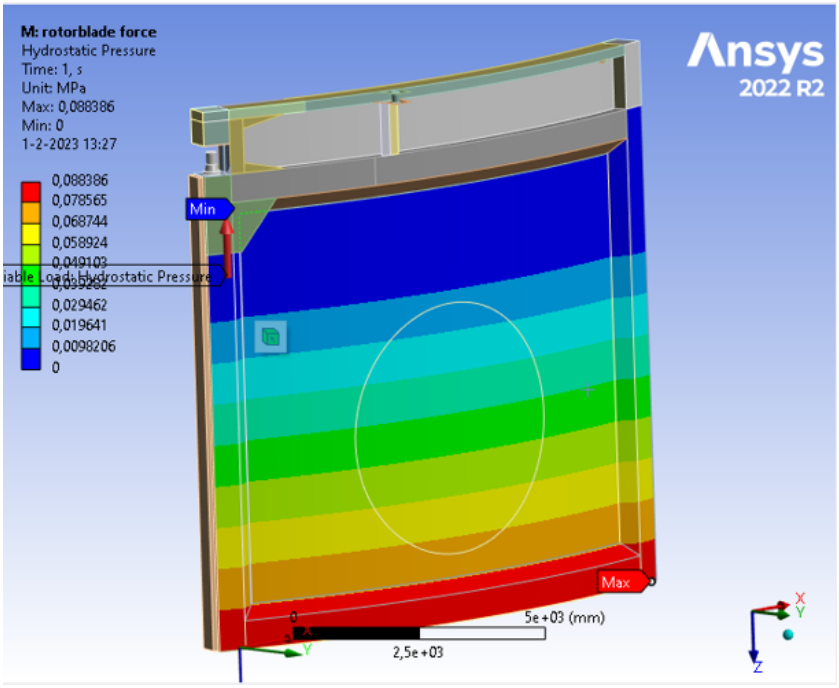

Figure L.7: Diffferential head high water level pressure as modelled in Ansys

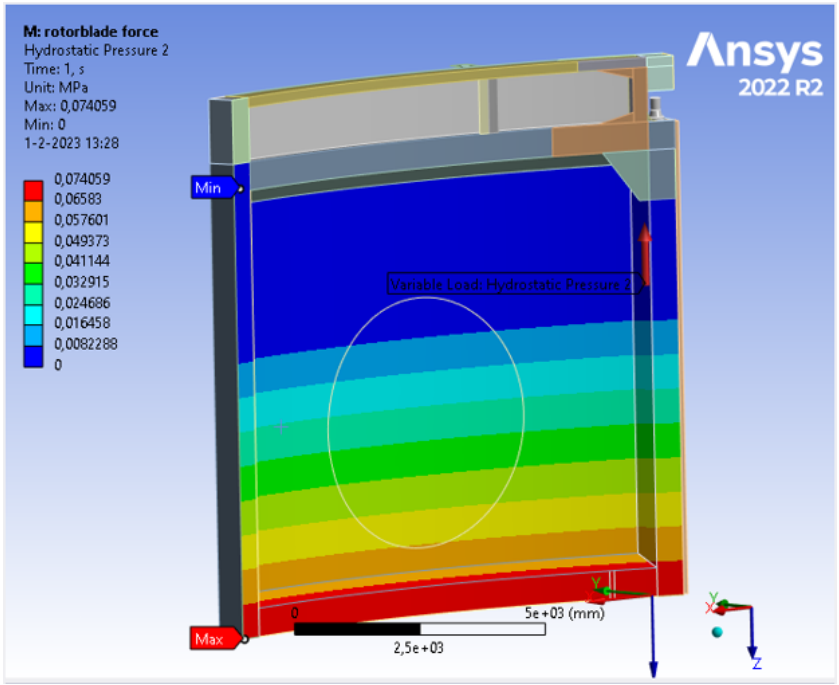

Figure L.8: Diffferential head low water level pressure as modelled in Ansys

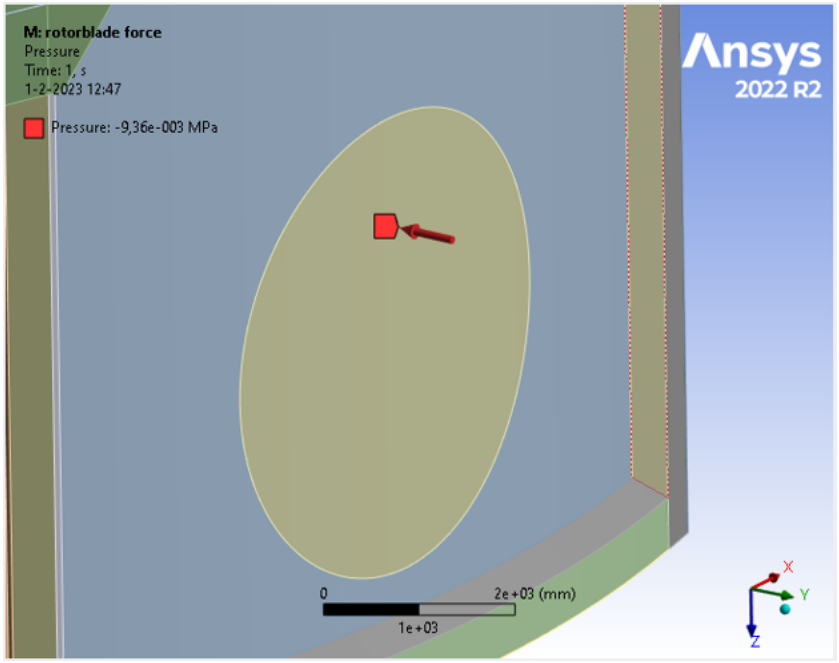

Figure L.9: Propeller load pressure as modelled in Ansys

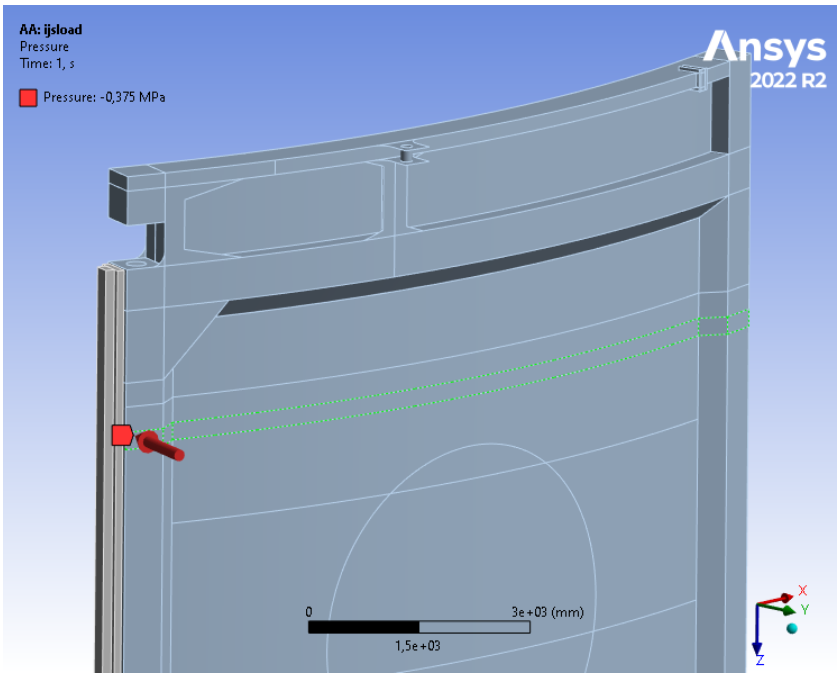

Figure L.10: Ice load pressure as modelled in Ansys

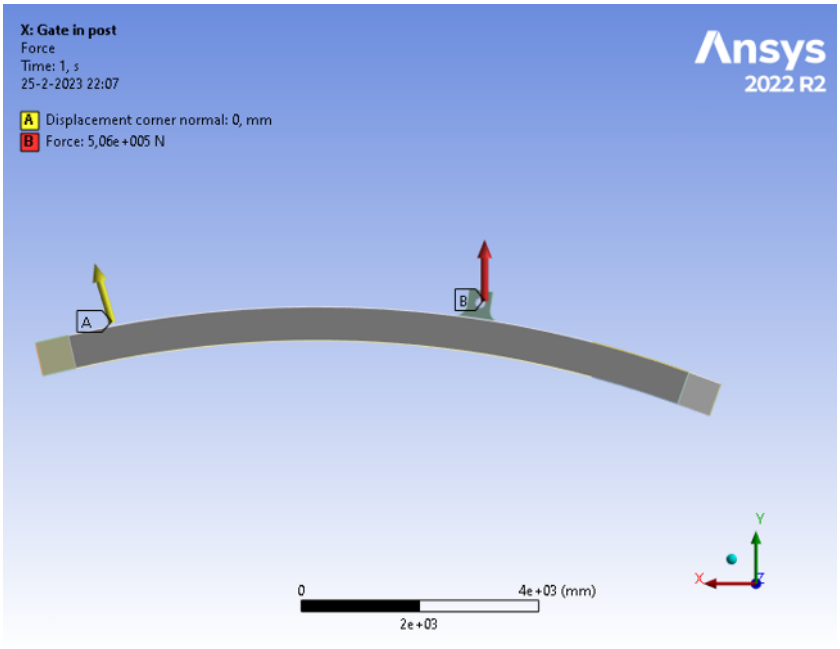

Figure L.11: Force applied to the top beam when the gate is simulated in its post.

L.2. Operational conditions

Figure L.12 shows how Ansys visualises the load combination on the design. In this figure, the extreme water head has been simulated on the gate. Also visualised are all separate components which play a role in the load combination.

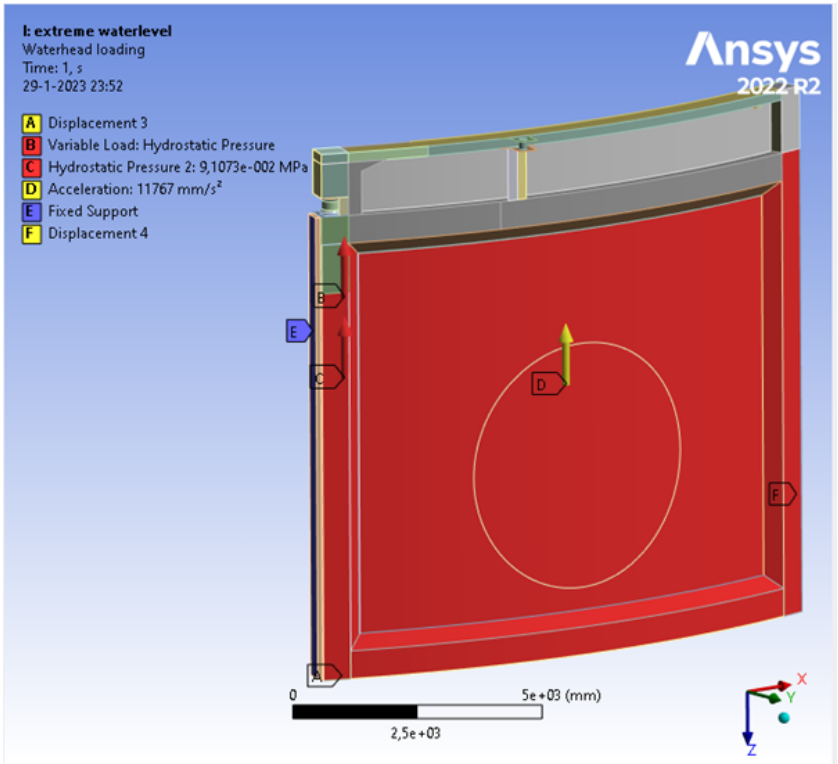

Figure L.12: Visualisation of the EWH load combination in Ansys Mechanical

L.13 in this figure the LC as used for the model in Ansys is presented

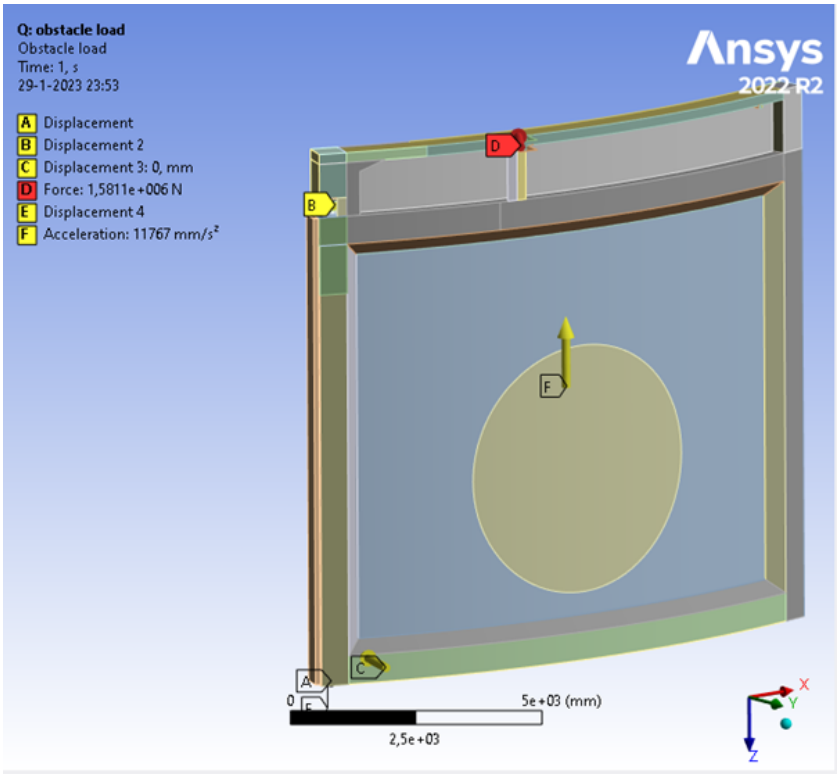

Figure L.13: Visualisation of the obstacle load combination in Ansys Mechanical

L.14 gives the figure of how the propeller load is made in the

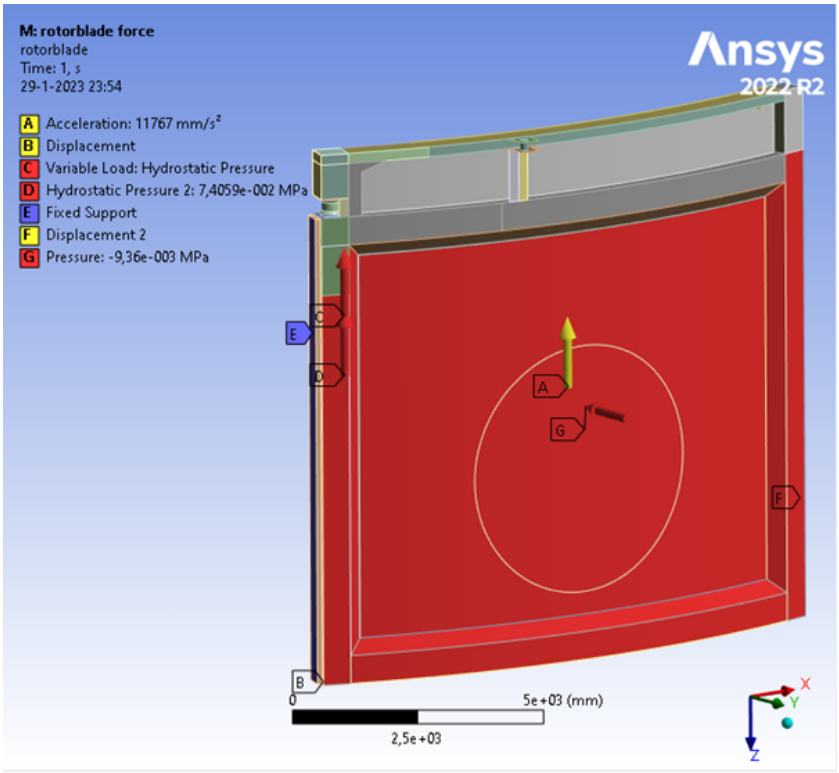

Figure L.14: Visualisation of the propeller load combination in Ansys Mechanical

L.15 gives the figure of how the gate is loaded if it is opened and is pulled against the gate post seal

in the left corner.

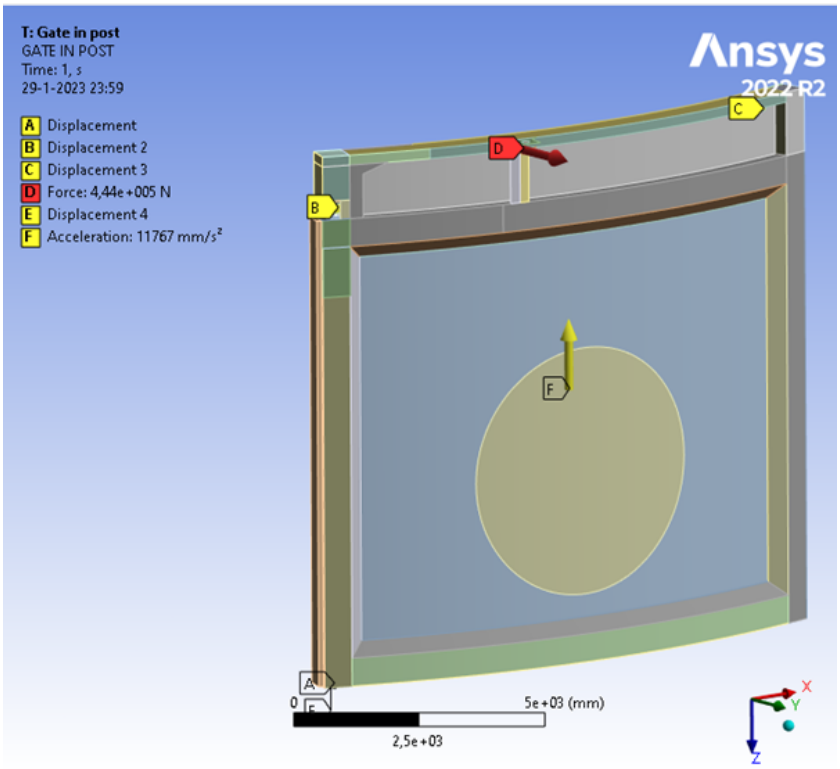

Figure L.15: Visualisation of the gate in its post load combination in Ansys Mechanical

The fatigue forces contain the different situations during opening and closing. There is also one crucial point in this process that is essential to check for the limit situations as the door is loaded in such a different manner than the two extreme cases that is needs to be taken into account when processing the larger forces acting on the door. Fatigue loads are shown in L.16 and L.17.

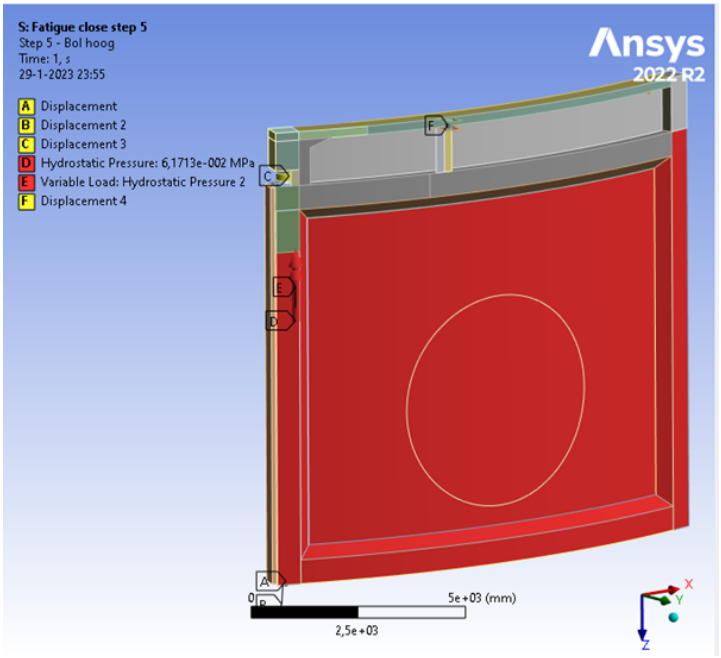

Figure L.17: Visualisation of the fatigue step 5 load combination in Ansys Mechanical

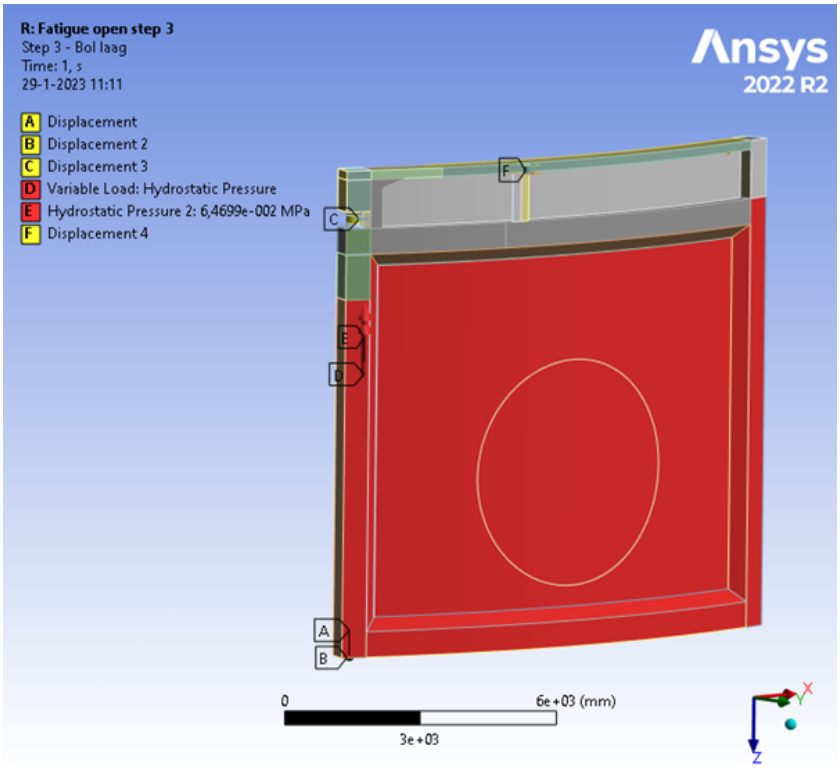

Figure L.16: Visualisation of the fatigue step 3 load combination in Ansys Mechanical

M

Results of gate simulations

M.1. EWH

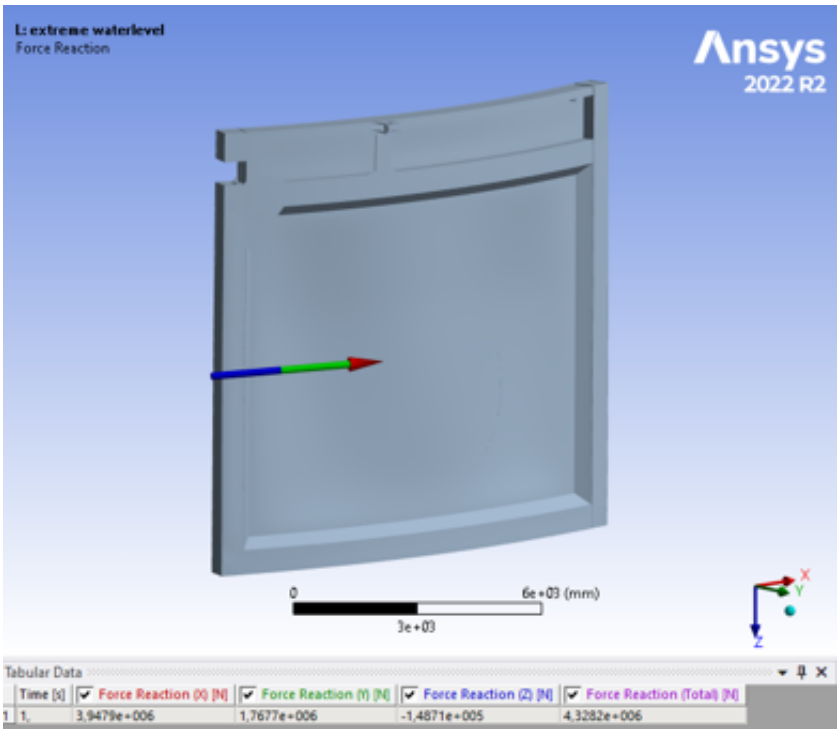

Figure M.1: Vertical reaction force on the inner seal due to firction

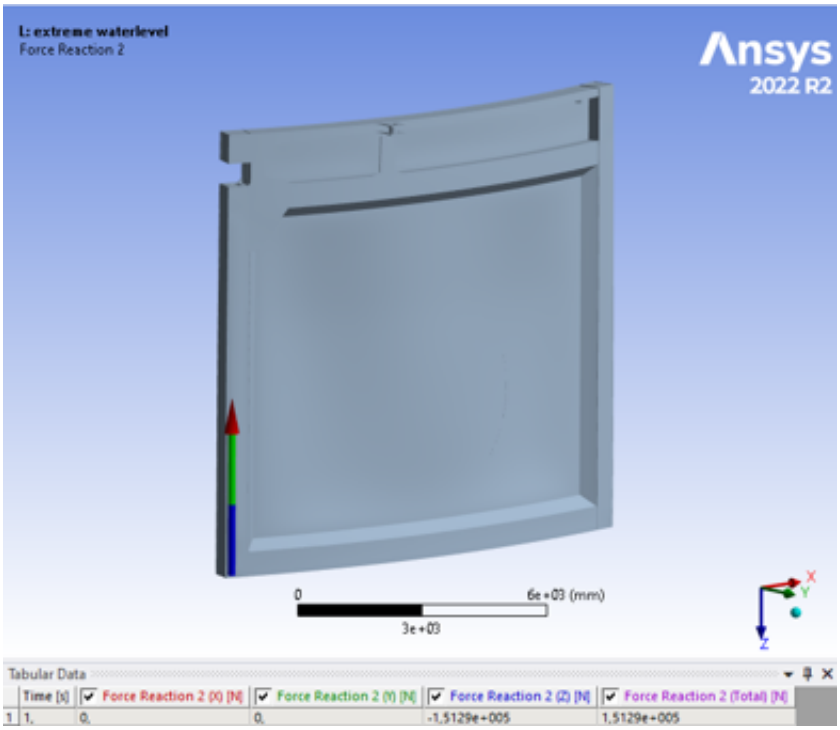

Figure M.2: Vertical reaction force of the pintle

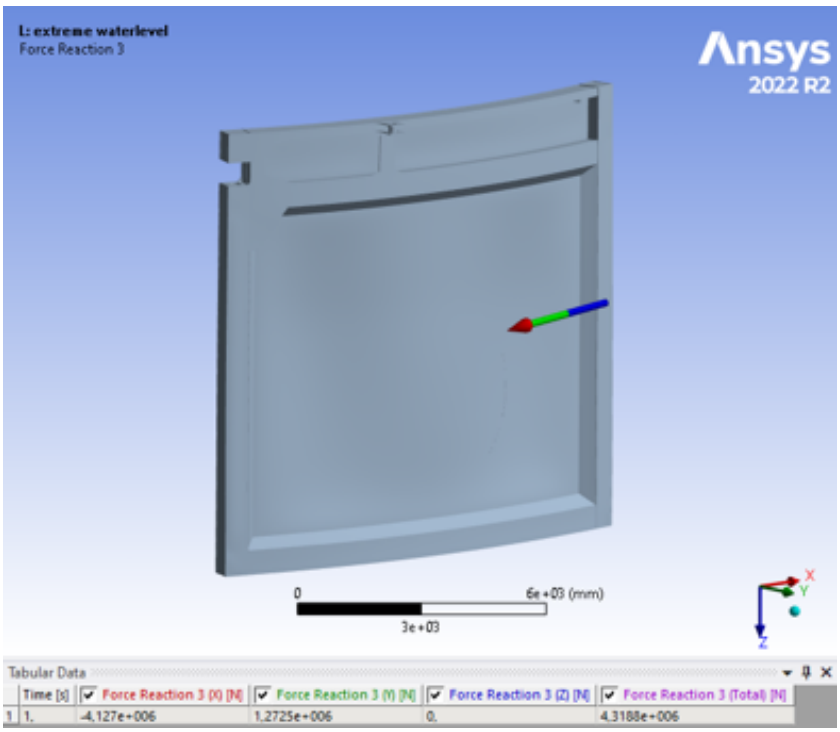

Figure M.3: Horizontal reaction of the middle seal of the lock

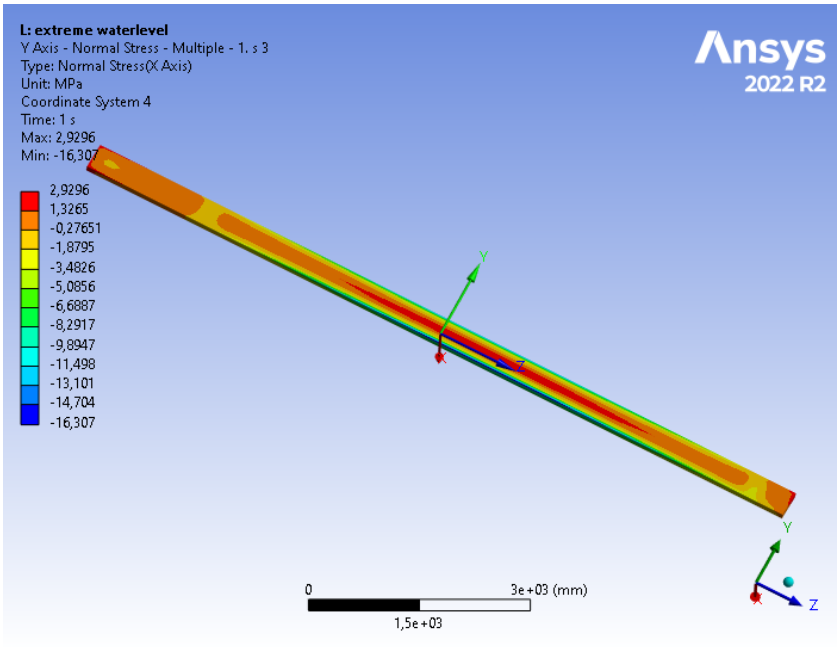

Figure M.4: Normal stresses perpendicular to the face of the seal in the middle of the lock

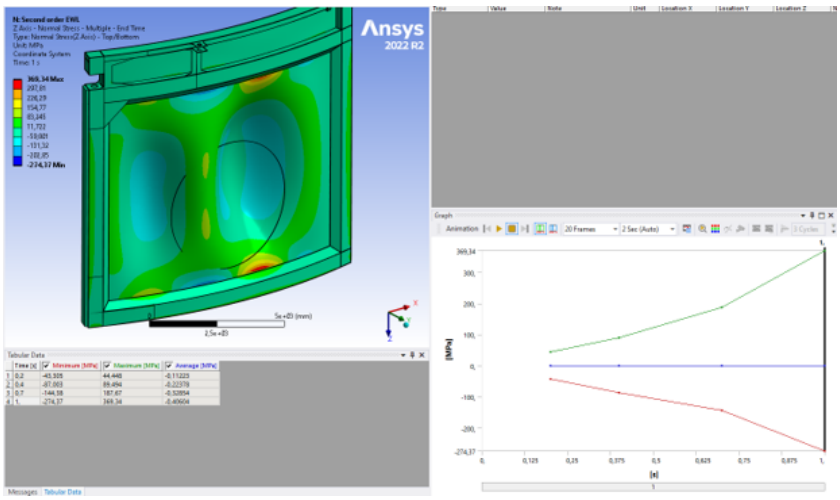

Figure M.5: Stability in the GNIA

The second buckling mode is similar to the first mode in the vertical direction. The horizontal buckles have increased over the width. As seen in figure 6.4b there are five buckles, and the middle of the plate buckles into the loading direction. The two buckles along the side of the largest buckle are deformed at 70% compared to the largest deformation. This makes the total deformation in the direction of the load larger than in the opposite direction. The deformation is sinus shaped, which results in large normal stresses where the plate is most bent and deformed. To determine if the second mode is more critical than the first, it will be used for the GNIA too. The plate has five buckles, of which the largest span is the middle one. The width of the buckle is approximately between a fourth and a fifth of the total plate width. A more conservative estimation would be to assume it to be 4, which enlarges the imperfection of the buckle. The imperfection is therefore equal to the imperfection in the first buckling mode analysis, which is 12 mm.

Figure M.6a shows the results from the second-order deformation. The minimum value, which is in absolute values the largest, is smaller than the first mode results. The location of the deformations is similar to the shape of the buckling mode itself, as the buckles next to the middle increase in size even

further. The middle buckle is bent in the opposite direction from the resultant loading and is opposite to the adjacent buckles. The general deformation of the plate is in the direction of the force and the value is, therefore, lower than the absolute deformation in the other direction. Figure M.6b presents the results from the equivalent Von Mises stresses. The plate shows no sign of yielding and the maximum stress is lower than in the first mode. The largest buckles have stresses at the bottom and top of the plate likewise to the first mode.

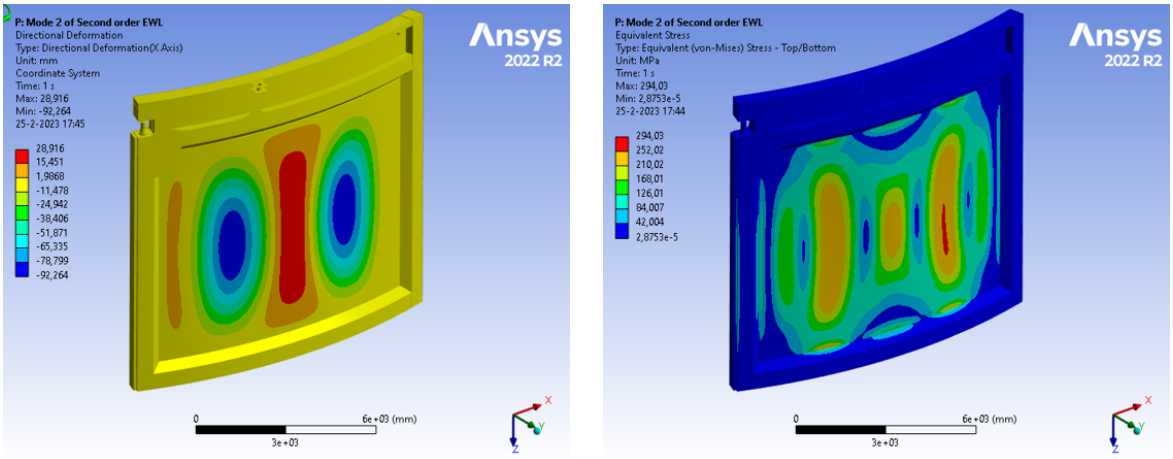

(a) Deformation of the construction

(b) Equivalent von Mises stress.

Figure M.6: Results of second order simulation for second buckling mode.

The observed values for the normal stress are lower than in the first buckling mode. When considering fatigue, the stress spots that might form at the top and bottom will be identical fatigue details to the critical spot in the first mode. They will not be more critical in the second mode due to the lower stresses present. The results of the normal stresses can be found in figures M.7a and M.7b. Figure M.7a gives the results from the normal stresses in Y along the plate. These values are slightly lower stresses than for the first buckling mode. Figure M.7b gives the results from the normal stresses in the Z direction in the plate.

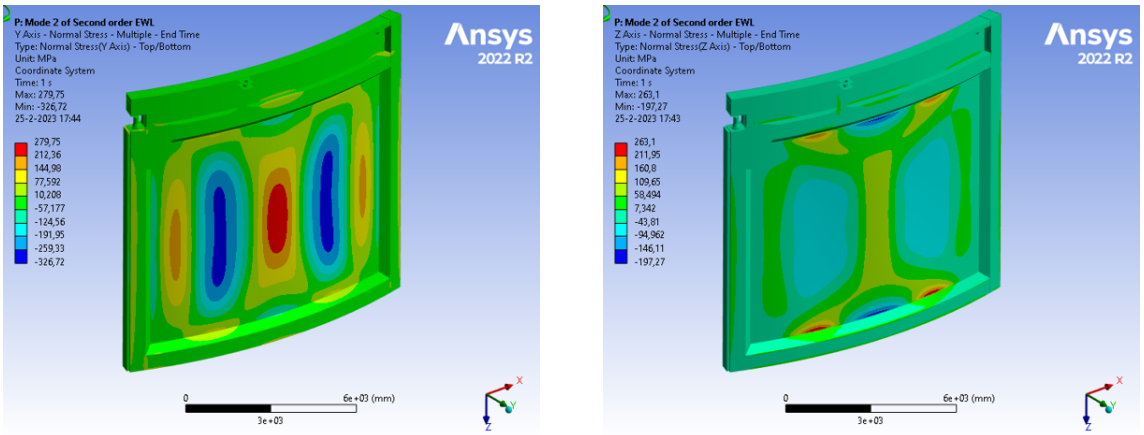

(a) Stresses along the horizontal curve of the plate.

(b) Vertical direction (z) stresses.

Figure M.7: Results of normal forces from second-order simulation for second buckling mode.

For this study the first mode is assumed to be critical. This is based on the results found in the EWH load combination. Higher buckling modes have been found to present more buckles on the plate which lead to smaller imperfections. Smaller imperfections in the plate lie closer to the perfect design in which the arch working of the plate is dominant, meaning that forces can be transferred more efficiently due to the global arch effect.

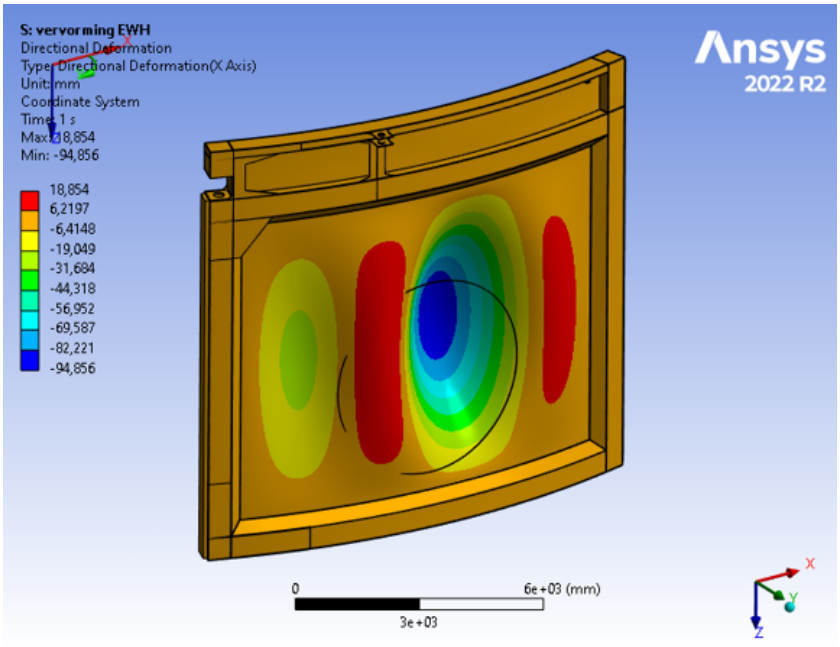

Figure M.8: Deformation in GNIA

M.2. Propellor load

The construction does not have extreme stresses. The highest stress is at the column which is in contact with the fixed support. This was also the case in the EWH load.

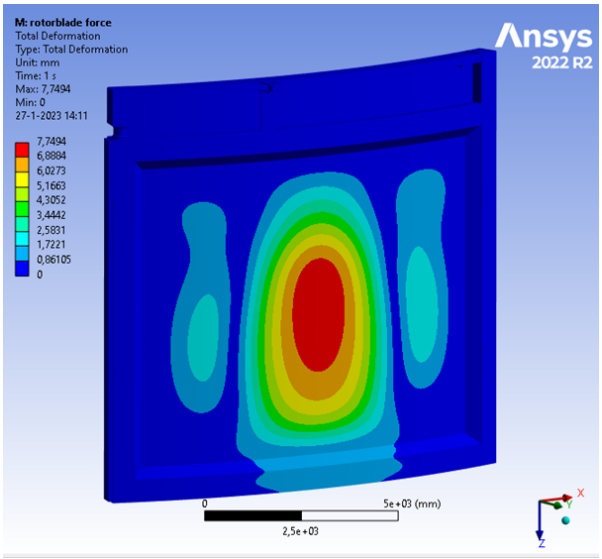

Figure M.9: Deformation of the gate with the propellor load in LA

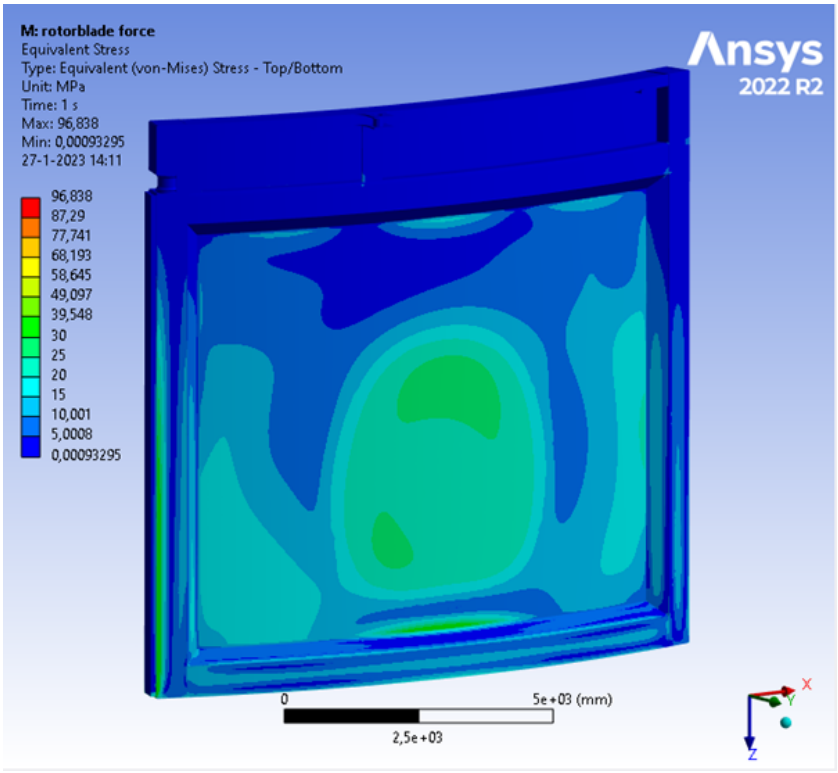

Figure M.10: Equivalent Von Mises stress for the first order propeller load combination.

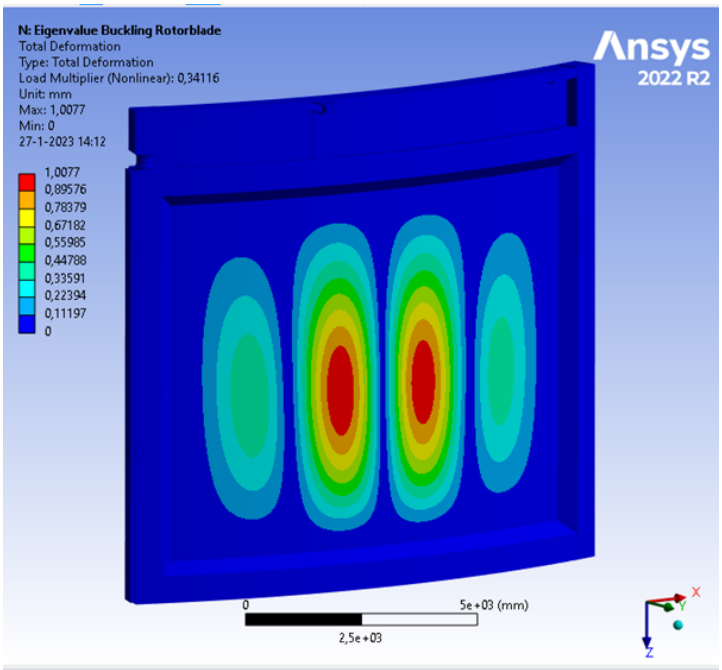

Figure M.11: Buckling shape of mode 1 due to Propeller load

Figure M.12 gives the results from the equivalent stresses in the second-order analysis. It is visible that yielding is not reached in the construction due to this load. The stresses are around the deformation like found in the other stress results.

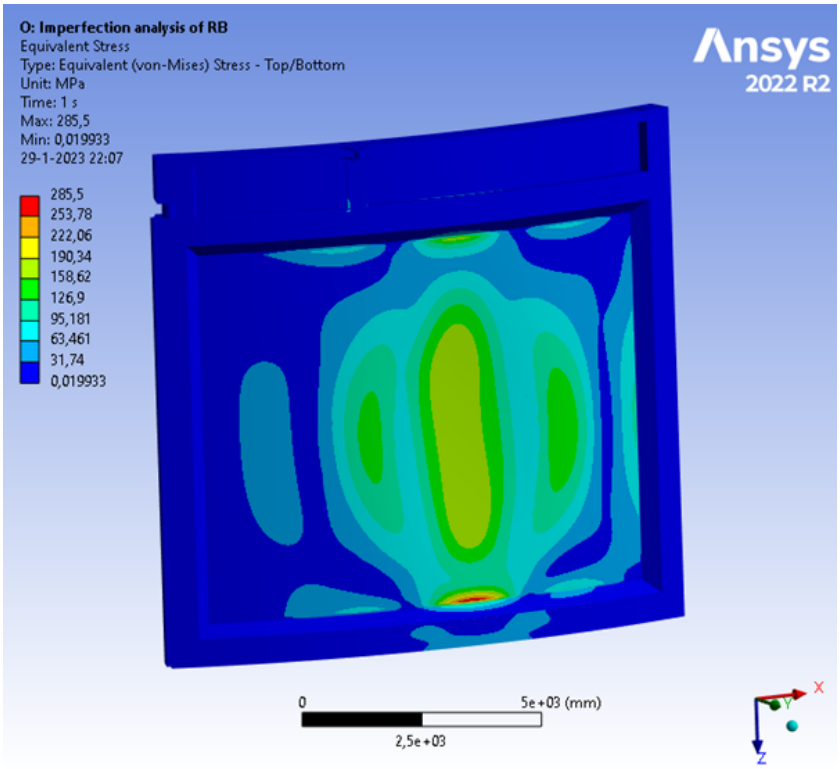

Figure M.12: Equivalent stresses

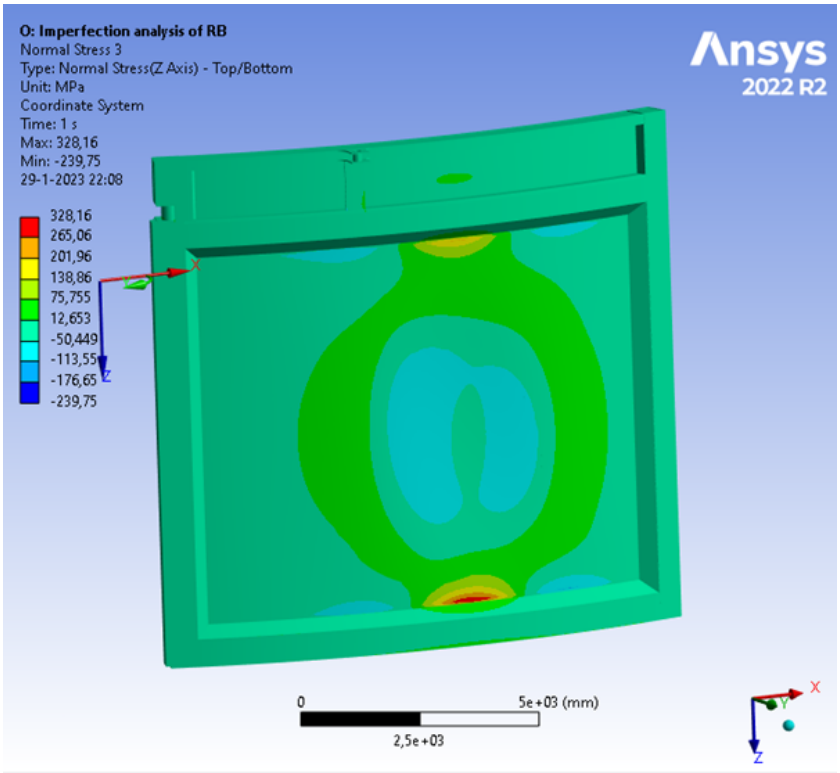

Figure M.13: The normal stresses in the vertical direction (Z) for the GNIA of the propeller load.

Figure M.14 gives the results from the normal stresses along the horizontal direction of the curved field. The larger stresses are mainly in the plate field which means that there are bending moments

there but they do not lead to yielding. In the no high stresses at the edge of the plate.

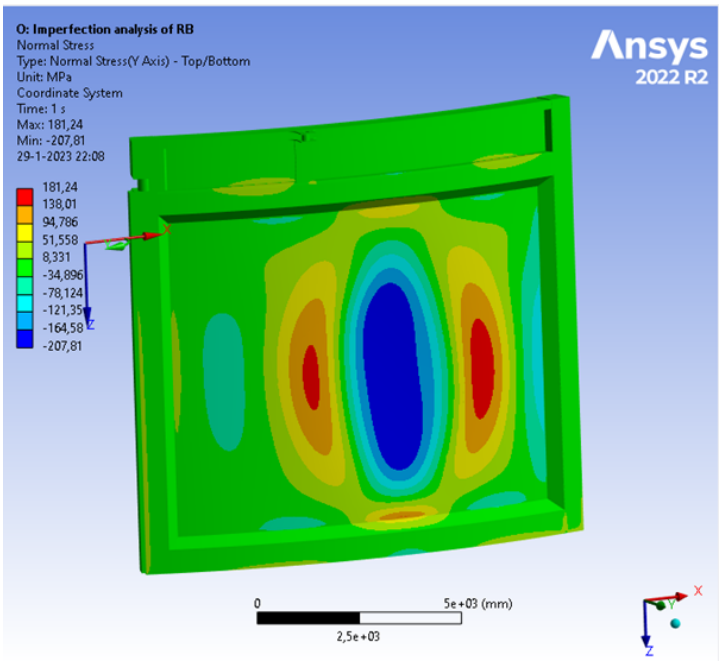

Figure M.14: The normal stresses in the horizontal direction along the curve of the main plate for the post-buckling analysis of the propeller load.

In figure M.15 the result of the deformations in a large deformation analysis is given.

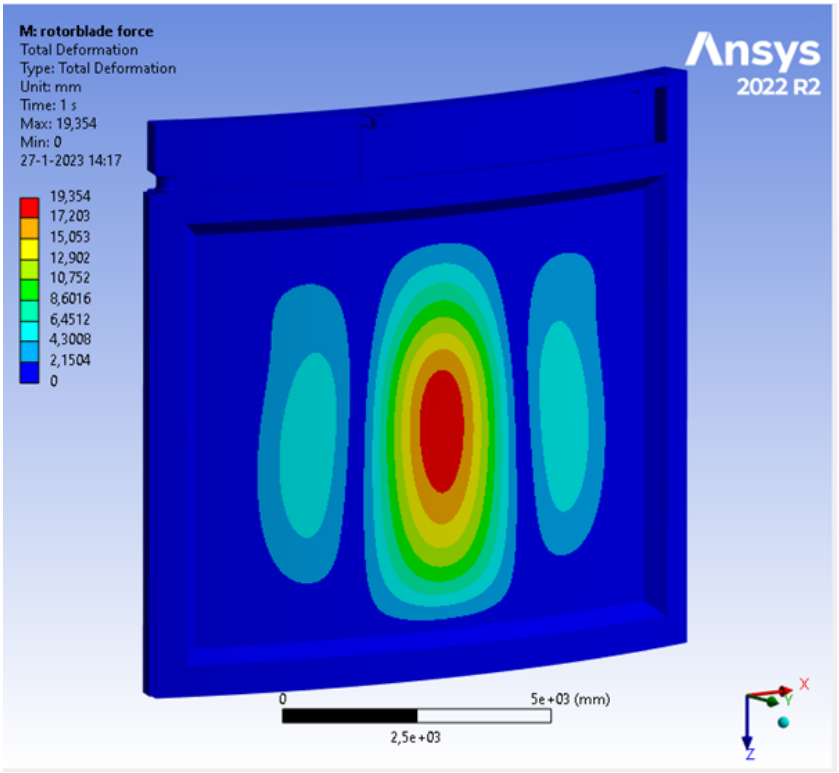

Figure M.15: Large deflections option in Ansys for a first-order analysis.

Figure M.16a gives the results from the large deformations option in Ansys for the normal stresses

in the y direction of the plate. Stresses are more than twice as high but do not approach yielding. Figure M.16b gives the results from the large deformations option in Ansys for the normal stresses in the y direction of the plate. the blue spot in the middle is smaller than in the regular calculation so less arch effect present. No extreme stresses are present.

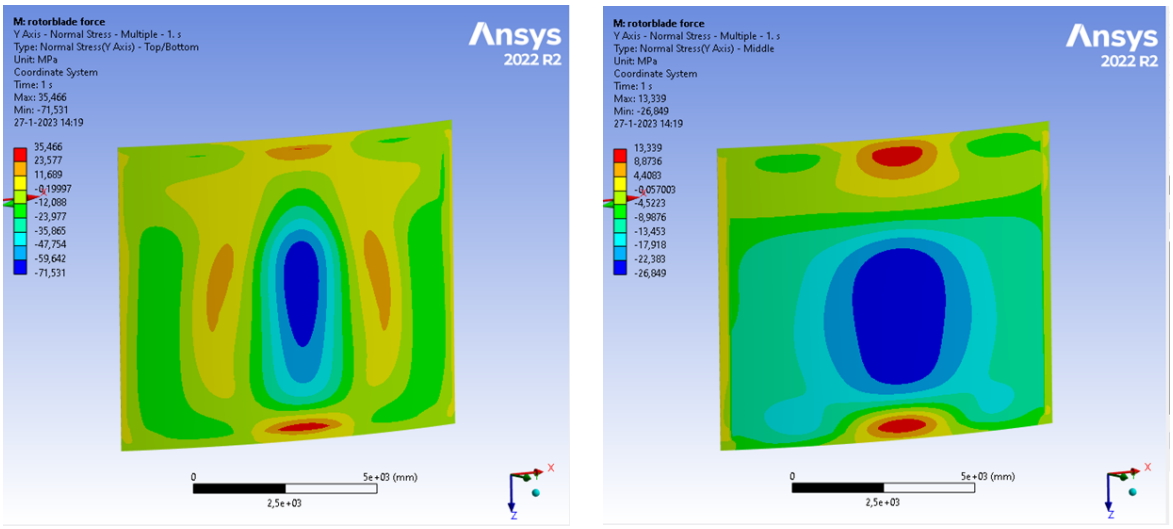

(a) Stresses on the top and bottom of the node.

(b) Stresses in the middle of the node.

Figure M.16: Normal stresses in the main plate

While not critical in the already simulated situation, the propellor load has the possibility to be critical if placed in a different location on the gate. As the buckling shape of the first mode of the EWH presented the largest issue thus far, it was used to determine the most critical imperfection shape in this situation. A GNIA is used, but it is based on the most critical buckling mode instead of its own buckling shape. Figure M.17a shows the results from the first buckling mode. The deformations that were found have been magnified to see where the buckle is in the direction of the load. The propeller load can be seen alligned with this deformation in M.17b. Changing the location to the other side, to align the load with the largest deformation in the opposite direction, has been tested and did not prove to be more critical.

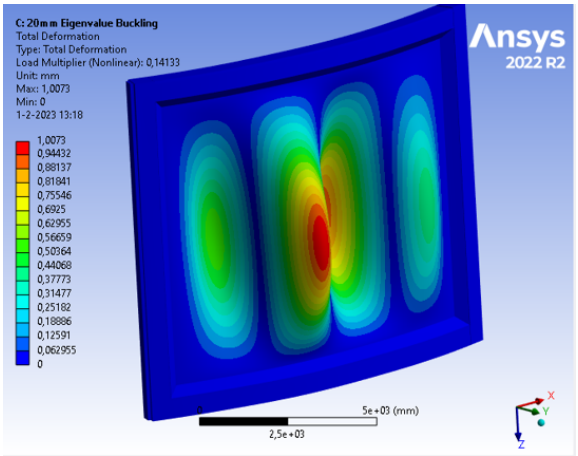

(a) The buckling shape of the first eigenvalue mode of the EWH with extreme deformations visualized.

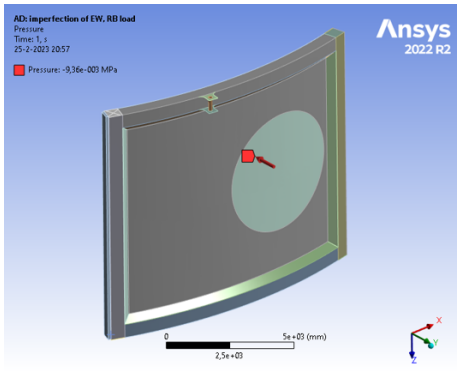

(b) location of the propeller load when shifted to the large deformation location.

Figure M.17: The model and the propeller load location used for the unideal location simulation.

As could be expected, the stresses are formed similarly at the top and bottom of the largest deformation. These values do not prove more critical than the results from the initial analysis of the propeller load. The location of the stress peak is in a different location than in the load in the middle of the plate

model and therefore fatigue can be discarded for this load situation. The asymmetrical propeller load will not be more critical than in the original location. In figure M.18 the results from the equivalent Von Mises stress due to the changed location of the load are shown. The results of the normal stresses in the plate can be found in figures M.19 and M.20.

The normal forces which are created in this Figure M.19 give the results from the normal forces in the y direction. At the end where the plate is attached to the frame, there are stresses which are interesting as seen from a fatigue perspective but the situation will not be as often repeated as the regular fatigue cycles. The weld at the location has the potential to be a good detail category. it can be a detail of 80 which can have the allowed stress of 270 MPa for half the cycles which would still be very conservative as there are not that many ships of this format that pass the lock.

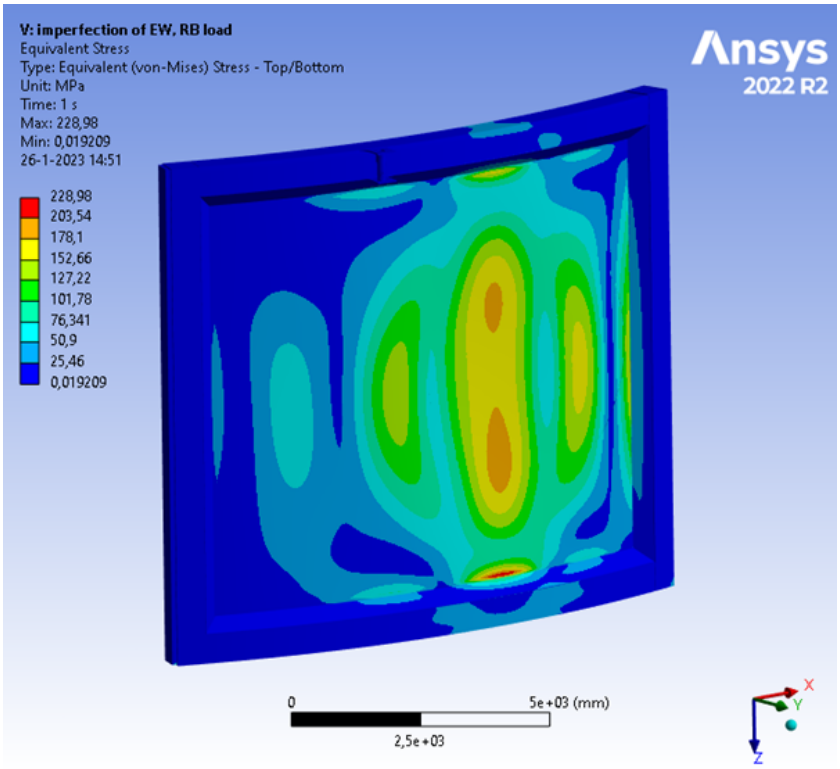

Figure M.18: Equivalent stress of the post-buckling analysis of the asymmetrical propeller load.

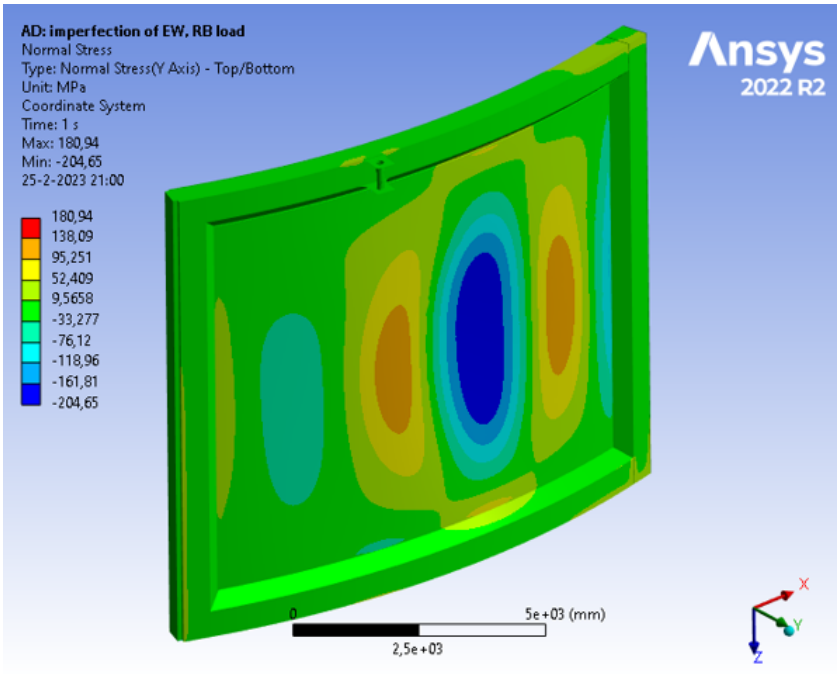

Figure M.19: Normal stress due to asymmetrical propeller load in Y direction

Figure M.20 gives the results from the z direction of the plate stresses. All comments for the results in the y direction of the plate are also valid for the z direction.

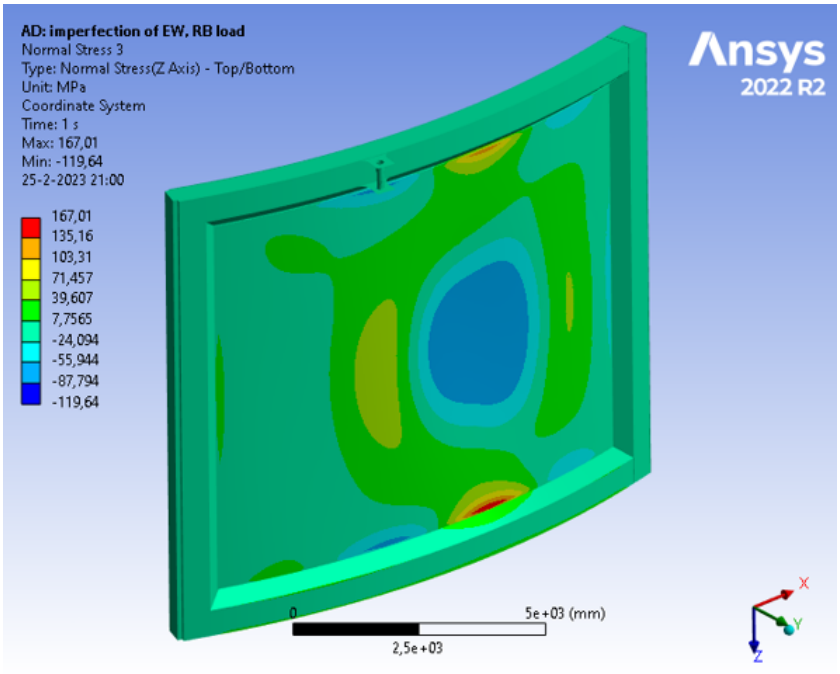

Figure M.20: Normal stress due to asymmetrical propeller load in Z direction

M.3. Ice load

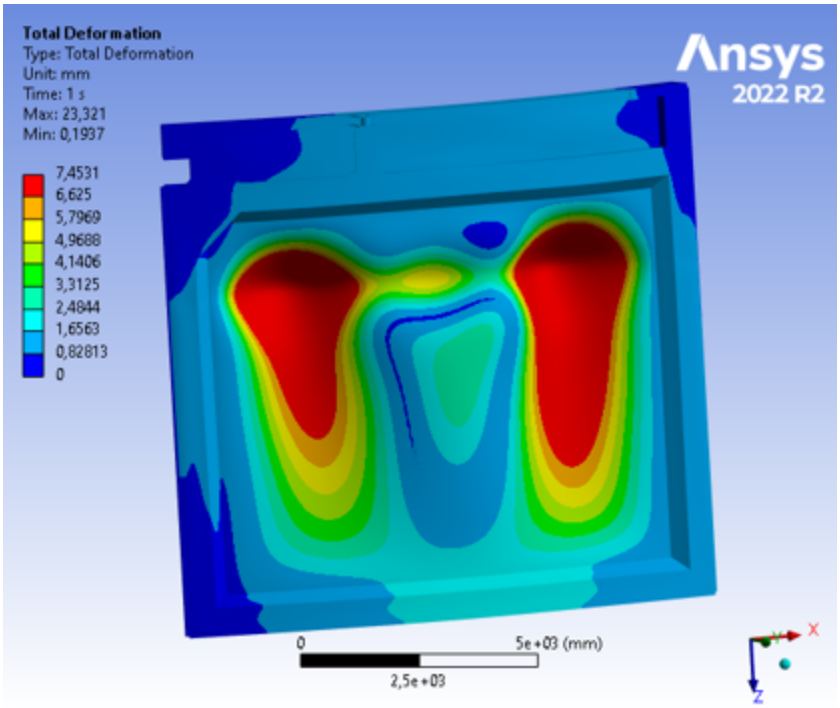

Figure M.21: Deformation of the gate due to ice load under ULS loads

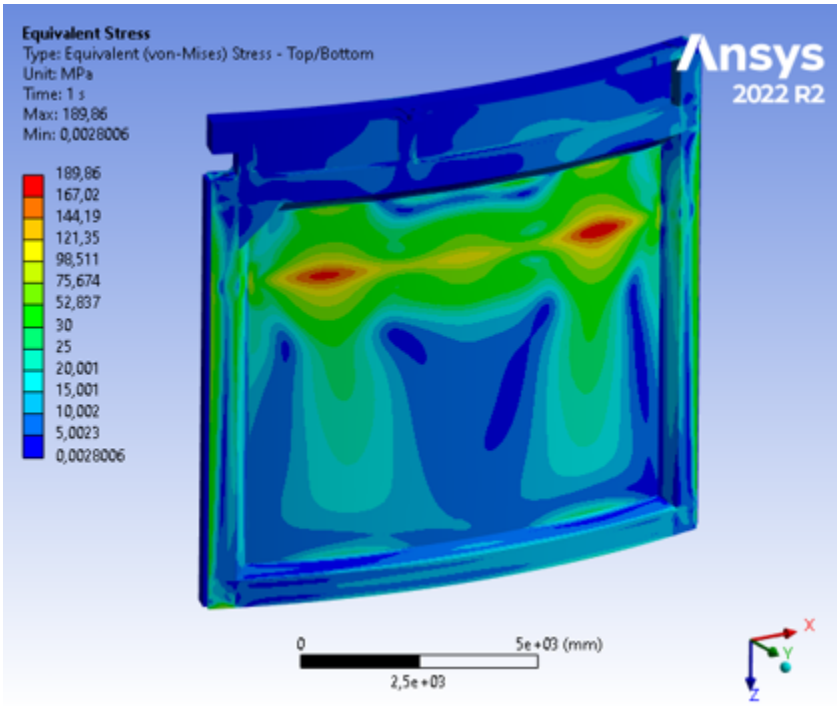

Figure M.22: Equivalent stresses in the gate under ice load.

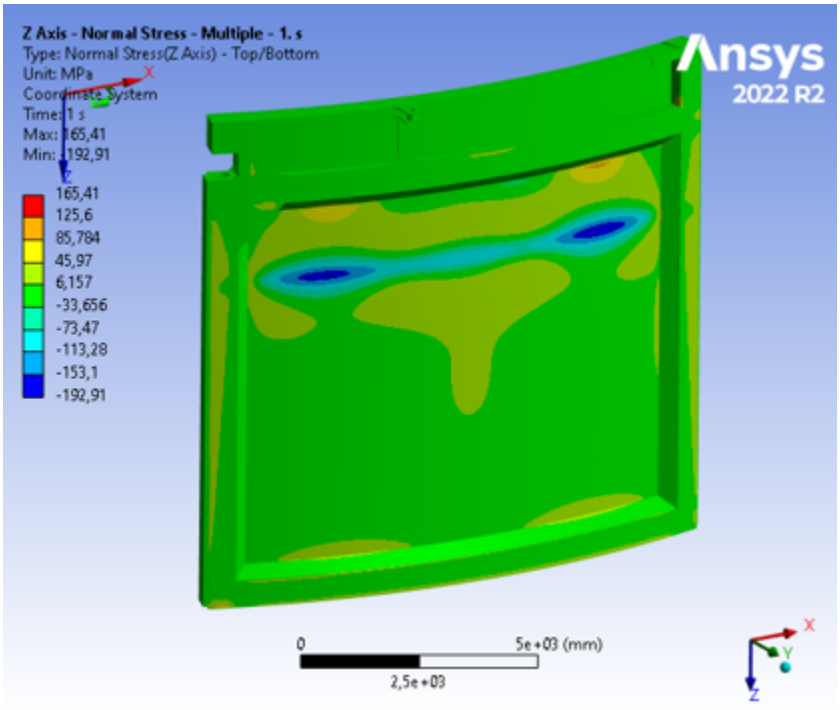

Figure M.23: Normal stresses in the vertical direction of the plate

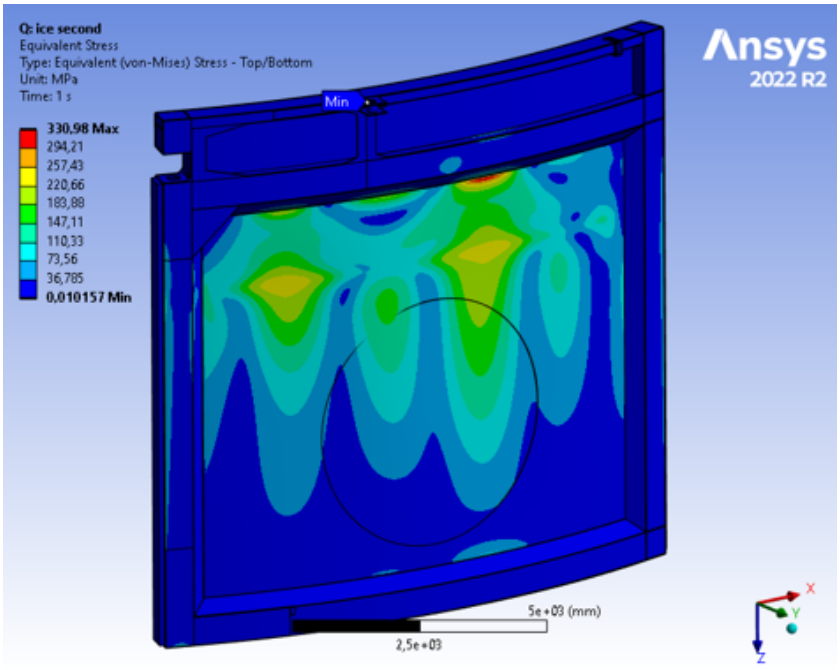

Figure M.24: Equivalent stress of the ice load in GNIA

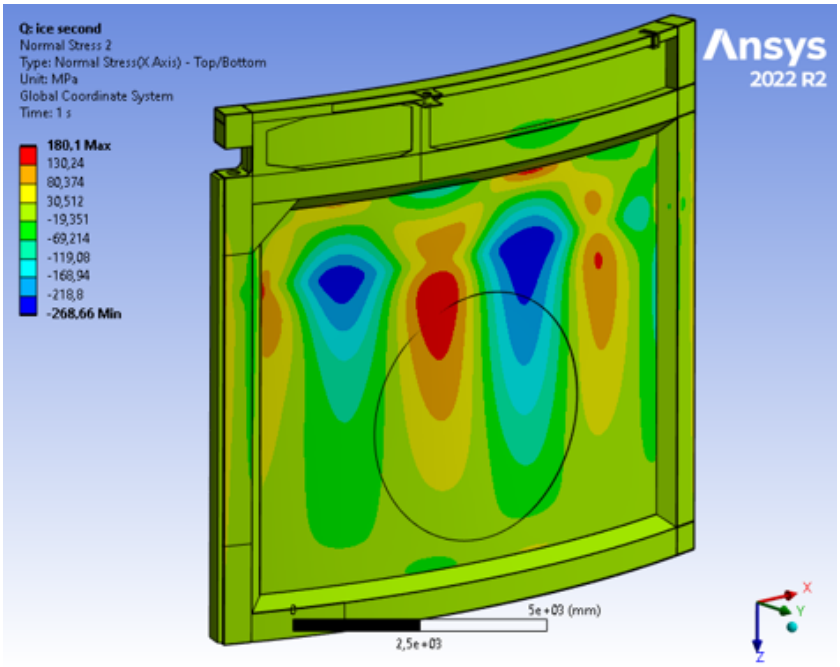

Figure M.25: Normal stress in the horizontal direction along the curve of the plate of the ice load in GNIA

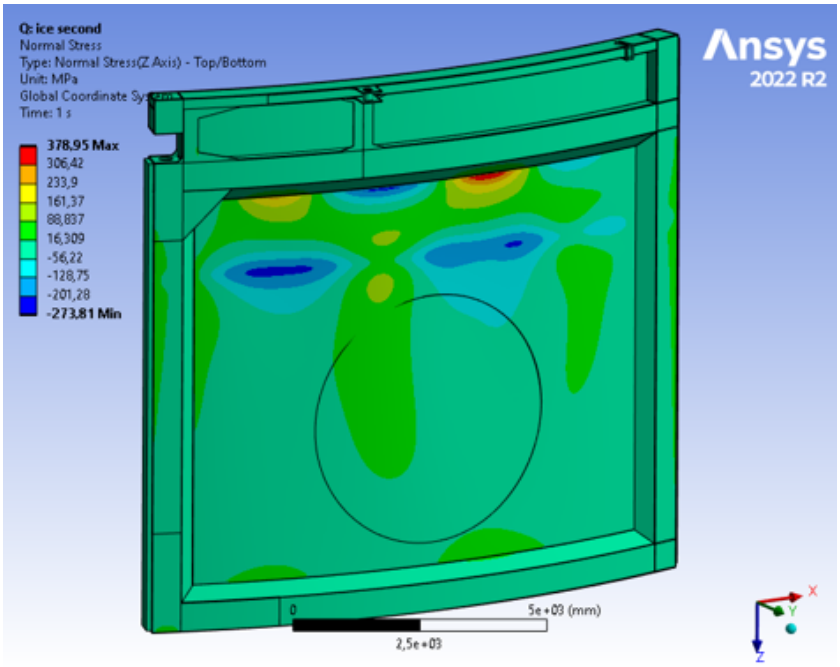

Figure M.26: Normal stress in the vertical direction of the ice load in GNIA

M.4. Obstacle load

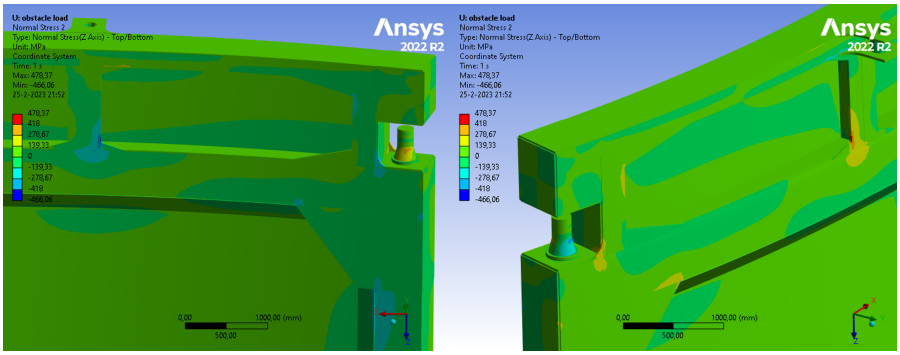

Figure M.27: Results of normal force in vertical direction due to obstacle load combination.

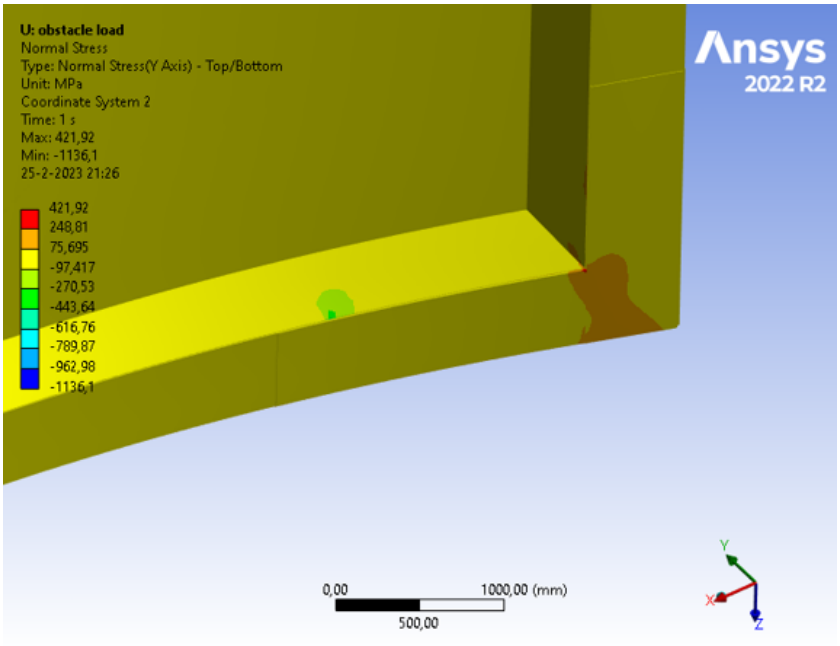

Figure M.28: Result of normal stresses perpendicular to the curve of the plate.

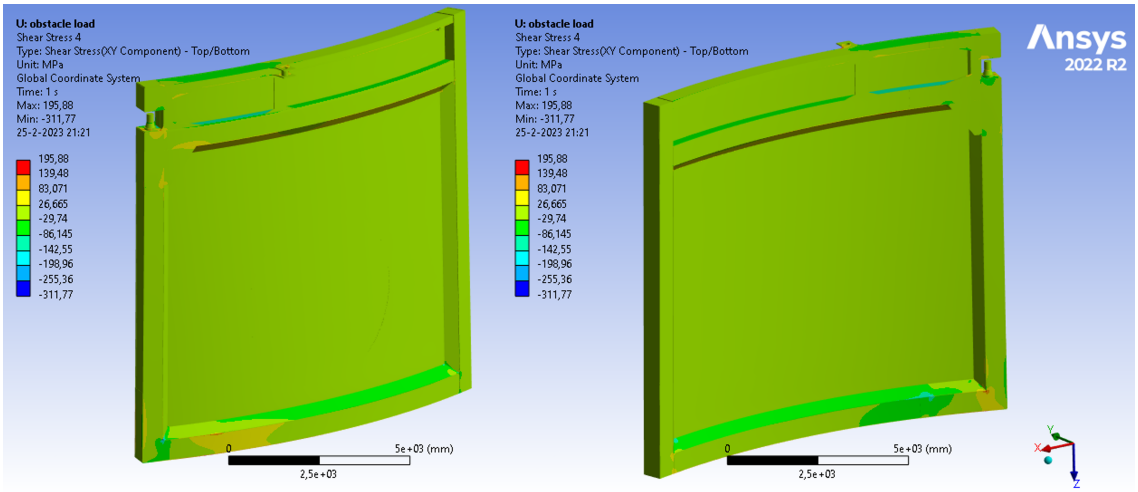

Figure M.29: Result of the shear stresses in the general YZ plane for the obstacle load.

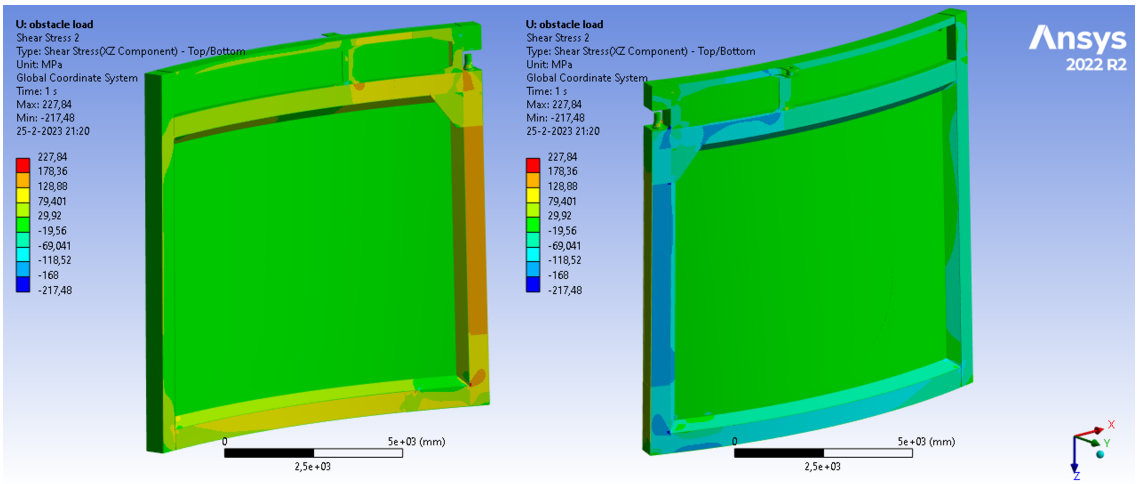

Figure M.30: Result of the shear stresses in the general YZ plane for the obstacle load.

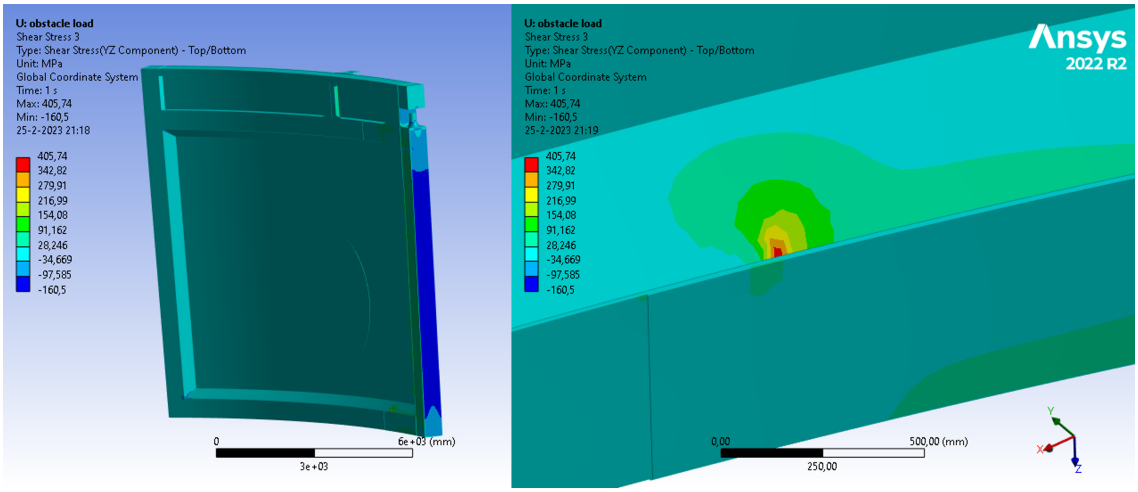

Figure M.31: Result of the shear stresses in the general YZ plane for the obstacle load.

M.5. Fatigue

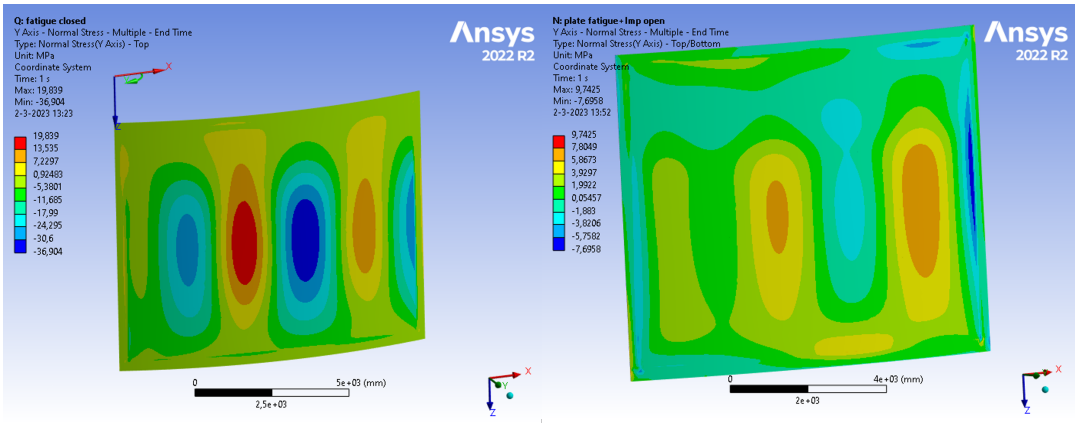

Figure M.32: Horizontal stress for Fatigue loading of the plate convex side

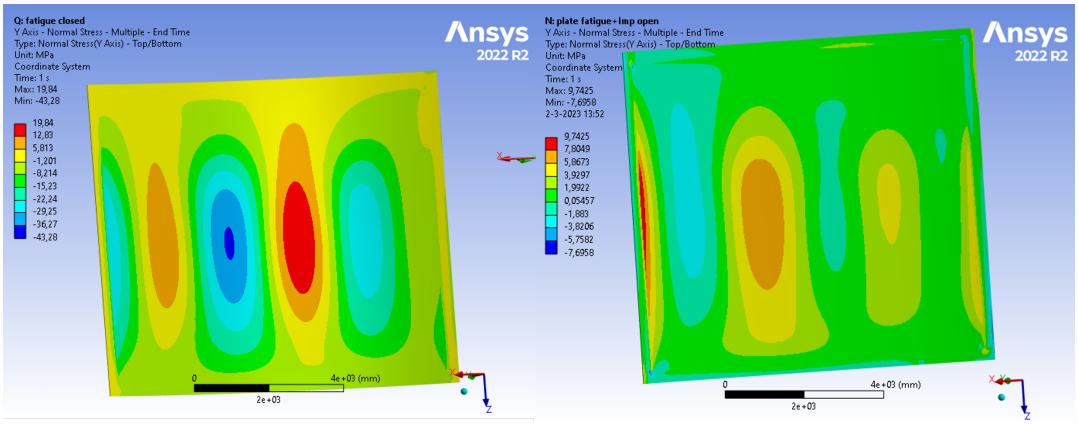

Figure M.33: Horizontal stress for Fatigue loading of the plate cancave side

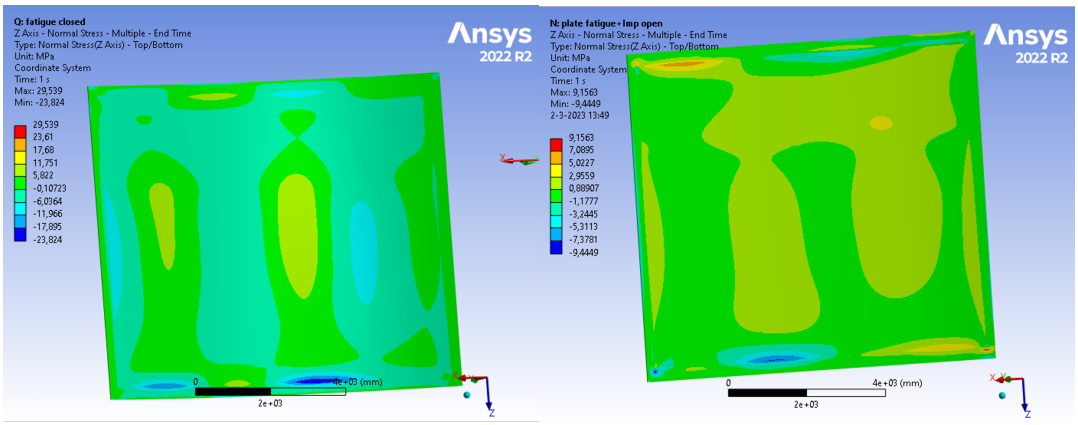

Figure M.34: Vertical stress for Fatigue loading of the plate convex side

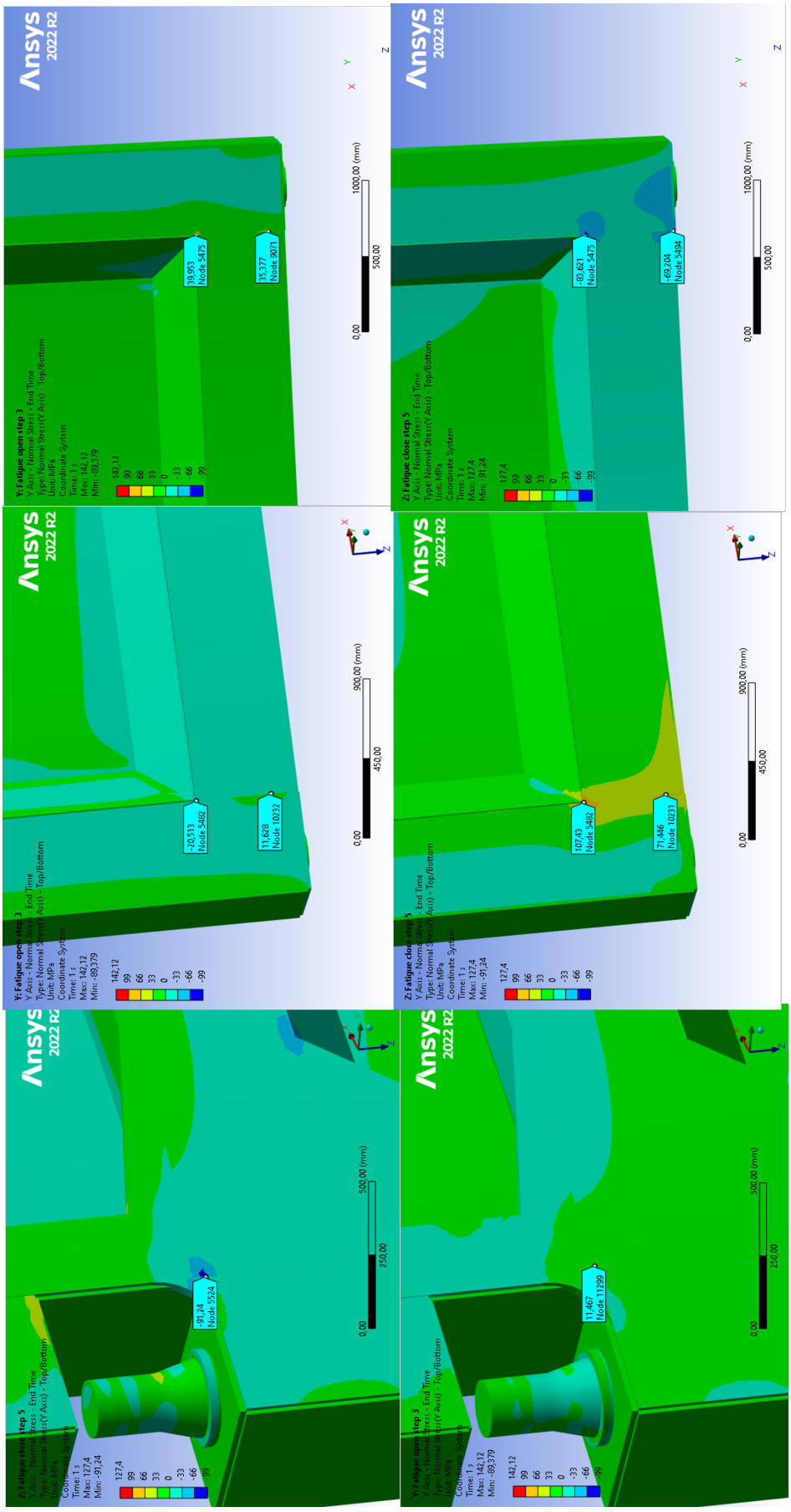

Figure M.35: Normal stresses in the frame due to fatigue loads on the construction.

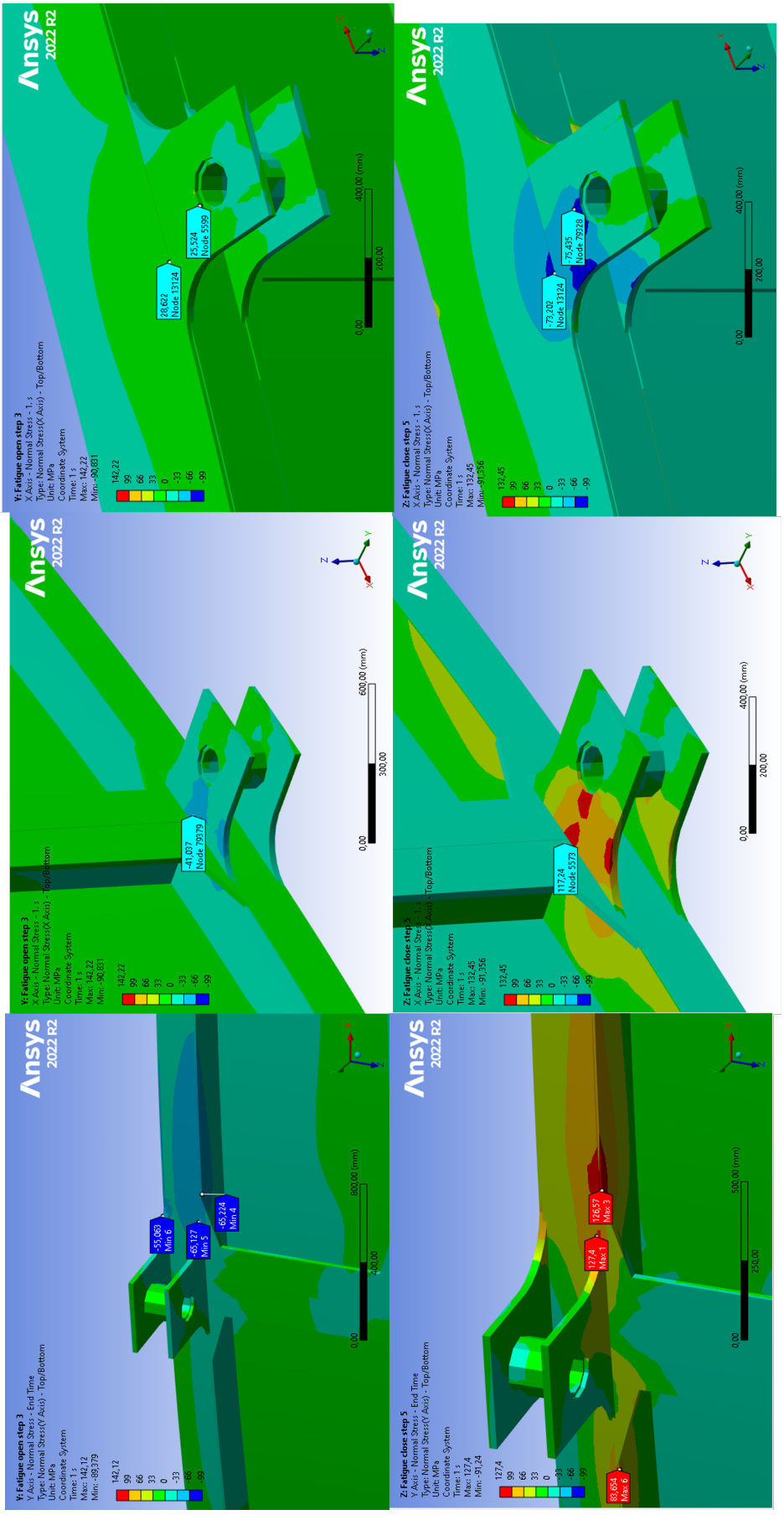

Figure M.36: normal stresses perpendicular to the main plate.

M.6. Gate in post

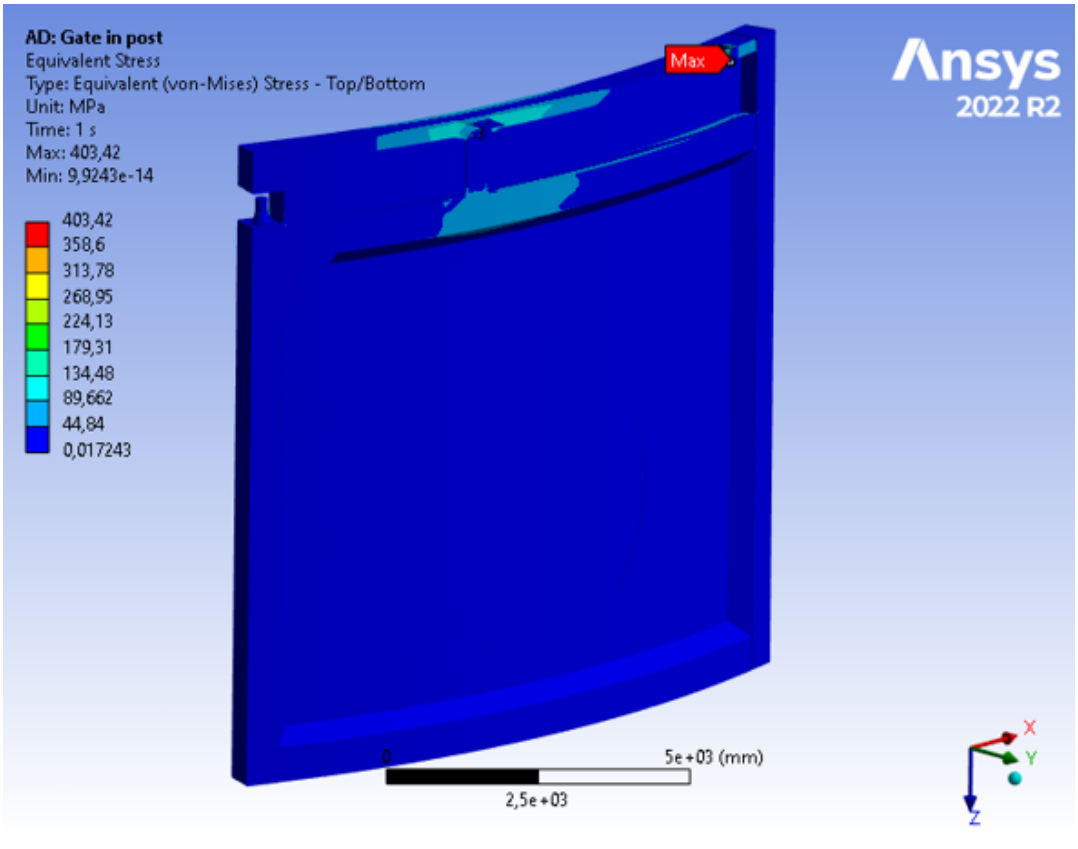

Figure M.37: Gate in post equivalent stress

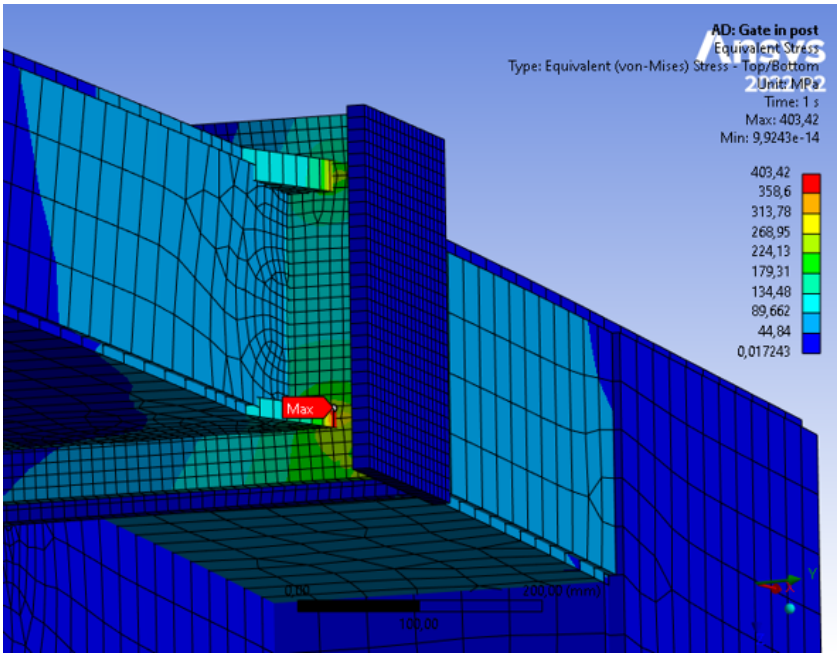

Figure M.38: The stress singularity of the support at the top beam.

M.7. Weight

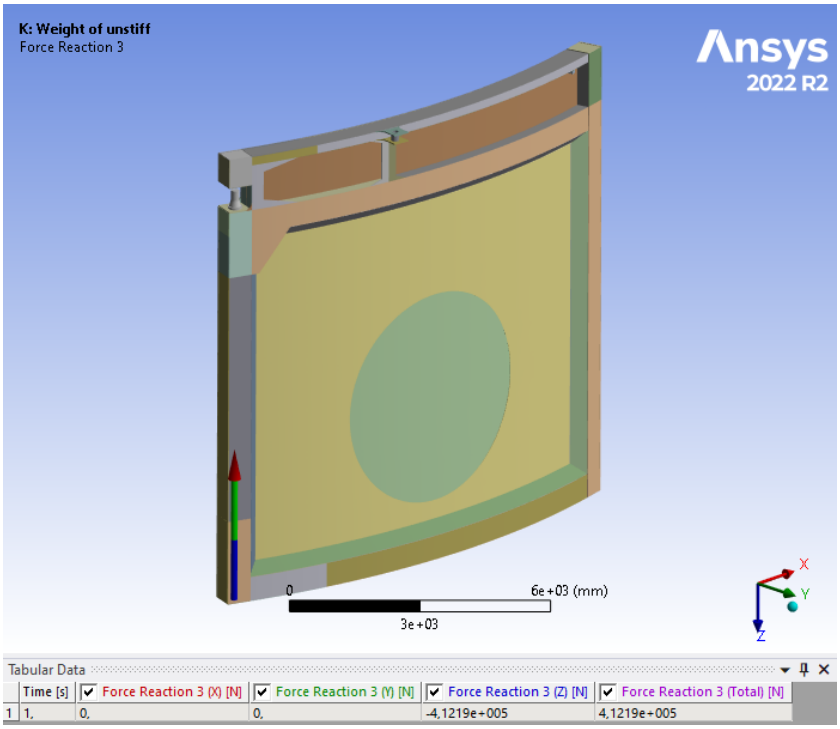

Figure M.39: The weight of the construction including weld weight

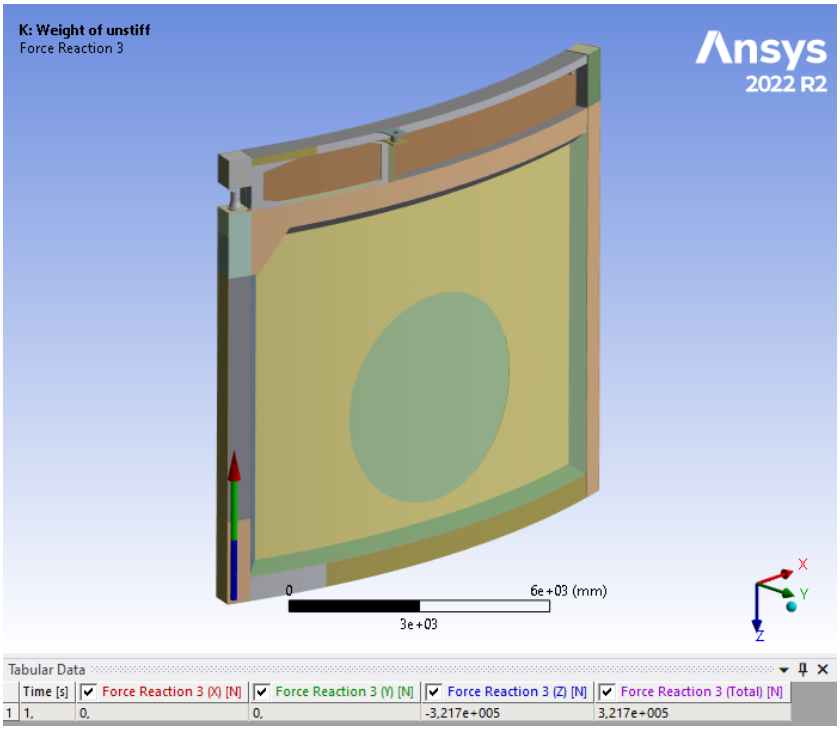

Figure M.40: The weight of the construction when the water is at the lowest level.

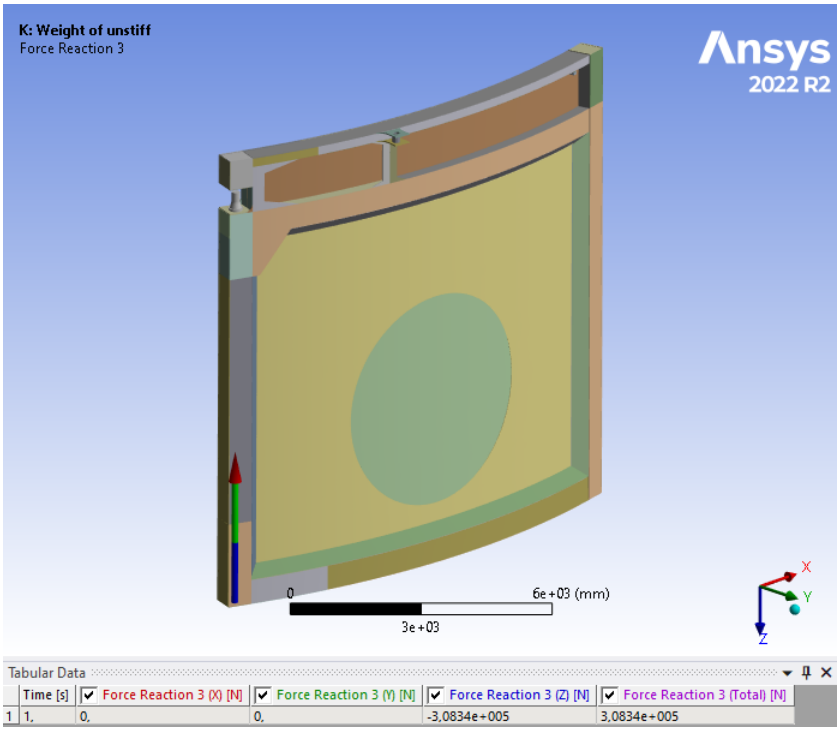

Figure M.41: The weight of the construction when the water is at the highest level.

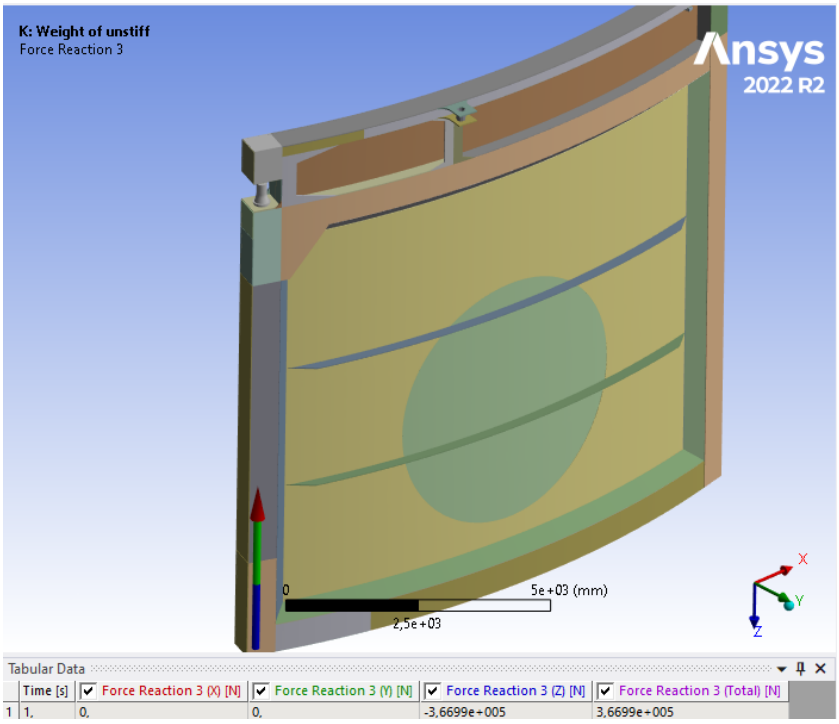

Figure M.42: Reaction force of the vertical support to determine the weight of the constructions

M.8. Welds

welds curved gate design								
no stiff								
	total height			10798				
	length along curve			11600				
	hoogte koker achter			570				
horizontals								
	#hor			3	#			
	#welds per hor			4	#			
	L			11600	mm	length	139200	mm
	t			26		area	3619200	mm2
diagonals hor				2	#			
	#welds per hor			4	#			
	L			10460	mm	length	83680	mm
	t			20		area	1673600	mm2
verticals								
	#ver			2	#			
	#welds			4	#			
	L			10798	mm	length	86384	mm
	thickness			26		area	2245984	mm2
diagonals ver				2	#			
	#welds per hor			4	#			
	L			8370	mm	length	66960	mm
	t			20		area	1339200	mm2
	plate							
	total plate height			9458				
	height plate bot			8370	2790	plate height for 3 plates		
	top plate	2						
	botplate	4						
	#welds			6				
	L			10460		length	62760	mm
	t			22		area	1380720	mm2
					total weld length			
						438984	mm	
						438,984	m	
			las volume is			0,55	x plaatdikte	
			gemiddelde plaat dikte			23,3692	mm	
			lasdikte			12,85306		
			weld area			82,60056		
			#welds per side			2		
			las volume			0,072521	m^3	
			difference			1,707599		

Figure M.43: Calculation of the weld length for the stiffened and unstiffened design.

N

Stiffened gate

The first-order results of the stiffened model can be seen in figure N.1.

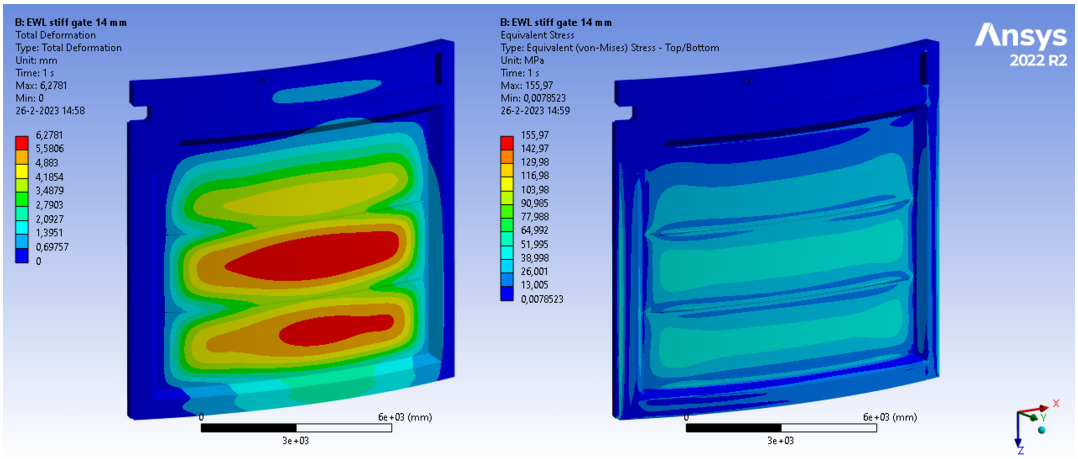

Figure N.1: Deformations and equivalent stress of mitre gate with 14 mm plate.

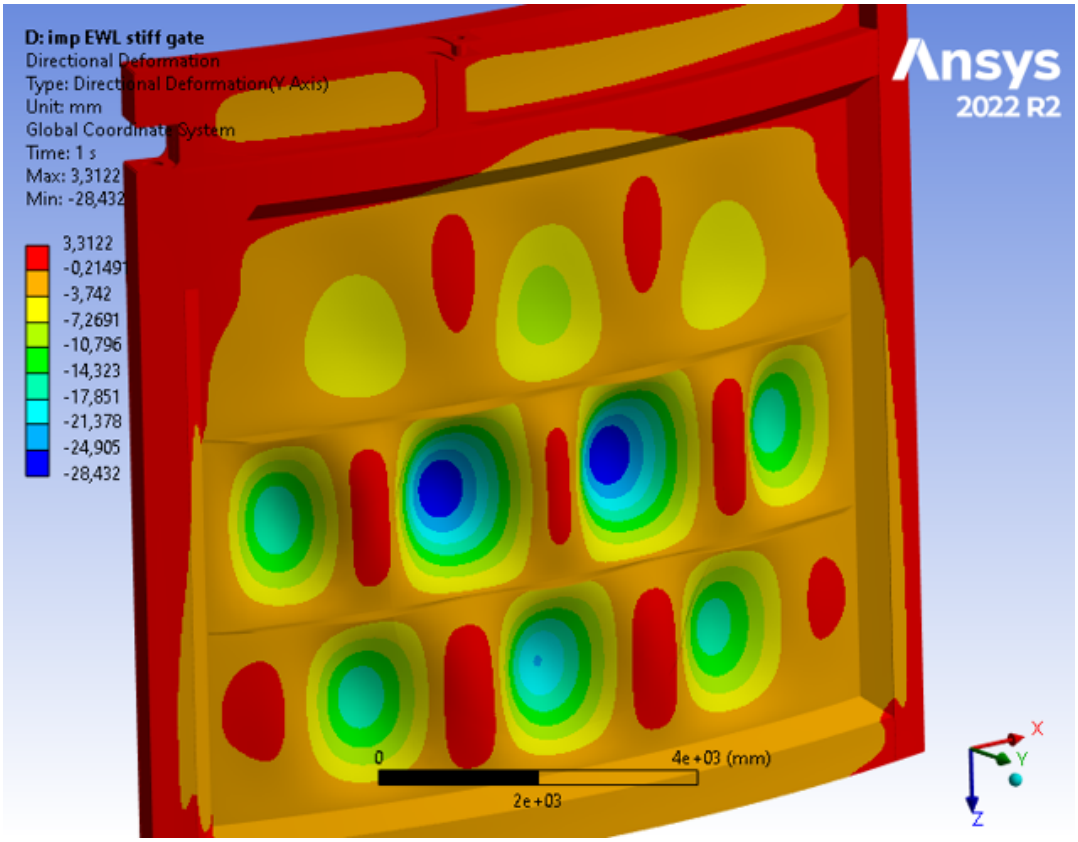

Figure N.2: Deformations for the model with 14 mm plate.

N.0.0.1. Thinner plates

An iteration was also executed for a plate thickness of 12 mm. This led to reasonable stresses and deformations in the first-order calculation. The GNIA, however, proved to be more complex. The first eight buckling modes became rather different from one another. The largest deformations in the buckling modes shift from the top plate to the middle plate and finally the bottom plate. The plates that do not have the largest deformations do however have small imperfections in them which are too small to see but are significant enough to present themselves in the second-order results. All buckling modes are between an eigenvalue of 0.02 and 0.3 which means the chance of all modes are relevant. Since the top plate is the largest it is not illogical that the first mode presents itself in the top segment. That higher modes present themself in the other plates can be explained by the slenderness of all main plates. For further reference with regards to the deformation and the equivalent stress of the first-order calculation, see figure N.4. For further reference with regards to the buckling modes see figure N.5.

When simulating the result for the buckling modes in a second-order calculation, the first mode has been used to evaluate the results. As there are higher modes which resemble the 14 mm plate these were not simulated separately: the effect is expected to be similar to the 14 mm plate with similar stress levels of the first buckling shape of the 12 mm plate (see figure N.3). A prediction could be made based on these results that the 12 mm plate would suffice, but this would have to be examined in further research. Higher alternative shape modes have not been assessed but can be relevant for further research and a final design. For the purpose of this study a conservative decision has been made to keep the design at the 14 mm thickness of the plate.

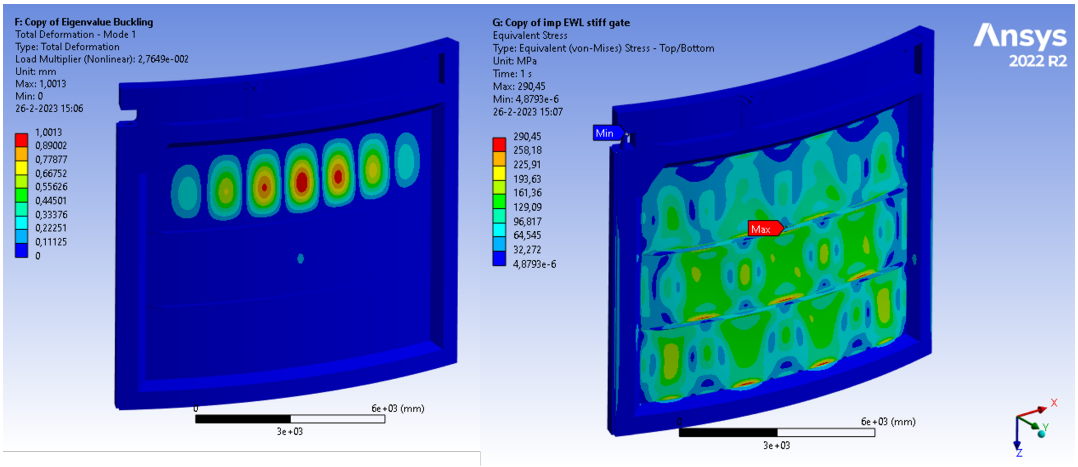

Figure N.3: Deformations and equivalent stress of mitre gate with 12 mm plate.

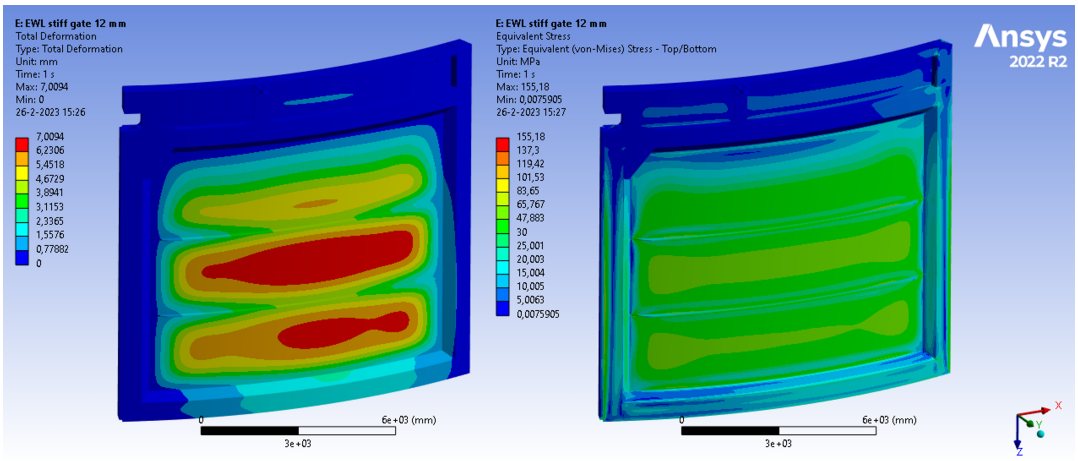

Figure N.4: Deformations and equivalent stress of mitre gate with 12 mm plate.

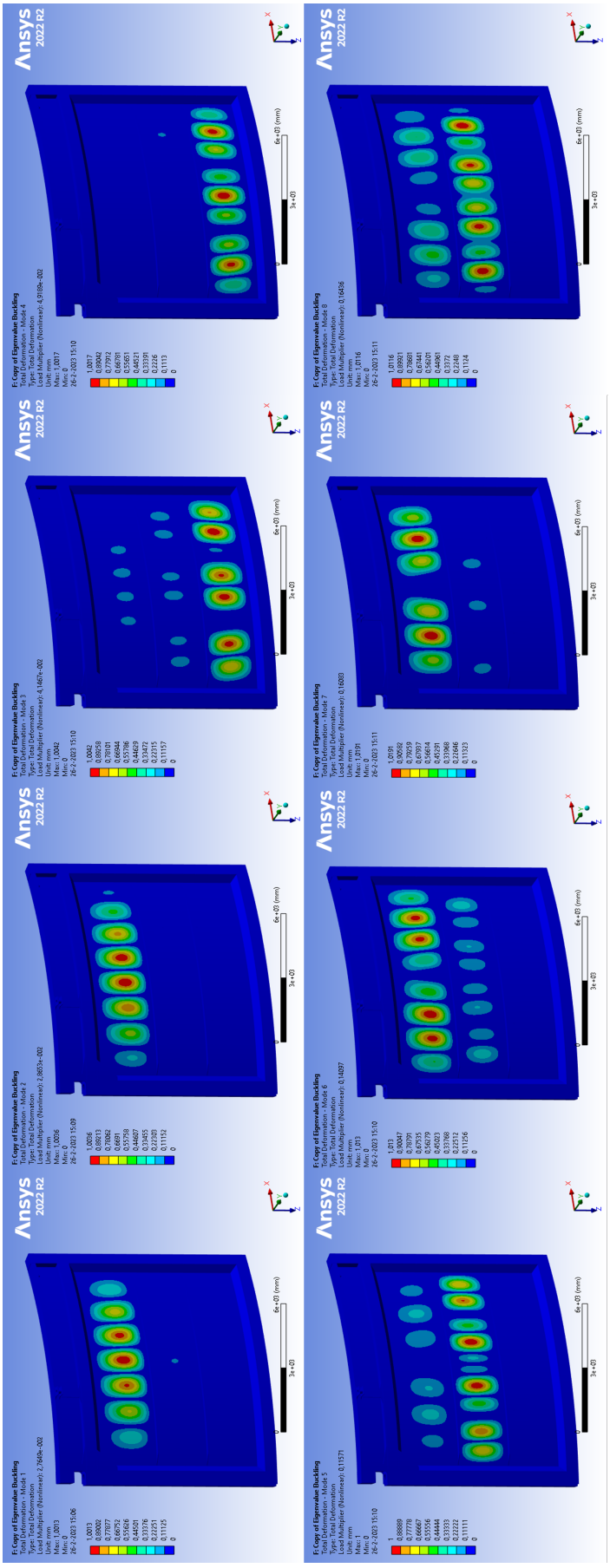

Figure N.5: Deformations and equivalent stress of mitre gate with 12 mm plate.

N.1. Welds

	With stiffeners in plate								
	total height			10798					
	length along curve			11600					
	hoogte koker achter			570					
horizontals									
	#hor			3	#				
	#welds per hor			4	#				
	L			11600	mm	length	139200	mm	
	t			26		area	3619200	mm2	
diagonals hor				2	#				
	#welds per hor			4	#				
	L			10460	mm	length	83680	mm	
	t			20		area	1673600	mm2	
verticals									
	#ver			2	#				
	#welds			4	#				
	L			10798	mm	length	86384	mm	
	thickness			26		area	2245984	mm2	
diagonals ver				2	#				
	#welds per hor			4	#				
	L			8370	mm	length	66960	mm	
	t			20		area	1339200	mm2	
	plate								
	total plate height			9458					
	height plate bot			8370	2790	plate height for 3 plates			
	top plate	2							
	botplate	6							
	#welds			8					
	L			10460		length	83680	mm	
	t			14		area	1171520	mm2	
					total weld length				
						459904	mm		
						459,904	m		
			las volume is			0,55	x plaatdikte		
			gemiddelde plaat dikte			21,85131	mm		
			lasdikte			12,01822			
			weld area			72,2188			
			#welds per side			2			
			las volume			0,066427	m^3		
			difference			0,91598			

Figure N.6: Weld volume approximated for the stiff gate design